Ion Pair Conductivity Model and Its Application for Predicting Conductivity in Non-Polar Systems

Sean Parlia

Submitted in partial fulfillment of the
requirements for the degree of
Doctor of Philosophy
under the Executive Committee
of the Graduate School of Arts and Sciences

COLUMBIA UNIVERSITY

2020

© 2020

Sean Parlia

All Rights Reserved

ABSTRACT

Ion-Pair Conductivity Model and Its Application for Predicting Conductivity in Non-Polar Systems

By Sean Parlia

While the laws of ionization and conductivity in polar systems are well understood and appreciated in the art, theories related to nonpolar systems and their conductivities remain elusive. Currently, multiple conflicting models, with limited experimental verification, exist that aim to explain and predict the mechanisms by which ionization occurs in nonpolar media.

A historical overview of the field of nonpolar electrochemistry, dating back to the 1800's, is presented herein with a focus on the work of prominent scientists such as Fuoss, Bjerrum, and Onsager, who's pioneering discoveries serve as the scientific foundation for our understanding of ionization in nonpolar systems, from which our knowledge of ion-pairs (i.e. re-associated solvated ions which do not contribute to the overall conductivity of the system) stems.

Recent work in the field of nonpolar electrochemistry has focused on ionization models such as the *Disproportionation Model* and the *Fluctuation Model*, which ignore ion-pair formation and the existence of these neutral entities altogether. While, the "*Ion-Pair Conductivity Model*", the novel conductivity model introduced and explored herein, primarily focuses on the critical role these neutral entities play with regards to the electrochemistry in these systems.

The "*Ion-Pair Conductivity Model*" for predicting and modeling the conductivity of mixtures of nonpolar liquids, arises from the *Dissociation Model*, a third ionization model for predicting conductivity in nonpolar systems which accounts for ion-pair formation, and is rooted in the foundational work of Fuoss, Bjerrum, Onsager, and others. The *Ion-Pair*

Conductivity Model's relationship to and derivation from the *Dissociation Model* is provided, including the justified assumptions and simplifications of the model to create a more concise approach for predicting conductivity in nonpolar systems that can be readily applied to real-world scenarios.

In order to substantiate this model as a reliable method for predicting conductivity in nonpolar solutions, experimental results from studies examining various two-component solutions comprised of an amphiphile and nonpolar liquid, analyzed under a variety of conditions, across the entire concentration spectra, from pure nonpolar liquid to pure amphiphile, are compared to the *Ion-Pair Conductivity Model*. The role additional properties such as water contamination, ion size, concentration of free ions, range of ion-pair existence, shear and longitudinal rheology in these nonpolar solutions are also explored.

The fitting of the experimental data and theoretical model demonstrates the ability of the *Ion-Pair Conductivity Model* to accurately predict conductivity in two-component solutions of an amphiphile and nonpolar liquid. Furthermore, it emphasizes the importance that ion-pairs play in the conductivity of such a system. Lastly, it reinforces the usefulness of the *Ion-Pair Conductivity Model* as a tool for investigating the mechanisms by which ionization in nonpolar media occur.

Ultimately, the goal of this study is to validate the *Ion-Pair Conductivity Model* as a robust and precise model for characterizing conductivity in nonpolar solutions across a diverse set of nonpolar systems. Allowing us, and others, to better understand and exploit the intrinsic properties of conductivity in these systems to advance a number of technologies in the field electrochemistry, such as a-polar paints, electrophoretic inks, and electrorheological fluids.

Table of Contents

LIST OF TABLES AND FIGURES

LIST OF TABLES

LIST OF FIGURES

LIST OF SYMBOLS

Symbol	Definition
α	Dissociation Constant, Attenuation
a	Distance of closest ion approach
β	Compressibility
C	Concentration
d	Distance
ε	Relative Permittivity
E	Intermolecular Energy
e	electron charge
ϕ	Volume fraction
F	Faraday's Constant
Λ	Conductance
γ	Activity
ΔG	Excess Activation Energy
I	Ionic Strength
J	Ionic Strength
κ	Debye Paramter (inverse Debye length)
$\mathbf{K_{eq}}$	Equilibrium Constant
K	Conductivity
k	Boltzmann's Constant
λ	Bjerrum Length
q	critical distance of ion-pair formation
r	distance
T	Temperature
U	Potential Energy
z	Valence

ACKNOWLEDGEMENTS

I would like to acknowledge my P.I., Dr. Ponisseril Somasundaran, for his advising throughout my years at Columbia University. Additionally, I would like to acknowledge Dr. Andrei Dukhin, who has served as not only my boss, but also as a mentor for the past decade.

DEDICATION

Dedicated to my wife, Alexandra Dudman, for the immeasurable help and support she has provided throughout this journey.

I. INTRODUCTION

The field of electrochemistry can be broadly defined as the study of electrical current in chemical solutions, driven, in part, by the behavior of ion transport and migration within these solutions[1]. Given the inherently ionic nature of polar systems, aqueous solutions serve as ideal media for electrochemical reactions. However, aqueous solutions have several limitations, most notably, the high number of chemical substances of potentially important electrochemical reactivity that are insoluble, highly reactive, or restricted by additional innate characteristics of these systems. Thus, the ability to understand and manipulate the properties of their more complex counterpart, nonpolar systems, allows for the exploration and exploitation of substances previously insoluble, unstable and unable to chemically react in polar systems.

Conductivity in non-polar media plays an important role in many modern applications, ranging from printer inks[2] to electrophoretic displays[3] to apolar paints[4,5].

Currently, multiple conflicting models, with limited experimental verification[6-8], exist that aim to explain and predict the mechanisms of conductivity in nonpolar media. These conflicting theories, and their limited application for modeling real-world systems, highlight the need for a more robust approach for predicting the behavior of these systems within the field of nonpolar electrochemistry.

The goal of this study is to expand upon the past discoveries of experts in the field and introduce a new model, called the "*Ion-Pair Conductivity Model*", as a means to accurately determine and predict conductivity in nonpolar systems. Initial experimentation and application of this model has shown promise. Further exploration of *the Ion-Pair Conductivity*

Model will provide additional insight into both the underlying mechanisms that drive nonpolar systems as well as provide a robust approach for accurately modeling these systems in real world environments.

1.1 BACKGROUND

1.1.1 THEORETICAL MODELS OF POLAR AND NON-POLAR MEDIA

To better understand electrochemistry in nonpolar systems, i.e. non-aqueous media, its best to begin by examining their less complex counterpart, polar systems, i.e. aqueous media. Polar systems are well studied and appreciated in the art and thus can serve as a reliable point of reference and provide valuable insight into the scientific foundation that governs the laws of nonpolar media. The electrochemistry of non-aqueous media and how its behavior deviates from that of its aqueous partner is the key to understanding, describing, and predicting conductivity in nonpolar systems.

1.1.1.1.1 MICHAEL FARADAY

In 1834, Michael Faraday first used the term "ion" to describe a charged particle that under the influence of an electric potential, carries an electric current[9]. Faraday believed that ions were produced via electrolysis, created by a peripheral source of electricity that provided a direct current to the system to form ions. To prove this theory, he began by studying how water, under various conditions, responded to electrolytic action. Faraday found that parameters such as electrode size and current intensity did not impact the waters chemical action when subjected to the same amount of electricity. From this he concluded the following about the dissociation of water into ions:

"…when subjected to the influence of the electric current, a quantity of it (water) is decomposed exactly proportionate to the quantity of electricity which has passed through it…"

This finding, and the tests he ran thereafter, resulted in Faraday's "table of ions", also

known as “Faraday’s Table of Equivalents”, which contains over 50 ions, separated into anions and cations, wherein a chemical equivalent is defined as the relative amount needed to react with or supply one mole of hydrogen ions (H^+) in an acid-base reaction[10]:

Faraday's Table of Equivalents

Anions		***Cations***			
Oxygen	8	Hydrogen	1	Silver	108
Chlorine	35.5	Potassium	39.2	Platina	98.6
Iodine	126	Sodium	23.3	Gold	-
Bromine	78.3	Lithium	10	Ammonia	17
Fluorine	18.7	Barium	68.7	Potassa	47.2
Cyanogen	26	Strontium	43.8	Soda	31.3
Sulphuric Acid	40	Calcium	20.5	Lithia	18
Selenic Acid	64	Magnesium	12.7	Baryta	76.7
Nitric Acid	54	Manganese	27.7	Strontia	51.8
Chloric Acid	75.5	Zinc	32.5	Lime	28
Phosphoric Acid	35.7	Lead	103.5	Magnesia	20.7
Carbonic Acid	22	Iron	28	Alumina	-
Boracic Acid	24	Copper	31.6	Protoxides	-
Acetic Acid	51	Cadmium	55.8	Quinia	171.6
Tartaric Acid	66	Cerium	46	Cinchona	160
Citric Acid	58	Cobalt	29.5	Morphia	290
Oxalic Acid	36	Nickel	29.5	Vegeto-alkalies	-
Sulphur (?)	16	Antimony	64.6		
Selenium	-	Bismuth	71		
Sulphoeyanogen	-	Mercury	200		

Table 1: Table of Ions reprinted from Faraday’s Table of Equivalents

1.1.1.2 SVANTE ARRHENIUS

Then, roughly fifty years later, Svante Arrhenius proposed that, even in the absence of an electric current, aqueous solutions contained ions[11,12]. Arrhenius argued that the chemical reactions occurring in these solutions were the result of reactions between oppositely charged ions, ***A+*** and ***B-***, which formed via dissociation of a neutral molecule, ***AB***, according to the following [2]:

$$AB \leftrightarrow A^{+} + B^{-} \qquad \textit{Eq. 1}$$

$$K_{eq} = \frac{[A^{+}][B^{-}]}{[AB]} \qquad \textit{Eq. 2}$$

Where [***A+***] and [***B-***] refer to the activity of the cations and anions, respectively, and [***AB***] refers to the activity of the neutral molecule, and K_{eq} is the equilibrium constant].

1.1.1.3 FRIEDRICH KOHLRAUSCH

From 1875-1879, Friedrich Kohlrausch measured the conductivity of various electrolytes as a function of concentration and established that, to a high degree of accuracy, in dilute solutions, molar conductance is the product of individual charge contributions of ions, known as ***Kohlrausch's law*** *of Independent Ionic migration*[14]:

$$\Lambda(C) = \frac{K(C)}{C} = \Lambda_0 - A\sqrt{C} \qquad \textit{Eq. 3}$$

Where, Λ is molar conductance, K is the additive's (i.e. electrolyte, amphihile, etc.) specific conductivity, C, is the molar concentration of the additive, Λ_0 is the limiting molar conductance and A is a proportionality constant.

Kohlrausch understood that a complex relationship between molar conductance (and, accordingly, equivalent conductance) of an electrolyte and the concentration of that electrolyte existed within these solutions. At low concentrations he noted that molar conductivity varied

by a fractional power of concentration. However, as concentration of the additive increased, he recognized this relationship became more convoluted.

At infinite dilution, Kohlrausch observed that conductivity, $\boldsymbol{K}$, was proportional to the molar concentration, $\boldsymbol{C}$, of the additive, where: $\boldsymbol{\lim_{C\to 0} K = \Lambda_0 C}$

At non-infinite dilution, Kohlrausch found that an increase in the concentration, $\boldsymbol{C}$, of the additive actually *decreased* the molar conductance, $\boldsymbol{\Lambda}$, of the system, which he assumed to be the result of the partial dissociation of the additive, according to equilibrium constant, $\boldsymbol{K_{eq}}$, defined as:

$$\boldsymbol{K_{eq} = \frac{\alpha^2 C}{1-\alpha}} \qquad \textbf{\textit{Eq. 4}}$$

Where $\boldsymbol{\alpha}$ is the dissociation constant, and its relationship to concentration, $\boldsymbol{C}$, is defined as:

$$\boldsymbol{[A^+] = [B^-] = \alpha C}$$

Degree of dissociation into free ions

$$\boldsymbol{[AB] = (1-\alpha)C}$$

Degree of re-association of ions into non-conducting species, e.g. neutral molecule/ion pair

Although, at the time, Kohlrausch could not assign any specific physical meaning to proportionality constant, $\boldsymbol{A}$, *Kohlrausch's law* was still able to accurately model the dependence of molar conductance of the system on the concentration of additive in very dilute solutions.

As the concentration of additive increased, the percentage of additive molecules that dissociated into ions, and remained as ions in the solution, decreased. Therefore, the molar conductance, which is defined as the conductance of solution per mole of additive, would thus decrease. Dissociation constant $\boldsymbol{\alpha}$ can be solved for as a quadratic with the non-extraneous root:

$$\boldsymbol{\alpha = \frac{-1+\sqrt{1+4\frac{C}{K_{eq}}}}{2\frac{C}{K_{eq}}}} \qquad \textbf{\textit{Eq. 5}}$$

Accordingly, the asymptotic limits for this dissociation constant can be determined at small and large concentrations[15]:

$$\lim_{C/K_{eq}\to 0} \alpha = 1 - \frac{C}{K_{eq}} + 2\left(\frac{C}{K_{eq}}\right)^2 + O\left[\left(\frac{C}{K_{eq}}\right)^3\right] \qquad \textit{Eq. 6}$$

$$\lim_{C/K_{eq}\to \infty} \alpha = \left(\frac{K_{eq}}{C}\right)^{1/2} - \frac{K_{eq}}{2C} + O\left[\left(\frac{K_{eq}}{C}\right)^{3/2}\right] \qquad \textit{Eq. 7}$$

At infinite dilution, the dissociation constant, α, is represented as the following:

$$\alpha(C) = 1 - O(C) \qquad \textit{Eq. 8}$$

Where O is a function of higher order terms of concentration C. In addition to the ionization work carried out in polar systems by Kohlrausch and others, ionization in nonpolar systems was explored by Arrhenius, Ostwald, and Kablukoff. They studied the effect Hydrochloric Acid (HCl) (i.e. the additive) had on the conductivity of non-aqueous liquids benzene, hexane, and ether[4]. In stark contrast to the work put forth by Kohlrausch, they found that the molar conductance in their nonpolar systems decayed as additive concentration decreased.

1.1.1.4 VLADIMIR ALEXANDROVICH PLOTNIKOV

Then, in the early 1900's, Ukrainian researcher Plotnikov demonstrated that two, virtually non-conducting liquids, ether and methylbromide, generated conductivity significantly higher than that of either individual liquid when mixed together, highlighting the important role of relative permittivity in controlling or influencing conductivity in non-aqueous solutions[16-19]. Approximately 100 years later, Dukhin and Goetz observed similar phenomena while studying steric stabilization of ions in nonpolar liquids using ionic surfactants, which themselves could dissociate and form ions[20]. However, this ability to dissociate is not a requirement for steric stabilization, and therefore the team set out to examine whether or not "non-ionic, non-dissociative substances can be used to control the conductivity and ionic

composition of non-polar liquids." While initially they noticed that non-ionic surfactants, based on their low relative permittivities (well below 10), yield higher-than-expected conductivity values, it wasn't until they mixed these surfactants with other nonpolar liquids that they confirmed the earlier work done by Plotnikov.

In their study, Dukhin and Goetz mixed nonpolar kerosene with a variety of materials with a low relative permittivity (i.e. below 10), and low Hydrophile-Lypophile Balance (HLB) number, and found that the conductivity of the solution, in many cases, increased as a function of the concentration of the additive. They also reported similar results for a variety of nonpolar liquids in which a nonionic surfactant was added. Additionally, the conductivity of these mixtures was higher than the conductivity of the individual components, which is in direct agreement with Plotnikov's work from 100 years prior.

During the same time period as Plotnikov's research into mixtures of nonpolar liquids, Latvian chemist Paul Walden became interested in electrochemistry of non-aqueous solutions[21,22]. In 1902, he proposed a theory of auto-dissociation of inorganic and organic solvents. In 1905, Walden discovered a relationship between the maximum molecular conductivity and viscosity of the medium, in which he asserted that the product of the viscosity, $\boldsymbol{\eta}$ and the ionic conductance in a nonpolar system at infinite dilution, $\boldsymbol{\Lambda_0}$ is constant, independent of the solvent[23]. The "*Walden Rule*", $\boldsymbol{\Lambda_0\eta} \approx constant$, as it is referred to today, is used to describe the linear function of concentration as a product of viscosity and conductivity in an electrolytic solution. The Walden Rule is regularly applied to the field of electrochemistry, and throughout this discussion, to delineate between classical electrochemistry (i.e. electrolytic solutions, wherein ion-pairs formed from solvated ions do not exist), and nonpolar electrochemistry (i.e. solutions wherein ion-pairs are present). In 1906,

Walden coined the term "solvation" and in 1914 he discovered and introduced ionic liquids to the field of electrochemistry.

The early electrochemistry work carried out at the end of the 19th century in aqueous solutions and at the beginning of the 20th century in non-aqueous solutions served as the basis for two prominent conductivity theories in polar and nonpolar systems: the Bjerrum theory of ion pairs[24] and the Debye-Hückel theory of the ion-cloud[25,26].

1.1.1.5 NIELS BJERRUM

In 1909, Niels Bjerrum proposed that an additional equilibrium, beyond that of neutral molecules, [$\boldsymbol{AB}$], and their oppositely charged ions, [$\boldsymbol{A^+}$] and [$\boldsymbol{B^-}$], also existed in these systems[27]. At this time, Bjerrum was exploring color changes (or lack thereof) that occur during electrolytic dissociation. He noted that in the case of chromium salts, the exact same absorption of light occurred regardless of concentration, however, the same did not hold true for all electrolytes he examined. More specifically, he found that only strong electrolytic solutions experience this lack of color change; while in weak electrolytic solutions the color of the solution is a function of electrolyte concentration. Bjerrum described this relationship by expanding on Arrhenius' initial hypothesis, arguing that strong electrolytes exhibit a unified color, across all concentrations, due to the full dissociation of the ions within the solution. However, for weaker electrolytes, a change in color is observed due to the incomplete dissociation of the ions, which ultimately re-associate within the solution.

Bjerrum then took a closer look at the behavior of molar conductivity within these two types of solutions and hypothesized that the phenomena occurring between the molar conductivity and freezing point of the solution must be related to the interaction of ions with each other within the solution. He noted that it is not a decrease in the number of ions that causes a decrease in the molar conductivity of the system, but rather the rate at which they

move. In other words, interactions between ions of weak electrolytes resulted in their mobility decreasing, which decreased their conductivity and molar conductance. This realization served as the basis for his theory of ion-pairs.

According to Bjerrum, if the electrostatic attraction between oppositely charged ions is sufficient, then it is possible for them to form neutral entities called ion-pairs, [A^+B^-], according to the following equilibrium relationship[28]:

$$A^+ + B^- \leftrightarrow A^+B^- \qquad \textit{Eq. 9}$$

$$K_{eq} = \frac{[A^+][B^-]}{[A^+B^-]} \qquad \textit{Eq.10}$$

While Bjerrum's ***Eq. 9*** looks very similar to Arrhenius' ***Eq. 1*** it is important to note that Arrhenius' ***Eq. 1*** can involve either an ionic or covalent bond while Bjerrum's ***Eq. 9*** pertains only to ionic bonds.

Using Coulomb's law to compute the electrostatic potential of two ions at some distance, ***r,*** and integrating the Boltzmann factor, ***k***, over all possible positions, Bjerrum calculated the fraction of ions which were within close enough proximity of one another to act as one neutral entity (i.e. ion-pair) rather than two separate ions. Accordingly, he defined the ***Bjerrum length***, λ, as the distance, ***r*** at which the electrostatic interaction between two ions is equal to thermal energy ***kT***:

$$\lambda = \frac{z^+z^-e^2}{\varepsilon kT} \qquad \textit{Eq. 11}$$

Where z^+ and z^- are the valences of the cation and anion, respectively, ***e*** is electron charge, ε is the relative permittivity of the solution, ***k*** is Boltzmann's Constant, and ***T*** is temperature.

Bjerrum length (***Eq. 11***) is determined by first calculating the fraction of ions which were, due to their attractive electrostatic forces, close enough together to behave as one

neutral entity instead of two distinct ions. Bjerrum further concluded that this fraction was inversely proportional to the equilibrium constant, $\boldsymbol{K_{eq}}$ in ***Eq. 10*** . Therefore, expanding on *Bjerrum length* (***Eq. 11***) as the negative ratio of the electrostatic potential energy (as a function of distance $\boldsymbol{r}$) versus thermal energy $\boldsymbol{kT}$, he determined[29]*:*

$$-\frac{U_{elec}(r)}{kT} = -\frac{\boldsymbol{z^+z^-e^2}}{\boldsymbol{4\pi r\varepsilon kT}} = \frac{\boldsymbol{\lambda}}{\boldsymbol{r}} \qquad \textbf{\textit{Eq. 12}}$$

With *Bjerrum length* defined in standard units in ***Eq. 12*** (with the addition of "$\boldsymbol{4\pi}$" in the denominator of the equation) and defined in Gaussian units in ***Eq. 11*** (where $4\pi\varepsilon_0 = 1$).

Using the theoretical approach described above, to estimate the value for $\boldsymbol{K_{eq}}$ in ***Eq. 10***., Bjerrum found that the electrolytes in the solution completely dissociated, implying that the partial dissociation described earlier by Kohlrausch does not explain the decreases in conductivity measured for such systems, despite adhering to ***Kohlrausch's law***.

Given the relationship illustrated in ***Eq. 11***, ion-pairs form when the collision diameter (the sum of the two ion radii) is less than *Bjerrum length*, at which point the thermal energy is no longer strong enough to break the pair apart. Thus, a large *Bjerrum length* means strong long-range electrostatic interactions between the ions with respect to thermal energy, $\boldsymbol{kT}$ and thus, the attractive forces between them will be sufficient for ion-pairs to exist in solution.

In the case of polar systems, relative permittivity is large and *Bjerrum length* is quite small, only 0.7 nanometers (nm). As a result, long-range electrostatic interactions are weak compared with thermal energy, $\boldsymbol{kT}$ and thus, ion-pairs are typically not found in these types of systems. However, the opposite is true for nonpolar systems in which relative permittivity is much lower, and long-range electrostatic interactions increase the likeliness of ion-pair formation.

Bjerrum also understood that long-range columbic interactions play an important role in nonpolar electrochemistry. If the *Bjerrum length* is sufficiently large, the electrostatic attractive forces from oppositely charged ions are strong enough to re-associate the ions into ion-pairs. The critical distance in formation of ion-pairs, $\boldsymbol{q}$, is defined as half the *Bjerrum length*, $\boldsymbol{\lambda}$[26]:

$$\boldsymbol{q} = \frac{\boldsymbol{\lambda}}{2} \qquad \textbf{\textit{Eq. 13}}$$

Bjerrum concluded, therefore, that ion-pair formation occurs when an ion of one charge (e.g. an anion) enters a sphere of radius $\boldsymbol{q}$ drawn around an ion of the opposite charge (e.g. a cation). Based on this notion ion-pair formation can be illustrated as the relationship between the "*distance of closest ion approach*", $\boldsymbol{a}$, and the "*critical distance in formation of ion-pairs*", $\boldsymbol{q}$. Wherein, when distance, $\boldsymbol{a}$, is less than distance $\boldsymbol{q}$, ion-pairs are forced to recombine into a neutral entity that does not contribute to the conductivity of the system. For simplification purposes distance of closest ion approach, $\boldsymbol{a}$, is used instead of ion size; because use of ion size would require additional information about the size ratio between the cation and the anion.

1.1.1.6 DEBYE AND HÜCKEL

In 1923, Debye and Hückel published their theory for the activity of strong electrolyte solutions, which was based on the idea that "a reference ion sitting at the origin of the spherical coordinate system is surrounded by the smoothed-out charge of the other ions.[30]" And while all ions are surrounded by this smoothed out charge, there exist local inequalities due to localized differences in ion concentration. This localized concentration difference being the case wherein the cloud of one ion will not necessarily cancel out the cloud of an oppositely charged ion. As a result, the ions are surrounded by clouds of charge opposite their own, due to the attractive forces of the opposing charge. As stated simply by Bockris & Reddy: "there is a local excess charge density of one sign opposite to that of the central ion."

In their ion-cloud model, the ion experiences a "smoothed-out cloud of charge around it", this creates, around each ion, an "ionic atmosphere" of oppositely charged ions with a mean radius of $\boldsymbol{\kappa^{-1}}$. The ***Debye-Hückel limiting law*** for low ionic strength is defined as[28]:

$$\ln \gamma_+\gamma_- = -\frac{\kappa\lambda}{1+\kappa a=1 \; for \; dilute \; solutions} = -\kappa\frac{z^+z^-e^2}{\varepsilon kT} = -Az_\pm^2\sqrt{I} \qquad \textbf{Eq.14}$$

Where $\boldsymbol{I}$ is ionic strength, $\boldsymbol{\gamma}$ is ion activity, and parameter $\boldsymbol{\kappa}$ is referred to as the "Debye parameter," which has the unit length^{-1}. Its inverse, $\boldsymbol{\kappa^{-1}}$, is commonly used and referred to as the *Debye screening length*[14] and is defined as $\boldsymbol{\kappa^{-1}} = \sqrt{\frac{e^2I}{\varepsilon kT}}$, which determines the range of electrostatic interactions and, consequently, the size of the ionic atmosphere. Debye length is the distance from a charged surface at which the electric potential has diminished by a value of 1/e. The most significant aspect of this theory is the prediction that the product of the activity coefficients, $\boldsymbol{\gamma_+}$ and $\boldsymbol{\gamma_-}$, are a function of *ionic strength*, $\boldsymbol{I}$, of the solution rather than the concentration of the additive, $\boldsymbol{C}$.

In the ion-cloud model described by Debye and Hückel, the ion experiences a "smoothed-out cloud of charge around it" and Poisson's continuum equation with its implication of a continuous charge distribution replaced Coulomb's law[14]. Thus, the time-average spatial distribution of the excess charge density described above needed to be determined next. To do so the following Poisson equation is applied:

$$\frac{1}{r^2}\frac{d}{dr}\left(r^2\frac{d\psi_r}{r}\right) = -\frac{4\pi}{\varepsilon}\rho_r \qquad \textbf{Eq. 15}$$

Where $\boldsymbol{r}$ is distance from the central ion, $\boldsymbol{\psi_r}$ is electrostatic potential, and $\boldsymbol{\rho_r}$ is the charge density. By applying the following linearized Poisson-Boltzmann equation and solving for the charge density, Debye and Hückel were able to determine the following:

$$\rho_r = -\frac{\varepsilon}{4\pi}\kappa^2\psi_r \qquad \textbf{Eq. 16}$$

Where

$$\boldsymbol{\kappa^2 = \frac{4\pi}{\varepsilon kT}\sum_i n_i^0 z_i^2 e_0^2} \qquad \textbf{\textit{Eq.17}}$$

And ε is relative permittivity, $\boldsymbol{k}$ is Boltzmann's constant, $\boldsymbol{T}$ is absolute temperature, $\boldsymbol{z}$ is valence, $\boldsymbol{e}$ is electron charge, and $\boldsymbol{n}$ is number of ions per unit volume. This equation served to not only describe the cloud surrounding a reference ion but, also describe the distribution of ions around said reference ion.

While at a sufficiently dilute concentration of ions, this "smoothed-out" description put forth by Debye and Hückel holds true, the same cannot be said as the concentration of ions in solution increases. Based on this theory, at sufficiently high ionic strength, e.g. 0.01 mol/L of electrolyte, half of the ionic atmosphere would come from a single ion, which is at odds with the "smoothed-out" cloud described earlier. According to work carried out by Bockris and Reddy, the concentration of 0.001 mol/L of electrolyte is the limit above which the Debye-Hückel ion-cloud theory is no longer applicable[26]. The phrase "coarse grained", coined by Bockris and Reddy, is often used to describe the ion-cloud model at high electrolyte concentrations, where the original theory is no longer valid because short range non-columbic interactions from neighboring ions now play a role in the ionic environment of the solution. In order for the ion cloud theory to be applicable, it is the long-range coulombic interactions which dominate, because it is those interactions that are responsible for the ion cloud itself.

There are different types of dissociation and equilibrium events that occur when an additive (electrolyte, amphiphile, surfactant, etc.) is introduced to a system.

By replacing Coulomb's law with Poisson's continuum equation, they were able to partially explain *Kohlrausch's law* via the product of ion activity coefficients $\boldsymbol{\gamma^+}$ and $\boldsymbol{\gamma^-}$:[29]

$$\boldsymbol{\ln \gamma^+ \gamma^- = -\frac{\kappa\lambda}{1+\kappa a}} \qquad \textbf{\textit{Eq. 18}}$$

Where

$$\boldsymbol{\kappa = \sqrt{\frac{e^2 \sum_i z_i^2 C_i}{\varepsilon k T}}} \qquad \textbf{\textit{Eq.19}}$$

If we opt to use ion activities, instead of ion concentrations, the equation for the equilibrium constant becomes the following:

$$\boldsymbol{K_{eq} = \frac{\alpha^2 C}{1-\alpha} \gamma^+ \gamma^-} \qquad \textbf{\textit{Eq. 20}}$$

Thus, while the Debye-Hückel theory resulted in the correct theoretical expression of *Kohlrausch's Law*, the proportionality constant, ***A***, predicted using ***Eq.3***, differed significantly from the experimental value of ***A***. In an attempt to correct this error, Swedish chemical engineer, Lars Onsager, derived a new theoretical expression for molar conductance, **Λ**, by incorporating Debye and Hückel's charge cloud distortion theory together with viscosity and electrophoretic effects of the system yielding the ***Debye-Hückel-Onsager theory***[31,32]

$$\boldsymbol{\Lambda = \Lambda_0 - S\sqrt{C}} \qquad \textbf{\textit{Eq. 21}}$$

Where, $\boldsymbol{S = (A + B\Lambda_0)}$ and ***A*** and ***B*** are proportionality constants that depend on the solvent's properties (relative permittivity and viscosity), the additives properties (ionic strength and ion charge) and temperature. More specifically:

$$\boldsymbol{A = \frac{e^2}{6\varepsilon k T (1+\sqrt{1/2}} \left(\kappa/\sqrt{C}\right)} \qquad \textbf{\textit{Eq. 22}}$$

$$\boldsymbol{B = \frac{eF^2}{3\pi\eta N} \left(\kappa/\sqrt{C}\right)} \qquad \textbf{\textit{Eq. 23}}$$

Where proportionality constant ***A*** defines the solutions relaxation effects, and ***B*** defines the solutions electrophoretic effects[21].

The square root dependence on concentration for conductance in ***Eq. 22*** and ***Eq. 23*** comes from a reimagining of the ion clouds deformation during movement. Debye and Hückel predicted that, while spherical when an ion is motionless, the cloud of counterions surrounding

an ion will deform as that ion moves, forming an ellipsoid shape. Due to drag effects, the cloud of counter ions will be slightly behind the actual ion located within. As a result, the attractive forces from the surrounding counter-ion serve to slow down the movement of the ions, hindering its mobility. From this they determined that a square root dependence on concentration was more accurately reflective of the behavior of these systems than the linear dependence they had previously suggested.

1.1.1.7 FUOSS AND ONSAGER

However, both *Kohlrausch's law* and the *Debye-Hückel-Onsager theory* break down as the concentration of the electrolyte in the solution increases, the result of which drives the average distance between the cation and anion to decrease, increasing the overall inter-ionic interactions within the system.

Accounting for the decreasing conductance of electrolytic solutions with increasing concentration was only partially resolved in the *Debye-Hückel-Onsager theory*. While this theory fixed certain aspects of the conductance problem, it still failed to accurately predict experimental conductance values even at rather low additive (i.e. electrolyte) concentrations. This shortcoming lies in the development of the theory itself, in which the ions were treated as point charges and terms orders higher than $\sqrt{C}$ were never evaluated. Follow up work carried out by Fuoss and Onsager highlighted the importance of investigating terms of order higher than $\sqrt{C}$, which gave way to the following ***Fuoss-Onsager Conductance Theory***[21]:

$$\boldsymbol{\Lambda = \Lambda_0 - S\sqrt{C} + EC \ln C + J(a)C} \qquad \textbf{\textit{Eq. 24}}$$

Where $\boldsymbol{C}$ is the concentration of the additive, $\boldsymbol{S}$ (*the Onsager limiting slope*) = $\boldsymbol{A + B\Lambda_0}$, and $\boldsymbol{A}$, $\boldsymbol{B}$, $\boldsymbol{E}$, and $\boldsymbol{J}$, are all proportionality constants that depend on the relative permittivity, viscosity, ionic strength, ionic charge and absolute temperature of the solution, with parameter $\boldsymbol{J}$ also serving as a function of $\boldsymbol{a}$, the distance of closest ion approach.

Additionally, this improved theory, with its accounting for higher order terms, allowed for an improved calculation of ion mobilities[33]:

$$\frac{\lambda_i}{\lambda_i^0} = 1 - \left(\kappa a_i + \frac{\omega}{6}\kappa\lambda_B\right) \qquad \textit{Eq. 25}$$

Where

$$\omega = z^+z^- \frac{2q}{1+\sqrt{q}} \qquad \textit{Eq. 26}$$

$$q = \frac{z^+z^-}{z^++z^-}\frac{\lambda^++\lambda^-}{\lambda^+z^+\lambda^-z^-} \qquad \textit{Eq. 27}$$

For 1-1 electrolytes, Prieve et al found that ω = 0.5859.[34]

In 1933, Fuoss and Kraus[25,26] noticed that many additives, particularly in solvents with a low relative permittivity, exhibit a minimum in equivalent conductance, Λ as concentration of additive, C increases. They explained this minimum conductance, Λ_m in terms of bilateral ion-triplet formation giving the following for the conductance of solutions containing ion-triplets[35]:

$$\Lambda\sqrt{C} = A + BC \qquad \textit{Eq. 28}$$

$$\Lambda_m\sqrt{C_m} = 2BC_m = 2 \qquad \textit{Eq. 29}$$

Where, Λ is conductance, and Λ_m, minimum conductance, C, is concentration of the additive and C_m, minimum concentration of the additive, and A and B are specific constants for a given solvent-solute system at a given temperature.

1.2 IONIZATION IN NON-POLAR SYSTEMS

To date, the mechanisms by which ions are maintained in non-aqueous media with low relative permittivity remains a source of debate among experts in the field of nonpolar electrochemistry. There are multiple competing models that attempt to explain the phenomena of ionization in nonpolar systems, the most common being:

1. The Dissociation Model
2. The Disproportionation Model
3. The Fluctuation Model

The *Dissociation Model* and the *Disproportionation Model* both aim to explain the process by which ions are solvated (i.e. stabilized) in nonpolar systems as the water content approaches zero, while the *Fluctuation Model*, conversely, focuses on inverse micro-emulsions wherein water is present. While all of these models provide significant contributions to our understanding of the field of nonpolar electrochemistry, this study will focus on the *Dissociation Model* and its relationship to the *Ion-Pair Conductivity theory*.

1.2.1 THE DISSOCIATION MODEL

The Dissociation Model defines ionization in nonpolar systems as the process wherein, first, ion formation occurs via the dissociation of polar or semi-polar molecules (e.g. surfactants or contaminants) or proton exchange between molecules (e.g. alcohols), followed by ion solvation via a solvating agent in the nonpolar system, which provides steric stability for the ion in solution[29].

In the case where ions form via dissociation of polar or semi-polar molecules, an additive (i.e. a surfactant or amphiphile) is introduced to the nonpolar system and serves as the solvating agent. The ion formation in this process is due to the dissociation of the additive

molecules, the result of contamination or another factor. The exact nature of ion formation is very difficult to predict due to the very low levels of overall ions in the system.

The mechanism by which ionization occurs in alcohol molecules is by way of proton exchange. First, the alcohol molecules undergo "self-dissociation", wherein the two alcohol molecules collide, causing the exchange of a proton, resulting in a cation and anion to form. Thus, for ethanol we have the following[26,36]: $C_2H_5OH + C_2H_5OH \leftrightarrow C_2H_5OH_2^+ + C_2H_5O^-$

In order for these ions to remain in the system, and not recombine into neutral ion-pairs, they need to be solvated. In the cases of alcohols, the solvating agent is other alcohol molecules that are capable of solvation due to their amphiphilic nature, which is referred to as "self-solvation," because both the ion and the solvating agent are the same species[26]. This ion-dipole interaction, between the alcohol ion and the neutral alcohol molecule, was first discovered by Fuoss and Kraus[37,38] and later expanded upon by others[39,40].

There are different types of dissociation and equilibrium events that occur when an additive (electrolyte, amphiphile, surfactant, etc.) is introduced to a nonpolar system.

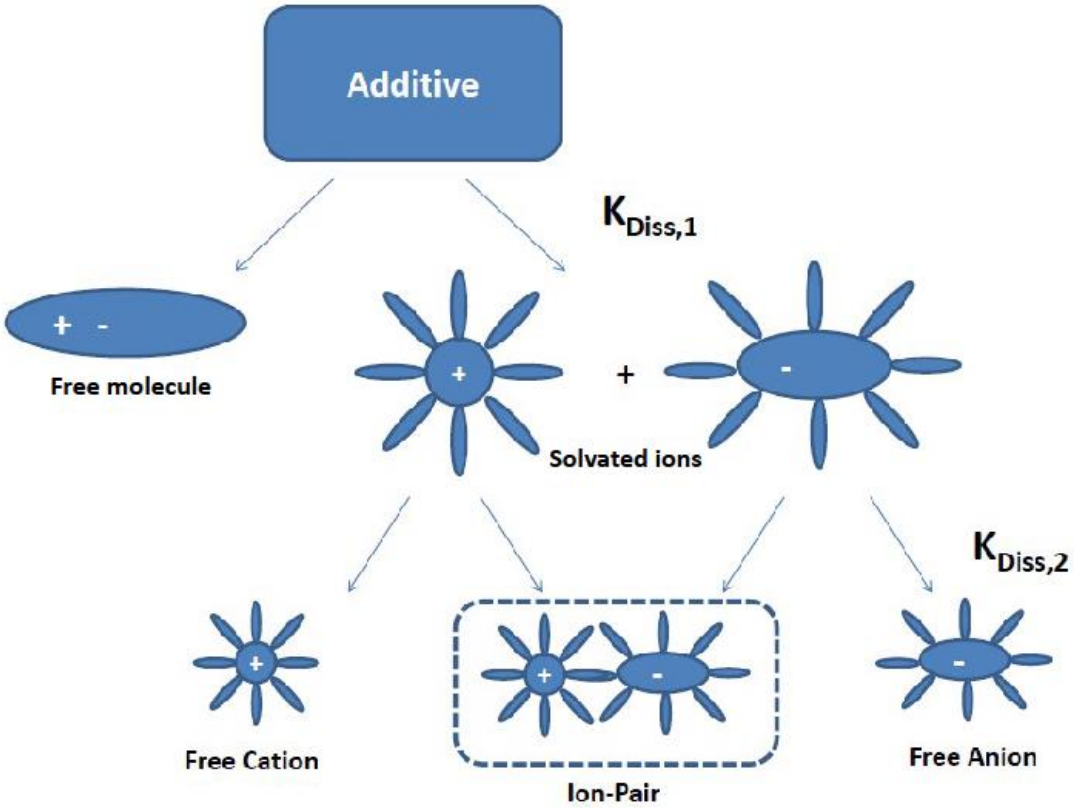

Figure 1. *Flow chart of Dissociation Model in Nonpolar Media, depicting initial equilibrium dissociation reaction between free molecules and solvated ions ($K_{Diss,1}$), as well as the second dissociation equilibrium reaction between free solvated ions and neutral ion-pairs ($K_{Diss,2}$)*

As illustrated in ***Figure 1***, above, initially, a first dissociation equilibrium, $\boldsymbol{K_{Diss1}}$, event occurs between free molecules and free ions. During this first dissociation a portion of the additive will remain undissociated as neutral molecules, ***AB***, while the remaining portion will dissociate into free ions, $\boldsymbol{A^+}$ and $\boldsymbol{B^-}$, and be solvated by a solvating agent (i.e. another additive molecule, surfactant, etc.). This reaction and corresponding equilibrium coefficient are represented as the following:

$$\boldsymbol{AB \leftrightarrow A^+ + B^-} \qquad \textbf{\textit{Eq. 30}}$$

$$\boldsymbol{K_{Diss1} = \frac{[A^+][B^-]}{[AB]}} \qquad \textbf{\textit{Eq. 31}}$$

Where, dissociation of neutral additive molecules into free ions is governed by ***thermal motion*** *and;*

$$\boldsymbol{AB \rightarrow A^+ + B^-}$$

Re-association of free ions into neutral additive molecules is governed by ***chemical reactions****:*

$$\boldsymbol{AB \leftarrow A^+ + B^-}$$

This is the same reaction proposed by Arrhenius in the late 1800's[13].

The chemical reactions, which govern the re-association of free ions back into neutral additive molecules are complex and only possible to define on a quantum physics level. These chemical reactions are further complicated by the presence of inevitable contamination in these systems, thus, the ability to accurately measure the total concentration of ions in the system, $\boldsymbol{C_{ions}}$, is virtually unattainable without a high degree of uncertainty. Contamination can come from a variety of sources: water contamination, contaminants in amphiphile, contaminants in nonpolar media, etc., and can be present in non-negligible concentrations. As a result, a single equilibrium dissociation reaction to describe the balance between neutral molecules and solvated ions, for all sources of solvated ions, is not feasible. Accordingly, ***Eq. 30*** and ***Eq. 31*** serve as purely theoretical representations of these relationships and thus, no attempt is made to predict the actual values for $\boldsymbol{C_{ions}}$ or equilibrium constant $\boldsymbol{K_{Diss1}}$.

Next, a second dissociation equilibrium, $\boldsymbol{K_{Diss2}}$, between free ions and ion-pairs takes place. During this second dissociation event a portion of the newly formed free ions will remain as such in solution, while others, due to electrostatic attractive forces, will recombine into neutral ion-pairs. These ions are still solvated (i.e. are still surrounded by a solvation layer of solvating molecules), however the attractive forces between anions and cations result in them combining to form (and behave as) a neutral entity, called an "ion-pair." $\boldsymbol{A^+B^-}$ is the newly created neutral ion-pair, explicitly bound by an ionic bond, which is not to be confused with the original neutral free molecule, ***AB***, from ***Eq. 30***and ***Eq. 31***, bound by either a covalent or ionic bond. Thus, this second dissociation reaction and corresponding equilibrium coefficient are governed by the laws of Bjerrum's ion-pair theory according to the following:

$$\boldsymbol{A^+B^- \leftrightarrow A^+ + B^-} \qquad \textbf{Eq. 32}$$

$$\boldsymbol{K_{Diss2} = \frac{[A^+][B^-]}{[A^+B^-]}} \qquad \textbf{Eq. 33}$$

Where, dissociation of neutral additive molecules into free ions is governed by ***thermal motion*** *and;*

$$\boldsymbol{A^+B^- \rightarrow A^+ + B^-}$$

Re-association of free ions into neutral additive molecules is governed by ***electrostatic interactions****:*

$$\boldsymbol{A^+B^- \leftarrow A^+ + B^-}$$

The long-range columbic interactions defined by Bjerrum length and described in ***Eq. 11***, serve as the driving force behind ion-pair formation in these solutions. Accordingly, we introduce a new parameter, $\boldsymbol{C_{ions}^{free}}$, defined as the concentration of free ions, $\boldsymbol{A^+}$ and $\boldsymbol{B^-}$, (labelled "free anion" and "free cation" in ***Figure 1***) that remain in the solution as such and do not recombine into neutral ion-pairs. Because electrostatic interactions, not chemical reactions, are the driving force behind this equilibrium coefficient, we are able to model $\boldsymbol{K_{Diss,2}}$, and measure $\boldsymbol{C_{ions}^{free}}$, according to Bjerrum's dissociation constant, $\boldsymbol{K_{Diss,2}}$, defined as[37]:

$$K_{Diss2} = 4\pi N_A \int_a^q EXP\left(\frac{2q}{r}\right) dr \qquad \textit{Eq. 34}$$

Where N_A is Avogadro's number and a is distance of closest ion approach. Later, K_{Diss2}, was redefined by Fuoss as[38]:

$$K_{Diss2} = \frac{4\pi N_A a^3}{3} EXP\left(\frac{2q}{a}\right) \qquad \textit{Eq. 35}$$

Fuoss, unlike Bjerrum, believed that physical contact was necessary for ion-pair formation and thus, subsequently expanded ***Eq. 24***, the *Fuoss-Onsager Conductance Theory*, by redefining molar conductance, Λ, as a function of additive concentration, C according to[14]:

$$\Lambda = \Lambda^0 - S\sqrt{C} + EC\ln C + J_1 C - J_2 C^{3/2} - \Lambda^0 C K_{Diss2} \qquad \textit{Eq. 36}$$

Where the newly introduced term $-\Lambda^0 C K_{Diss2}$, considers ion association in the solution. Experimental data for molar conductance, Λ, vs concentration of additive, C, and adjustable parameters, Λ^0 and K_{Diss2}, allow for theoretical modeling and prediction of ion size, which is directly related to the distance of closest ion approach, a from ***Eq. 34***.

Fuoss, in his later papers from 1957[41] defined this final term using slightly different nomenclature, as such:

$$-K_{Diss2} C \gamma_c^2 \Lambda^0 \qquad \textit{Eq.37}$$

From this he defined the fraction of ions that are associated into ion-pairs as (1-α) as:

$$(1-\alpha) = K_{Diss2} \alpha C \gamma_c^2 \Lambda^0 \qquad \textit{Eq.38}$$

However, ***Eq.36***, by design, is robust enough to be applicable in all solutions, both aqueous and non-aqueous, thus, it can be substantially simplified for nonpolar liquids with rather low ionic strength. Given nonpolar systems often exhibit very large Debye lengths due to large distances between ions, relaxation and electrophoretic effects along with long range ion interactions can be ignored giving the following, ***Onsager-Fuoss Conductivity Theory for Non-Polar Liquids[29]***:

$$\Lambda = \Lambda^0 - \Lambda^0 C K_{Diss2} \qquad \textit{Eq. 39}$$

While the *Onsager-Fuoss Conductivity Theory for Non-Polar Liquids* was a significant contribution to the field of non-polar electrochemistry, it remains limited by restrictions on ion concentration and can only be used to model conductivity in systems in which that concentration is low. Above a critical concentration[42]:

$$C > C_{critical} = \frac{1}{K_{Diss2}} \qquad \textit{Eq. 40}$$

The calculated conductivity is negative, which is fundamentally impossible. Additionally, the more the second dissociation reaction favors solvated ions (i.e. higher values of $K_{Diss,2}$), the lower this critical concentration becomes. Therefore, a theory for non-polar systems that overcomes this critical concentration limit and allows for the modeling of non-aqueous solutions across a broad range of ionic concentrations is imperative. It is this gap in understanding that the "*Ion-Pair Conductivity Model*" aims to fulfill.

1.2.2 THE DISPROPORTIONATION MODEL

The Disproportionation Model attributes ionization of nonpolar liquids to interactions of inverse micelles[43,44]. It postulates that when the concentration of surfactant exceeds the "critical micelle concentration", the surfactant molecules readily rearrange into spherical molecules, called inverse micelles, providing a more energetically favorable configuration for ionization to transpire in nonpolar media.

Nelson and Pink among the first to study charged inverse micelles in 1954[45], focusing predominantly on neutral micelles prior to that point. Additionally, Matton and Mathews also published work on charged inverse micelles around that time in 1949[46]. Their work focused on inverse micelles formed from the surfactant Aerosol OT (AOT), which would in turn behave as a charge carrier.

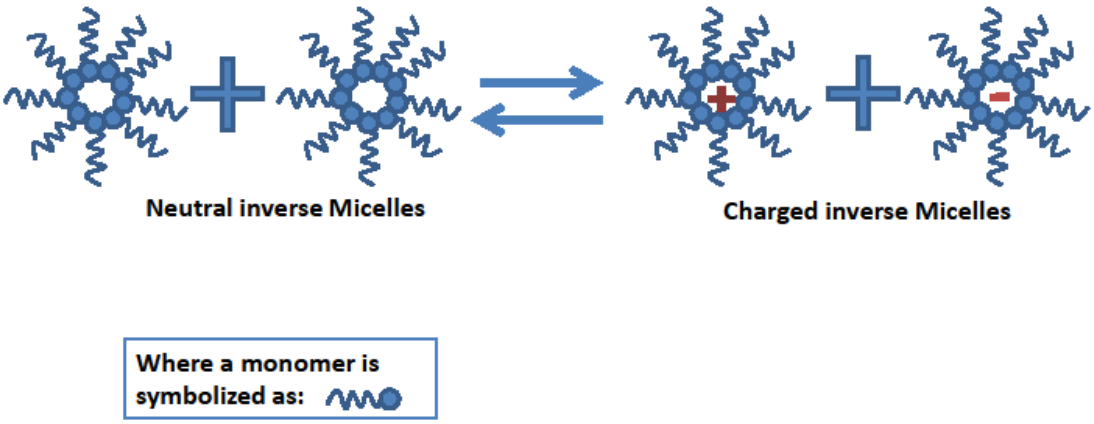

Figure 2. *Exchange of charge between inverse micelles, as described by the Disproportionation Model. Legend describes symbol for monomer. Ion exchange is the result of collision between inverse micelles, resulting in them becoming charged.*

As depicted in ***Figure 2,*** these inverse micelles then collide, due to Brownian motion as a result of localized temperature variations within the media, and exchange charges during collision resulting in the formation of an anion and a cation. The reaction, and corresponding equilibrium constant, $\boldsymbol{M_{Disp}}$, for this charge exchange are as follows:

$$\boldsymbol{A^+ + B^- \leftrightarrow A + B}$$

$$\boldsymbol{M_{Disp} = \frac{[A][B]}{[A^+][B^-]}}$$

Where $\boldsymbol{M_{Disp}}$ is the equilibrium constant and the parameters in brackets correspond to the concentrations of the respective ions [$\boldsymbol{A^+}$], [$\boldsymbol{B^-}$] or neutral inverse micelles [$\boldsymbol{A}$] [$\boldsymbol{B}$]. Notably, in the case of *The Disproportionation Model*, the reaction is second order in both directions, while in *The Dissociation Model*, it is first order in the forward direction and second order in the reverse direction.

If we apply a dissociation constant **α,** then $\boldsymbol{M_{Disp}}$ can be re-written as:

$$\boldsymbol{M_{Disp} = \frac{(1-\alpha)^2}{\alpha^2}} \qquad \textbf{\textit{Eq. 41}}$$

If we assume that all of the surfactant monomers with a concentration $\boldsymbol{c_s}$ are arranged into inverse micelles, with $\boldsymbol{m}$ monomers in each micelle, then the total amount of micelles can be written as $\boldsymbol{c_s/m}$ and we can solve for ionic strength, $\boldsymbol{J}$, of such a system according to:

$$\boldsymbol{J = \frac{1}{1+\sqrt{M_{Disp}}}\frac{c_s}{m}} \qquad \textbf{\textit{Eq. 42}}$$

Eq. 42 implies that ionic strength, $\boldsymbol{J}$, and, accordingly, conductivity, are linear functions of concentration, while molar conductivity is independent of concentration, a notable departure from the assumptions made in *The Dissociation Model* described above.

This model has been popularized in recent years by Morrisson[6], Berg[4,5], and others[28,47] who've demonstrated its usefulness in describing electric phenomena in nonpolar liquids. However, upon closer examination, this model is plagued by a number of issues. This model is

dependent upon the presence of micelles for ionization. Ionization cannot occur below the critical micelle concentration (CMC) because there would be no micelles present in the solution for collision, exchange of charge and anion/cation formation rendering the solution unable to maintain a charge in a nonpolar system. Additionally, this model assumes that conductivity is a linear function of surfactant concentration, which does not always hold true[48].

Furthermore, *The Disproportionation Model* assumes that inverse micelle size is equal for both anions and cations. While this is possible, the physical shape of a typical surfactant molecule makes this unlikely. The polar head of a typical micelle has a dipole moment. This dipole moment will interact with the ion that the inverse micelle is surrounding differently, depending on the charge of that ion. Moreover, that ion-dipole interaction is not symmetrical. The interaction will either be attractive or repulsive, depending on the charge of the ion. Accordingly, the way that the surfactant molecules orient themselves around an ion will depend on the charge of that ion. Therefore, the assumption that ion size is the same regardless of the charge contained within the inverse micelle is not inherently valid. Such an effect has been described in aqueous systems by Verwey[49,50]. Water molecules, which serve as solvating agents in aqueous systems, will orient themselves in opposite directions for anions and cations. As a result, the size differs between anion and cation.

Lastly, *The Disproportionation Model* completely ignores the law of ion-pairing of inverse micelles, even in the case where micelle size is significantly less than half the *Bjerrum length* (**q**), with no theoretical justification or experimental validation. This study argues that ion-pairing cannot be simply removed from the model when measuring conductivity in nonpolar liquids, as their presence dramatically affects the overall conductivity of the system and serves as the catalyst for the exponential decrease in conductivity at low surfactant concentrations.

1.2.3 THE FLUCTUATION MODEL

There is one type of ion that does not form ion-pairs in nonpolar liquids even when ion size is very small: these ions are charged microemulsion droplets. A microemulsion is an energetically favorable scenario in which droplets form when water, oil, and surfactant are present, wherein the surfactant molecules sit at the interface between the water and oil to minimize free energy of the system. These droplets are thermodynamically stable, and form spontaneously. The focus of this model, known as "*The Fluctuation Model*", is on inverse microemulsions, in which droplets filled with water are spontaneously formed in a continuous oil phase with surfactant molecules present at the interface. These microemulsion droplets are typically very small in size, and thus behave similarly to charged ions, as they are able to carry and transport charge in a similar fashion. This theory based on ionization of microemulsions was developed by Eicke, Borkovec and Das-Gupta in 1989[51] and asserts that the microemulsion droplets serve as the charge carriers in nonpolar systems.

According to Eicke et al., the conductivity of a nonpolar system with charged microemulsion droplets is related to the mean value of the square of that charge, which is locally never zero even if the average across the entire system is zero. *The Fluctuation Model* assumes that microemulsion droplets are charged via collision and charge exchange, resulting in the following:

$$K_{me}^{fluct} = \frac{\varepsilon_m \varepsilon_0 kT}{2\pi\eta} \frac{\varphi}{r^3} \qquad \textbf{Eq. 43}$$

Where $\boldsymbol{\varepsilon_m}$ is relative permittivity, $\boldsymbol{\varepsilon_0}$ is permittivity in a vacuum, $\boldsymbol{\eta}$ is viscosity, $\boldsymbol{\phi}$ is volume fraction of water, and $\boldsymbol{r}$ is water droplet radius. This model, similarly to *The Disproportionation Model*, of which it was derived from, also ignores the law of ion-pairs. However, unlike *The Disproportionation Model*, this model's predictions of conductivity in

systems with microemulsions stabilized by ionic surfactants is in good agreement, experimentally, with the assumptions of its theory[52].

The *Fluctuation Model*, while confirmed experimentally, is only applicable to systems in which sufficient water is present in order for inverse microemulsions to form. For solutions in which these conditions are not met, such as those explored in this work, the *Fluctuation Model* is not appropriate, and instead a model such as the *Dissociation Model*, and the corresponding *Ion-Pair Conductivity Model*, are necessary.

1.3 ION-PAIR CONDUCTIVITY MODEL

The *Dissociation Model*, illustrated in ***Figure 1*** via the second dissociation reaction, K_{Diss2}, serves as the genesis for the *Ion-Pair Conductivity Model*. The key advantage of the *Dissociation Model* is that ionization occurs first, via the breakup of some neutral entities, molecules or ion-pairs, followed by solvation, resulting in steric stability of the ions in the nonpolar solution, which, if sufficient, will allow them to remain in the solution as ions, and contribute to the overall conductivity of the system.

The *Dissociation Model* asserts that an equilibrium ionic environment is the result of a balance between a first order reaction, the breakup of entities, e.g. free ions A^+ and B^-, and a second order reaction, the association of ions into neutral entities, e.g. ion-pairs A^+B^-, which is reflected as the following:

$$A^+ + B^- \leftrightarrow A^+B^-$$

With concentrations of the free ions and ion-pairs in solution determined by the *Mass Action Law* for ion-pairs, a first order reaction illustrating the balance between free ions and ion-pairs as the following:

$$M_{Diss} = \frac{[A^+B^-]}{[A^+][B^-]}$$

Where M_{Diss} is the equilibrium constant and the parameters in brackets correspond to the concentrations of the respective ions [A^+], [B^-] or ion-pairs [A^+B^-].

An expression for this equilibrium constant was derived by Fuoss in 1957[37] as:

$$M_F = \frac{4\pi N_A a^3}{3} EXP\left(\frac{z^+z^-e^2}{\varepsilon kTa}\right) \qquad \textit{Eq. 44}$$

Where T is temperature, k is Boltzmann's constant, e is electron charge, z^+ and z^- are valencies of the cation and anion, respectively, N_A is Avagardo's number, and a is the distance of closest approach for the ions.

In the case of the classical *Dissociation Model*, the added material is expected to dissociate, thus we introduce a dissociation constant, $\boldsymbol{\alpha}$, that relates to the concentration of cations, $\boldsymbol{A^+}$ and anions, $\boldsymbol{B^-}$, where the total concentration of ions, $\boldsymbol{C_i}$, derived from dissociation, equals ionic strength, $\boldsymbol{I}$:

$$\boldsymbol{I = [A^+] = [B^-] = \alpha C_i} \qquad \textbf{Eq. 45}$$

And for ion-pairs:

$$\boldsymbol{[A^+B^-] = (1-\alpha)C_i} \qquad \textbf{Eq. 46}$$

All of the ions in solution are either free ions or ion-pairs, with the dissociation constant $\boldsymbol{\alpha}$ dictating the ratio between the two.

If we incorporate ***Eq. 45*** and ***Eq. 46*** into mass action law, we get the following (which was similarly predicted in the work carried out by Bockris and Reddy in 1977[26]):

$$\boldsymbol{M_{Diss} = \frac{[AB]}{[A^+][B^-]} = \frac{(1-\alpha)C_i}{\alpha^2 C_i^2} = \frac{C_i - I}{I^2}} \qquad \textbf{Eq. 47}$$

$$\boldsymbol{I^2 M_{Diss} + I - C_i = 0} \qquad \textbf{Eq. 48}$$

The above equation can be re-written as a quadratic equation solving for $\boldsymbol{I}$:

$$\boldsymbol{I = \frac{\sqrt{1+4M_{Diss}C_i}-1}{2M_{Diss}}} \qquad \textbf{Eq. 49}$$

For simplicity, we assume that all ions are monovalent (i.e. $\boldsymbol{z^+}$ and $\boldsymbol{z^-}$ are equal to 1), allowing us to derive conductivity, $\boldsymbol{K}$, by multiplying the ionic strength, $\boldsymbol{I}$ from ***Eq. 49***, by electron charge $\boldsymbol{e}$, Faraday constant $\boldsymbol{F}$, and electron mobilities $\boldsymbol{\mu^+}$ and $\boldsymbol{\mu^-}$ to give:

$$\boldsymbol{K = (\mu^+ + \mu^-)eF\frac{\sqrt{1+4M_{Diss}C_i}-1}{2M_{Diss}}} \qquad \textbf{Eq. 50}$$

In order to expand upon ***Eq. 50*** to generate a new model for conductivity in nonpolar systems , the following assumptions are made:

Assumption #1: We assume that the non-aqueous liquid does not impact the structure of ions in solution, or the ability of the solvating agent to solvate said ions.

Assumption #2: The expanded *Onsager-Fuoss theory* outlined in ***Eq. 36*** implies that the dissociation reaction that causes ions to form in the nonpolar solution (additive+ non-aqueous liquid) is the same dissociation reaction that would occur in the pure additive alone. However, there will be fewer ions present in the nonpolar solution than in the pure additive alone, thus, we assume that the ratio between the total concentrations of ions in solution (additive+ non-aqueous liquid), C_i, is a function of the additive volume fraction, φ of the total concentration of ions in the pure additive, C_A, according to:

$$C_i = \varphi C_A \qquad \textit{Eq. 51}$$

Assumption #3: We assume that the distance of closest ion approach, ***a,*** is independent upon concentration of the additive in the solution. This allows for a single value for ***a*** to be used across the entire concentration spectra of non-polar media with added amphiphile.

Assumption #4: We assume that electrostatic interactions in nonpolar solutions are dictated by the overall relative permittivity of the system, where localized relative permittivity is neglected.

Assumption #5: We assume, for simplicity that all ions are monovalent.

Assumption #6: We assume that Stoke's equation can be used to describe the mobility of ions in these binary nonpolar solutions:

$$\mu^+ + \mu^- = \frac{1}{6\pi\eta}\left(\frac{1}{a_i^+} + \frac{1}{a_i^-}\right) \qquad \textit{Eq. 52}$$

Where η is dynamic viscosity, and a_i^+ and a_i^- are hydrodynamic radii of the cation and anion, respectively. Unfortunately, there is not enough information derived from the conductivity curves to determine the size of the oppositely charged ions, a_i^+ and a_i^- , individually. Instead we simplify the equation by introducing the effective hydrodynamic ion size, d_h, assuming it to be equal to the real ion diameter given that the cation and anion are also the same size:

$$d_h = \frac{4a_i^+ a_i^-}{a_i^+ + a_i^-} \qquad \textit{Eq. 53}$$

And, ion mobilities are redefined as: $$\boldsymbol{\mu^{+} + \mu^{-} = \frac{2}{3\pi\eta d_h}}$$ ***Eq. 54***

Lastly, we redefine *Bjerrum length*, considering additive volume fraction, $\boldsymbol{\varphi}$, as:

$$\boldsymbol{\lambda = \frac{e^2}{\varepsilon(\varphi)kT}}$$ ***Eq. 55***

If we insert ***Eq. 44***, ***51***, and ***54*** into ***Eq. 50***, and according to ***Assumption #3***, assume that all ions are monovalent, we have following equation for conductivity, $\boldsymbol{K}$:

$$\boldsymbol{K = \frac{eF}{4\pi^2\eta N_A a^3 d_h}\left(\sqrt{1 + \frac{16}{3}\pi N_A a^3 \varphi C_A e^{\lambda/a}} - 1\right) EXP\left(\frac{-\lambda}{a}\right)}$$ ***Eq. 56***

Next, an assumption based on the *Onsager-Fouss theory* with regard to parameter $\boldsymbol{a}$, distance of closest ion approach, and hydrodynamic radius, $\boldsymbol{d_h}$ must be made where:

$$\boldsymbol{d_h = a}$$ ***Eq. 57***

Of note, some uncertainty regarding the validity of ***Eq. 39*** exists, and thus, in our earlier published work, in order to differentiate between the two, we assume $\boldsymbol{a}$ to be proportional to, rather than equal to, $\boldsymbol{d_h}$, according to an arbitrary multiplier, $\boldsymbol{R}$: $$\boldsymbol{d_h = Ra}$$ ***Eq. 58***

However, in our opinion ***Eq. 57***, while not perfect, is the best approach, to date, to accurately model and predict conductivity in nonpolar solutions. By assuming such, we're only left with two adjustable parameters: $\boldsymbol{a}$ and $\boldsymbol{C_A}$, which are both solvable using the conductivity curve data.

Yielding the final mathematical representation of the ***Ion-pair Conductivity Model***[42]:

$$\boldsymbol{K = \frac{eF}{4\pi^2\eta N_A a^4}\left(\sqrt{1 + \frac{16}{3}\pi N_A a^3 \varphi C_A e^{\lambda/a}} - 1\right) EXP\left(\frac{-\lambda}{a}\right)}$$ ***Eq. 59***

1.3.1 ION-PAIR CONDUCTIVITY MODEL VS. THE FLUCTUATION MODEL

Given the *Fluctuation Model's* ability to ignore ion-pairs, but remain experimentally sound questions the need to consider ion-pairs at all when modeling conductivity in non-polar liquids. In their 2015 paper, Dukhin and Parlia[29] explored the work of Eicke et al., and Morrisson[6], Berg[4,5], and others[28,47] as to whether or not the ignoring of ion-pairs is justified in the *Fluctuation* and *Disproportionation Models*. As discussed earlier, Bjerrum theory dictates that when the ratio of ion particle size to *Bjerrum length* is small enough ion-pairs form within the solution. In polar liquids that distance is quite short due to the abundance of polar molecules which can shield the charge between ions; in water it is about 0.7 nm. However, that distance in nonpolar liquids is much larger due to the inability of the nonpolar continuous phase to shield any of the electrostatic attraction between oppositely charged ions.

During their 2015 work Dukhin and Parlia discovered that how the solution relevant *Bjerrum length* (which is directly related to relative permittivity) is measured is of paramount importance to *The Fluctuation Model's* success. According to Dukhin and Parlia the *Fluctuation Model* is able to ignore ion-pairs because ion-pairs simply do not exist, because the relevant *Bjerrum length* is not the *Bjerrum length* in nonpolar media, but rather the *Bjerrum length* in water. Although micelle size is quite small and *Bjerrum length* is quite large in nonpolar systems, *The Fluctuation Model* remains successful in predicting conductivity in such systems due to the makeup of the microemulsion droplet itself, which at its core is made up of water, not oil, allowing the ion present inside of the droplet to be solvated by water and thus, significantly shortening its *Bjerrum length* of relevance (roughly 40x shorter, depending on the oil phase). While the *Bjerrum length* of the continuous phase remains quite large in the solution, implying favorable circumstances for ion-pair formation, this *Bjerrum length* is not the *Bjerrum length* experienced by the ion itself since the ion is contained within a microemulsion

droplet, the center of which is water, in this model. Therefore, the environment experienced by that ion is actually that of the surrounding water; an aqueous solution contained within the microemulsion droplet. Accordingly, the surrounding water is able to adequately shield the electrostatic forces it exerts on (and has exerted upon it by) other ions. Therefore, even if the microemulsion droplet is very small, the ratio of droplet size to *Bjerrum length* remains large enough that ion-pairs do not form within the solution, allowing *The Fluctuation Model* to ignore ion-pairs, but maintain its experimental validity.

Additionally, because of the aqueous environment inside the microemulsion core, the electrostatic interactions between the ion and the surfactant molecules that surround it is suppressed. Therefore, there is justification for assuming that cations and anions have the same size: the ion-dipole interaction is limited and therefore its effects on ion size will be minimized. And in the case of ionic surfactants, this phenomenon can serve to facilitate dissociation of the ionic surfactant itself. The dissociated ionic surfactant molecules carry charge, but do so in the solvating layer where they are located. The counter-ions would be located inside of the water core, where they migrate. However, interaction between them would be limited due to the very short Bjerrum length. This hinders the possibility of the dissociated surfactant and counter ion from recombining into a neutral pair. Hence, the dissociation of the surfactant molecule, and its remaining as a dissociated charged molecule, is helped by the ionic nature of the water core.

1.3.2 ION-PAIR CONDUCTIVITY MODEL VS. THE DISPROPORTIONATION MODEL

While the above is true for *The Fluctuation Model*, the same cannot be said for *The Disproportionation Model*. *The Disproportionation Model*, while derived from *The Fluctuation Model*, is instead modeled around the principle that ion solvation occurs as the water content approaches zero in a nonpolar system, allowing for the inverse microemulsion to become an inverse micelle. Since there is no water present in this model, the *Bjerrum length* of relevance remains dependent upon the properties of the oil phase. Therefore, the ratio of inverse micelle size to *Bjerrum length* dictates that ion-pair formation will likely occur within the solution and consequently cannot be ignored, which is likely why *The Disproportionation Model* tends to deviate from the law of linear dependence of conductivity to concentration at low concentrations of surfactant (i.e. the concentration region where ion-pairs are present).

Both models suggest that surfactant molecules form structured entities (inverse micelles in the case of *The Disproportionation Model* and microemulsion droplets in the case of *The Fluctuation Model*), and ionization occurs as a result of collisions between these entities when charge exchange occurs. However, the environment within the surfactant molecules is very different within the two models. In the case of *The Fluctuation Model*, the microemulsion droplet contains an inner core that consists of water, while no such scenario exists at the inner core of inverse micelles; an ion inside an inverse micelle is not shielded by an aqueous environment in *The Disproportionation Model*. Therefore, the *Bjerrum length* experienced by that ion is much larger, because the relative permittivity of the surrounding oil is much lower (around 40x lower) than that of a typical aqueous system. And so, while the *Bjerrum length* experienced by an ion inside a microemulsion droplet was around 0.7 nm, the *Bjerrum length* inside of an inverse micelle is closer to 28 nm (corresponding to a relative permittivity of the

nonpolar phase equal to 2). Thus, the ability to assume that ion pairs are not present in solution, and therefore can be omitted entirely from this theoretical model, is no longer valid.

Even if the environment experienced by the ion in an inverse micelle is considered to be not that of the surrounding liquid, but that of the surrounding surfactant molecules which serve to solvate the ion, ion-pairs must still be considered. The relative permittivity of typical amphiphilic molecules (surfactants in particular), as will be demonstrated throughout this study, are much closer to that of a nonpolar liquid than that of water.

1.4 CRITICISMS OF THE ION-PAIR CONDUCTIVITY MODEL

1.4.1 MASS ACTION LAW FOR THE DISSOCIATION MODEL

A 1993 paper by Morrison et al.[6] criticized *The Dissociation Model* and its application for conductivity in nonpolar systems, stating: *"… what is surprising is that conductivity is linear over quite a range of concentration… for weak electrolytes, the degree to which dissociation varies with concentration and conductivity should vary (at low concentration) with the square root of concentration…"*

The Dissociation Model and corresponding *Ion-Pair Conductivity Model* do both predict a non-linear dependence of conductivity on concentration at low concentration of additive when ion-pairs are present, while in practice both models report a linear dependence between concentration and conductivity at low concentrations (see paper *Bombard et al*[48]). However, this deviation between theoretical approach and experimental result is not due to a failure of either model's legitimacy, but rather, the result of increased viscosity causing decreased ion mobility and limiting conductivity. Certain amphiphiles, particularly nonionic surfactants, have viscosities that are orders of magnitude larger than that of the nonpolar liquid in which they reside. As a result, the effects of viscosity on the conductivity of the system cannot be ignored.

In order to consider the effect viscosity has on conductivity it is best to investigate conductivity multiplied by viscosity versus concentration, which will be examined through validation of the *Ion-Pair Conductivity Model* herein. *The Walden Rule* states that conductivity multiplied by viscosity is a linear function of concentration when ion-pairs are not present (i.e. $K\eta = \alpha C$). When mixtures of nonpolar media with viscous non-ionic surfactant are explored using the Walden Rule (see ***Discussion*** Section) we found that the relationship for such systems is in fact exponential. In fact, we found that, for these systems, the relationship is not only exponential at very low concentrations of added amphiphile, but rather across the entire concentration spectra, implying that ion-pairs are present even in pure non-ionic surfactant (this phenomenon is explored in detail in ***Section 3.11***). As is such, the *Ion-Pair Conductivity Model* is still an accurate representation for the systems described by Morrison.

1.4.2 ION PAIRS AS POINT CHARGES

The *Ion-Pair Conductivity Model* places a great deal of emphasis on the importance of ion-pair formation and the impact ion-pairs have on the overall conductivity in nonpolar systems. Ion-pairs form when the electrostatic attractive forces within the nonpolar media are sufficient to result in the reassociation of free ions into a neutral entity.

So far, only the importance of ion-pair formation in influencing overall conductivity of the nonpolar system has been discussed. Additionally, parameters such as shape and structure of the ion-pairs need to be considered.

In 2002, Kosuke Izutsu[30] published his textbook on *Electrochemistry in Nonaqueous Solutions* wherein he schematically illustrated and described three different types of ion-pairs that may form in nonpolar media depending on the strength of ion-solvent interactions:

1. Solvent-separated ion-pair
2. Solvent-shared ion-pair
3. Contact ion-pair

After exploring the three types of ion-pair formation structures, it is clear, particularly in the case of the solvent-separated ion-pair, that a dipole moment exists within the core of the structure. Such a dipole moment could potentially impact the movement (i.e. mobility) of other ions or ion-pairs and the relative permittivity of the system[53].

Consideration of the ion-pair structure, which is influenced by various ion-solvent interaction factors, only further complicates the treatment of ion-association. Given that the mechanisms which govern the formation of specific ion-pair structures fall outside the scope of this work, we chose, for simplicity purposes, to consider ion-pairs as neutral single point elements with respect to conductivity. Effects caused by the presence of dipole moments in ion-pairs, such as electrophoretic effects described by Debye, Huckel, and Onsager for aqueous systems (***Eqs. 21*** and ***23***) are ignored.

While the exact nature by which ion-pair structural formation occurs within nonpolar media is not specifically analyzed herein, their importance should not be overlooked when studying and modeling nonpolar systems in which ion-pair formation plays an integral role. Therefore, the nature of the dipole moment within an ion-pair and other factors influencing the ion-pairs structural formation serves as a source of future work.

1.4.3 SHORTCOMING OF DYNAMIC LIGHTS SCATTERING FOR ION SIZE

Within the field of nonpolar electrochemistry, Dynamic Light Scattering (DLS) is a commonly employed tool for studying inverse micelle size[54]. However, the sizes of neutral inverse micelles and charged inverse micelles (or solvated ions) are not necessarily the same. The presence of an ion within the inner core of the structure will impact the orientation of solvating amphiphile molecules due to electrostatic interactions between the polar headgroups of the amphiphile molecules and the ion. This change in orientation can potentially affect the size of these structures when an ion is present.

Additionally, conductivity in nonpolar systems is very low. This is due to very low concentration of ions present in such systems. The concentration of solvated ions (i.e. charged inverse micelles) is much lower than the concentration of neutral inverse micelles. Therefore, ion size measured by DLS would be dominated by the size of neutral inverse micelles, overshadowing solvated ion size due to this difference in concentration between structures. Because of this, DLS was not considered a viable means of determining ion size in nonpolar systems, and for that reason was not included as a measurement technique in this work.

1.4.4 ACID-BASE REACTIONS

When discussing nonpolar electrochemistry, it has become common to describe ionization in nonpolar media within the framework of acid-base reactions[6]. This is typically done within the context of the *Disproportionation* and *Fluctuation Models,* in which ionization is the result of charge exchange due to the collision of inverse micelles (in the case of the *Disproportionation Model*) or inverse microemulsion droplets (in the case of the *Fluctuation Model*). For inverse microemulsion droplets described by the *Fluctuation Model*, the water inside the core can serve as both an acid and a base, with a proton being exchanged between inverse microemulsion droplets according to this donor-acceptor model. The *Disproportionation Model* describes the same mechanism for ionization in nonpolar media, albeit between inverse micelles instead of inverse microemulsion droplets. Therefore, describing this mechanism via acid-base reactions is equally valid, although the species participating as proton donor and acceptor are more ambiguous as water content goes to zero.

In the case of the *Dissociation Model*, however, the mechanism of ionization is different. Ionization occurs due to dissociation followed by solvation. These ions can be the result of dissociation of the added amphiphile, which is then solvated by additional amphiphile molecules. However, conductivity is so low in nonpolar systems that trace contamination can also serve as a source of ions in nonpolar media, whether that contamination is from water or another contaminant. Accordingly, acid-base reactions are not as well suited for describing ionization in nonpolar media within the context of the *Dissociation Model* (which serves as the basis of the work contained here within), when compared to the *Disproportionation Model* and *Fluctuation Model.* It is for this reason that ionization is not described within the framework of acid-base reactions in this work.

In the case of alcohols as added amphiphile, the auto-dissociation reaction described by Bockris & Reddy[26] can be described as an acid-base reaction, with alcohol serving as both acid and base in the reaction. However, water contamination will be demonstrated to be a potential source of ions in these systems, limiting the usefulness of representing ionization this way.

II. METHODS AND MATERIALS

2.1 MATERIALS

2.1.1 ALCOHOLS

For measurements in which alcohols were used as the amphiphile/semi-polar component, high purity primary straight-chain alcohols were used. The alcohols used were methanol, ethanol, 1-propanol, 1-butanol, 1-pentanol, 1-hexanol, 1-heptanol, and 1-octanol. Straight-chain alcohols were chosen to minimize additional effects caused by branching, or similar scenarios where the molecule has multiple "hydrophobic sections." Primary straight-chain alcohol isomers are closest in shape to surfactant molecules, which typically have rigidly defined hydrophilic and hydrophobic (polar and nonpolar, respectively) sections. In the case of the alcohol molecule, the hydroxyl group would by analogous to the polar head of a surfactant, and the straight chain of methyl groups would be analogous to the hydrophobic tail of the surfactant. All alcohols were purchased from Sigma Aldrich, with purity > 99% in all cases except for Hexanol which had a purity of only 95% due to availability[55,56]. Anhydrous alcohols were used in all cases to minimize water contamination.

2.1.2 NON-POLAR LIQUIDS

Within the framework of the *Ion-Pair Conductivity Model (IPCM)*, relative permittivity is the driving factor which affects Bjerrum length, which impacts the ability of ion-pairs to form. As is the case, relative permittivity is the parameter by which, within the context of this research, a material is classified as "nonpolar." For the purpose of this work, nonpolar liquids are classified by their low relative permittivities, typically below 5. Heptane, hexane, and toluene were used as the nonpolar liquids in the binary mixtures studied during this research,

all of which have a relative permittivity below 3. The straight-chain isomers of heptane and hexane were used, to avoid any additional effects cause by branched structuring. These liquids were chosen because they are miscible/compatible with all (or, at least, most) of the amphiphilic materials used. Anhydrous versions of all non-polar liquids were purchased from Sigma Aldrich, with purity >99% in all cases.

2.1.3 SURFACTANTS

Two different series of surfactants were used in these experiments. The first of which was the Xiameter® series of surfactants manufactured by Dow Corning[57]. Surfactants OFX-5098 and OFX-0400 were chosen for these experiments[58,59]. Both materials are polyalkylene oxide-modified polydimethylsiloxanes. They are also referred to as silicone-ethylene oxide copolymers. The Xiameter series of surfactants was chosen because of its high purity, and that it remains liquid at 100% purity. OFX-5098 and OFX-0400 were chosen specifically because they have similar viscosities and endcaps (OAc). Their differences arise in differing Hydrophile-Lipophile Balance (HLB) numbers. This allowed for studying the effect of HLB number on conductivity, dielectric permittivity, etc.

The second series of surfactants used were from the SPAN series Croda. SPAN 20 and SPAN 80 were used (described in more detail in the Discussion).[60,61] These surfactants are referred to as Sorbitans, and tend to be more common in typical laboratory application than the Xiameter series.

2.1.4 WATER

For experiments in which water was added to the solutions, deionized water was used. The trace water measured using Karl-Fischer titration experiments was not added intentionally to the liquids measured, but was rather contamination presumably from the manufacturing process or introduced after the bottles had been opened initially.

2.1.5 MOLECULAR SIEVE BEADS

In scenarios where it was desirable to remove as much trace water as possible from a specific solution, 3A 4x8 molecular sieve beads were used. These beads were purchased from Delta Enterprises, Inc. These beads have 3 Angstrom pores which are small enough that water can enter the bead, whereas larger molecules such as toluene (or the other nonpolar liquids used in these studies) cannot. Accordingly it is an effective means of removing water contamination from a nonpolar liquid[62].

2.2 METHODS

2.2.1 NON-POLAR CONDUCTIVITY

The instrument used for measuring the conductivity in these systems was the DT-700 Non-Aqueous Conductivity Probe by Dispersion Technology. This instrument is capable of measuring conductivities as low as 1E-12 S/m[63], which is necessary when measuring samples where the continuous phase is a non-polar medium.

The manufacturer specifies the range of conductivities this instrument can measure as 1E-11 to 1E-4 S/m, with a single-measurement precision of ±(1%+10E-11 S/m) over the complete range. The precision can be improved by taking multiple measurements at a single data point. For the purpose of this research, many measurements were taken at each data point (typically exceeding 20 measurements) and the results were then averaged to yield the final result.

The DT-700 probe consists of two concentric coaxial cylindrical electrodes: an inner one and an outer one, along with a guard electrode which serves to prevent leakage. Measurements are made by dipping the probe into the sample such that the holes of the outer electrode are covered, and the area between the electrodes is filled with liquid. After measurements are made, the outer electrode is removed to allow for cleaning.

The DT-700 employs a log-amplifier to measure current. Improvements have been made over initial versions of the instrument, such that there is no "range selection" required in the present model. Simultaneously a voltage waveform is applied to the outer electrode while the log-amplifier is captured by the second channel of the Analog-to-Digital converter. The log-amp values are then used to calculate the desired waveform through an inverse log calculation.

Using this approach allows for measurements to be made over many decades of current, hence the instruments vast range of measureable conductivities.

The amplitude and phase of both the voltage and current waveforms are calculated using first order Fourier coefficients. The Complex Conductance of the cell contents is then computed from the current voltage ratio. Finally, the specific conductivity of the sample material is determined by computing the real part of the complex conductance and then multiplying it by a cell constant, which is determined via instrument calibration.

Figure 3 *- Setup for Non-Aqueous Conductivity Measurements: Mixing was provided by a magnetic stir-bar to ensure homogeneity of the solution. A narrow vial was used to hold sample, allowing part of the Conductivity probe to serve as a cap to the sample chamber, preventing evaporation or effects caused by vapor pressure.*

2.2.2 RELATIVE PERMITTIVITY

Relative Permittivity measurements were made using a Brookhaven Instruments Corporation BI-870 Dielectric Constant Meter[64]. The probe component of the instrument is comprised of two cylindrical concentric electrodes. A low distortion 10 KHz sine wave is applied to the outer electrode of the probe, and the response from the inner electrode is measured and used to determine relative permittivity . The amplitude of the sine wave is approximately 7 volts for low dielectric fluids (i.e. fluids with a relative permittivity below 20). However, the instrument is capable of measuring relative permittivities from 2 – 200, by adjusting the voltage of the applied sine wave. An absolute accuracy of 2% has been determined for this instrument.

2.2.3 VISCOSITY

Viscosity measurements were performed using Cannon-Fenske Viscometers. These viscometers are very simple tools which allow for determining the viscosity of a homogeneous fluid by measuring its flow rate through a narrow section of glass tubing. The viscometers are given difference "sizes" corresponding to the range of viscosities they can measure. The viscometer is loaded with fluid, and the time it takes to travel down the tube is recorded. A cell constant, unique for each sized viscometer, is then multiplied by the recorded time to determine the viscosity of the fluid. In order to improve the reliability of the data, ensure reproducibility, and establish error bars with regards to variation, multiple measurement were made for each fluid[65].

2.2.4 ACOUSTIC SPECTROMETRY

Acoustic spectrometry was used in examining the materials in this study in order to study particle size. A Dispersion Technology DT-1202 Acoustic & ElectroAcoustic spectrometer was used for these experiments[66]. The DT-1202 has a sample chamber, into which the sample is loaded, situated between two piezocrystal transducers which face one another – a receiving and a transmitting transducer. The receiving transducer is attached to a stepping motor, which allows for the distance between the two transducers to be controlled.

An electric signal is generated via the electronics of the DT-1202, which is then sent to the transmitting transducer which converts it to a sound pulse. That sound pulse is then propagated through the sample, where it is attenuated (i.e. dampened). That attenuated signal is captured by the receiving transducer, where it is converted back to an electric signal and sent back the electronics where it is compared against the initial inputted transmitted signal. These sound pulses are sent at a multiple frequencies in the MHz range, from 3 – 100 MHz. Also, the

distance between the two transducers is varied, in multiple steps from <1mm up to 20 mm. These many data points (typically at 18 frequencies and 21 gaps, yielding 378 data points) are converted into an attenuation curve, in which normalized attenuation (attenuation divided by frequency) is plotted against frequency.

The raw data yielded from these measurements are attenuation (versus frequency) and sound speed (at 10 MHz). From this raw data the following information can be calculated:

- From Attenuation
    - Longitudinal rheology
        - Longitudinal viscosity versus frequency
        - A Newtonian test to determine if the material is Newtonian or non-Newtonian under longitudinal stresses on the megahertz scale, based on whether or not the viscosity is dependent on frequency
        - Bulk viscosity for Newtonian liquids, and an estimation for non-Newtonian liquids which can be used to measure the oscillational and rotational degrees of freedom in non-newtonian systems
        - Loss modulus G''
    - Particle Size distribution
        - Particle size distribution with a lower limit of 5 nm and an upper limit of over 1 micron.
- From Sound Speed
    - Elastic modulus G'
    - Isothermal compressibility β

This attenuation spectra is useful for studying a material in 2 ways, depending on the scale at which the sample is being examined. From a macroscopic level, at which the sample is

considered a homogenous fluid, rheological properties can be explored. Sound speed (also measured) is related to compressibility of a fluid, and attenuation is related to storage modulus. Accordingly, using this instrument one can determine if a sample is Newtonian or Non-Newtonian under the stress of a MHz frequency longitudinal stress.

Alternatively, if the sample is examined from the standpoint that it is a heterogeneous fluid, then particle size can be explored. In the case of the samples in this research, the most common structures would most likely be inverse emulsions of amphiphile in non-polar liquid, or emulsions of nonpolar liquid in amphiphile, depending on the concentration. The instrument applies relevant theory, in which intrinsic properties of the materials are inputted and particle size can be calculated from the measured attenuation curve[67].

2.2.5 KARL-FISCHER TITRATION

Karl Fischer titration experiments were performed in order to determine the amount of water contaminant in each material used in these experiments. An 870 Karl-Fischer Titrino Plus, manufactured by Metrohm, was used[68]. The instrument was run in KFT Ipol mode, which follows the Karl Fischer Titration method with adjustable polarization current, determining the amount of water contamination on a volumetric basis. The procedure is based on the following reaction:

$$ROH + SO_2 + R'N \rightarrow [R'NH]SO_3R + H_2O + I_2 + 2R'N \rightarrow 2[R'NH]I + [R'NH]SO_4R$$

Where ROH signifies an acid, R'N is a base, [R'NH]SO_3R is sulfonite salt, 2[R'NH]I is hydroiodic acid salt, and [R'NH]SO_4R is alkylsulfate salt. In the above reaction, water (H_2O) and iodine (I_2) are consumed in a 1:1 ratio. Accordingly, the Metrohm 870 Karl-Fischer Titrino Plus works by titrating iodine into the system, and then using an indicator electrode to detect when excess iodine is present. The point at which excess iodine is present indicates the point in which all of

the water initially present in the system has been consumed. Thus, by measuring the amount of iodine needed to reach this point, the instrument can determine the amount of water that was present in the system to begin with.

III. RESULTS AND DISCUSSION

3.1 ALCOHOL AND TOLUENE SOLUTIONS

The first group of nonpolar systems examined consisted of eight alcohol-nonpolar liquid (toluene) solutions. The eight straight chain alcohols, with a carbon chain of increasing length, from methanol to octanol, were chosen specifically due to their distinctive structural isomers, where the effects of branching, which could impact parameters such as HLB number, can be ignored allowing the effects that increased carbon chain length may have on the conductivity, dielectric permittivity, etc. of these mixtures to be exclusively studied. This class of alcohols are often referred to as amphiphiles because they contain both a hydrophilic polar component (hydroxyl group), and a hydrophobic nonpolar component (carbon chain of varying length depending on alcohol). Toluene was chosen as the nonpolar liquid because it is miscible with all eight of the alcohols being investigated[42].

3.1.1 MATERIALS AND METHODS

The eight alcohol-toluene solutions were prepared according to one of two approaches. First, for mixtures with a higher alcohol content (from 100 wt. % pure alcohol down to 40 wt. %), toluene was added to the pure alcohol to dilute the solution and measurements were taken at specific setpoints during the dilution process. This approach is referred to as the "path of reducing alcohol content." Second, for mixtures with lower alcohol content (from 0 wt. % alcohol up to 40 wt. %), alcohol was added to the pure toluene to concentrate the solution and measurements were taken at specific setpoints during the concentration process. This approach is referred to as the "path of increasing alcohol content."

The eight solutions were prepared by weight, at room temperature (~ 25°C), to allow for easier preparation, with a total solution weight of 20 grams, which was maintained throughout formulation by re-calculating how much original material should be kept and how

much additional liquid (toluene in the case of the "path of reducing alcohol content," and alcohol in the case of the "path of increasing alcohol content") should be added prior to each dilution or concentration step. An average of twenty alcohol to toluene concentration measurements were taken, across the entire concentration spectra from pure alcohol to pure toluene, for all eight of the alcohol-toluene solutions analyzed. Each solutions alcohol to toluene concentration ratio overlapped at 40 wt. %, meaning the data, regardless of the solutions preparation path, is reproducible at 40 wt. %, which served as a meaningful check point to confirm solution formulation accuracy throughout the preparation process. To further ensure reproducibility of the data, the entire experiment was repeated multiple times.

A setup utilizing a narrow vial as the sample chamber for measurement prevented evaporation of mixture components, allowing for vapor pressure, and differences in vapor pressure between material, to be ignored (see ***Figure 3***).

3.1.2 RESULTS

Conductivity and relative permittivity across the full range of possible concentrations of alcohol and nonpolar liquid, from pure alcohol to pure toluene, were analyzed.

Table 2 and ***Table 3*** provide each liquids molecular weight, viscosity, density, and relative permittivity, and where available, each liquids literature value of conductivity as well.

Figure 4 illustrates the relationship between relative permittivity and alcohol concentration of the solution and ***Figure 5*** shows the relationship between conductivity and alcohol concentration of the solution for all eight alcohol-toluene samples examined. ***Figures 6a*** and ***6b*** expand the range of low concentration of added alcohol in ***Figure 5.*** ***Figure 7*** presents the relationship between conductivity and viscosity.

Material	Formula	Molecular Weight	Viscosity (at 20°C) [Pa s][69]	Density (at 20°C) [g/cm^3][69]
methanol	CH_3OH	32.04	0.00055	0.792
ethanol	C_2H_5OH	46.08	0.00109	0.789
propanol	C_3H_7OH	60.14	0.00195	0.803
butanol	C_4H_9OH	74.12	0.00253	0.810
pentanol	$C_5H_{11}OH$	88.15	0.00347	0.811
hexanol	$C_6H_{13}OH$	102.17	0.00459	0.814
heptanol	$C_7H_{15}OH$	116	0.00597	0.819
octanol	$C_8H_{17}OH$	130.23	0.00759	0.824
toluene	C_7H_8	92.14	0.00059[70]	0.867[70]

***Table 2**: Properties of Alcohols and Toluene*

	Relative Permittivity		K exp [10^{-6} S/m]	K lit[72] [10^{-6} S/m]
	ε exp	ε lit[71]		
methanol	33.2	32.6	245	120
ethanol	24.1	24.3	78	55.4
propanol	19.6	20.1	42.5	38.5
butanol	17.3	17.1	7.3	3.6
pentanol	14.7	13.9	6.4	4.1
hexanol	12.6	13.3	7.79	
heptanol	11.3	12.1	2.43	
octanol	9.4	10.3	1.53	
toluene	2.37	2.38	<0.000001	

***Table 3**: Macroscopic Properties of Alcohols and Toluene, from known literature.*

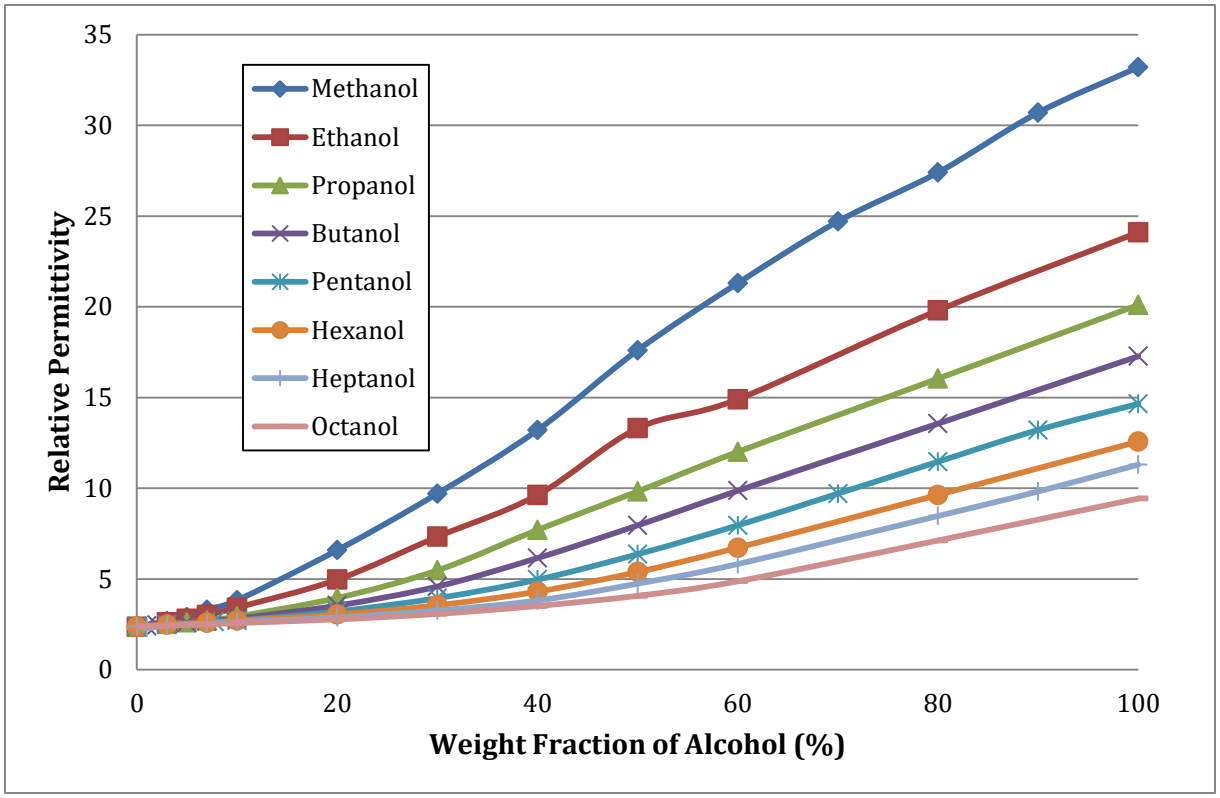

Figure 4. *Relative Permittivity versus Concentration of Alcohol for Alcohol-Nonpolar Liquid Solutions. Nonpolar liquid is Toluene for all solutions. Legend Denotes Alcohol used as Amphiphile. Linear Scale*

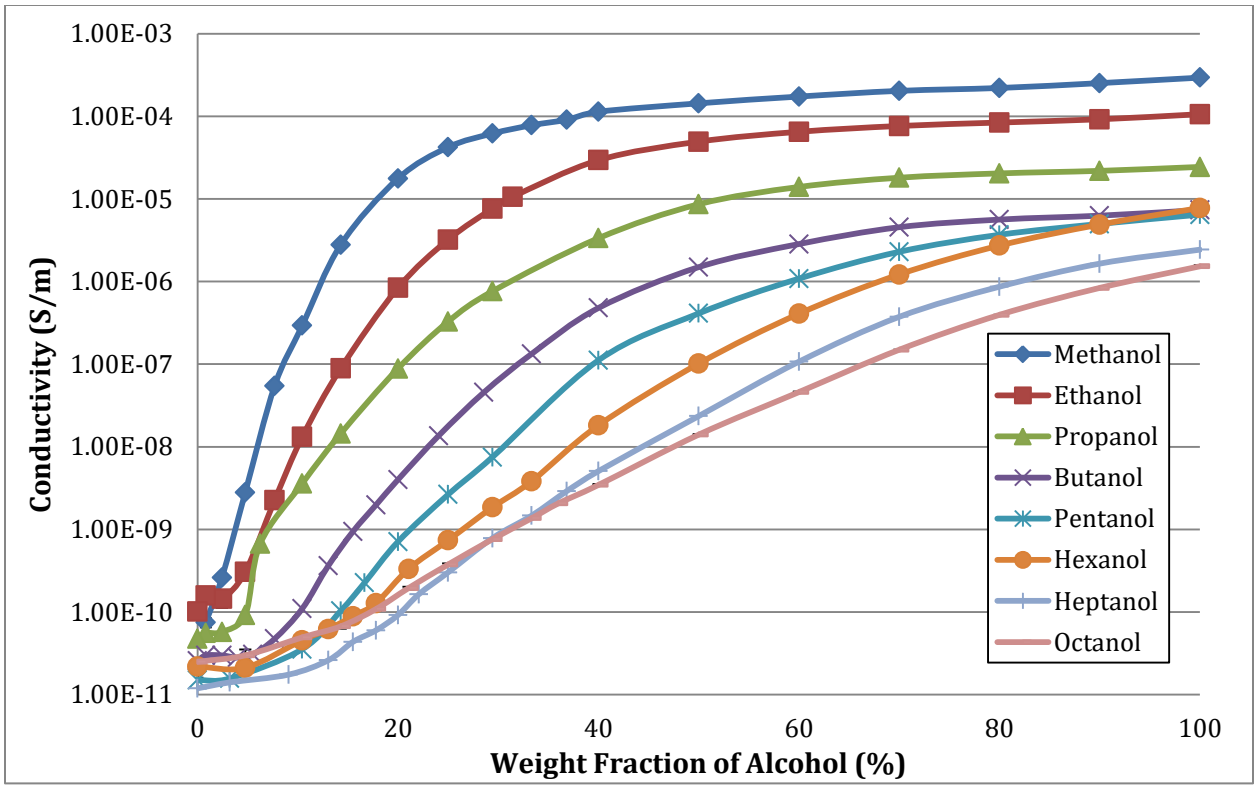

Figure 5. *Conductivity versus Concentration of Alcohol for Alcohol-Nonpolar Liquid Solutions.*

Nonpolar liquid is Toluene in all mixtures. Legend Denotes Alcohol used as Amphiphile.

Logarithmic Scale

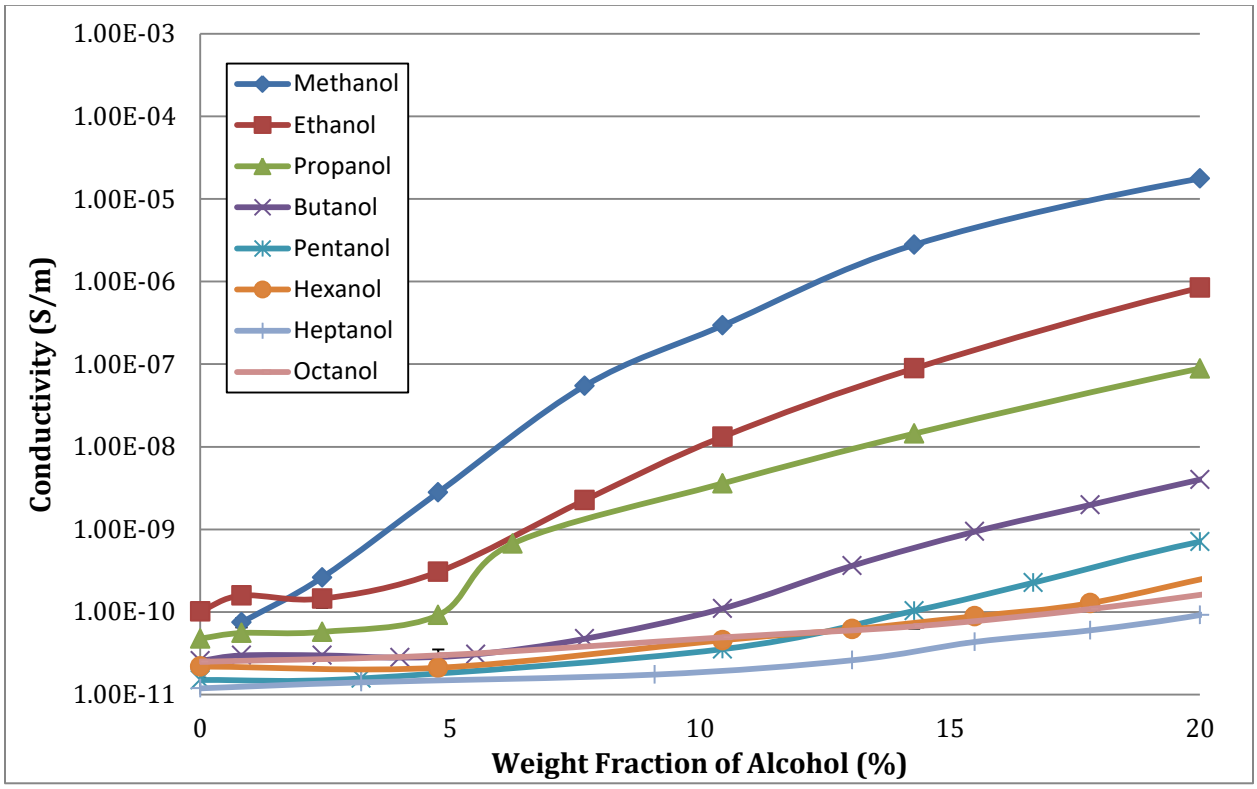

Figure 6a. *Conductivity versus Concentration of Alcohol for Alcohol-Nonpolar Liquid Solutions. Nonpolar liquid is Toluene in all mixtures. Legend Denotes Alcohol used as Amphiphile. Expanded low concentration range of added Alcohol to Alcohol-Toluene mixture. Logarithmic Scale*

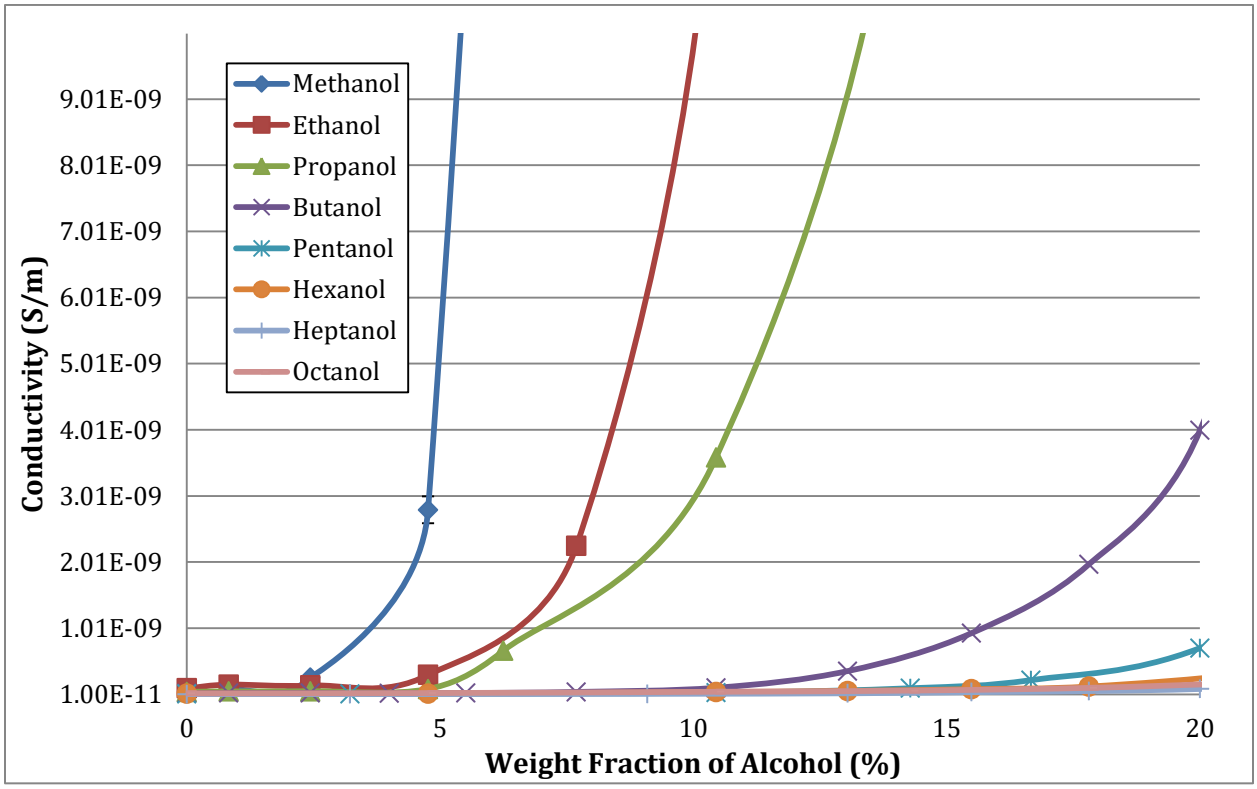

Figure 6b. *Conductivity versus Concentration of Alcohol for Alcohol-Nonpolar Liquid Solutions. Nonpolar liquid is Toluene in all mixtures. Legend Denotes Alcohol used as Amphiphile. Expanded low concentration range of added Alcohol to Alcohol-Toluene mixture. Linear Scale*

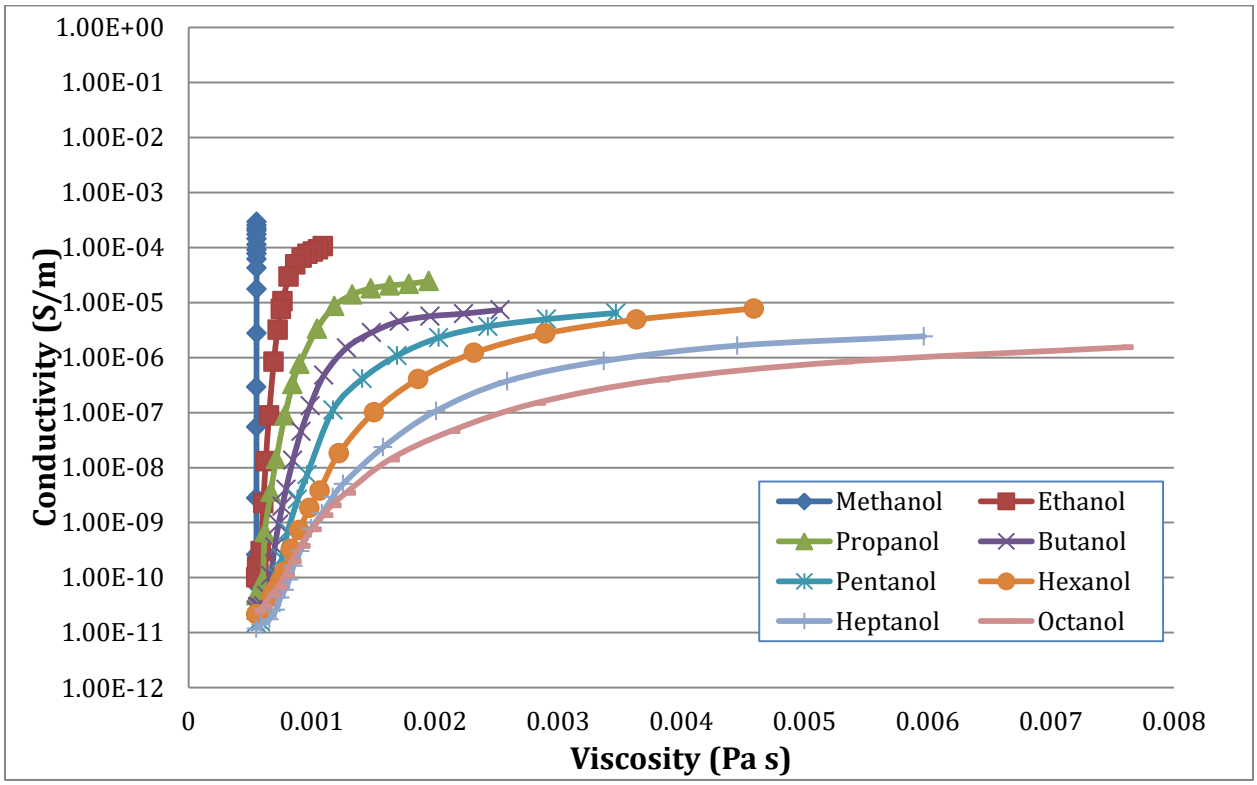

Figure 7. *Conductivity versus Viscosity of Solution for Alcohol-Nonpolar Liquid Solutions. Nonpolar liquid is Toluene in all mixtures. Legend Denotes Alcohol used as Amphiphile. Linear Scale*

3.1.3 DISCUSSION

As shown in ***Figure 4*** and ***Figure 5***, the shorter the chain length of alcohol and higher the concentration, the higher the relative permittivity and conductivity of the solution. This correlates with the expected relationship between the solution's relative permittivity and conductivity, both of which are expected to decrease with increasing alcohol chain length.

Three distinctly different trends are found in most, if not all, of the eight alcohol-toluene solutions; a "high alcohol content" range, an "intermediary alcohol content" range and a "low alcohol content" range. Each of these three trends is characterized by a specific relationship between conductivity and concentration of alcohol in the system.

The curves for all eight alcohol-toluene solutions, exhibit the same trends: at low alcohol concentrations in the mixture with nonpolar liquid there is a non-linear, exponential dependence exhibited between conductivity and concentration of amphiphile, indicative of ion-pair formation within the solution. At sufficiently high alcohol concentrations in the mixture with nonpolar liquid there is a linear relationship between conductivity and amphiphile concentration, as predicted by classical electrochemistry.

Conductivity is plotted versus viscosity of the liquid mixture in ***Figure 7***. For this data viscosity was modeled using a volume fraction-based average of the viscosities of the individual components. The corresponding curves depict a relationship between conductivity and viscosity that is neither linear nor exponential, implying that the relationship between the two is more complex and dependent on other factors (i.e. relative permittivity).

3.1.3.1 High alcohol content range: linear dependence on the alcohol volume fraction.

For mixtures with shorter chain alcohols, a linear dependence between concentration and conductivity is present when alcohol concentration in the mixture is high. The concentration of amphipihle at which this transition to a linear dependence of conductivity

occurs is dependent on the alcohol in the mixture or, more specifically, the chemistry of that alcohol. The shorter the carbon chain of the alcohol (i.e. the lower the molecular weight), the longer this linear relationship is observed, even evident in some solutions at extremely low alcohol concentrations. For methanol, the shortest carbon chain of the alcohols analyzed, this linear dependence of conductivity on amphiphile concentration is observed from 100 wt. % down to roughly 30 wt. %. While this linear relationship ends at approximately 40 wt. % for ethanol, 40 wt. % for propanol, 50 wt. % for butanol, and for higher molecular weight alcohols it appears to not exist at all.

This linear relationship between conductivity and concentration is the result of the high alcohol content subsequently providing a high concentration of the solvating agent (i.e. alcohol molecules) to solvate the free ions in solution. During solvation the free ions are sterically stabilized by a concentric solvent shell that enlarges the ions size, suppressing their re-association into neutral ion pairs, allowing them to remain as free ions and contribute to the overall conductivity of the system[17].

As demonstrated by the data in ***Figure 4***, ideal solvation conditions are not the only characteristic of this concentration range; an increase in relative permittivity, a limiting factor for *Bjerrum length*, **λ**, is also evident in this high ionic environment. This agrees with the *Ion-Pair Conductivity Model* wherein an increase in alcohol concentration is expected to raise the macroscopic relative permittivity of the entire system. Accordingly, *Bjerrum length*, **λ** will decrease as concentration of alcohol increases. This decrease in *Bjerrum length*, **λ** results in a decrease in the *critical distance in formation of ion-pairs*, ***q*** defined in ***Eq. 13***. As ***q*** decreases, it will eventually become less than ion size, ***a***, and the circumstances for ion-pair formation within the solution will no longer exist. At this point the conductivity of the solution is dictated

by the same classical electrochemistry that governs polar systems wherein conductivity is a linear function of concentration according to the following[34]:

$$K(\varphi) = \varphi K_A = \varphi(\mu^+ + \mu^-)eFC_A \qquad \textbf{Eq. 60}$$

This concentration range, and ***Eq. 60***, serve as justification for ***Assumption 1*** and ***2*** made earlier in the *Ion-Pair Conductivity Model*. This linear dependence between concentration and conductivity implies that the nonpolar liquid (i.e. toluene) does not affect the ionic structure or the solvation of the ions in these solutions.

3.1.3.2 Low alcohol content range: Exponential (non-linear) dependence on the alcohol volume fraction.

At very low alcohol concentrations, an exponential dependence between concentration and conductivity is observed. ***Figures 6a*** and ***6b*** shows an expansion of the low concentration range of added alcohol to the toluene-alcohol mixtures. This non-linear relationship presented in ***Figures 6a*** and ***6b*** is the result of a decrease in the overall relative permittivity of the system, and consequently an increase in *Bjerrum length,* **λ**. Accordingly, long range interactions between ions, and a potential lack of sufficient solvating agent to solvate all of the free ions in the solution, increases the likeliness of neutral ion-pair formation, drastically lowering the conductivity in this region. Thus, the *Dissociation Model*'s mass action law, not the linear model of classical electrochemistry, drives the overall conductivity of the system in this low alcohol concentration range.

Reduction of the alcohol content results in a decrease in the relative permittivity of the alcohol-toluene mixtures. Accordingly, this decrease in relative permittivity causes an increase in the *Bjerrum length,* **λ**. As *Bjerrum length,* **λ**, increases, the *critical distance in formation of ion-pairs*, ***q*** defined in ***Eq. 13*** also increases, eventually growing larger than ion size, ***a***, and the circumstances for ion-pair formation exist within the nonpolar solutions. As this happens, the electrostatic attractive forces that cause the re-association of ions into neutral ion-pairs are

comparable to the forces of thermal motion during the dissociation process. This ion-pair formation results in a decrease in the amount of free charged ions within the solutions, creating an exponential dependence of conductivity on concentration in this region.

Of note, at very low alcohol concentration for some of the solutions, particularly in the higher molecular weight alcohols, deviation from this relationship is observed. This deviation is thought to be the result of either measuring error or contamination. The conductivity of pure toluene is 1E-11 S/m, independent of the amphiphile being added to it. And so any deviation from this value is presumed to come from error. Anhydrous materials, including anhydrous toluene, were used to minimize contamination (particularly from water) but, the systems measured here within have very low conductivities, which is the result of very small concentrations of ions, and so it may turn out that some contamination is inevitable. Contamination and the role of contamination plays with regards to ionization in nonpolar media are discussed in later sections.

This exponential behavior at low concentration of added amphiphile, depicted in ***Figure 5***, and expanded upon in ***Figures 6a*** and ***6b***, could not be accurately modeled by the *Disproportionation model*, which predicts a linear dependence of conductivity on concentration.

3.1.3.3 Intermediate concentration range

Between the low and high alcohol content ranges a transition region exists evidenced by an inflection point at which the solution's conductivity transitions between a non-linear to a linear dependence on alcohol concentration. The length of this transition region is a function of the molecular weight of the alcohol. As the chain length of the alcohol molecule increases, the inflection point at which the solution's conductivity transitions between non-linear and linear is not seen until much higher levels of alcohol are present in the solution and for the largest

alcohol molecules (e.g. octanol, heptanol, etc.) it's not clear that this inflection point is ever reached. This behavior is likely due to the larger alcohol molecules, like octanol, having significantly lower relative permittivities (~10) than the shorter-chain alcohols, like methanol, (~33), thus, the *Bjerrum length,* $\boldsymbol{\lambda}$, is never small enough to prevent ion-pair formation and short-range interactions become the driving force of conductivity. Accordingly, as alcohol concentration of the solution increases, the rate of change is more gradual for the longer chain alcohols than it is for the shorter chain alcohols (i.e. alcohols with higher relative permittivities).

An effort was made to graph this inflection point as a function of chain length of the alcohol. This data is presented below:

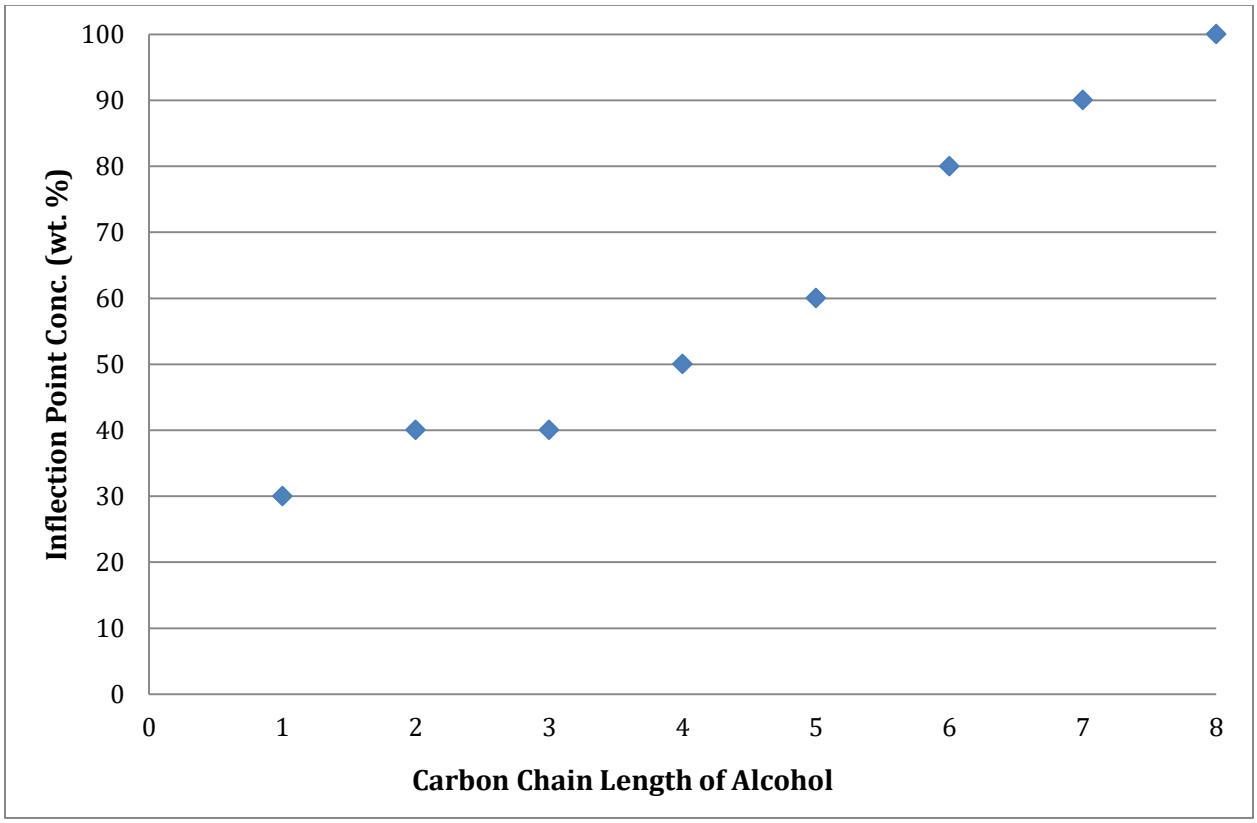

Figure 8*: Concentration at which Inflection Point occurs versus Chain Length of Alcohol as Amphiphile in Mixture With Toluene. The Inflection point represents the transition at which the dependence of conductivity on concentration of amphiphile switches from linear to nonlinear. Linear Scale.*

Figure 8 depicts an increase in the concentration at which the inflection point occurs as chain length of the alcohol additive increases. This behavior is consistant with the *IPCM,* which states that the transition from a non-linear dependence of conductivity on concentration of added amphiphile to a linear dependence is dependent on relative permittivity of the system. As chain length increases, relative permittivity of the alcohol (and, as a result, the relative permittivity of the mixture at any given concentration of added amphiphile) decreases. At sufficiently low relative permittivity, long-range electrostatic interactions are sufficiently strong enough (i.e. Bjerrum length is sufficiently large) for ion-pair formation.

The data presented in ***Figure 8*** is qualitative not quantitative, and serves only as an approximation for the inflection points of the curves. Determination of an exact inflection point for these graphs is not easily attainable due to the complex nature of the curves. Attempts to fit them with complex polynomial best-fit lines (of order 4) and solving for the second derivative were inadequate for determining inflection point. Instead, the low end of the curves were fit with exponential best-fit lines, and the concentration at which the experimental data began to deviate from this exponential best-fit line was deemed the "inflection point." Therefore this data serves only as an approximation meant to display a trend, rather than exact values for inflection point.

3.2 BUTANOL-NONPOLAR LIQUID SOLUTIONS

Next, to study the impact that nonpolar chemistry has on conductivity, the alcohol in these binary solutions was kept constant and the nonpolar liquid was varied. Two-component mixtures of butanol and nonpolar media were prepared and measured across the entire concentration spectra: from pure butanol to pure nonpolar liquid.

Anhydrous primary straight-chain Butanol was chosen as the amphiphile because it's both an intermediary in the group of alcohols from the first experiment[73], and the conductivity of pure butanol falls roughly in the middle of the measurable conductivity range of the DT-700[63] Non-Aqueous Conductivity Meter used for these experiments. Additionally, butanol is considered a low hygroscopic (i.e. readily absorbs moisture) material, in comparison with more hygroscopic alcohols such as ethanol, which is beneficial in minimizing the effects of contamination via water absorption from the surrounding air, allowing for simplified handling procedures during sample preparation.

The three nonpolar liquids studied were: toluene, hexane, and heptane. These nonpolar liquids are all miscible with butanol, as to avoid any incompatibility issues. Their chemical structures are illustrated in ***Figure 9***.

Measurements were performed in a narrow vial in order to minimize the exposure to open air. Additionally, the top of the conductivity probe is sufficiently wide to serve as an effective cap for the sample chamber (Relative permittivity measurements, by comparison, require much less time, on the scale of a few seconds). This minimized the possibility of evaporation of materials from occurring, allowing us to ignore vapor pressure effects of both the nonpolar media and added amphiphile.

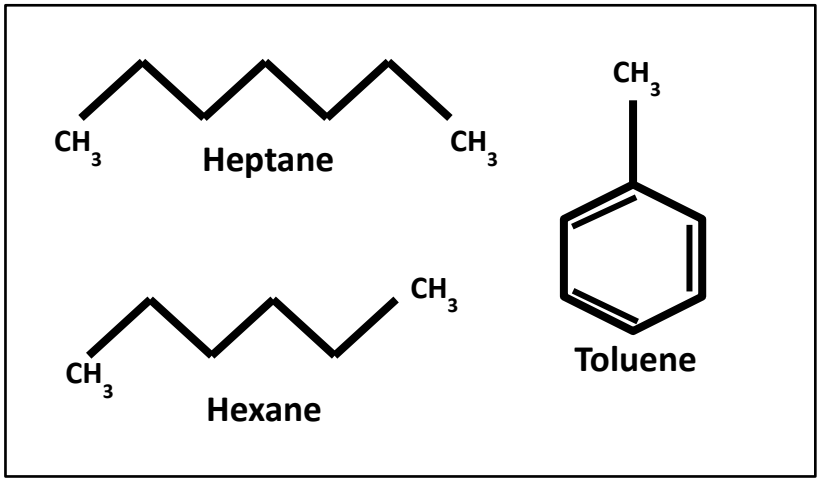

Figure 9: *Chemical Structures of Heptane, Hexane & Toluene*[74, 75, 76]

Material	Formula	Molecular Weight	Viscosity (at 20°C) [Pa s][69]	Density (at 20°C) [g/cm3][69]	Relative Permittivity [at 20°C]
Toluene	C_7H_8	92.141	0.00059	0.87	2.36
Heptane	C_2H_5OH	46.08	0.00109	0.789	1.9
Hexane	C_3H_7OH	60.14	0.00195	0.803	1.88

Table 4: *Material properties of Heptane, Hexane & Toluene*

As illustrated in ***Figure 9***, hexane and heptane are both straight-chain alkanes of varying carbon length (6 for hexane, 7 for heptane), and toluene is an aromatic hydrocarbon (i.e. it has a benzene ring) with an additional methyl group attached. Anhydrous versions of these nonpolar liquids were selected to minimize the effects of water contamination. Additionally, all three have nearly identical relative permittivities (~2) and viscosities (~1 cP). Therefore, by comparing the conductivity curves of these butanol-nonpolar liquid solutions, we can examine whether the chemistry of the nonpolar liquid in solution serves as the driving force behind ion-pair formation and thus the conductivity of these butanol-nonpolar media mixtures.

3.2.1 MATERIALS AND METHODS

We employed the same "path of reducing alcohol content" for preparation of samples with concentrations from 100 wt. % to 40 wt. % butanol and the "path of increasing alcohol content" approach for butanol concentrations from 0 wt. % (100 wt. % nonpolar liquid) up to 50 wt. % butanol. For each solution we had overlapping concentration data points for both 40 and 50 wt. % of butanol, which again served as a meaningful check point to ensure solution reproducibility and confirm solution formulation accuracy throughout the preparation process independent of the solutions preparation path.

Again, all solutions were calculated and prepared on a weight basis, with a total solution weight of 50 grams, which was maintained throughout formulation by re-calculating how much original material should be kept and how much additional material (nonpolar in the case of the "path of reducing alcohol content," and butanol in the case of the "path of increasing alcohol content") should be added to achieve the desired solution concentration ratio. Increasing the sample weight to 50 grams allowed for more precise dilution/concentration of the sample because larger volumes are easier to accurately pipette than small volumes.

3.2.2 RESULTS

Figure 10a and 10b show the conductivity curves for the two-component mixtures of butanol and nonpolar liquid measured across the entire concentration spectra: from pure nonpolar liquid to pure butanol. ***Figure 10a*** presents the data on a linear scale and ***Figure 10b*** on a logarithmic scale, which allows for easier viewing of the conductivity and concentration data at different scales. ***Figure 10c*** expands the low concentration region of ***Figure 10b***, allowing for the behavior in this region viewed.

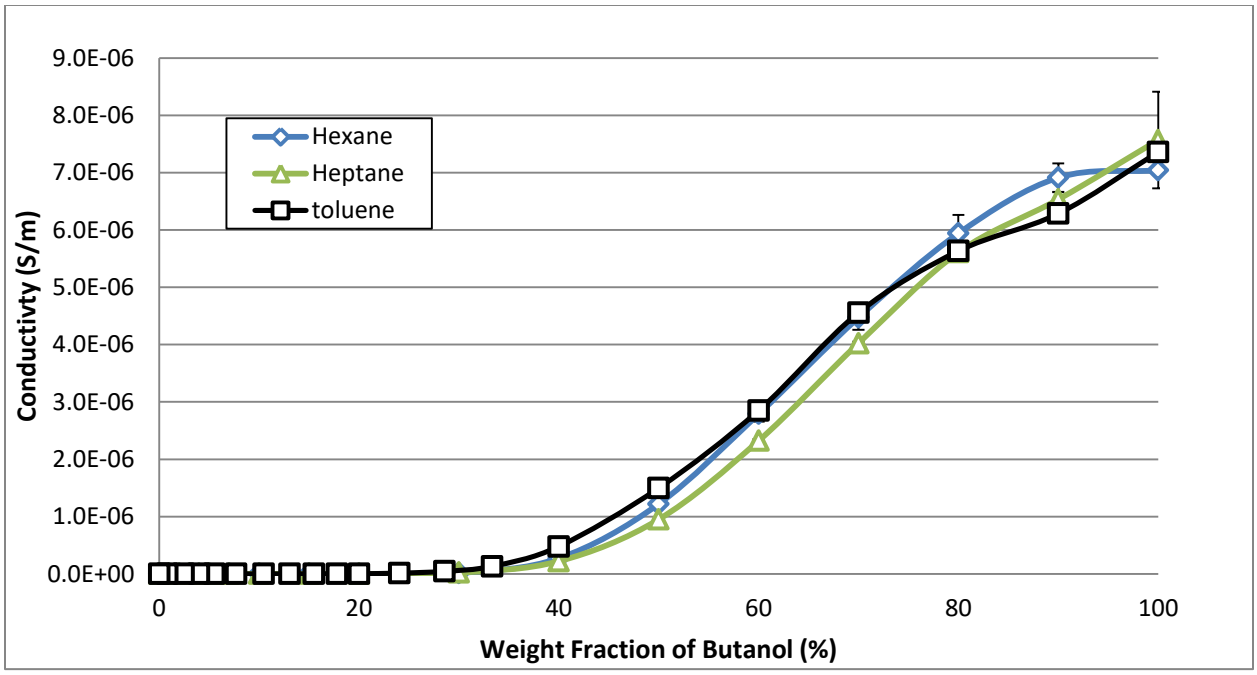

***Figure 10a**: Conductivity versus Concentration of Butanol for Butanol-Nonpolar Liquid Solutions.*

Legend Denotes Nonpolar liquid in Solution. Linear Scale

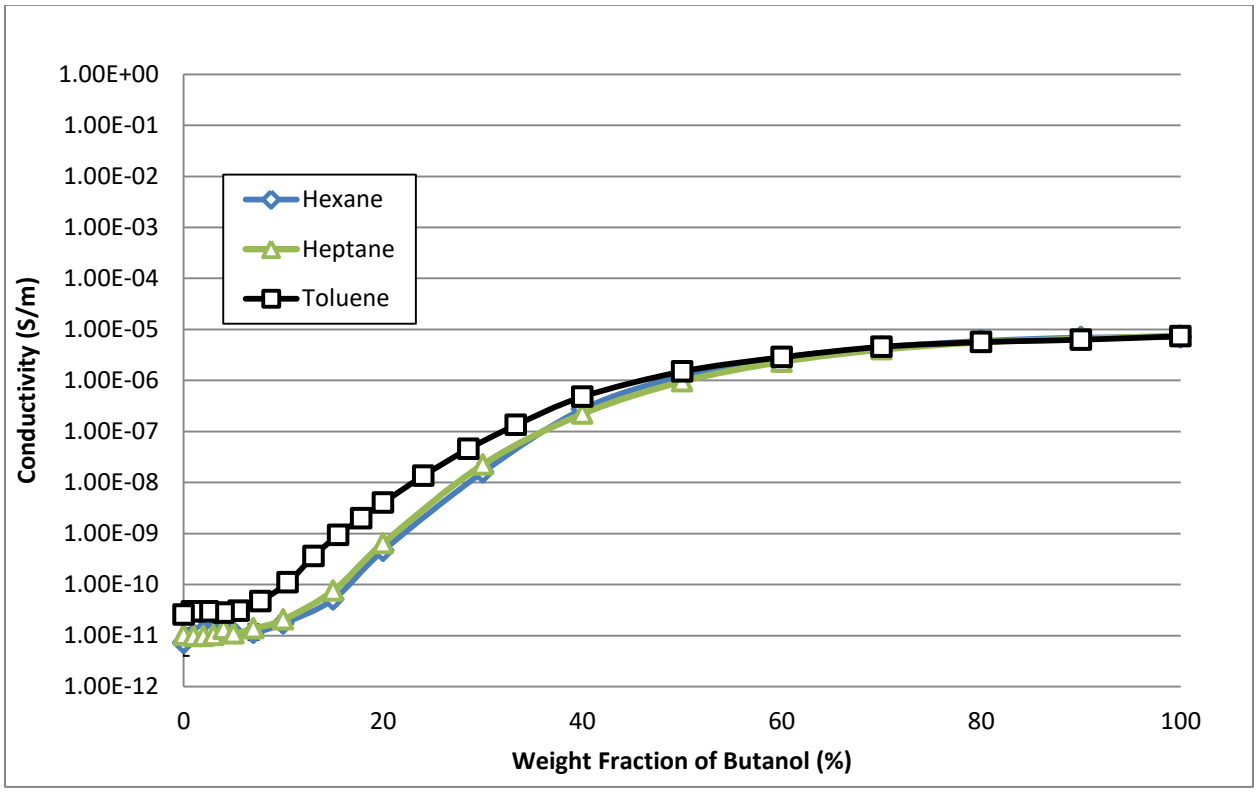

***Figure 10b**: Conductivity versus Concentration of Butanol for Butanol-Nonpolar Liquid Solutions.*

Legend Denotes Nonpolar liquid in Solution. Logarithmic Scale

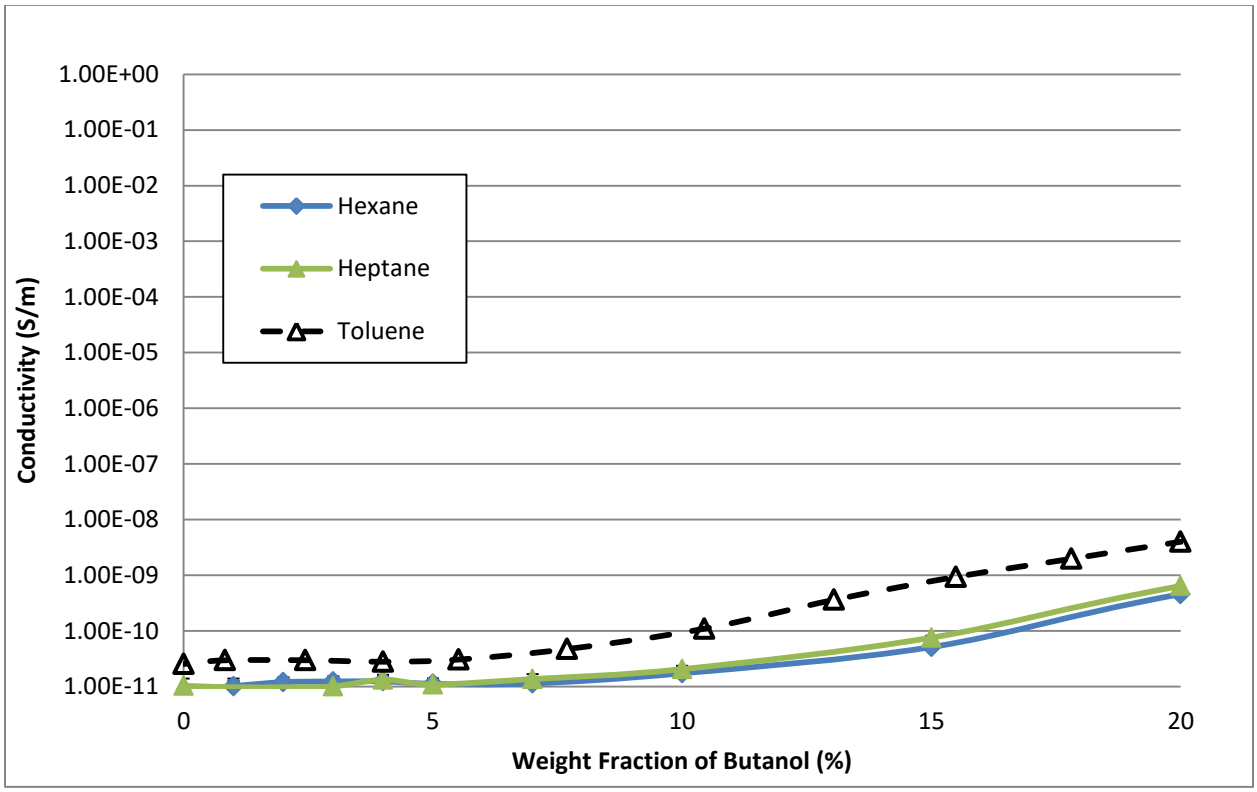

***Figure 10c**: Conductivity versus Concentration of Butanol for Butanol-Nonpolar Liquid Solutions. Expansion of region of low concentration of added Butanol. Legend Denotes Nonpolar liquid in Solution. Logarithmic Scale*

3.2.3 DISCUSSION

Similarly, to those results found in **Section 3.1**, we observe three distinctly different relationships between conductivity and alcohol (i.e. butanol) concentration in the conductivity curves for all three of the butanol-nonpolar liquid solutions; a "high alcohol content" range, an "intermediary alcohol content" range and a "low alcohol content" range. And accordingly, the same conclusions can be drawn for those three regions for all three of the butanol-nonpolar liquid solutions:

- High alcohol content range: a linear relationship, as predicted by classical electrochemistry, between conductivity and concentration is observed and no ion-pairs present. Depicted in **Figure 10a** above concentrations of 40 wt. % of added amphiphile.
- Low alcohol content range: a non-linear, exponential dependence is exhibited between conductivity and concentration, indicative of an increase in ion-pair formation and a decrease in the conductivity of the overall system (see **Figure 10c**). This dependence is in disagreement with the linear behavior predicted by the *Disproportionation Model*, and in direct agreement with the *Dissociation model* and the *IPCM*, which predict this behavior due to ion-pair formation.
- Intermediate range: transition between the other two ranges.

Additionally, the *Ion-Pair Conductivity Model (IPCM)* predicts that conductivity of nonpolar media with alcohol added as the amphiphile is independent of the chemistry of the nonpolar phase. Despite differing lengths of carbon chain, or the benzene ring present in toluene, the conductivity data is the same for all three sample when mixed with butanol as the added amphiphile, displaying the same conductivity trends across the entire concentration spectra.

The relevant parameters of the nonpolar media in the *IPCM* are relative permittivity and viscosity, which are very similar for all three nonpolar liquids examined, explaining why they show the same behavior.

3.3 PURE BUTANOL AND BUTANOL-HEXANE SOLUTIONS

As stated previously, ionization in mixtures of nonpolar media with added alcohol as amphiphile can be attributed to the auto-dissociation of the alcohol (e.g. in the case of butanol: $C_4H_9OH + C_4H_9OH \Leftrightarrow C_4H_9OH_2^+ + C_4H_9O^-$). Additionally, in this section, we will also explore ionization as the result of water contamination.

In **Section 3.1**, we simply characterized the concentration of total ions in the pure alcohol as $\boldsymbol{C_A}$ and attributed ion formation solely to auto-dissociation of the alcohol molecules. However, to better understand the complexity of the conductivity in these systems, it's also important to consider how water contamination contributes to $\boldsymbol{C_A}$ as well[73].

3.3.1 MATERIALS AND METHODS

Experiments were performed using both treated and untreated butanol. Treated butanol was dried with 3A molecular sieve beads, which are porous, with pores 3 angstroms in size, in order to remove water. These beads allow for water molecules to enter and become trapped within the pores, while the larger butanol molecules are able to remain free in solution[77]. In experiments where dried butanol was used, the mixture of the beads and butanol were placed in a sealed glass container and left to equilibrate overnight to allow for the complete, or nearly complete, removal of water. This preparation process of drying the butanol was carried out with the goal of examining how water removal affects the conductivity of dried pure butanol and dried butanol-nonpolar liquid solutions. The efficiency of the beads was not a focus, and so these results are more qualitative than quantitative.

Experiments were then conducted to determine the effect contamination, via exposure to ambient air, had on dried pure butanol and on a dried butanol-nonpolar liquid solution. Dried pure butanol, as well as a mixture of dried butanol and hexane (70 wt. % butanol, 30 wt. % hexane), were placed in an uncapped 100 mL bottle with a 1.5-inch diameter and exposed to

ambient air in the laboratory at room temperature (~25 °C). Conductivity measurements, taken at regular time intervals, were used to track any changes that this exposure may have caused to the overall conductivity of the solution. By examining the effects ambient air contamination had on both dried pure butanol and the dried butanol-hexane mixture, we were able to analyze the relationship between dried butanol concentration and contamination and the impact it has on overall conductivity of the solution.

Lastly, in order to further explore the effects that contamination has on conductivity, water was manually added into the dried pure butanol solution (i.e. via a titration experiment). The amount of water added in each experiment was recorded, with the concentration of water never exceeding 5 wt. %.

3.3.2 RESULTS

Figure 11 shows the conductivity curves for the butanol and nonpolar liquid solutions and dried butanol solution measured across the entire concentration spectra: from pure nonpolar liquid to pure butanol.

Figure 12 depicts the conductivity curves for dried pure butanol and the dried butanol-hexane solution across the entire air contamination exposure spectra.

Figure 13 displays the conductivity curve for dried pure butanol across the entire water titration spectra.

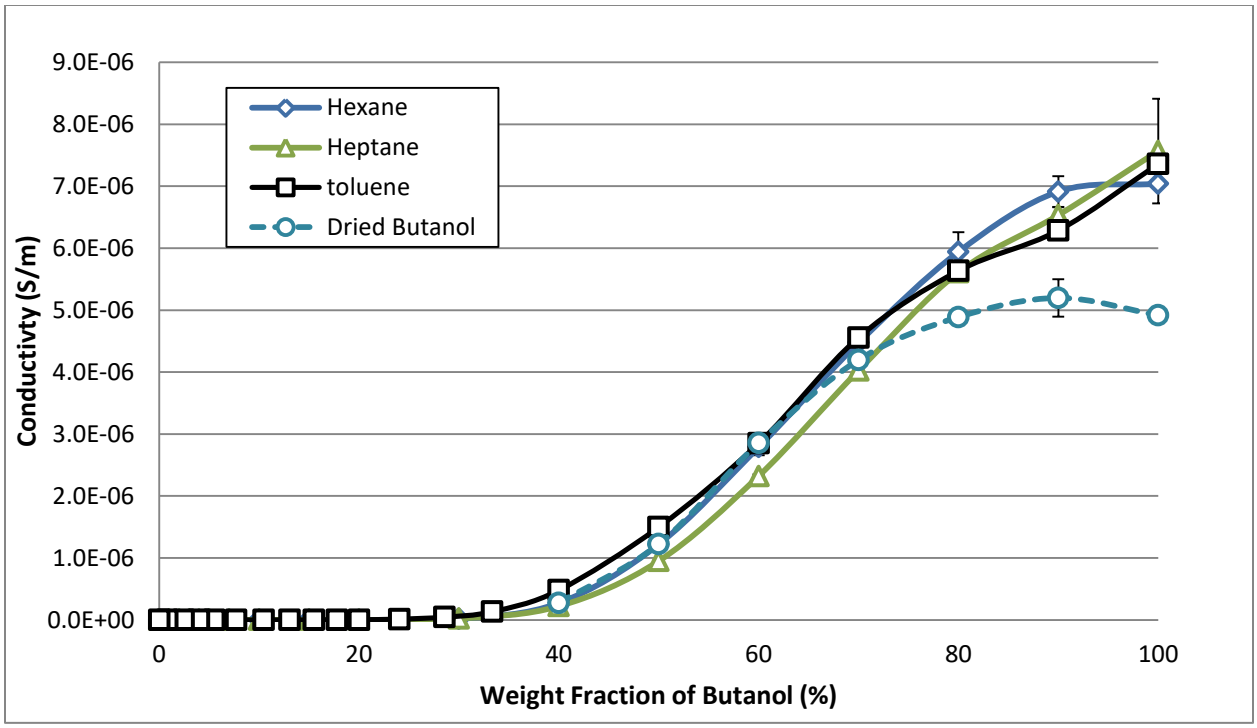

Figure 11*: Conductivity versus Concentration of Butanol for Butanol-Nonpolar Liquid and Dried Butanol Solutions. Legend Denotes Nonpolar liquid in Solution. "Dried Butanol" in Legend refers to Hexane-Butanol Mixture in which Dried Butanol was used. Linear Scale*

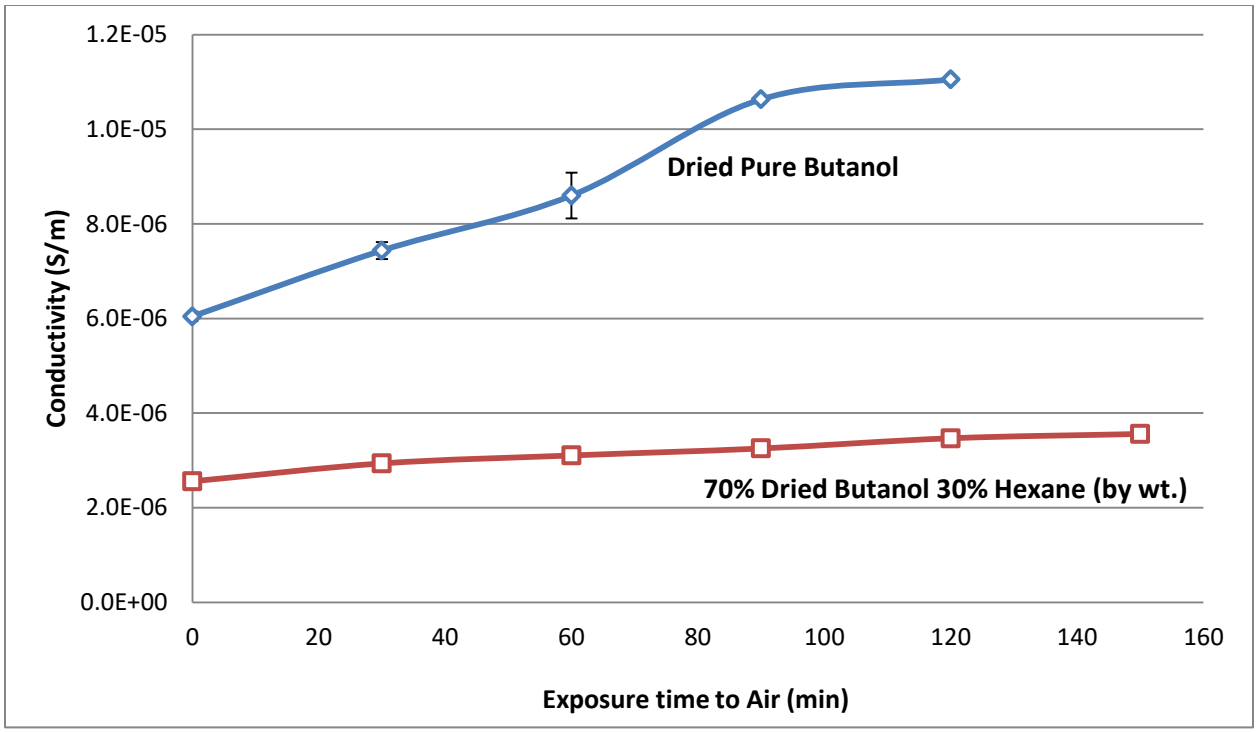

***Figure 12**: Conductivity versus Exposure time to Air for Dried Pure Butanol and Dried Butanol-Hexane Solutions. Linear Scale*

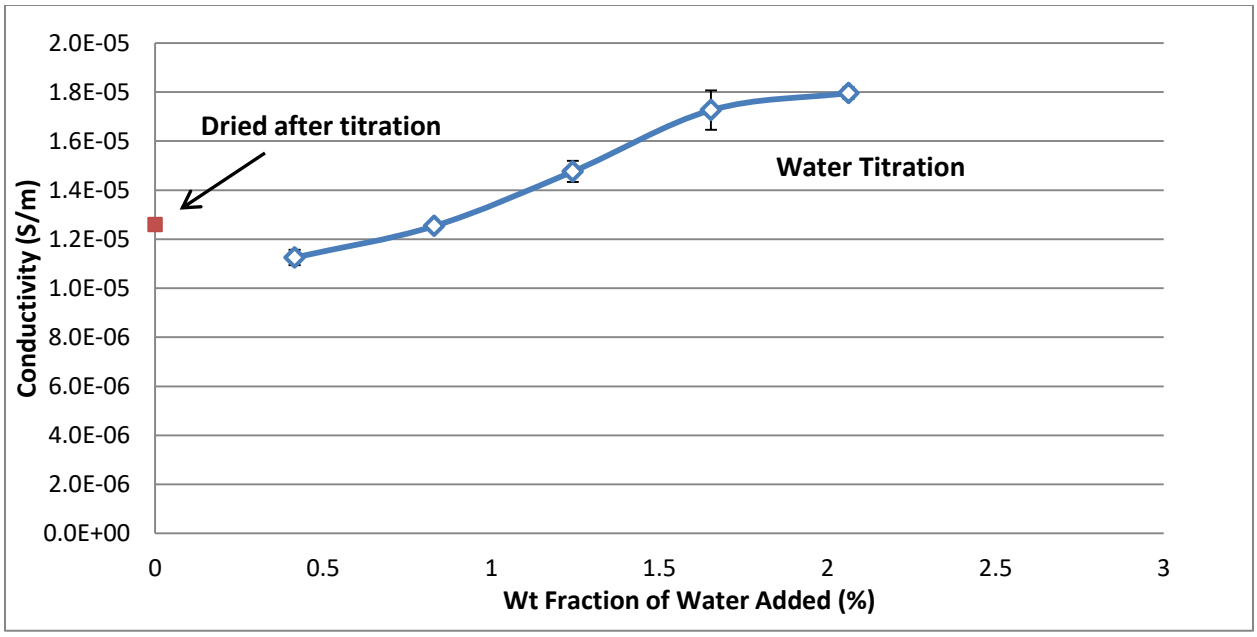

***Figure 13**: Conductivity versus Concentration of Added Water for Dried Pure Butanol Solution.*

Linear Scale

3.3.3 DISCUSSION

The conductivity curves in ***Figure 11*** show that dried butanol has a significantly lower conductivity than that of non-dried butanol (evidenced by the butanol-nonpolar liquid data points at 100 wt. % butanol). In ***Figure 12*** the conductivity of dried butanol increases the longer the solution is exposed to air (i.e. contamination). However, this increase in conductivity due to exposed air contamination in the butanol-hexane solution appears to weaken until it eventually becomes negligible as exposure time lengthens.

3.3.3.1 Water Absorption by Ambient Air

Dried pure butanol and a dried butanol-hexane (at a concentration of 30 wt. % hexane) solution were exposed to ambient air in the laboratory, over a course of several hours, with conductivity measured at specific time intervals to allow for examination of the change in conductivity of the system over time. As seen in ***Figure 12*** it is clear that in the case of dried pure butanol the increase in conductivity of the solution as a result of contamination is rather significant, nearly doubling after 120 minutes. For the mixture of dried butanol and hexane the effect of contamination on conductivity was far less pronounced.

The relationship between length of contamination and conductivity of the system in the two solutions conductivity curves illustrated in ***Figure 12*** is exactly what one would expect given butanol and hexane's intrinsic physical properties. Butanol is hygroscopic by nature[78]. Butanol, and other alcohols like it, readily absorb moisture from ambient air. While hexane, a hydrophobic nonpolar liquid, does not readily absorb water under any condition. This is due to water and hexane being immiscible[73]. Accordingly, pure hexane, when exposed to ambient air for prolonged periods of time, shows negligible changes in conductivity. This indicates that only the butanol portion of the butanol-hexane solution is being contaminated by the moisture in the ambient air.

Of note, in this section we are choosing to assume that the source of contamination from the ambient air is water. However, it is possible that other contaminants, not just water, are at play in these systems during prolonged periods of exposure to ambient air. One example being carbon dioxide, which can also be adsorbed by these types of solutions.

While acknowledging that exposure to water contamination via ambient air can affect conductivity in these systems, accounting for and attempting to avoid such contamination is very complicated. The source of contamination can come from, for example, the manufacturer's bottle when it is opened to pour out butanol to be used for experiments, or simply due to the cap not being sufficiently airtight. Additionally, given that the conductivities being measured in these nonpolar systems are very low, even the slightest contamination anywhere along the solution preparation process can have a substantial effect on the overall conductivity of the system. Accordingly, contamination is likely the source of variation between the measured conductivity of dried butanol found in ***Figure 11*** (5E-06 S/m) at 100 wt. % of pure butanol and dried pure butanol at time zero in ***Figure 12*** (6E-06 S/m).

3.3.3.2 Water Titration

As stated above, the source of contamination due to exposure to air is difficult to pinpoint in these systems. In an effort to validate our assumption that water contamination via ambient air exposure played a role in our contamination study illustrated in ***Figure 12***, we next examined the effects titrating water, exclusively, into dried pure butanol had on the overall conductivity of the solution. Water contamination will be explored further in ***Section 3.12*** by means of Karl-Fischer titration.

As demonstrated in ***Figure 13***, titration of water into dried pure butanol caused an increase in conductivity of the solution. The values for water contamination on the x-axis refer

to the amount of water specifically added to the butanol; it does not account for any initial contamination to the solution caused by exposure to ambient air.

Following completion of the water titration into the dried pure butanol experiment, 3A molecular sieve beads were added to the now water-butanol solution and left to equilibrate to demonstrate that these beads are in fact a viable means for removing water from these systems.

As evidenced in ***Figure 13***, these 3A molecular sieve beads are capable of removing most, if not all, water from these nonpolar systems. However, the concentration of water following the 3A molecular sieve bead drying was not actually zero, and we do not claim that the molecular beads were able to remove all of the water from the system; rather it seemed an appropriate location to place the data point to demonstrate the effect adding the 3A molecular sieve beads had on removing water from the system, and the subsequent effect the water removal had on the conductivity of the solution. The purpose of demonstrating the efficacy of the 3A molecular sieve beads was not to quantify how much water they could remove from these systems, but validate their ability to remove water from these water-butanol solutions all together.

3.4 NON-IONIC SURFACTANTS: XIAMETER SURFACTANTS

While solutions consisting of alcohols (i.e. amphiphiles) and nonpolar media do have real world applications, they are rather limited in scope. Accordingly, the next step was to analyze amphiphiles that are more commonly utilized in real-world applications: non-ionic surfactants. More specifically, we opted to study the conductivity of binary mixtures in which non-ionic surfactant was used as the amphiphile[79]. While it has been known that ionic surfactants increase the conductivity of nonpolar systems, the acknowledgement that increased nonpolar conductivity can come from nonionic surfactants as well is a relatively recent conclusion[80-82]. To date, to our knowledge, there have been no published studies examining these types of systems across the entire concentration range, from pure nonpolar liquid to pure non-ionic surfactant. The goal in measuring these systems was to determine if the *Ion-pair Conductivity Model* is applicable to mixtures in which the amphiphile is a nonionic surfactant.

3.4.1 MATERIALS AND METHODS

The first non-ionic surfactants chosen for these experiments were OFX-5098 and OFX-0400. They are both manufactured by Dow Corning, and are part of their Xiameter line of silicone-based polyether surfactants. More specifically both materials are polyalkylene oxide-modified polydimethylsiloxanes, also referred to as silicone-ethylene oxide copolymers. The Xiameter series of surfactants were chosen because of their high purity, and their ability to remain as liquids at 100% purity. Accordingly, conductivity, relative permittivity, and viscosity of these materials could all be measured at 100% purity without having to perform additional dilution or other modification steps prior to analysis (i.e. they could be measured as is). Similarly, these two nonionic surfactants have the following relevant properties:

Material	Molecular Weight	Viscosity (at 25°C) [Pa s]	End Cap	HLB
OFX-5098	3,225.90	0.25	OAc	11.7
OFX-0400	3,101.10	0.282	OAc	6.6

Table 5*: Material Properties of Non-Ionic Xiameter Surfactants OFX-5098 and OFX-0400*

As evidenced above in ***Table 5***, OFX-5098 and OFX-0400 have nearly the same viscosity and the exact same end cap. Therefore, by specifically choosing these two nonionic surfactants as the amphiphile in these systems the effect the Hydrophile-Lipophile Balance (HLB) number of the amphiphiles has on conductivity and relative permittivity, particularly when mixed with a nonpolar liquid, can be exclusively studied.

Toluene was chosen as the nonpolar liquid because both Xiameter nonionic surfactants are miscible in toluene, allowing for the nonionic surfactant-toluene solutions to be easily measured at all concentrations, from pure toluene to pure nonionic surfactant.

Sample preparation was again carried out in the same fashion as **Section 3.1**. The *"reducing surfactant content"* approach was performed for mixtures with high concentrations of nonionic surfactant: from pure (100 wt. %) nonionic surfactant down to 40 wt. %. While the *"increasing surfactant content"* approach was performed for mixtures with low concentrations of nonionic surfactant: from pure toluene (0 wt. % surfactant) up to 50 wt. %. Accordingly, we again saw sample overlap at both 40 and 50 wt. % of nonionic surfactant, which again served as a meaningful check point to ensure solution reproducibility and confirm solution formulation accuracy throughout the preparation process independent of the solutions preparation path.

Next, conductivity, relative permittivity, and viscosity measurements were taken for each nonionic surfactant-toluene solution across the entire concentration spectra. Experiments in this section were performed in such a way that all three measurements could be taken on each solution in succession, avoiding the need for excess sample preparation (i.e. performing titrations) for each measurement. This served to decrease error potential during sample preparation by limiting the total amount of sample required for testing. The measurements performed on these samples (conductivity, relative permittivity, and viscosity)

are all classified as “non-destructive measurement techniques”, so performing the experiments in this fashion had no adverse impact on the data collected.

Sample measurements were performed with the same sample setup as in ***Sections 3.1*** and ***3.2*** to minimize evaporation of mixture components.

3.4.2 RESULTS

Figure 14a and ***Figure 14b*** illustrate the conductivity curves as a function of concentration of nonionic surfactant for the two Xiameter nonionic surfactant-toluene solutions, on logarithmic and linear scales, respectively. The data is displayed on both scales because the range of conductivities is so large that each scale is better suited for examining a different end of the concentration spectrum. ***Figure 14c*** expands the low region of ***Figure 14b*** in order to further explore the range of low amphiphile concentration.

Figure 15 illustrates the relationship between relative permittivity the system and concentration of added nonionic surfactant. The relationship between viscosity of the system and concentration of added nonionic surfactant is shows in ***Figure 16***.

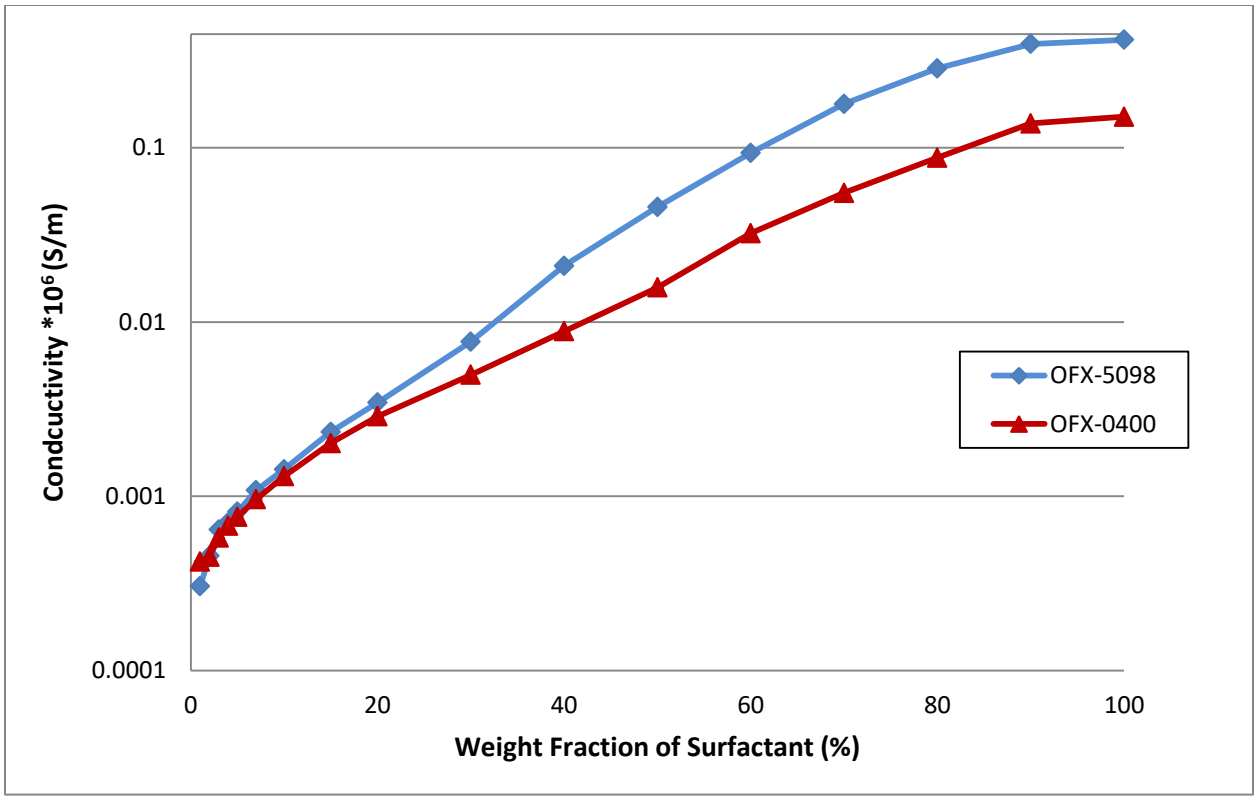

***Figure 14a**: Conductivity versus Concentration of Nonionic Surfactant for Xiameter Nonionic Surfactant-Toluene Solutions. Legend Denotes Nonionic Surfactant in Solution. Logarithmic Scale.*

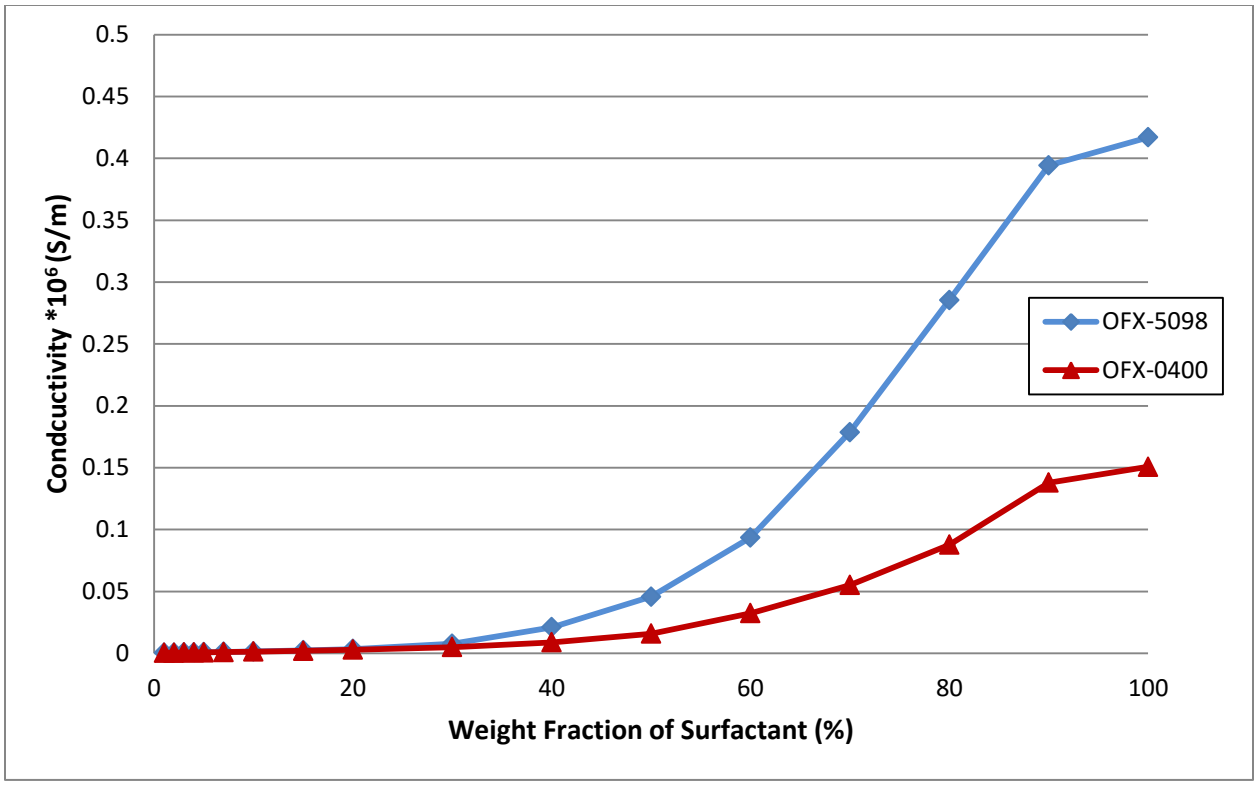

***Figure 14b**: Conductivity versus Concentration of Nonionic Surfactant for Xiameter Nonionic Surfactant-Toluene Solutions. Legend Denotes Nonionic Surfactant in Solution. Linear Scale.*

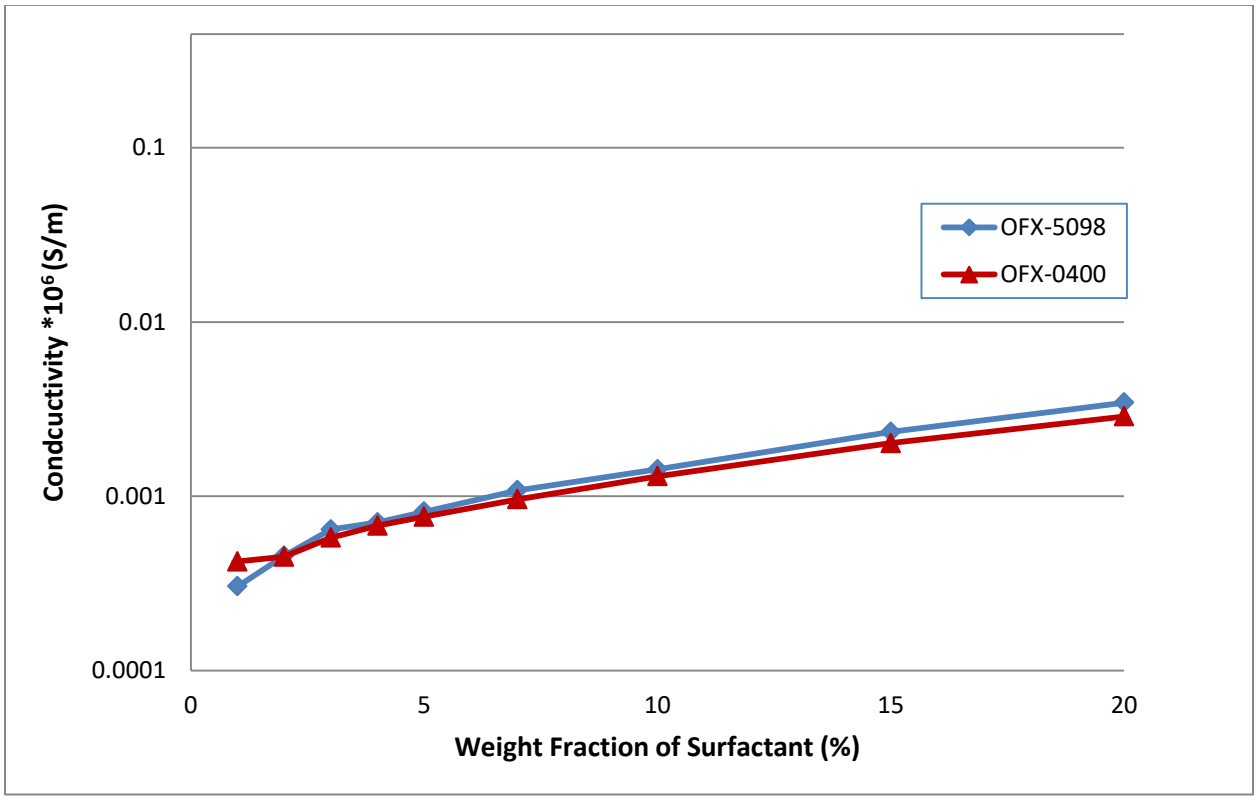

***Figure 14c**: Conductivity versus Concentration of Nonionic Surfactant for Xiameter Nonionic Surfactant-Toluene Solutions, Expanded region of low amphiphile concentration. Legend Denotes Nonionic Surfactant in Solution. Logarithmic Scale.*

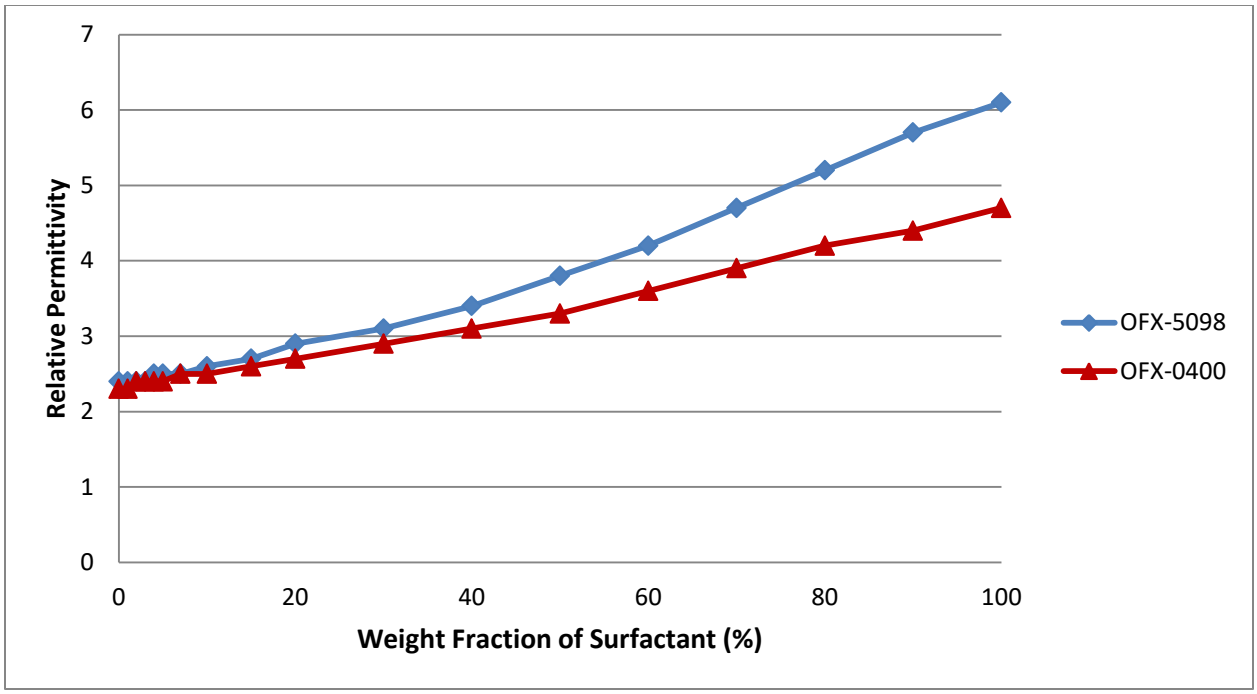

***Figure 15**: Relative Permittivity versus Concentration of Nonionic Surfactant for Xiameter Nonionic Surfactant-Toluene Solutions. Legend Denotes Nonionic Surfactant in Solution. Linear Scale*

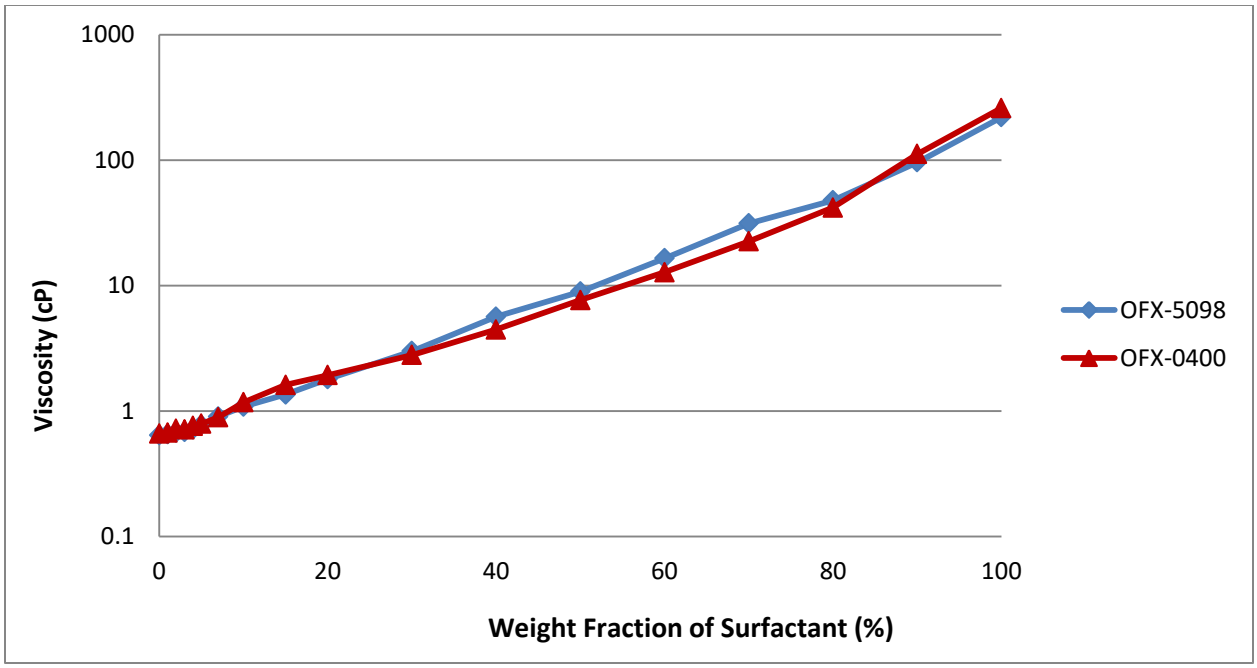

***Figure 16**: Viscosity versus Concentration of Nonionic Surfactant for Xiameter Nonionic Surfactant-Toluene Solutions. Legend Denotes Nonionic Surfactant in Solution. Logarithmic Scale*

3.4.3 DISCUSSION

3.4.3.1 Conductivity vs. Concentration of Xiameter Nonionic Surfactant

As seen in ***Figure 14a*** and ***Figure 14b*** an increase in concentration of nonionic surfactant significantly increases the conductivity of the solution for both Xiameter surfactants analyzed. The conductivity increases four orders of magnitude from pure toluene to pure nonionic surfactant.

Based on the conductivity curves shown in both ***Figure 14a*** and ***Figure 14b***, keeping in mind that ***Figure 14a*** is plotted on a logarithmic scale, it appears that the conductivity is exponentially dependent on nonionic surfactant concentration across the entire concentration range. This exponential relationship between conductivity and nonionic surfactant concentration implies that ion-pairs are present at all concentrations of these binary mixtures. Even at 100 wt. % of nonionic surfactant, the relative permittivity of the solution remains low enough to allow for a sufficiently large *Bjerrum length*. This large *Bjerrum length* provides a favorable environment for the attractive electrostatic forces between the oppositely charged ions in this nonpolar solution comparable to the repulsive forces of thermal motion. As *Bjerrum length* approaches and/or exceeds the distance of closest ion approach, ***a***, solvated ions will recombine into neutral ion-pairs. These formed ion-pairs, while containing solvated ions within, are neutral from a conductivity perspective and, accordingly, do not contribute to the conductivity of the overall system. Thus, an exponential dependence of conductivity on concentration is observed in these systems. This exponential dependence yields conductivities at a given concentration that are lower than would be predicted by classical electrochemistry, in which the dependence of conductivity on concentration is linear.

Figure 14c expands the region of low concentration of added nonionic surfactant, allowing the relationship between conductivity and concentration to be explored. The curves

in ***Figure 14c***, for both mixtures with nonionic surfactant as amphiphile, show an exponential dependence of conductivity on concentration, even in this region of low amphiphile concentration. This non-linear dependence is in disagreement with the *Disproportionation Model,* which predicts a linear dependence of conductivity on concentration of amphiphile. However, the exponential dependence exhibited agrees with the *IPCM.* Given that this non-linear relationship exists for nonpolar mixtures when both a nonionic surfactant and alcohol (***Figure 5***) are used as the amphiphile, confirms that this phenomenon is not unique to only alcohol-toluene nonpolar solutions.

As the concentration of the nonionic surfactant increases beyond 10 wt. %, the two conductivity curves for the Xiameter nonionic surfactant-toluene solutions begin to diverge. ***Figure 14b***, with data plotted on a linear scale, better illustrates this variance. As nonionic surfactant concentration continues to increase the divergence between the two conductivity curves also grows. At 100 wt. % nonionic surfactant the conductivity of pure OFX-5098 is roughly 2.5 times greater than that of pure OFX-0400.

Given the endcaps and viscosities for both Xiameter nonionic surfactants are approximately equal, the differences in the conductivity of the two solutions can likely be attributed to variations in their respective HLB numbers. The hydrophilic-lipophilic balance (HLB) number of a material is used to characterize how hydrophobic or lipophilic a molecule is. An amphiphilic (i.e. surfactant) molecule, by definition, has both a hydrophobic and a lipophilic component, and its HLB number is a numerical representation of how heavily a role each component plays in the behavior of the molecule. A high HLB number implies that the hydrophilic portion of the molecule plays a more dominant role in the materials behavior, while a low HLB number implies that the lipophilic portion of the molecule is more impactful. While Xiameter nonionic surfactant OFX-5098 has an HLB number of 11.7, OFX-0400 only has

an HLB number of 6.6. OFX-5098 is more hydrophilic than OFX-0400, and therefore OFX-5098 surfactant's polar component is more prominent than that of OFX-0400. In view of the fact that the ability of a surfactant molecule to conduct electricity is derived from the polar component of the molecule, OFX-5098 should, and does, yield a higher conductivity than OFX-0400.

Lastly, in the case of conductivity of these nonpolar systems we assume that the nonionic surfactants, not the toluene, serve as the solvating agents in these solutions, and postulate that the nonionic surfactants themselves may also serve as the dissociating molecules. However, given the fact that impurities at the low levels of conductivity discussed within this work are nearly impossible to eliminate, it is virtually impossible to zero in on a single dissociating agent, making it unfeasible to confirm, with any degree of certainty, that we know the exact chemical nature of the dissociating molecules. However, the concentration of solvating agent in such a system can be controlled, and in doing so allows us to derive and implement a model which can serve to quantitatively predict conductivity in such systems.

3.4.3.2 Relative Permittivity vs. Concentration of Xiameter Nonionic Surfactant

As shown in ***Figure 15***, the Xiameter nonionic surfactant-toluene solutions relative permittivity was linearly dependent upon nonionic concentration across the entire concentration spectra for both nonpolar systems. The relative permittivities for the Xiameter nonionic surfactants, OFX-5098 and OFX-0400 are 6 and 4.7, respectively, which, while still quite low, fall on the higher end of the "nonpolar liquid" classification range and closer to the "low polar" category. This further reinforces the fact that ion-pairs are present within these nonpolar systems across the entire nonionic surfactant concentration range, because even when the solution is pure surfactant the relative permittivity remains low. This low permittivity results in a large *Bjerrum length*, allowing for a favorable environment for the re-combination of the solvated ions into neutral ion-pairs, minimizing the overall conductivity of

the system. Furthermore, an examination of the relative permittivity data reinforces the conclusions drawn above, and the relationship between HLB number and conductivity.

As demonstrated in the alcohol-toluene solutions from **Section 3.1**, as amphiphile concentration increases, amphiphiles with higher relative permittivities have a greater impact on the overall conductivity of the system. This same relationship holds true for the nonionic Xiameter surfactants as well: OFX-5098 has a higher relative permittivity than OFX-0400 and accordingly yields higher conductivities as its concentration within the system increases.

3.4.3.3 Viscosity vs. Concentration of Xiameter Nonionic Surfactant

As revealed in ***Figure 16*** the relationship between viscosity and nonionic surfactant concentration for both Xiameter nonionic surfactant-toluene solutions is exponential across the entire concentration spectra (hence appearing linear when plotted on a logarithmic scale). While both Xiameter nonionic surfactants measured viscosities are roughly 10% lower than the manufacturers reported values, both viscosities of surfactnt still exhibited an exponential dependence on concentration as evidenced in ***Figure 16***. The reason for this deviation between reported and measured viscosity is possibly due to measurement technique: Canon-Fenske viscometers were used to make shear viscosity measurements in the experiments conducted within this work. The methods performed by the manufacturer to measure viscosity were not given.

In the experiments carried out in **Section 3.1**, viscosity of the alcohols was not measured directly, but rather estimated using a mole fraction-based average of the viscosities of the individual components, which was considered sufficient because the overall viscosities of the alcohols and nonpolar liquids were very close to begin with. However, in the case of these nonionic surfactants the difference in viscosity between pure toluene and pure surfactant varies by 2 orders of magnitude. Furthermore, it is clear from the graph, and the exponential

dependence displayed within, that using a mole fraction-based average would not have been adequate and would have instead yielded an incorrect approximation.

3.5 NON-IONIC SURFACTANTS: SPAN SURFACTANTS

Next the examination of nonionic surfactant as the amphiphile in two-component nonpolar systems was continued, switching from the Xiameter series of nonionic surfactants to the SPAN series of nonionic surfactants, manufactured by Sigma Aldrich. The SPAN surfactants are well-known nonionic surfactants based on the sorbitan molecule and are widely used in both research and commercial applications for such functions as an emulsifier, wetter, and stabilizer. A depiction of a sorbitain molecules can be found below in ***Figure 17***.

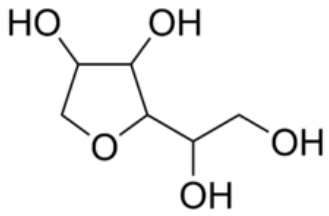

Figure 17*: Chemical Structure of a Sorbitan Molecule*[83]*.*

The specific SPAN surfactants chosen for these experiments were SPAN 20 and SPAN 80, which have the following properties:

Material	Chemical Name	Chemical Structure	Hydrophobic Tail	Molecular Weight	Viscosity (at 25°C) [Pa s]	HLB
SPAN-20	Sorbitan Monolaurate	$C_{18}H_{34}O_6$	C12	346.46	3.5	8.6
SPAN-80	Sorbitan Monooleate	$C_{24}H_{44}O_6$	C18	428.60	1.047	4.3

***Table 6**: Material Properties of SPAN-20 and SPAN-80 Nonionic Surfactants*

SPAN 20 is Sorbitan monolaureate, whereas SPAN 80 is Sorbitan Monooleate. The difference between these two molecules pertains to the fatty acid used as the hydrophobic part of the surfactant molecule. In the case of SPAN20, the surfactant is derived from lauric acid, whereas SPAN 80 is derived from oleic acid. Accordingly, they have different properties, including HLB number, conductivity, viscosity, and relative permittivity.

These nonionic surfactants also have very similar densities, and therefore comparing these two materials, and the conductivities of binary mixtures in which they are the amphiphile, allows us to further explore the effect that HLB number has on conductivity.

3.5.1 MATERIALS AND METHODS

Toluene was again chosen as the nonpolar liquid because both SPAN nonionic surfactants are miscible in toluene, allowing for the nonionic surfactant-toluene solutions to be easily measured at all concentrations, from pure toluene to pure SPAN nonionic surfactant. Additionally, keeping the nonpolar liquid consistent for all of the nonionic surfactant experiments allowed us not only to compare SPAN 80 to SPAN 20, but also to Xiameter OFX-5098 and OFX-0400.

Sample preparation was again carried out in the same fashion as **Section 3.1**. The *"reducing surfactant content"* approach was performed for mixtures with high concentrations of SPAN nonionic surfactant: from pure (100 wt. %) nonionic surfactant down to 50 wt. %. While the *"increasing surfactant content"* approach was performed for mixtures with low concentrations of SPAN nonionic surfactant: from pure toluene (0 wt. % surfactant) up to 50 wt. %. Accordingly, we saw sample overlap at 50 wt. % of SPAN nonionic surfactant, which again served as a meaningful check point to ensure solution reproducibility and confirm solution formulation accuracy throughout the preparation process independent of the solutions preparation path.

Next, conductivity, relative permittivity, and viscosity measurements were taken for each SPAN nonionic surfactant-toluene solution across the entire concentration spectra. Experiments in this section were performed in the same fashion as with the Xiameter series in **Section 3.4** with all three measurements taken on each solution in succession, avoiding the need for excess sample preparation (i.e. performing titrations) for each measurement. As a result, material waste was minimized and the potential for human error during sample preparation decreased. The measurements performed on these samples (conductivity, relative permittivity, and viscosity) are all classified as "non-destructive measurement techniques", so performing the experiments in this fashion had no adverse impact on the data collected.

Sample setup was consistent with the sample setup described in ***Sections 3.1*** and ***3.2*** to minimize evaporation of mixture components.

3.5.2 RESULTS

Figure 18a and ***Figure 18b*** illustrate the conductivity curves as a function of concentration of nonionic surfactant for the two SPAN nonionic surfactant-toluene solutions, on linear and logarithmic scales, respectively. The data is displayed on both scales because the range of conductivities is so large that each scale is better suited for examining a different end of the concentration spectrum.

Figure 19 shows the relative permittivity curves as a function of concentration of nonionic surfactant for the two SPAN nonionic surfactant-toluene solutions.

Figure 20 shows the viscosity curves as a function of concentration of nonionic surfactant for the two SPAN nonionic surfactant-toluene solutions.

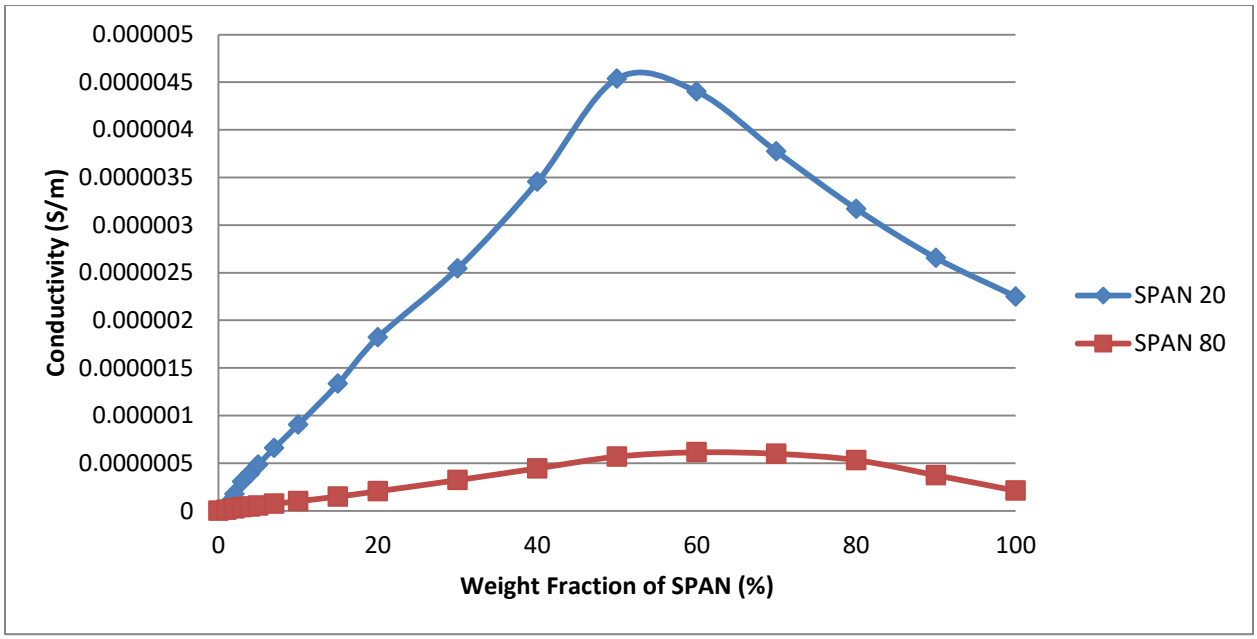

***Figure 18a**: Conductivity versus Concentration of Nonionic SPAN Surfactant for Nonionic SPAN Surfactant-Toluene Solutions. Legend Denotes Nonionic Surfactant in Solution. Linear Scale.*

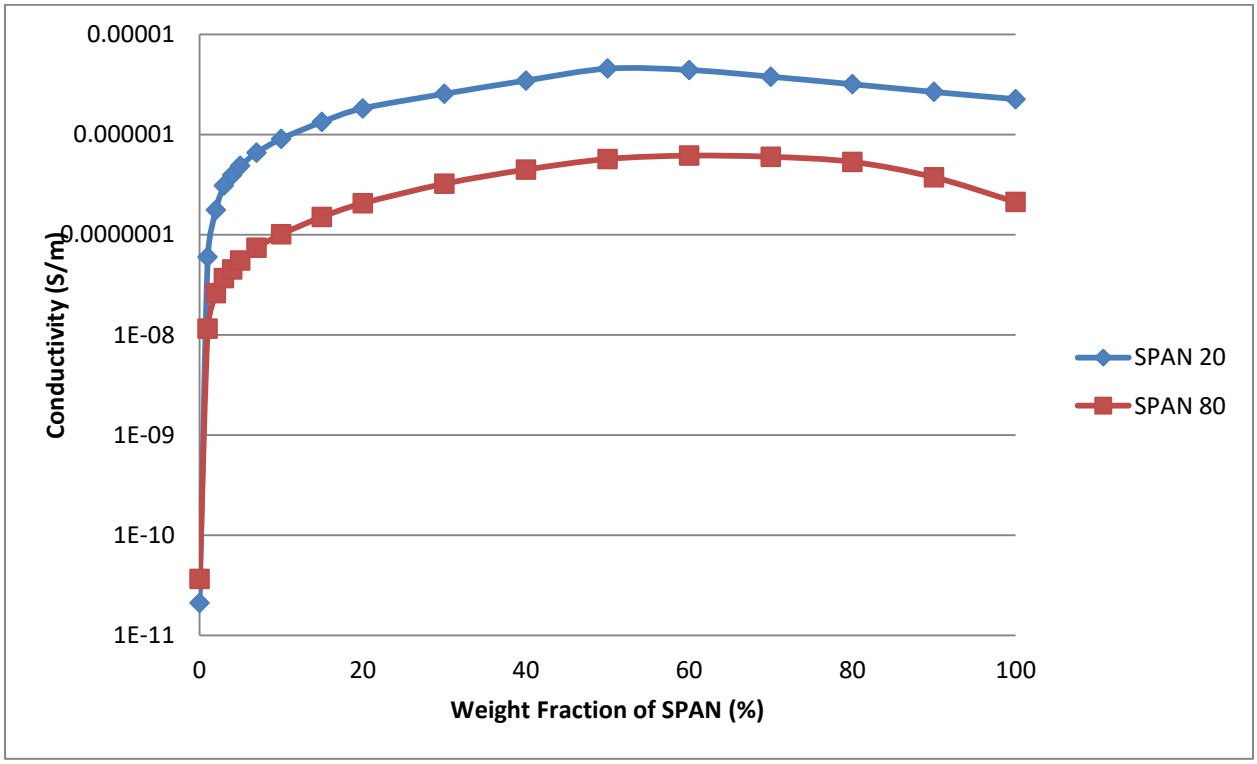

***Figure 18b**: Conductivity versus Concentration of Nonionic SPAN Surfactant for Nonionic SPAN Surfactant-Toluene Solutions. Legend Denotes Nonionic Surfactant in Solution. Logarithmic Scale.*

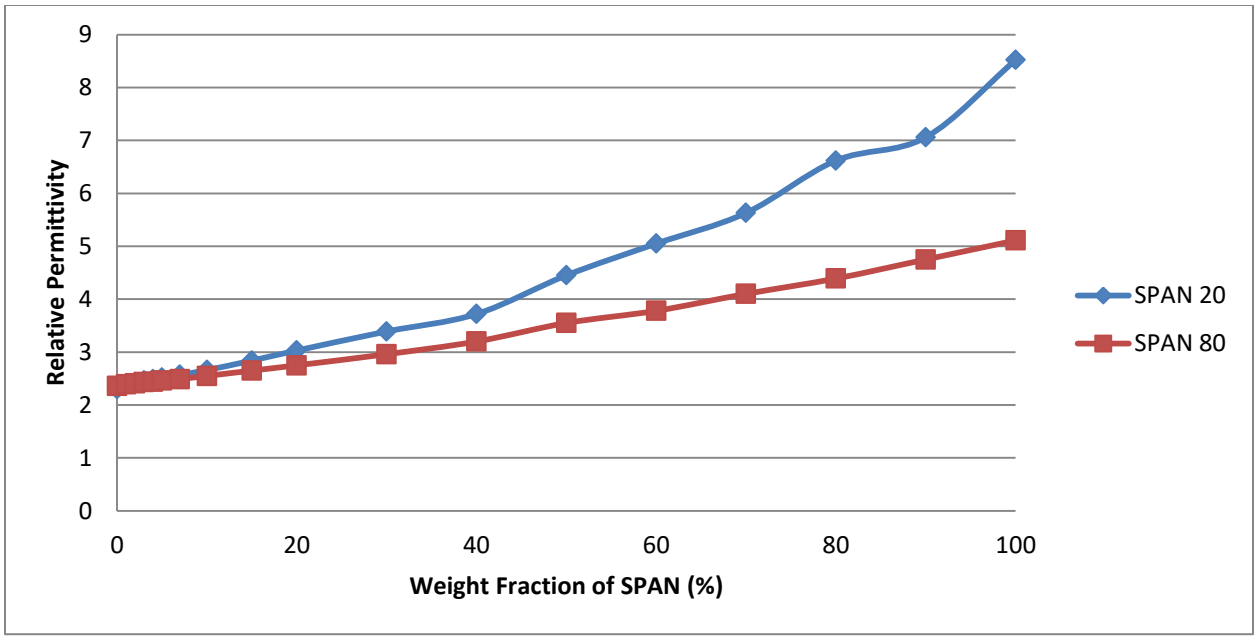

***Figure 19**: Relative Permittivity versus Concentration of Nonionic SPAN Surfactant for Nonionic SPAN Surfactant-Toluene Solutions. Legend Denotes Nonionic Surfactant in Solution. Linear Scale*

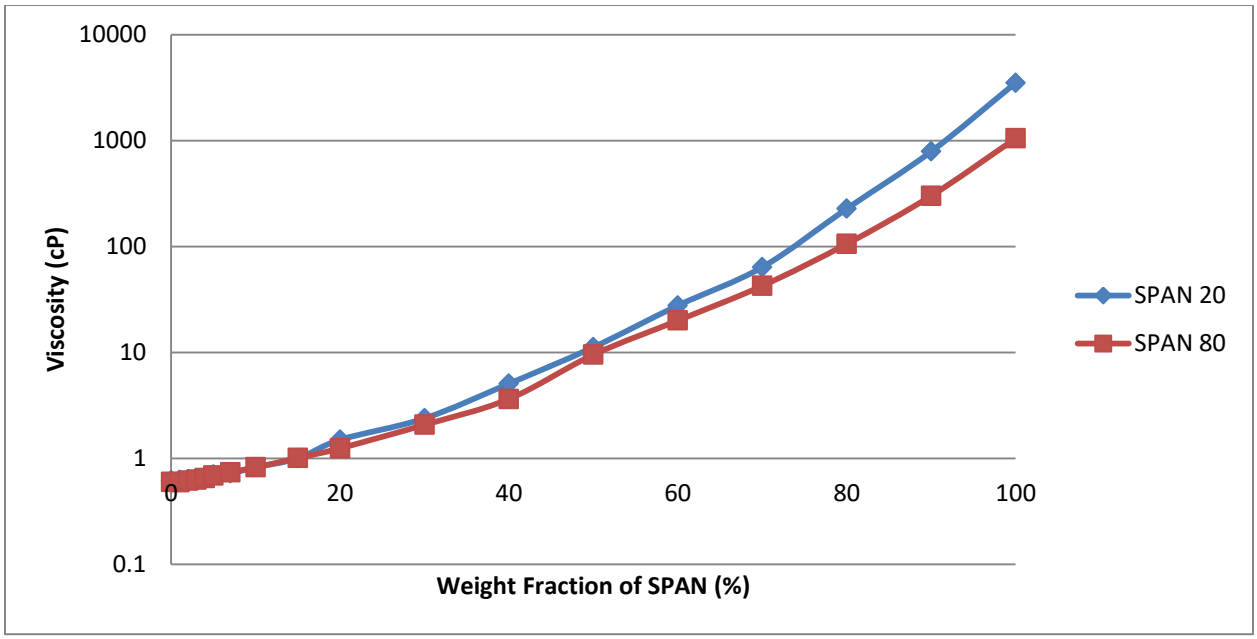

***Figure 20**: Viscosity versus Concentration of Nonionic SPAN Surfactant for Nonionic SPAN Surfactant-Toluene Solutions. Legend Denotes Nonionic Surfactant in Solution. Logarithmic Scale*

3.5.3 DISCUSSION

3.5.3.1 Conductivity vs. Concentration of SPAN Nonionic Surfactant

Past experiments using these materials implied there was a linear dependence of conductivity on concentration. However, those tests were limited in scope, measuring only at dilute concentrations of surfactant never going above 10 wt. %.

Figure 18a confirms the data from previous work that conductivity is a linear function at significantly low (<10 wt. %) nonionic surfactant concentration for binary mixtures in which SPAN 20 or SPAN 80 is the amphiphile. However, as seen in ***Figure 18b***, as SPAN concentration increases (>10 wt. %) within these nonpolar solutions this linear relationship between conductivity and concentration no longer exists. Additionally, an interesting trend in the data begins to emerge in ***Figure 18a*** at the SPAN nonionic surfactant concentration range of roughly 40 wt. %, in which conductivity actually starts to decrease as concentration of SPAN continues to increase. This data is in direct agreement with a phenomenon observed many years ago by Plotnikov, who showed that the conductivity of a solution can be higher than that of either of its individual components. This finding by Plotnikov is further substantiated by our data in the 40-60 wt. % SPAN concentration range for both nonpolar solutions where the conductivity of the system is higher than that of pure toluene or pure SPAN nonionic surfactant. While we did not see this exact same trend in **Section 3.4** with the Xiameter surfactants, we did notice that the rate at which conductivity increases as a function of Xiameter surfactant concentration did diminish at very high concentrations.

We currently do not have an answer as to why these phenomena occur, but we do have some hypotheses as to why it might happen. Firstly, these nonionic surfactants are very viscous, and so the overall viscosity of the mixture increases significantly as we get to higher concentrations of surfactant. Viscosity impedes upon mobility of the ions in solution, which

may inhibit the overall conductivity in such a way as was measured. Furthermore, these surfactants are non-Newtonian liquids, and so their viscosity is not constant, but rather a function of the stress applied upon them. This as well could be responsible for some of the behavior we see in the conductivity curves, or possibly why there is deviation from the applied model, as will be discussed in a later section.

3.5.3.2 Relative Permittivity vs. Concentration of SPAN Nonionic Surfactant

As seen in earlier sections, where alcohols and Xiameter non-ionic surfactants served as the amphiphiles in the nonpolar systems, ***Figure 19***, also shows relative permittivity as a linear function of SPAN nonionic surfactant concentration in the SPAN-toluene solutions investigated herein. The relative permittivities of pure SPAN 20 and pure SPAN 80 are 8.52 and 5.11 respectively. As discussed with regards to the Xiameter surfactants in **Section 3.4**: the amphiphile with the higher HLB number had the higher relative permittivity, resulting in a higher conductivity for the SPAN 20-toluene solution across the entire SPAN 20 concentration range, than that of the SPAN 80-toluene solution.

3.5.3.3 Viscosity vs. Concentration of SPAN Nonionic Surfactant

The viscosity data plotted in ***Figure 20*** shows the relationship between viscosity and SPAN concentration was exponential, not linear for both SPAN-toluene solutions. Additionally, the viscosity data for both SPAN 20 and SPAN 80 are nearly identical across the entire concentration spectra, which varied over three orders of magnitude from pure toluene to pure SPAN surfactant.

Referring back to the conductivity data illustrated in ***Figures 5***, ***10a***, ***10b***, ***14a*** and ***14b***, in which the amphiphile was an alcohol or Xiameter nonionic surfactant, an exponential dependence is reported between conductivity and concentration at low concentrations of amphiphile. However, in the SPAN nonionic surfactant solutions a linear dependence is

reported between conductivity and concentration at low concentrations of amphiphile. This contradiction in data forces us to question whether or not ion-pair formation exists in these solutions at low concentrations of SPAN nonionic surfactant, or if it exists at all in these SPAN-toluene nonpolar systems.

To better understand the driving force behind this interesting finding, further investigation into the role that viscosity plays in the conductivity of these systems is required. For starters, the viscosity of both SPAN 20 and SPAN 80 is over 1,000 times greater than that of pure toluene. Given that an increase in viscosity limits ion mobility, and thus diminishes conductivity in a nonpolar system, it can be postulated that in solutions with incredibly high viscosities this dependence of conductivity on concentration is forced to shift from exponential to linear. The *Walden Rule*, which takes into consideration the impact viscosity has on a system, can therefore be used to confirm (i) whether or not ion-pairs are present in these SPAN-toluene solutions and (ii) validate whether or not the previous assumption on the shift in conductivity dependence on concentration has any merit. Accordingly, the *Walden Rule* states that conductivity multiplied by viscosity ($K^*\eta$) is a linear function of concentration if no ion-pairs are present[84]. Consequently, ***Figure 21*** shows conductivity multiplied by viscosity for both the SPAN-toluene solutions as well as the Xiameter-toluene solutions.

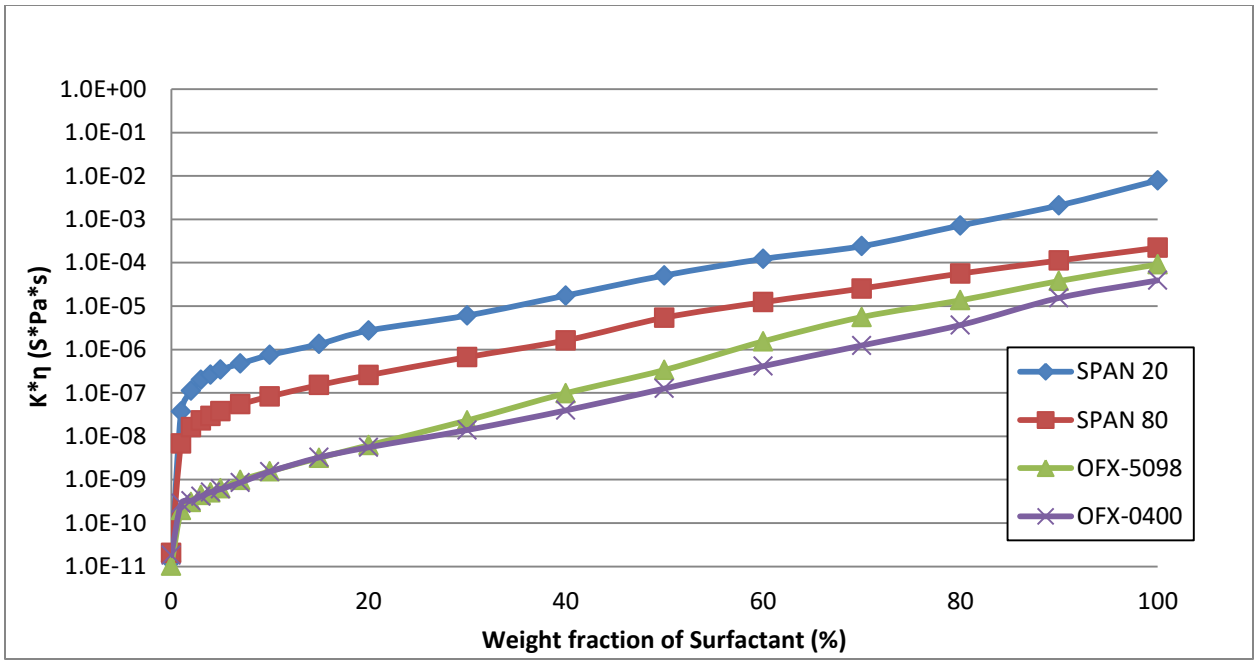

***Figure 21**: "Walden Rule" plot of Conductivity multiplied by Viscosity versus Concentration of Nonionic Surfactant for Nonionic Surfactant-Toluene Solutions. Legend Denotes Nonionic Surfactant in Solution. Logarithmic Scale*

Figure 21shows that in the case of all four nonionic surfactant-toluene solutions, the "Walden plots" (conductivity (K) of the solution multiplied by the viscosity (η) of the solution) are exponentially, not linearly, dependent on surfactant concentration. Based on the *Walden Rule*, this exponential relationship indicates that ion-pairs are present in all four solutions. Conversely, in the case of the alcohol-toluene solutions in **Section 3.1**, at high amphiphile concentrations a linear dependence between conductivity and amphiphile concentration was observed, implying that ion-pairs were not forming in those solutions (due to shorter *Bjerrum lengths*) and conductivity continues to increase in that concentration range. While, in the case of the highly viscous nonionic surfactants, as surfactant concentration increases, so does the solutions viscosity and in turn the systems ion-mobility is further limited, resulting in an additional decrease in the conductivity of these systems in that concentration range.

Lastly, conductivity plotted versus viscosity can provide additional insight into the relationship between the two:

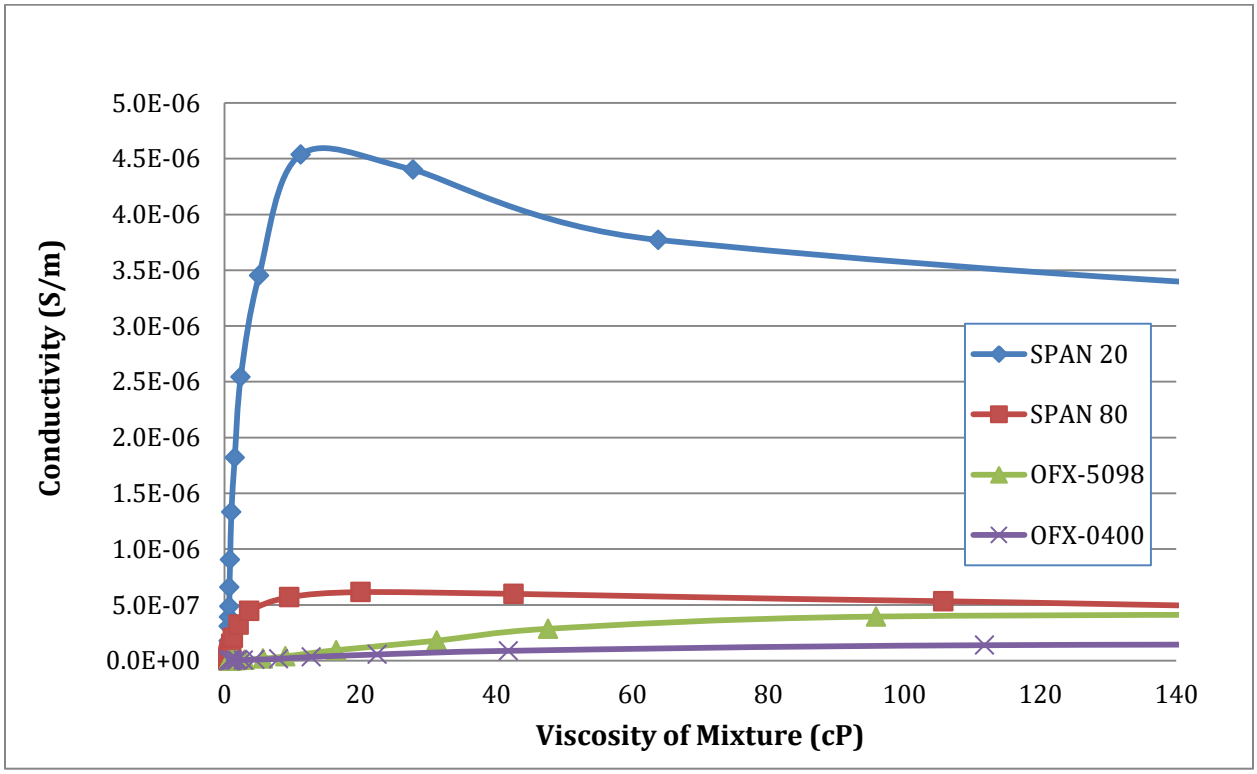

***Figure 22a**: Conductivity versus Viscosity of Mixture for Mixtures of Toluene with Non-ionic Surfactant as Amphiphile. Viscosity range is limited to 140 cP in order for trends to be better visible. Legend Denotes Nonionic Surfactant in Solution. Linear Scale*

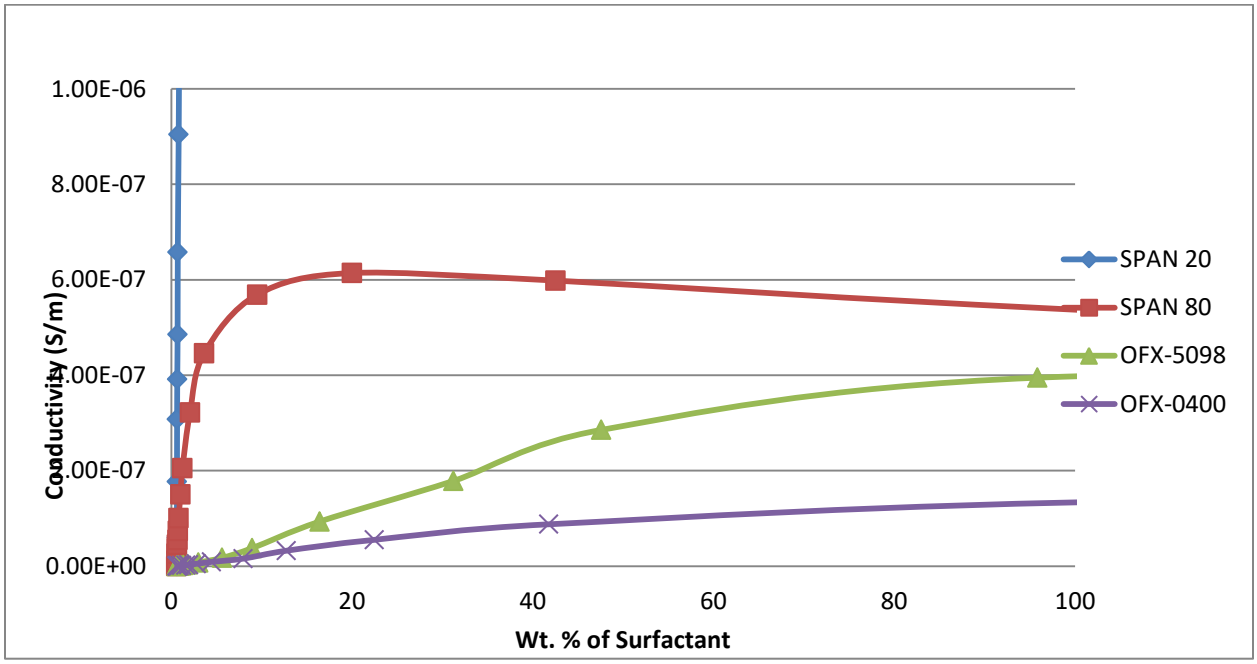

***Figure 22b**: Conductivity versus Viscosity of Mixture for Mixtures of Toluene with Non-ionic Surfactant as Amphiphile. Viscosity range is limited to 140 cP in order for trends to be better visible. Conductivity range is limited to 1E-06 S/m in order to display trends of mixtures with Non-ionic surfactants other than SPAN 20. Linear Scale*

Figures 22a and ***22b*** show the relationship between conductivity and viscosity for nonpolar media with added nonionic surfactant as amphiphile. In both graphs the range of viscosity is limited to display the prominent parts of the graphs for all data. Beyond 140 cP conductivity continues to decrease as a function of concentration for mixtures in which both SPAN 20 and SPAN 80 are the added amphiphile. ***Figure 22b*** limits conductivity range to 1E-06 S/m in order to display the trends of mixtures with nonionic surfactants other than SPAN 20.

The data in ***Figures 22a*** and ***22b*** show that there is no single trend across all four mixtures. Mixtures of toluene with SPAN surfactants showed a critical viscosity at which conductivity reaches a maximum, beyond which conductivity decreases as a function of concentration. This critical viscosity implies that there is a concentration of added SPAN surfactant at which the balance between concentration of free solvated ions in solution (which increase as a function of surfactant concentration), and mobility of said ions in solution (which decreases as a function of concentration due to increased viscosity), yields the highest conductivity.

For mixtures of toluene with Xiameter nonionic surfactants no such critical viscosity exists: Conductivity continues to increase as viscosity increases, reaching a maximum when the solution is pure nonionic surfactant, when both conductivity and viscosity are highest.

3.5.3.4 Overlay of All Toluene-Amphiphile Graphs

Figures 23 and ***24***, presented below, overlay the data for all mixtures of nonpolar media with added amphiphile with toluene as the nonpolar liquid. ***Figure 23*** shows relative permittivity plotted versus concentration for all 8 alcohols as amphiphile, as well as all 4

nonionic surfactants as amphiphile. ***Figure 24*** displays the graphs of conductivity versus concentration for the same 12 mixtures.

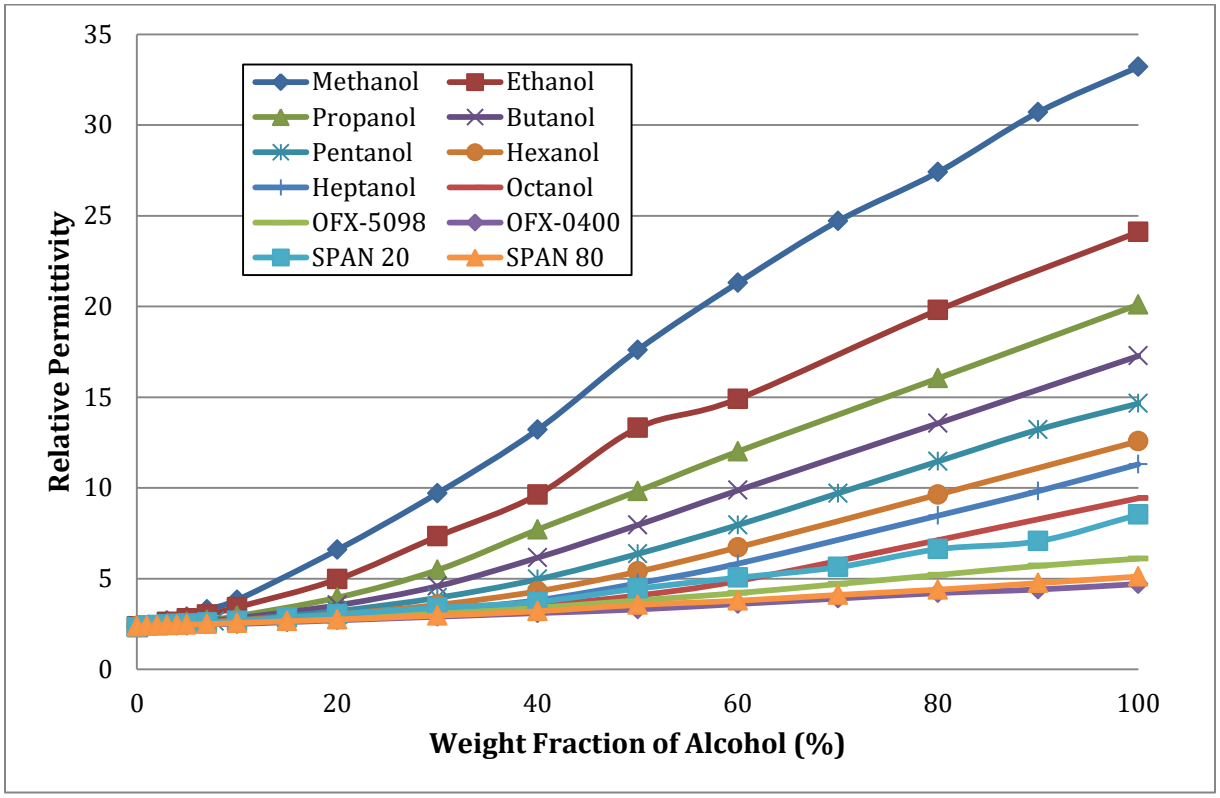

Figure 23: *Relative Permittivity versus Concentration of Amphiphile for All Amphiphile-Nonpolar Liquid Solutions. Nonpolar liquid is Toluene for all solutions. Legend Denotes Amphiphile in Solution. Linear Scale*

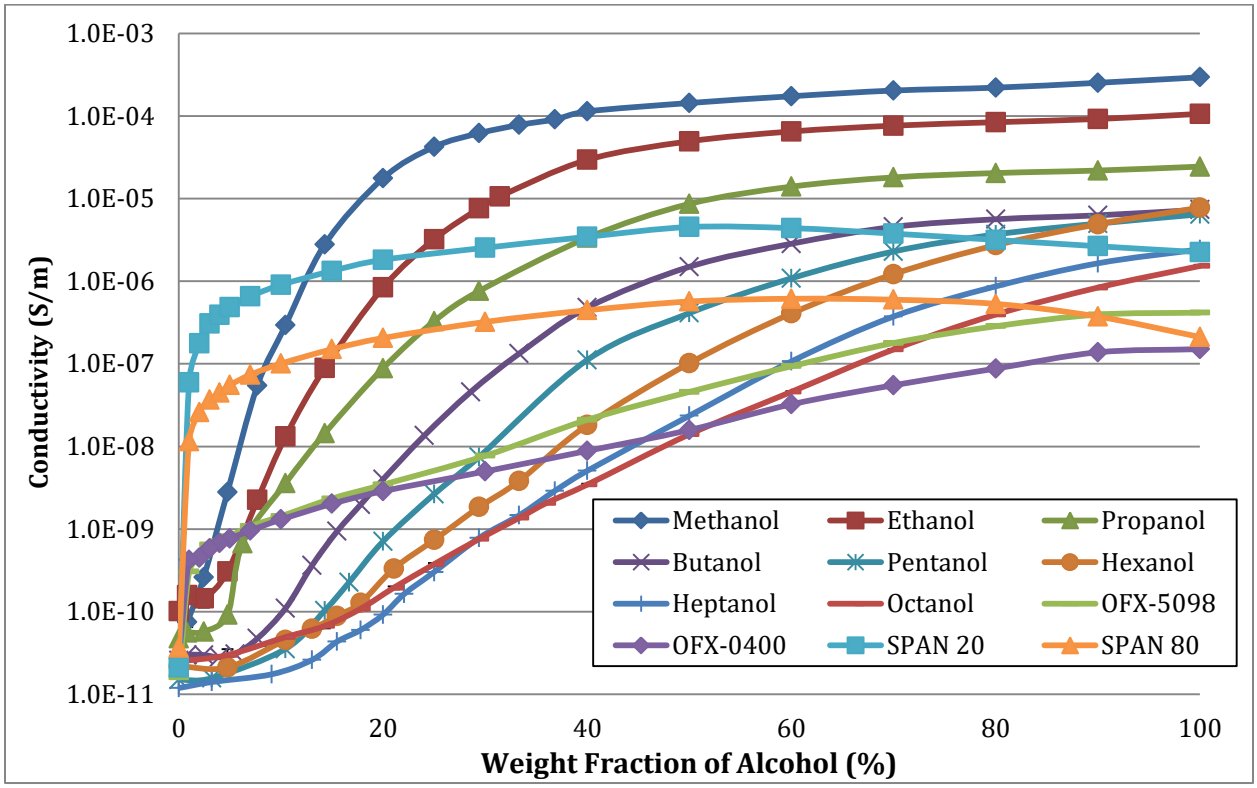

Figure 24: *Conductivity versus Concentration of Amphiphile for All Amphiphile-Nonpolar Liquid Solutions. Nonpolar liquid is Toluene for all solutions. Legend Denotes Amphiphile in Solution. Logarithmic Scale*

Figure 23 shows a linear dependence of relative permittivity on concentration of added amphiphile for all 12 mixtures studied. ***Figure 24*** shows that the relationship between conductivity and concentration is more complex and not consistent across all mixtures of toluene with added amphiphile. Conductivity is impacted both relative permittivity and viscosity. Relative permittivity affects Bjerrum length, which dictates whether ion-pairs form in solution or not. For the mixures in which the added amphiphile is alcohol, viscosity effects are minimal due to the small variation in viscosity between mixture components. Regions of linear and non-linear dependence of conductivity on concentration of added amphiphile are observed.

For mixtures in which the added amphiphile is nonionic surfactant, viscosity differences between mixture components are substantial (i.e. the viscosity of nonionic surfactant is orders of magnitude higher than that of nonpolar toluene). Increased viscosity serves to limit ion mobility, decreasing conductivity in these systems. Such effects are responsible for the linear dependence of conductivity on concentration seen for mixtures of SPAN surfactants and toluene (see ***Section 3.5.3.3***), and justify the use of Walden Plots versus concentration for examining conductivity in these systems.

3.6 ION-PAIR CONDUCTIVITY MODEL (IPCM): THEORETICAL MODEL VS. EXPERIMENTAL DATA

The experimental data put forth in the previous sections demonstrates our ability to measure the conductivity (as well as relative permittivity and viscosity) of two-component mixtures of amphiphile and nonpolar liquid and the role that parameters such as viscosity, relative permittivity, and HLB number play in the overall conductivity of these systems. Data from ***Figures 4***, ***15***, and ***19*** showed a linear relationship between amphiphile concentration and relative permittivity, while ***Figures 16*** and ***20*** showed an exponential relationship between amphiphile concentration and viscosity. The relationship between amphiphile concentration and conductivity proved more complex.

Next, the ability of the *Ion-Pair Conductivity Model* to accurately model the relationships found in the experimental data put forth in **Sections 3.1-3.5** from the alcohol-toluene and nonionic surfactant-toluene studies must be examined. The goal of this comparison is to provide an assessment of the validity of the *Ion-Pair Conductivity Model*, the methodology used and the resulting data in order to determine the value of this technique as a robust model for predicting conductivity in nonpolar systems and as a tool to further investigate the mechanisms by which ionization in nonpolar media occur.

Accordingly, the *Ion-Pair Conductivity Model (IPCM)*, ***Eq. 59***, states conductivity is defined as:

$$\boldsymbol{K = \frac{eF}{4\pi^2 \eta N_A a^4}\left(\sqrt{1 + \frac{16}{3}\pi N_A a^3 \varphi C_A e^{\lambda/a}} - 1\right) EXP\left(\frac{-\lambda}{a}\right)}$$

Where, ion size, $\boldsymbol{a}$, and the total ionic concentration of the amphiphile, $\boldsymbol{C_A}$, serve as the variable parameters.

3.7 IPCM VS. ALCOHOL-TOLUENE SOLUTIONS

In the case where the amphiphile was an alcohol, ***Figure 5***, three distinct behaviors were observed in all eight alcohol-toluene solutions across the entire alcohol concentration spectra: at a low alcohol concentration range conductivity was exponentially dependent on concentration, at a high alcohol concentration range conductivity was linearly dependent on concentration, and an intermediate region (i.e. an inflection point) between the two.

3.7.1 RESULTS

Please note, the theoretical analysis carried out in this section focuses on conductivity specifically, and accordingly uses experimental relative permittivity data to that end. The determined values for the concentration of ions in the pure amphiphile $\boldsymbol{C_A}$, and distance of closest ion approach ***a*** are presented in ***Table 7***.

Figures 25 a-h illustrate the theoretical vs. experimental conductivity curves for all eight alcohol-toluene solutions.

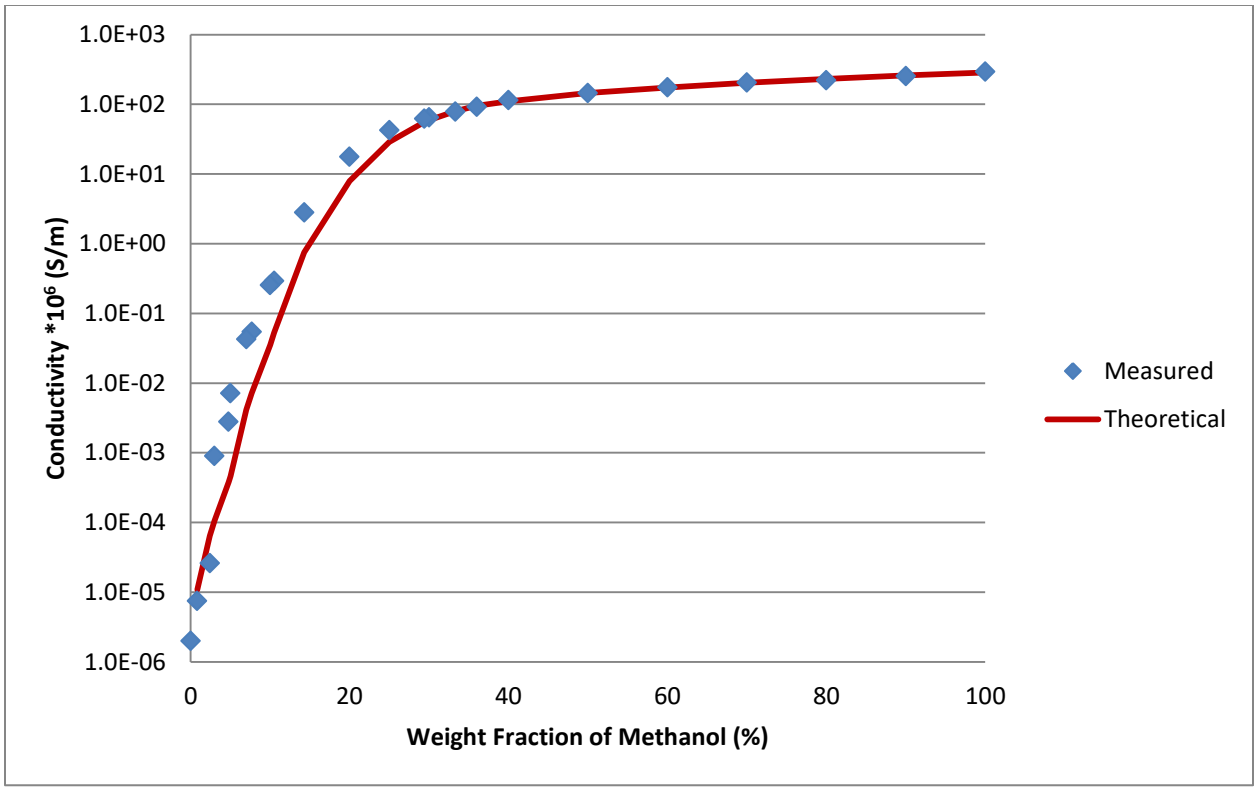

***Figure 25a**: Ion-Pair Conductivity Theoretical Fitting of Alcohol-Toluene Solution: Methanol. Logarithmic Scale*

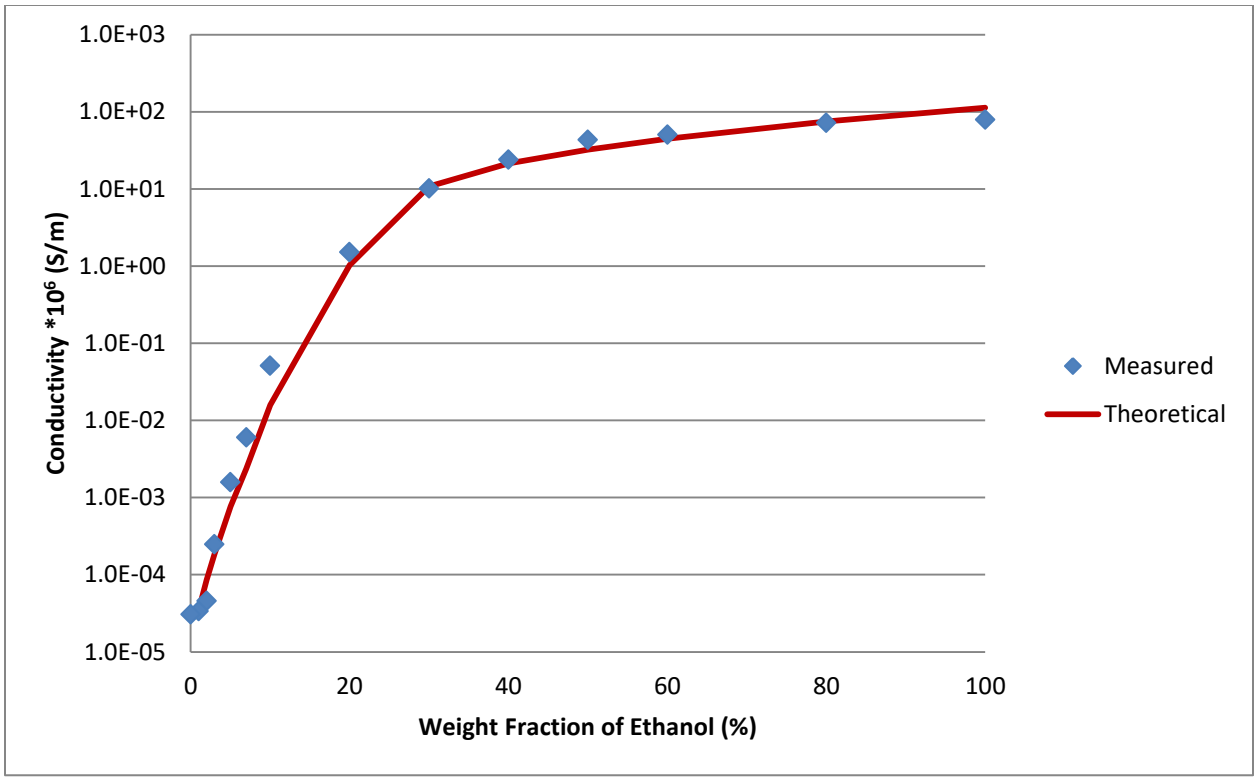

***Figure 25b**: Ion-Pair Conductivity Theoretical Fitting of Alcohol-Toluene Solution: Ethanol. Logarithmic Scale*

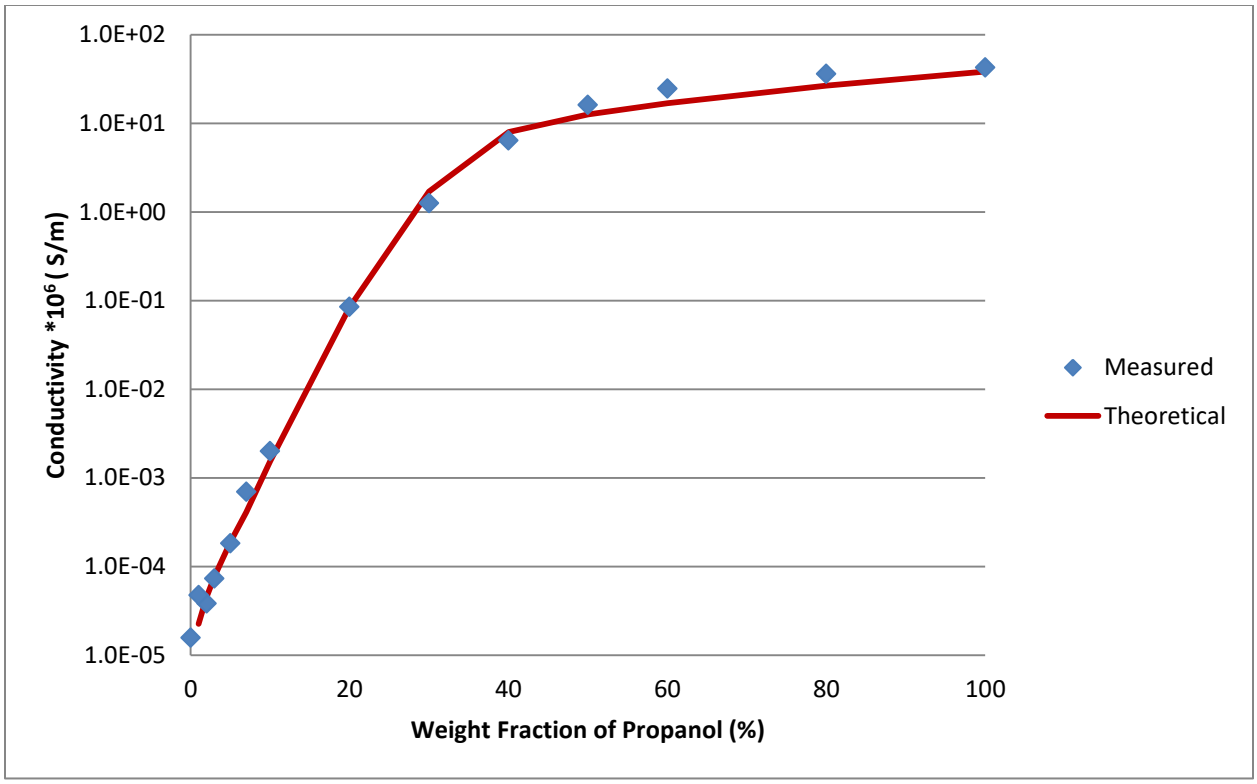

***Figure 25c**: Ion-Pair Conductivity Theoretical Fitting of Alcohol-Toluene Solution: Propanol. Logarithmic Scale*

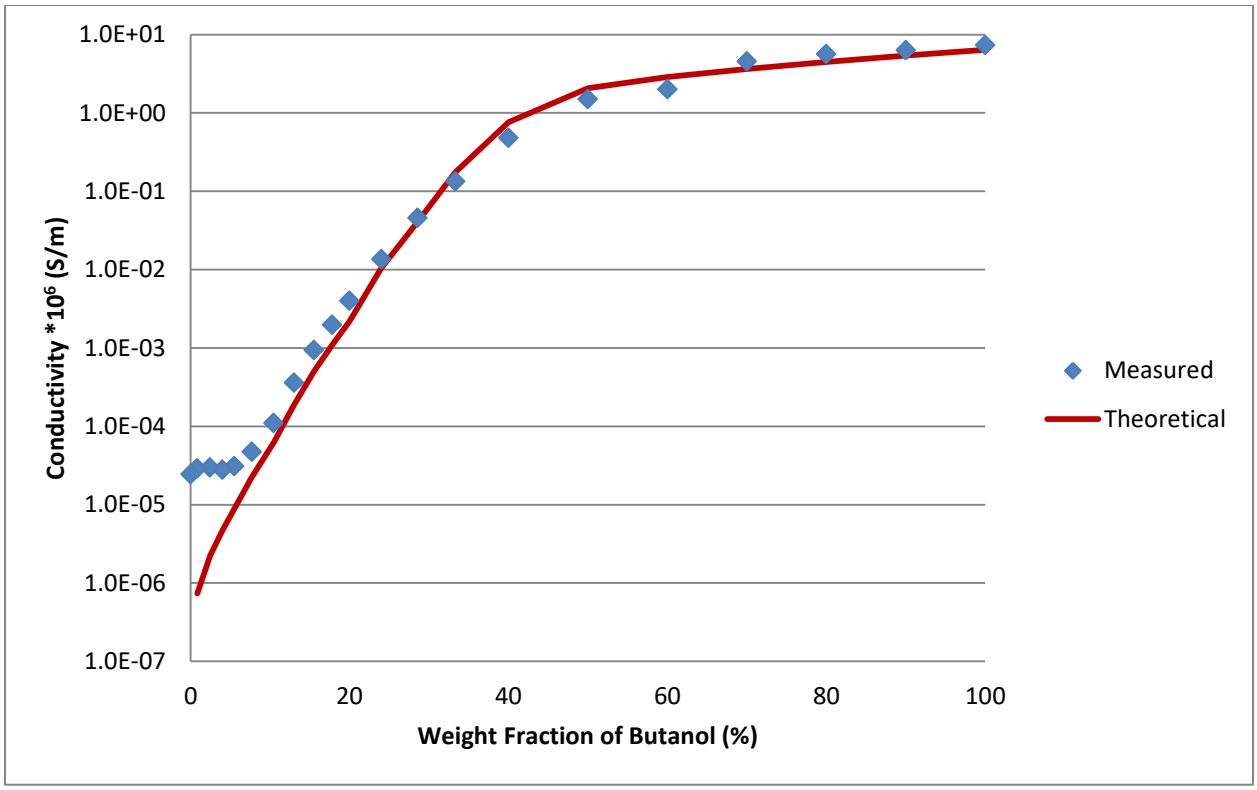

***Figure 25d**: Ion-Pair Conductivity Theoretical Fitting of Alcohol-Toluene Solution: Butanol.*

Logarithmic Scale

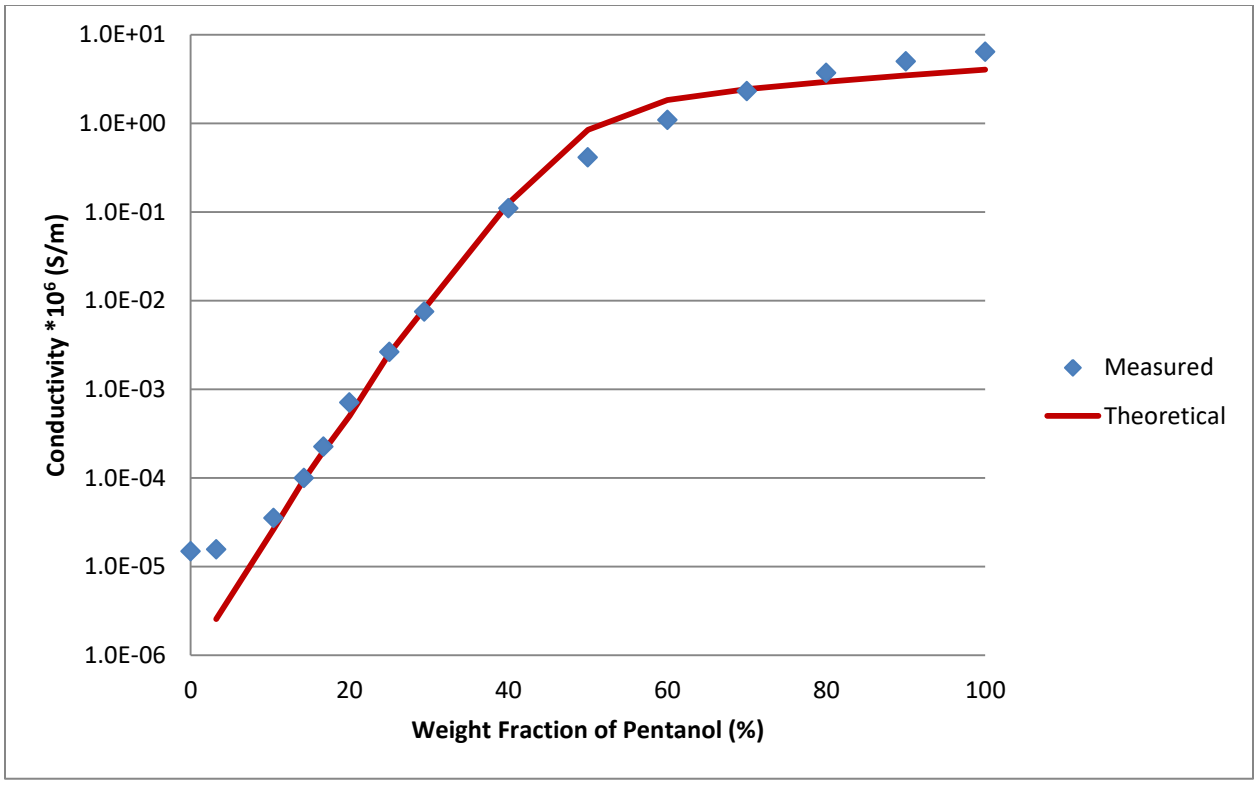

***Figure 25e**: Ion-Pair Conductivity Theoretical Fitting of Alcohol-Toluene Solution: Pentanol. Logarithmic Scale*

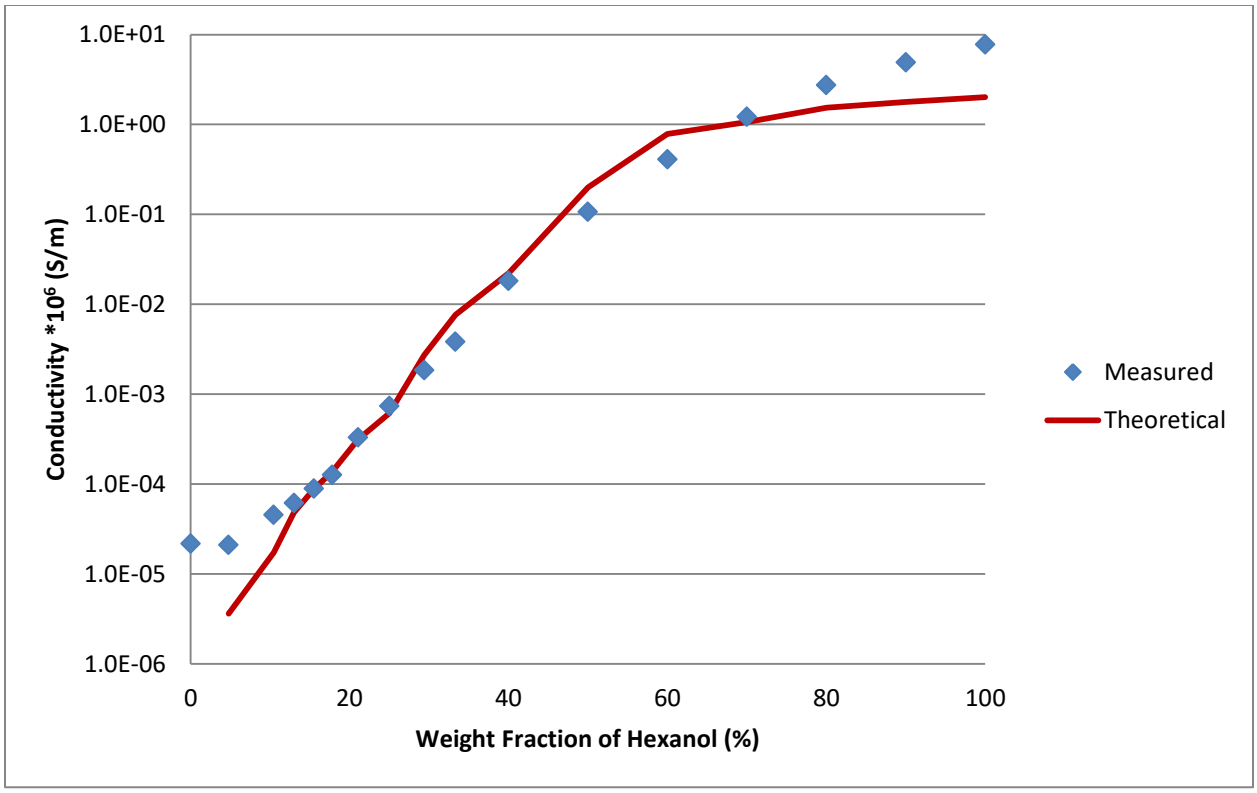

***Figure 25f**: Ion-Pair Conductivity Theoretical Fitting of Alcohol-Toluene Solution: Hexanol. Logarithmic Scale*

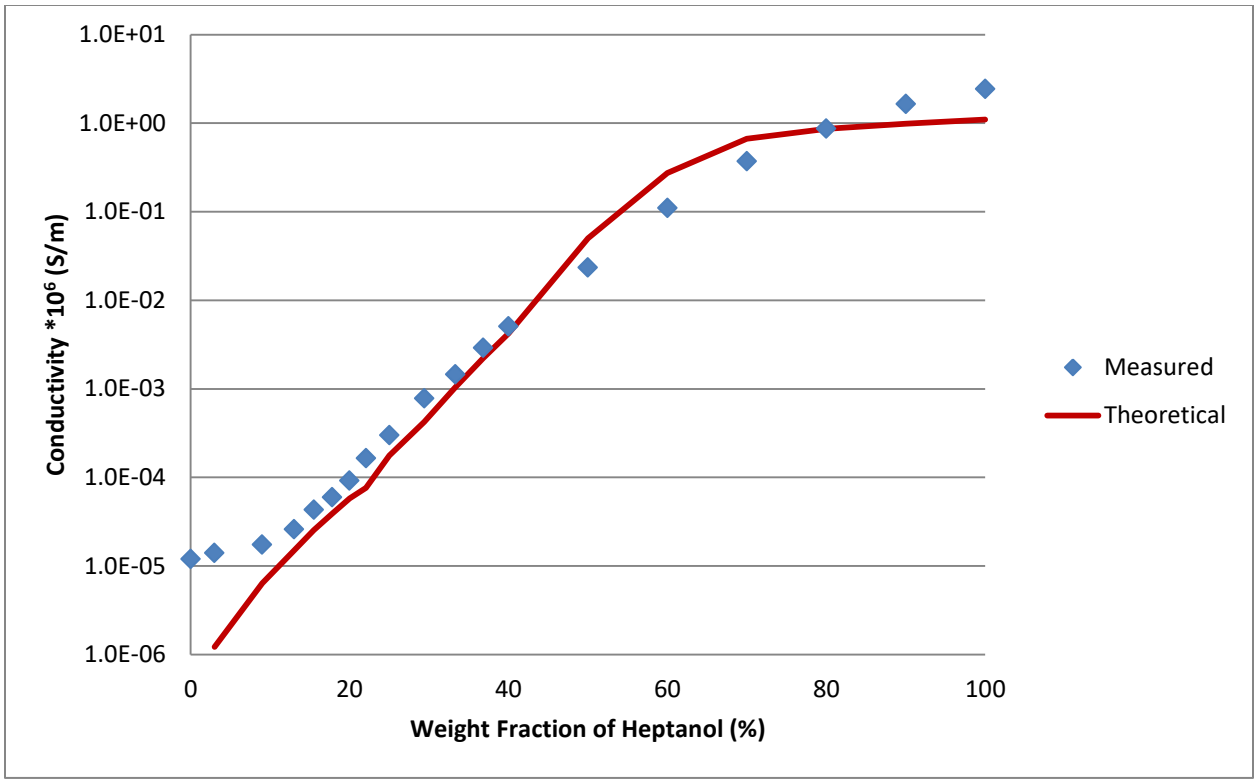

***Figure 25g**: Ion-Pair Conductivity Theoretical Fitting of Alcohol-Toluene Solution: Heptanol. Logarithmic Scale*

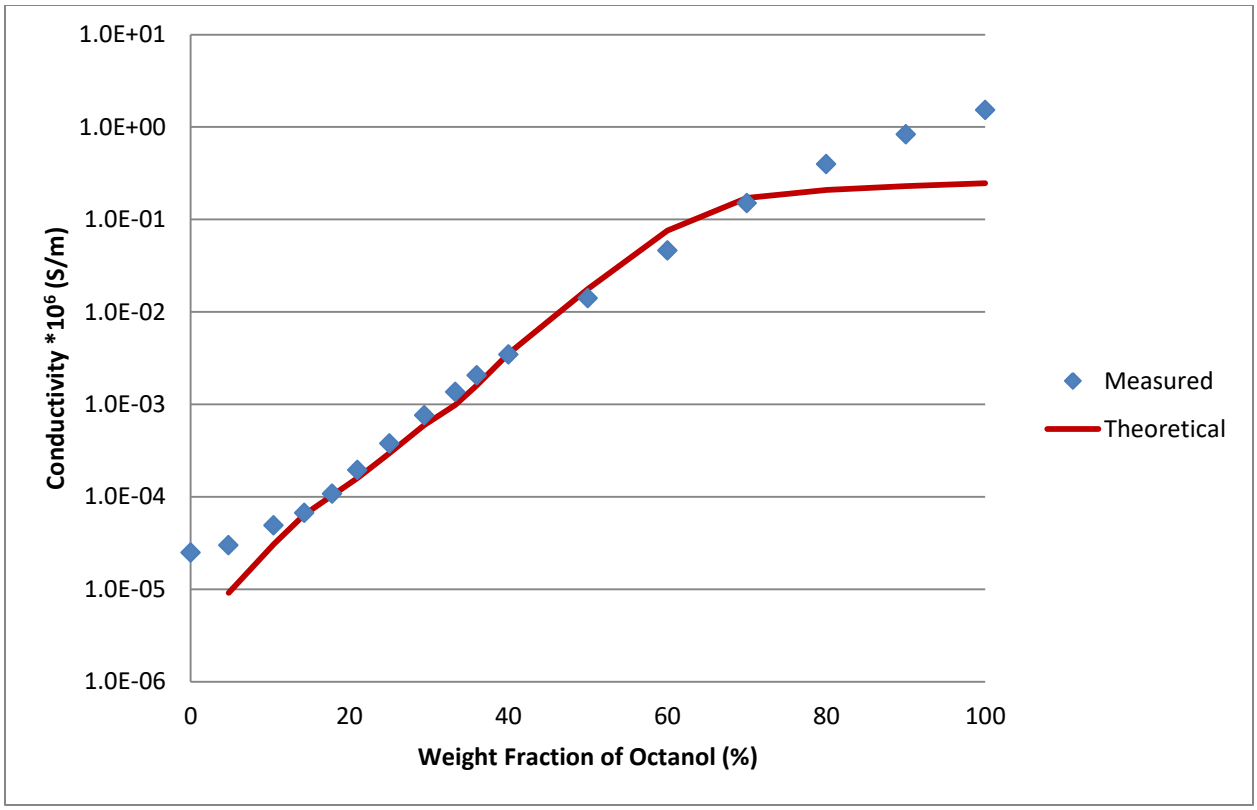

***Figure 25h**: Ion-Pair Conductivity Theoretical Fitting of Alcohol-Toluene Solution: Octanol. Logarithmic Scale*

	a [nm]	d_h [nm]	C_a [10^{-6} mol/l]
methanol	0.63	0.63	290
ethanol	0.61	0.61	135
propanol	0.6	0.6	8
butanol	0.56	0.56	1
pentanol	0.54	0.54	1
hexanol	0.54	1.08	2
heptanol	0.57	1.14	1
octanol	0.63	1.26	1

***Table 7**: Hydrodynamic Radii and Distance of Closest Ion Approach for Alcohols*

3.7.2 DISCUSSION

Figures 25 a-h show that the theoretical model and experimental data were in good agreement with one another for all eight alcohol-toluene solutions. Some variation in the quality of the fit is seen as the length of the carbon chain in the alcohol increases, from methanol to octanol. Using ***Figure 25a*** for reference, we see that the *IPCM* theoretical model is able to fit the experimental data across seven orders of magnitude, from $10E^{-11}$ to $10E^{-4}$ S/m.

For the *IPCM* curves in ***Figures 25 a-h***, only one, not both the distance closest ion approach, $\boldsymbol{a}$, and hydrodynamic radius, $\boldsymbol{d_h}$, of the size variables from ***Table 7*** was used. The assumption made, according to ***Eq. 57***, states:

$$\boldsymbol{d_h = a}$$

However, as stated earlier, ***Eq. 57*** is not perfect, and it is not necessarily true that distance of closest ion approach, $\boldsymbol{a}$, and hydrodynamic radius, $\boldsymbol{d_h}$, are equal. While, according to ***Table 7***, for the methanol, ethanol, propanol, butanol and pentanol solutions, it appears these two values are in fact equal, there was simply not enough information contained within the graph to discern any differences between $\boldsymbol{a}$ and $\boldsymbol{d_h}$ for this group of shorter chain alcohols.

Yet, for the three longer chain alcohol solutions (i.e. hexanol, heptanol, and octanol), we assume $\boldsymbol{a}$ to be proportional to, rather than equal to, $\boldsymbol{d_h}$, according to an arbitrary multiplier, $\boldsymbol{R}$, according to ***Eq. 58***, which states:

$$\boldsymbol{d_h = Ra}$$

By solving for $\boldsymbol{R}$ we were able to further understand and differentiate between the size variables $\boldsymbol{a}$ and $\boldsymbol{d_h}$.

Interestingly, as seen in ***Table 7***, the distance of closest ion approach, $\boldsymbol{a}$, for all alcohols, independent of carbon chain length, is approximately 0.6 nm. Even when modifying the search routine, this value of 0.6 nm was repeatedly found to be the best solution. We believe that the

rationale behind this nearly identical approximation for $\boldsymbol{a}$, across all eight alcohol-toluene solutions, is based on the work carried out by Izutsu and his subsequent theory on "solvent shared ion-pairs." According to Izutsu's theory, the solvating layers for ions created by an amphiphiles molecules are not necessarily rigid; they can instead be soft and malleable/compressible. All of the eight alcohol molecules investigated herein are on the scale of 0.4-0.5 nm, with little to no deviation in size from the shortest carbon chain alcohol (methanol) to the longest (octanol). And so, according to Izutsu's description of partially overlapped soft solvating layers[30], if the ion is solvated by a single molecule layer, the size of the solvated ion should not exceed twice the length of the molecule itself (i.e. in this case the length should not exceed 1 nm).

Unfortunately, the second adjustable variable of the *Ion-Pair Conductivity Model*, the concentration of ions in the pure alcohol, $\boldsymbol{C_A}$, is significantly dependent upon the size variables ($\boldsymbol{a}$ and $\boldsymbol{d_h}$) of the solution, making its impact on the conductivity of the system very difficult to study independently. The *Ion-Pair Conductivity Model* is not a reliable model for accurately determining $\boldsymbol{C_A}$, but rather serves as a first approximation. Therefore, in this case, the predicted value of $\boldsymbol{C_A}$ for the shorter chain alcohols, when the solution is pure amphiphile, is closely tied to the ionic strength of the system due to the lack of ion-pairs formed at 100 wt. % alcohol. While, based on their conductivity curves, the opposite appears to be true for the longer chain alcohols. For these longer chain alcohols, not all of the free ions represented by $\boldsymbol{C_A}$ will contribute to the conductivity of the system, due to the formation of neutral ion-pairs at pure amphiphile concentrations.

Further complicating what $\boldsymbol{C_A}$ represents in these nonpolar systems is the understanding that ions can also form in alcohols via an auto-dissociation process and/or via contamination to the liquid itself, either from water contamination or other foreign substance.

Accordingly, in the case of the *Ion-Pair Conductivity Model*, due to the low conducting nature of these systems, $\boldsymbol{C_A}$ is simply considered the total concentration of ions present in the nonpolar solution, regardless of the mechanism by which the ions formed (e.g. solvated alcohol ions or solvated ions from another source) because distinguishing between the two would be very difficult, if even possible, and would be of minimal use for practical application. Efforts were made to minimize contamination (i.e. using of anhydrous materials), but absolute avoidance of contamination was likely impossible in the laboratory setting. All in all, the conductivity curves of the theoretical model and the experimental data illustrated in ***Figures 25 a-h*** demonstrate the ability of the *Ion-Pair Conductivity Model* to accurately predict conductivity in two-component solutions of nonpolar liquid and alcohol. Furthermore, they reinforce the validity of the *Ion-Pair Conductivity Model* and *Dissociation Model* as a means for describing the phenomena by which ionization occurs in nonpolar solutions and emphasizes the importance that ion-pairs play in the conductivity of such systems.

3.8 IPCM VS. BUTANOL-NONPOLAR LIQUID SOLUTIONS

In **Section 3.2** the impact that nonpolar chemistry had on conductivity was examined by keeping the alcohol (i.e. butanol) constant and varying the nonpolar liquid (i.e. heptane, hexane, and toluene) within the solutions. It was hypothesized that the nonpolar chemistry would not have an impact on the conductivity of the mixtures. Through experimentation, this theory was confirmed, as evidenced by ***Figures 10***, wherein the conductivity curve data, for all three butanol-nonpolar liquid solutions produced the same results, regardless of the nonpolar liquid used in the mixture. The relative permittivities of all three nonpolar liquids (the parameter by which they are defined as nonpolar) are very similar, and all below 3. Therefore, the ability for ion-pairs for form, under the conditions of the same added amphiphile, is equally similar. These experimental results are in direct agreement with the *Ion-Pair Conductivity Model*, which argues that ion-pair formation (or the lack thereof) within nonpolar media dictates the conductivity of a system, not the chemistry of the nonpolar liquid. Accordingly, it is relative permittivity of the mixture (a function of the relative permittivity of the components of the mixture) which dictates whether or not ion-pairs are present.

3.8.1 RESULTS

Therefore, since the IPCM model was able to accurately predict the conductivity curve for the butanol-toluene solution in **Section 3.7** (***Figure 25d***), and given all three conductivity curves in ***Figures 10a*** and ***10b*** are aligned, it can be inferred that the *Ion-Pair Conductivity Model* is also capable of modeling the butanol-heptane and butanol-hexane solutions as well.

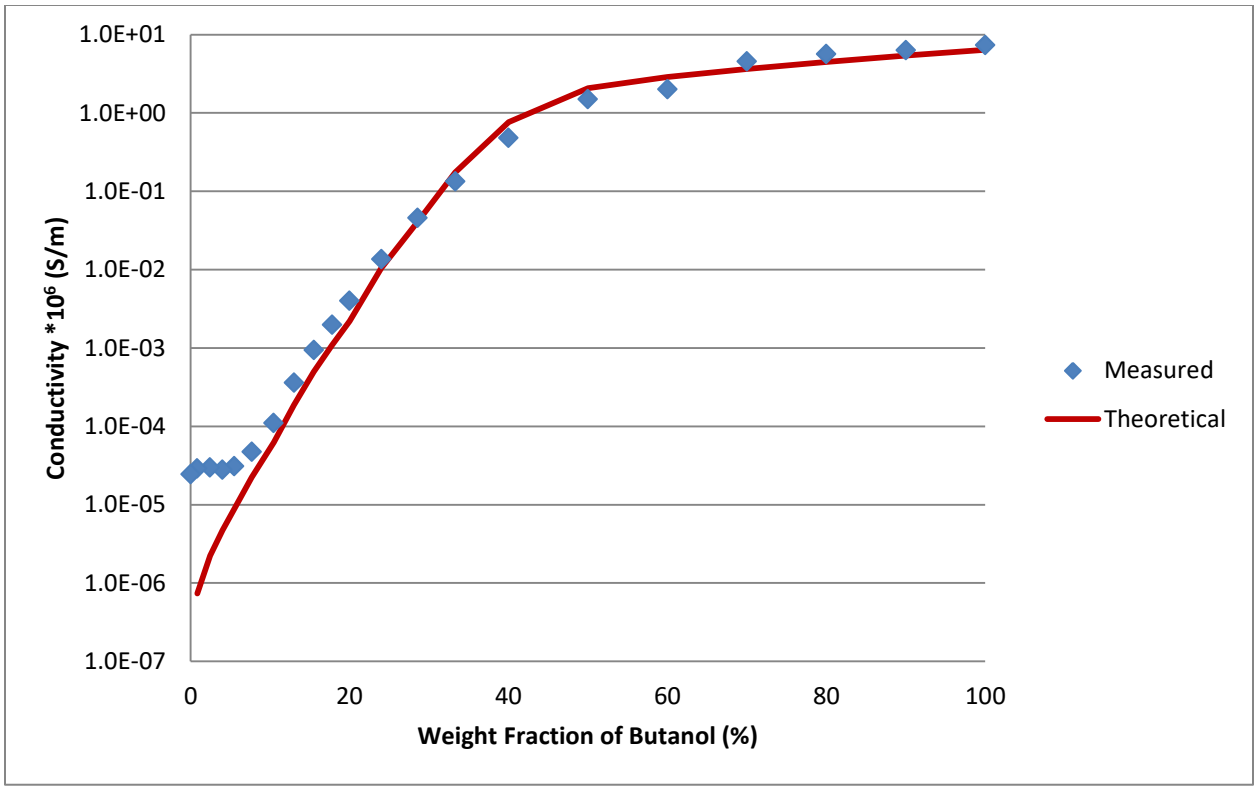

***Figure 26**: Ion-Pair Conductivity Theoretical Fitting of Alcohol-Toluene Solution: Butanol-Nonpolar Liquid Solution. Logarithmic Scale*

3.8.2 DISCUSSION

Figure 26 demonstrates how the experimental data from ***Figures 10a***, ***10b,*** and ***10c*** are able to be accurately predicted by the IPCM. In fact, as evidenced by ***Figure 10c***, both the butanol-heptane and butanol-hexane solutions report experimental conductivities of $1E^{-11}$ S/m at 0 wt. % butanol (i.e. 100 wt. % nonpolar liquid heptane/hexane), thus, as seen in ***Figure 26***, at low alcohol concentration (i.e. high nonpolar liquid concentration) the IPCM is able to more accurately predict conductivity of the nonpolar system for heptane and hexane than for toluene. Deviation at this low alcohol concentration range between the experimental and IPCM theoretical curves for the heptane and hexane solutions would disappear.

While *the Ion-Pair Conductivity Model* does not consider the chemical structure of the nonpolar liquid to be of any significance, specifically, it is worth noting that changes to the chemical structure of a nonpolar liquid can directly impact other properties of a nonpolar solution, such as relative permittivity and viscosity, which are treated by the *Ion-Pair Conductivity Model* as important factors in modeling conductivity in nonpolar systems.

According to the *Ion-Pair Conductivity Model* relative permittivity is important for determining the *Bjerrum length* of the system, which dictates the likeliness of ion-pair formation within the solution, and viscosity is important for determining ion mobility within the system, which dictates the degree of limitation placed on the ion mobilities within the solution, both of which significantly impact the overall conductivity of the system. Consequently, the uniform behavior in conductivity, seen across the entire concentration spectra for all three solutions in ***Figures 10a***, ***10b*** and ***26***, was driven, at least in part, by the nonpolar liquids having nearly identical relative permittivities (~2) and viscosities (~1 cP).

Ultimately, ***Figure 26*** reinforces the fact that the *Ion-Pair Conductivity Model* applies to alcohol-nonpolar liquid solutions beyond those in which toluene serves as the nonpolar liquid

and demonstrates that the chemistry of the nonpolar liquid does not, in and of itself, play an integral role in driving the conductivity of nonpolar systems. Rather, it is the nonpolar relative permittivity and viscosity of the solution that are vital for modeling the conductivity of a nonpolar system.

3.9 IPCM VS. XIAMETER NONIONIC SURFACTANT-TOLUENE SOLUTIONS

Sections 3.7 and **3.8** demonstrated the ability of the *Ion-Pair Conductivity Model* predict conductivity in alcohol-nonpolar liquid solutions across the entire alcohol concentration spectrum. In these models the alcohols served as the amphiphiles. Next the ability of the *Ion-Pair Conductivity Model* to predict conductivity for amphiphiles other than alcohols must be investigated. To begin, the experimental data from **Section 3.4**, Xiameter nonionic surfactant-toluene solutions, ***Figures 14 (a, b, and c)*** , ***15*** and ***16***, conductivity, relative permittivity, and viscosity, respectfully, will be used to determine the ability of the *Ion-Pair Conductivity Model* to model conductivity in these two component systems.

3.9.1 RESULTS

Similarly to **Sections 3.7** and **3.8**, the experimental values for conductivity, viscosity, and relative permittivity from the data exhibited in ***Figures 14a***, ***14b***, ***14c***, ***15*** and ***16***, were inserted into the *Ion-Pair Conductivity Model* (***Eq. 59***) and the unknown variables, distance of closest ion approach, $\boldsymbol{a}$, and concentration of ions in the pure amphiphile $\boldsymbol{C_A}$, were determined.

For these calculations we assumed that distance of closest ion approach, $\boldsymbol{a}$, was equal, not proportional (according to an arbitrary multiplier, ***R***, ***Eq. 58***) as done previously in **Section 3.7** and **3.8**, to hydrodynamic radius, $\boldsymbol{d_h}$, according to ***Eq. 57:*** $\boldsymbol{a = d_h}$

Consequently, limiting the total number of adjustable parameters in ***Eq. 59*** to only two: distance of closest ion approach, $\boldsymbol{a}$, and concentration of ions in the pure amphiphile $\boldsymbol{C_A}$.

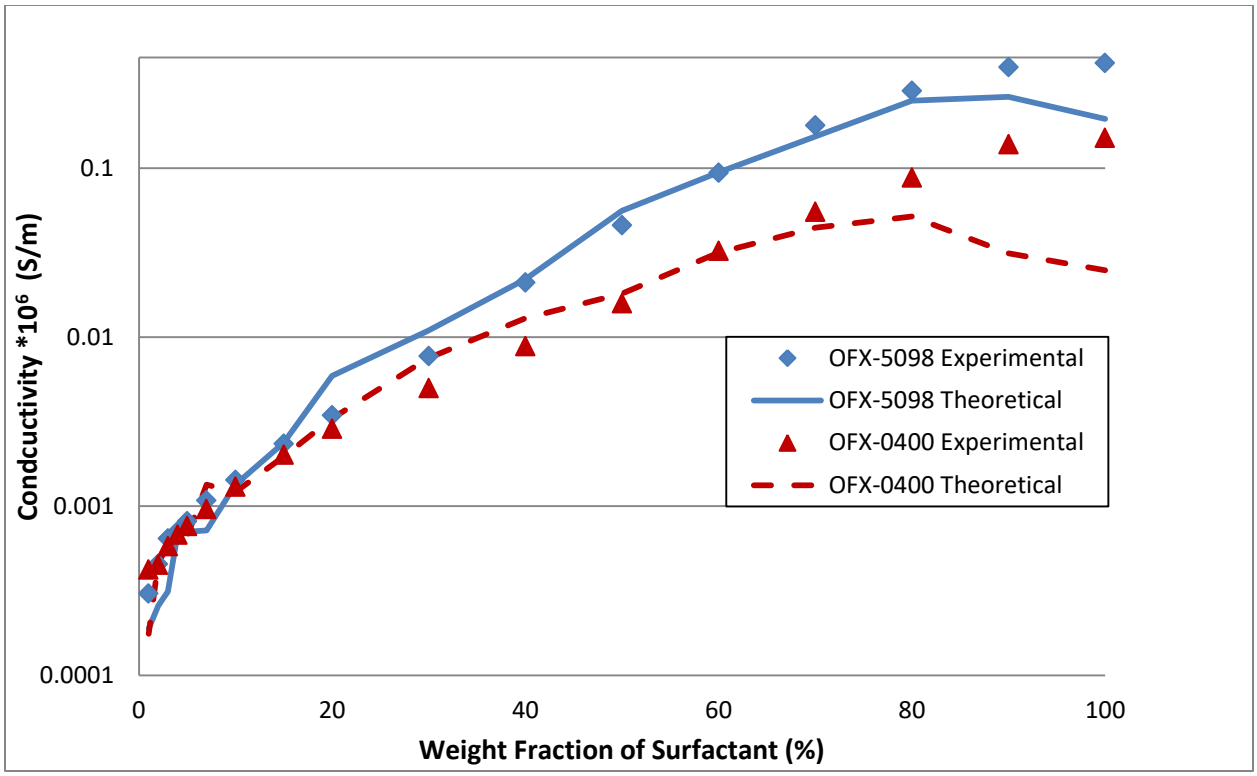

***Figure 27**: Ion-Pair Conductivity Theoretical Fitting of Experimental Data for Xiameter Nonionic Surfactant-Toluene Solutions. Legend denotes Nonionic Surfactant in Mixture. Logarithmic Scale*

Surfactant	$a = d_h$ [nm]	C_A [10^{-6} mol/l]
OFX-5098	0.68	53
OFX-0400	0.72	33

***Table 8**: Hydrodynamic Ion Size and Ionic Strength of Non-Ionic Surfactants.*

3.9.2 DISCUSSION

The theoretical curves calculated by fitting $\boldsymbol{a}$ and $\boldsymbol{C_A}$ are not entirely smooth. This seems peculiar for theoretical data. However, measured data was inputted into the *Ion-Pair Conductivity Model* equation in order to fit the data. It is because of this inputted measured data that the curves do not appear entirely smooth, but rather have kinks. An alternative approach would have been to apply a best-fit line to the viscosity data, and use the equation for that best-fit line for viscosity values in the *IPCM.* However, this would have introduced additional error (between theoretical and measured viscosity data) that would need to be considered. Additionally the graphs presented here are consistent with the publication of this work in the Journal of the Electrochemical Society[79].

As presented in ***Figure 27***, the *IPCM* theoretical model is in good agreement with the experimental data across nearly the entire Xiameter concentration range with some deviation between the theoretical and experimental conductivity curves observed at very high concentrations of Xiameter nonionic surfactant (~70-100 wt. % Xiameter concentration). We hypothesize that this deviation has to do with viscosity of the surfactant and, more specifically, the non-Newtonian nature of these surfactants. The viscosities measured for these calculations were determined using Cannon-Fenske viscometers, which measure the viscosity on a macroscopic level, i.e. they measure the overall viscosity of the liquid under the stress of gravity. Imagine ions moving inside of cages formed by the larger surfactant molecules. This results in the measured viscosity being quite high, while, the experienced viscosity by the ions is actually quite low, allowing for increased ion mobility and therefor increased conductivity of the system. Thus, since conductivity is a function of ion mobility, viscosity of the ions is actually measured on a microscopic level, i.e. on the scale of nanometers. Due to the non-Newtonian nature of these materials, it is feasible that the micro and macro viscosities of these

nonpolar solutions differ, and these differences cause the deviation observed in the theoretical model and experimental data in this concentration range. However, as the sample is diluted with nonpolar liquid, this macromolecular structure breaks down until the viscosity of the entire solution is just the singular micro viscosity experienced by the ions, which is why deviation between the two curves is not seen in the lower Xiameter nonionic surfactant concentration range.

Using the *Ion-Pair Conductivity Model* to best-fit the experimental conductivity data with the IPCM theoretical model ion size, $\boldsymbol{d_h}$, along with distance of closest ion approach, $\boldsymbol{a}$, and concentration of ions in the pure Xiameter surfactant, $\boldsymbol{C_A}$, were determined (***Table 8***). Interestingly, according to the data in ***Table 8*** both Xiameter surfactants have roughly the same hydrodynamic radii (~ 0.7nm), despite their distinctly different conductivities shown in ***Figure 27***. Notably, the ion sizes for the Xiameter nonionic surfactants are nearly identical to the ion sizes calculated for the alcohols in **Section 3.7**, ***Table 7***, which correlates with the literature data reported for ion size by Fuoss and others.

On the other hand, according to the data in ***Table 8***, the concentration of ions in the pure amphiphile $\boldsymbol{C_A}$, for Xiameter surfactant OFX-5098 is nearly double that of OFX-0400. This discrepancy in $\boldsymbol{C_A}$, for the two Xiameter surfactants is in line with what the physical properties, specifically their respective HLB numbers, of OFX-5098 and OFX-0400, outlined in **Section 3.4**, tell us about the role the polar part of the nonionic surfactant molecule plays with regards to influencing the overall conductivity of the system. Given OFX-5098's inherently higher relative permittivity and HLB number than that of OFX-0400, implies that the polar part of the OFX-5098 surfactant molecule plays a more prominent role in than it does in OFX-0400 and as such, FX-5098 contains a higher concentration of ions in the pure amphiphile $\boldsymbol{C_A}$, than OFX-0400.

Overall, the data presented in ***Figure 27*** and ***Table 8*** proves the even broader usefulness of the *IPCM* for modeling nonpolar systems with amphiphiles other than alcohols, specifically, in this case, for the amphiphile family of Polyalkylene Oxide-modified Polydimethylsiloxanes nonionic surfactants such as Xiameter OFX-5098 and OFX-0400.

3.10 IPCM VS. SPAN SURFACTANT-TOLUENE SOLUTIONS

Next, the experimental data from **Section 3.5**, solutions of SPAN nonionic surfactant and toluene, ***Figures 18a***, ***18b***, ***19*** and ***20***, conductivity, relative permittivity, and viscosity, respectfully, will be used to determine the ability of the *Ion-Pair Conductivity Model* to model conductivity in these two component systems.

3.10.1 RESULTS

As was done in the previous section, ***Section 3.9***, experimental values for conductivity, viscosity, and relative permittivity from the data presented in ***Figures 18a***, ***18b***, ***19*** and ***20***, were inserted into the *Ion-Pair Conductivity Model* (***Eq. 59***) and the unknown variables, distance of closest ion approach, $\boldsymbol{a}$, and concentration of ions in the pure amphiphile $\boldsymbol{C_A}$, were determined.

Likewise, for these calculations we assumed that distance of closest ion approach, $\boldsymbol{a}$, was equal, not proportional (according to an arbitrary multiplier, $\boldsymbol{R}$, ***Eq. 58***), to hydrodynamic radius, $\boldsymbol{d_h}$, according to ***Eq. 57:*** $\boldsymbol{a = d_h}$

Again, limiting the total number of adjustable parameters in ***Eq. 59*** to only two: distance of closest ion approach, $\boldsymbol{a}$, and concentration of ions in the pure amphiphile $\boldsymbol{C_A}$.

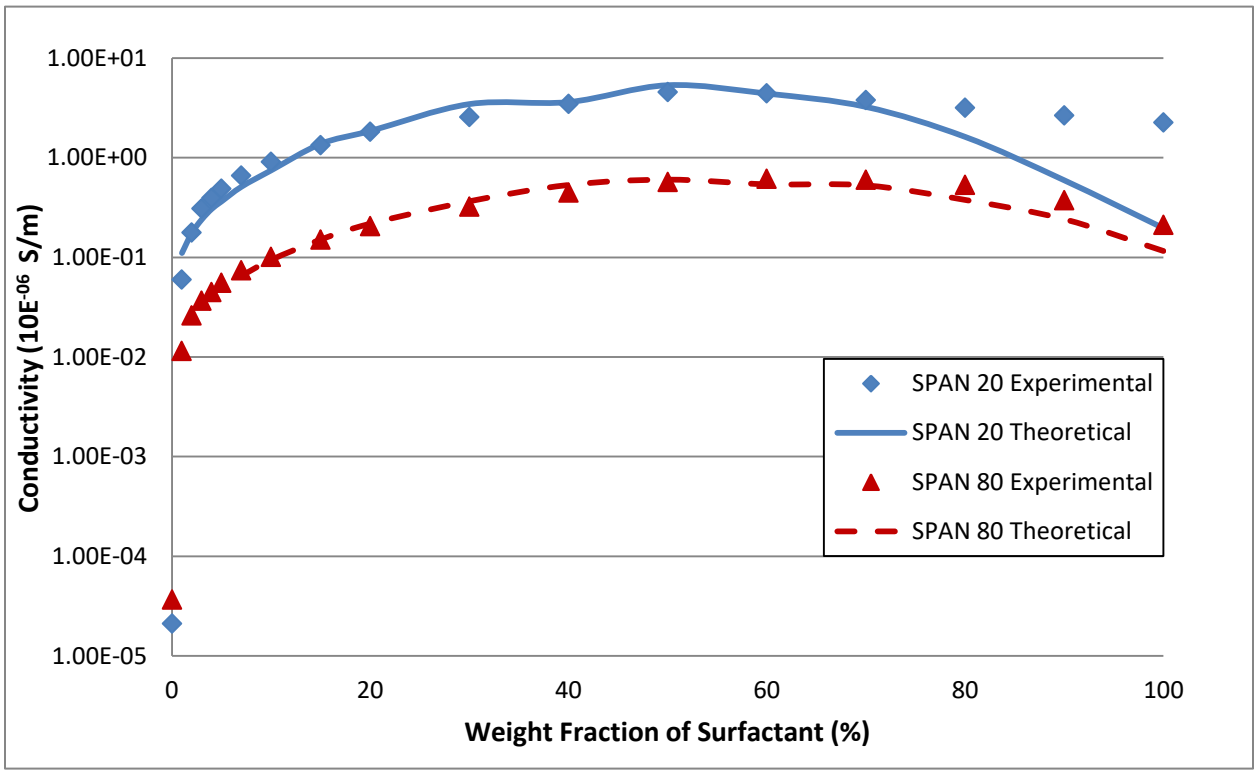

***Figure 28**: Ion-Pair Conductivity Theoretical Fitting of Experimental Data for Nonionic Surfactant SPAN-Toluene Solution. Legend denotes Nonionic Surfactant in Mixture. Logarithmic Scale.*

3.10.2 DISCUSSION

As illustrated in ***Figure 28***, the IPCM theoretical data is in good agreement with the experimental data across nearly the entire SPAN concentration range with some deviation between the theoretical and experimental conductivity curves observed at very high concentrations of SPAN nonionic surfactant (~70-100 wt. % SPAN concentration). Based on the data presented in ***Figure 28***, the deviation between theoretical and experimental at high concentration of SPAN nonionic surfactant appears more pronounced for the SPAN 20-toluene solution than the SPAN 80-toluene solution.

As was the case in ***Section 3.9***, measured viscosity data was inputted into the *IPCM.* The graphs presented here are consistent with the peer-reviewed published data[85].

According to the experimental viscosity data for the SPAN nonionic surfactant series put forth in ***Figure 20***, it is apparent that, again, at very high concentrations of SPAN nonionic surfactant (~70-100 wt. % SPAN concentration) the SPAN 20-toluene solution has a higher macroscopic viscosity than the SPAN 80-toluene solution, and so, as stated before, the difference between the microscopic viscosity experienced by the ions[86,87], and the measured macroscopic viscosity of the overall solution, is, again, likely the cause in the deviation between the experimental and theoretical results evident in ***Figure 28***.

3.11 IPCM VS. CONCENTRATION, CRITICAL ION SIZE, AND RANGE OF ION-PAIR EXISTANCE

The fitting of experimental data demonstrates the ability of the *Ion-Pair Conductivity Model* to accurately predict conductivity in two-component solutions of non-polar liquid and amphiphile. Furthermore, it reinforces the validity of *The Dissociation Model* as a means of describing the phenomena by which ionization occurs in nonpolar liquids. Lastly, it emphasizes the importance that ion-pairs play in the conductivity of such a system.

According to the *Ion-Pair Conductivity Model*, there are five critical parameters of a nonpolar system that impact the conductivity of any two-component amphiphile-nonpolar liquid solution:

1. The relative permittivity of the amphiphile, $\boldsymbol{\varepsilon_a}$,
2. The volume fraction of the amphiphile in the overall solution, $\boldsymbol{\varphi}$,
3. The concentration of ions in the pure amphiphile, $\boldsymbol{C_A}$, and
4. Ion size in solution, $\boldsymbol{a}$
5. Viscosity of the system, $\boldsymbol{\eta}$

While the relative permittivity of the nonpolar liquid, $\boldsymbol{\varepsilon_n}$, also plays a role in these systems, given the inherent nature of media characterized as such, the relative permittivity of these liquids are typically very low (~2) and do not vary much. Thus, for the purposes of this discussion, it can be ignored.

Additionally, the *Ion-Pair Conductivity Model* further states that only when the environment of the system, and subsequently the five driving properties of such a system allow for it, will ion-pair formation occur within the nonpolar solution. Ion-pairs will only be present within a nonpolar system, across a specific concentration range, when the solutions properties create an ideal atmosphere for ion-pairs to form.

3.11.1 RESULTS

Through application of theoretical graphs for the *Ion-Pair Conductivity Model* (i.e. ***Eq. 59***), the concentration ranges at which ion-pairs are present within a nonpolar system can be predicted.

To begin, the relative permittivity of the nonpolar liquid is assumed to be equal to that of pure toluene ($\boldsymbol{\varepsilon_n}$ = 2.36), and the relative permittivity of the entire solution can be estimated as the volume-based average of its components according to:

$$\boldsymbol{\varepsilon(\varphi) = \varepsilon_n(1 - \varphi) + \varepsilon_a\varphi} \qquad \textbf{Eq. 61}$$

Where, $\boldsymbol{\varepsilon_A}$ is the relative permittivity of the amphiphile, and $\boldsymbol{\varphi}$ is the volume fraction of the amphiphile in the overall solution. Conductivity multiplied by viscosity, as a function of amphiphile concentration, across the entire volume-based amphiphile concentration spectra for amphiphiles with a range of theoretical relative permittivities, from $\boldsymbol{\varepsilon_a}$ = 5 to $\boldsymbol{\varepsilon_a}$ = 30 was explored.

Given the viscosity of these theoretical systems can span multiple orders of magnitude the theoretical data in this section is presented as the Walden product (conductivity multiplied by viscosity) versus concentration/ion size.

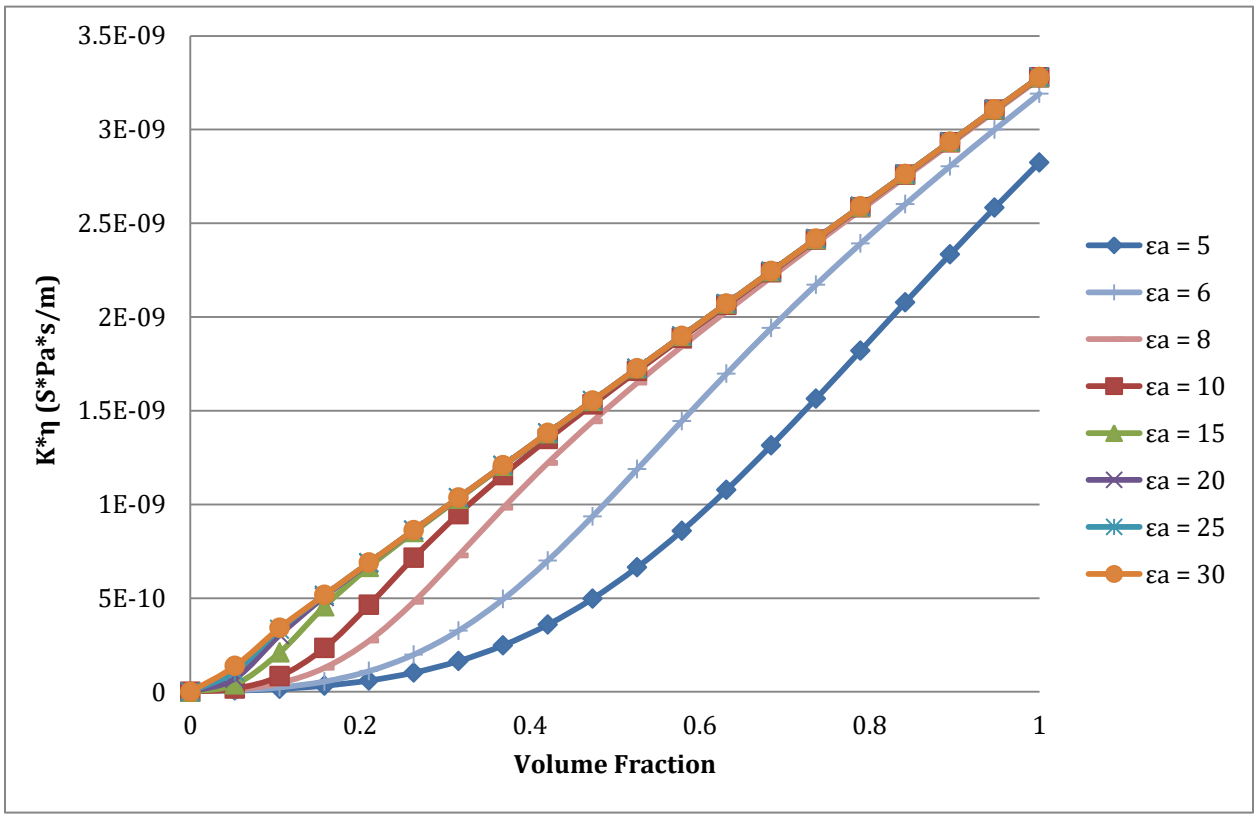

***Figure 29a**: Walden product versus Volume Fraction: ion size = 1 nm. C_A = 10^{-6} M. Linear Scale.*

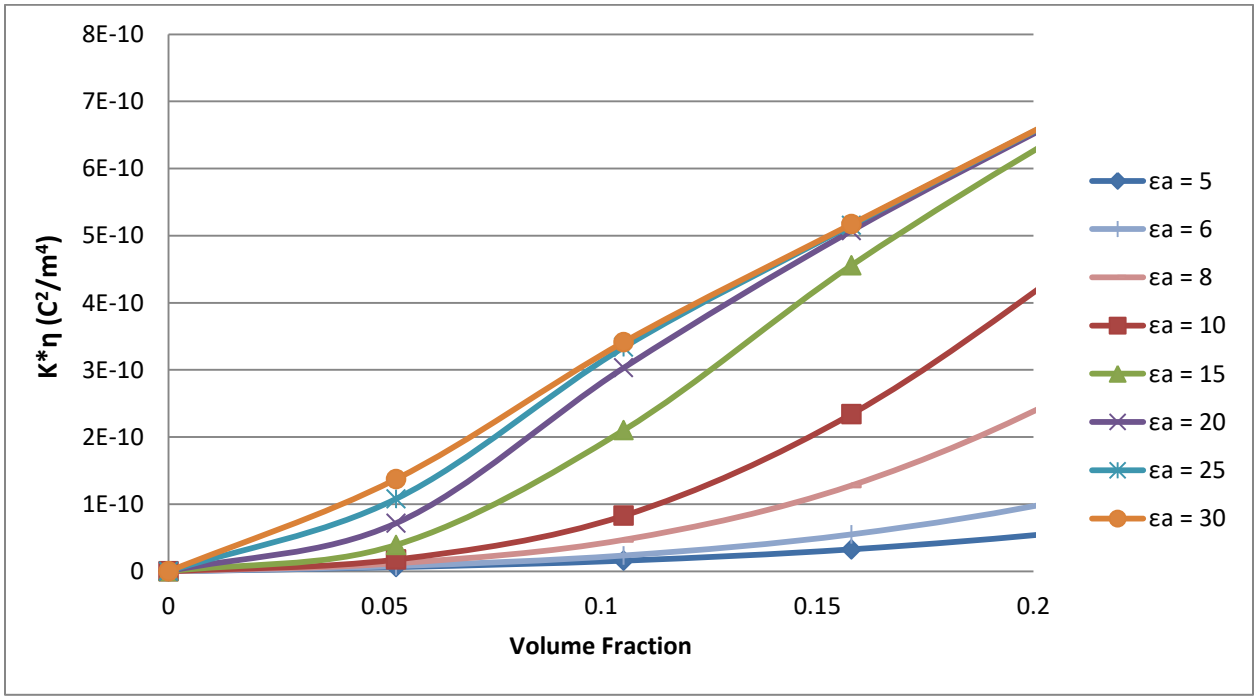

***Figure 29b**: Walden product versus Volume Fraction: ion size = 1 nm. C_A = 10^{-6} M. Expanded Range of Low Concentration of Added Amphiphile. Linear Scale.*

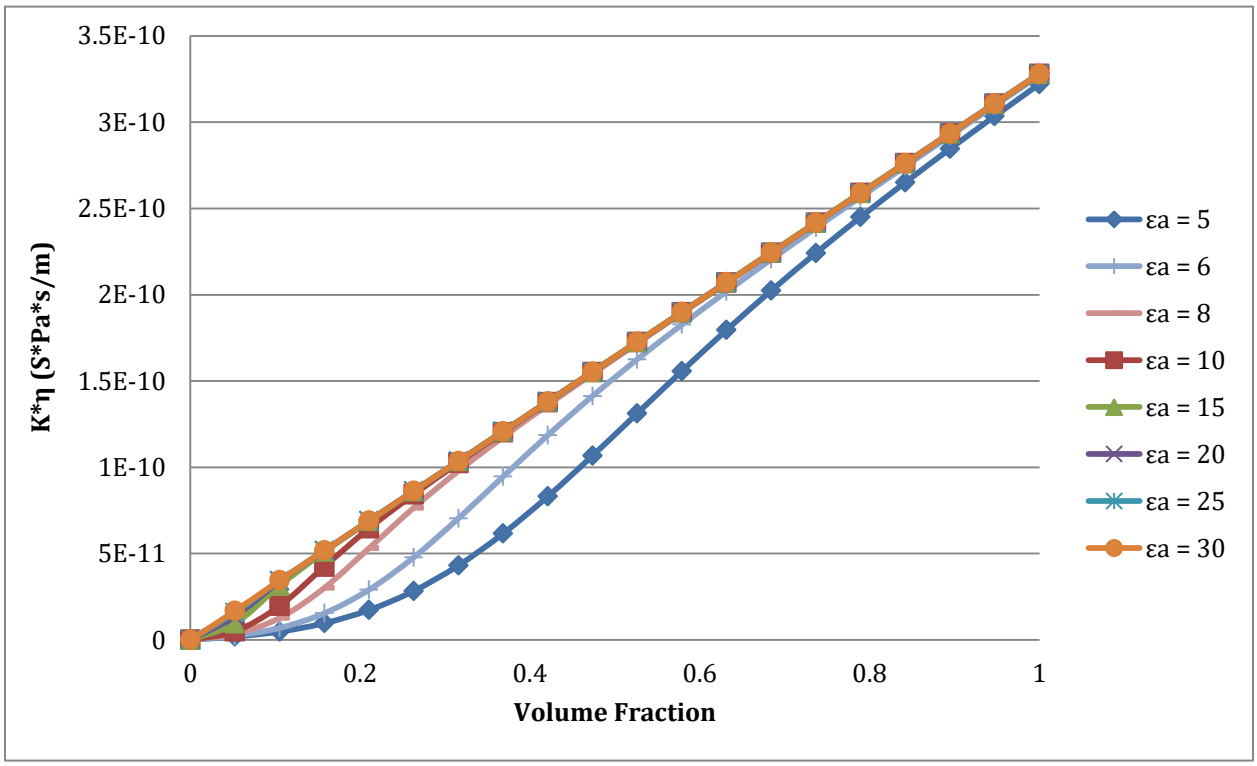

***Figure 30**: Walden product versus Volume Fraction: ion size = 1 nm. $C_A = 10^{-7}$ M. Linear Scale*

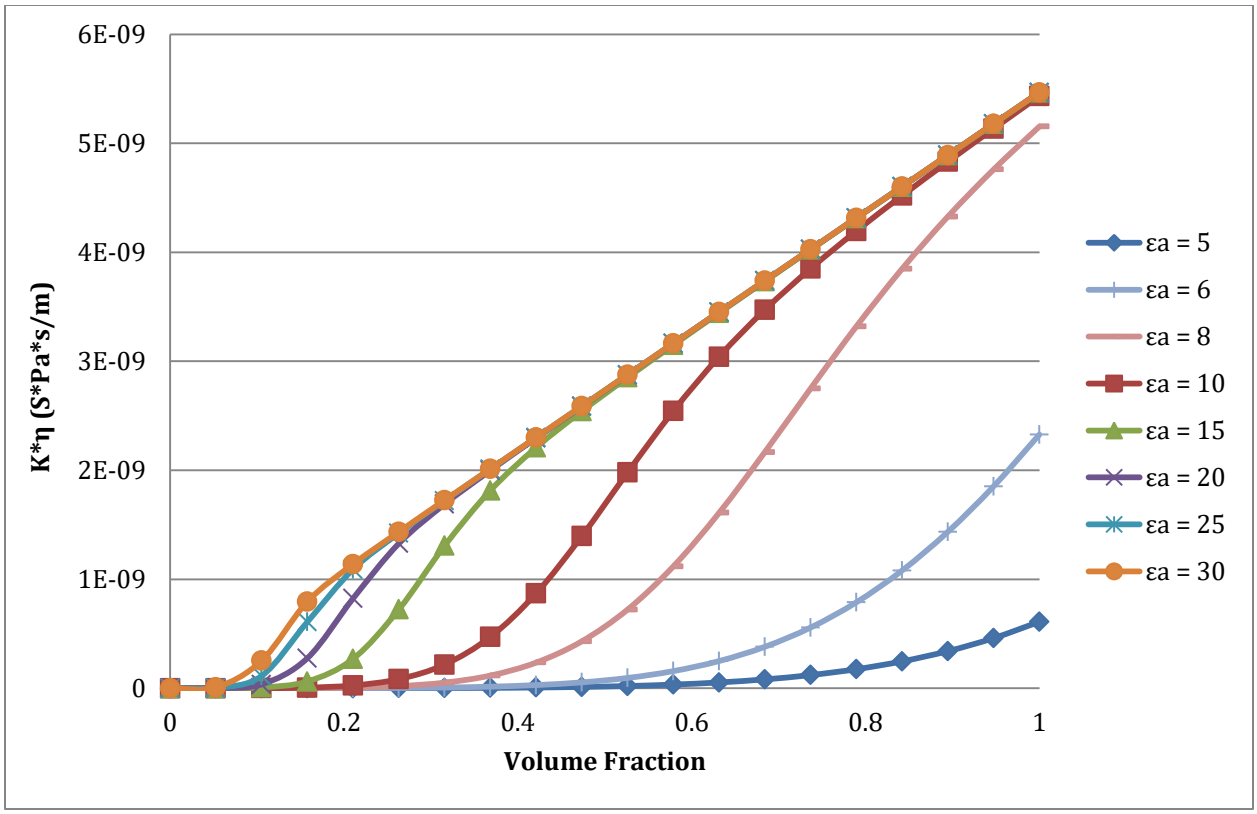

***Figure 31**: Walden product versus Volume Fraction: ion size = 0.6 nm. C_A = 10^{-6}M. Linear Scale*

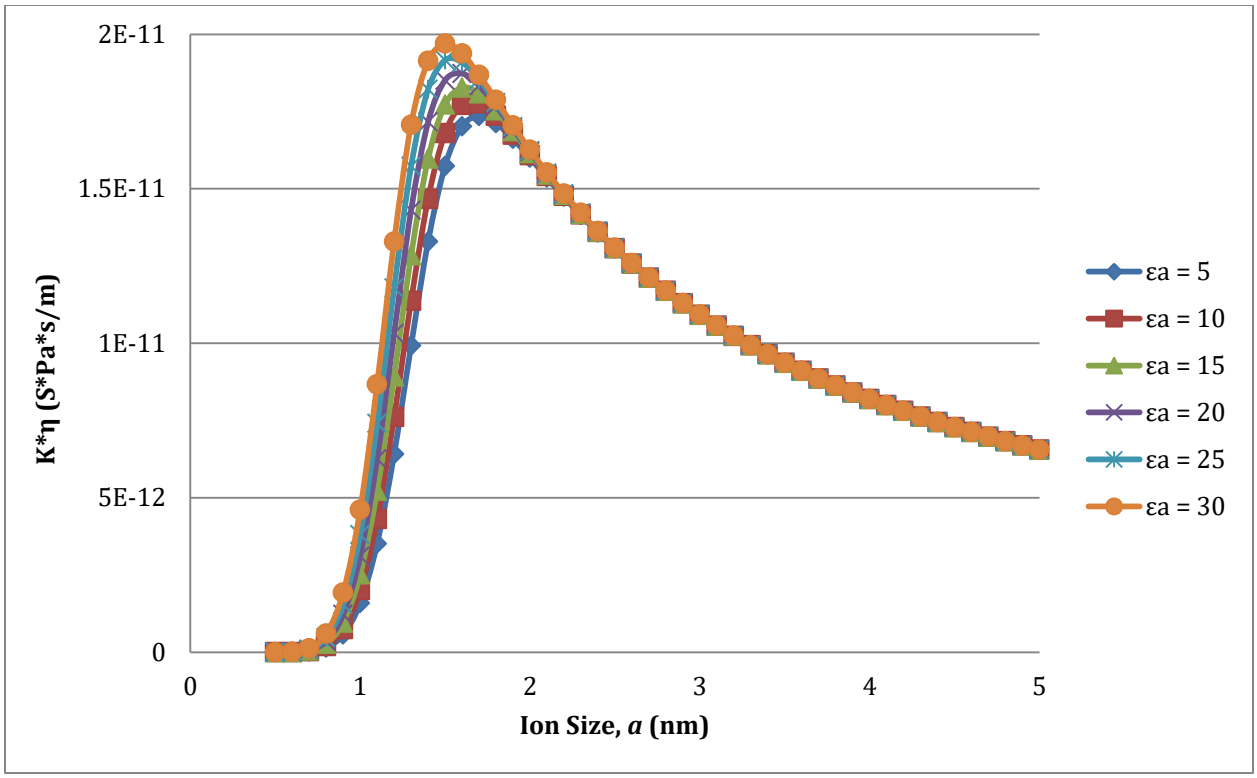

***Figure 32**: Walden product versus Ion Size for Theoretical Solutions with Varying Relative Permittivities of the Amphiphile. $C_A = 10^{-8}$M. Linear Scale*

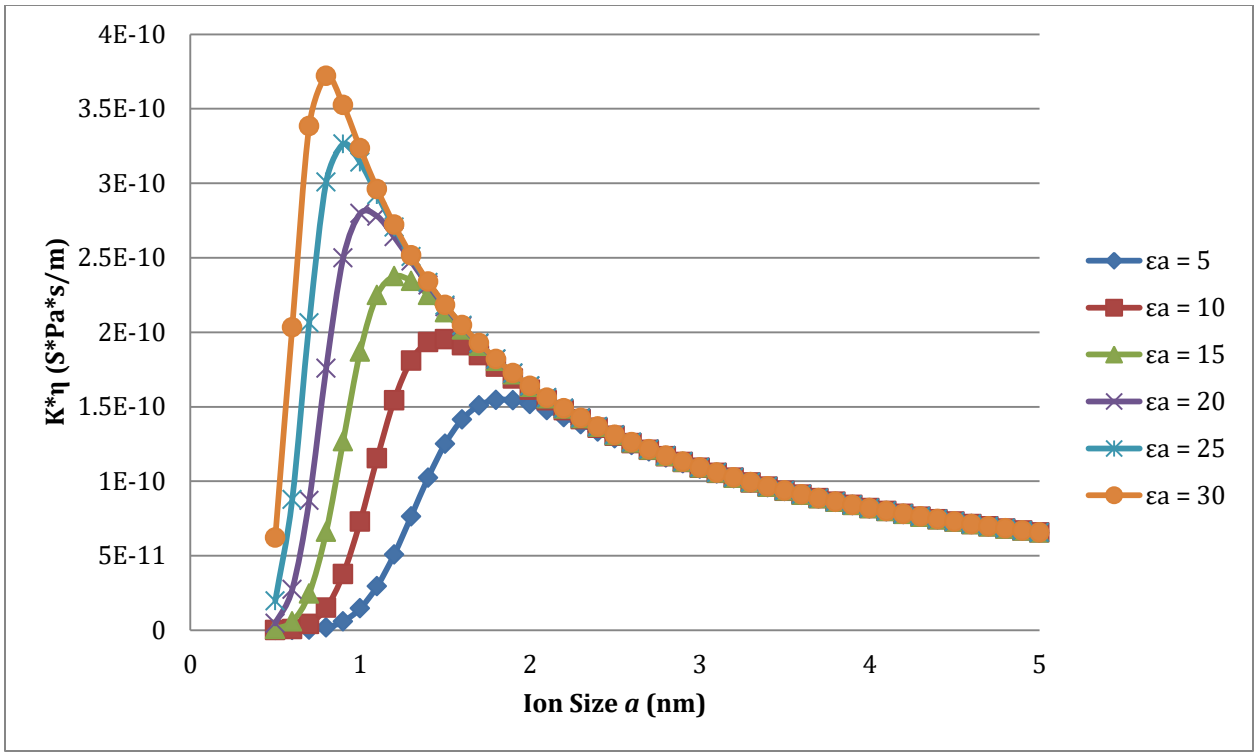

***Figure 33**: Walden product versus Ion Size for Theoretical Solutions with Varying Relative Permittivities of the Amphiphile. $C_A = 10^{-7}$M. Linear Scale*

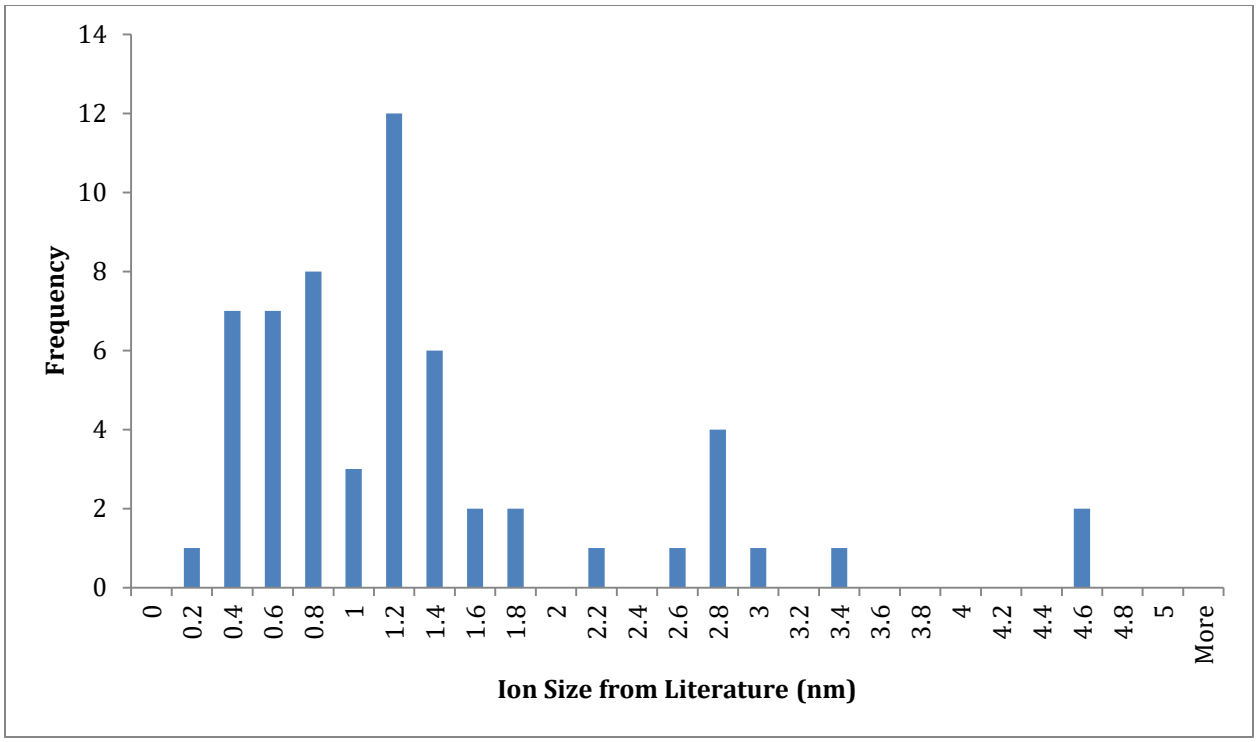

***Figure 34**: Histogram of reported Ion Sizes in Nonpolar Media from Literature Sources.*

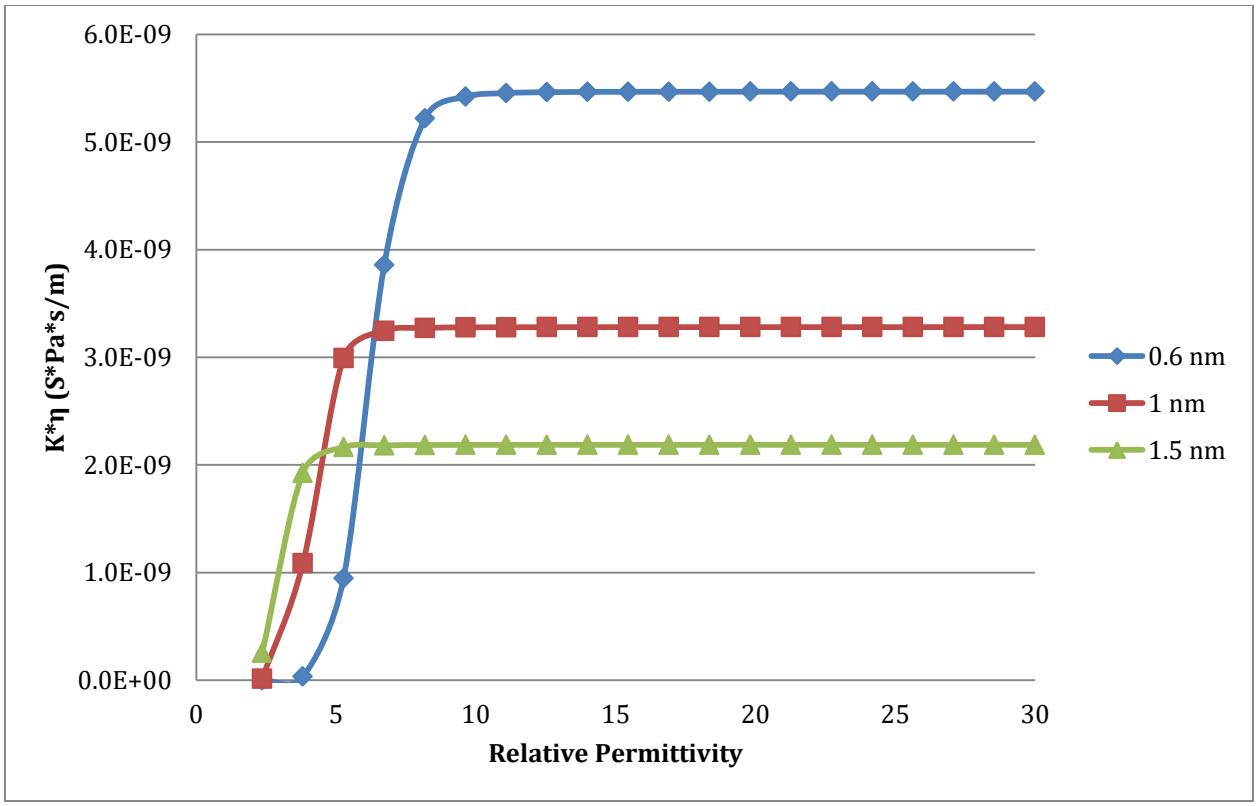

***Figure 35**: Walden plot versus Relative Permittivity for Theoretical Ion Sizes.* $C_A = 10^{-6}$ *M. Linear Scale*

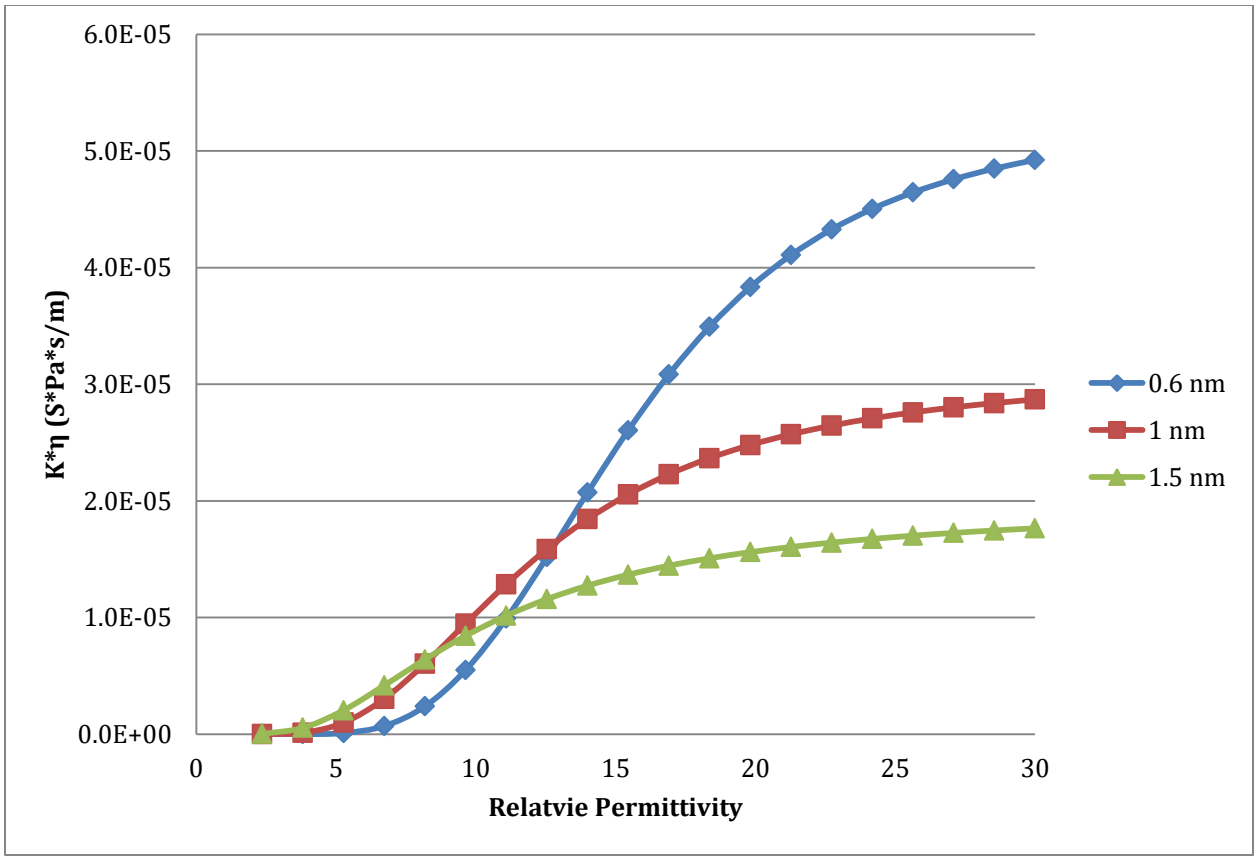

***Figure 36**: Walden plot versus Relative Permittivity for Theoretical Ion Sizes. C_A = 10^{-2} M. Linear Scale*

3.11.2 DISCUSSION

3.11.2.1 Amphiphile Concentration

Figures 29a, ***29b***, ***30***, and ***31*** show the eight theoretical Walden product curves for all 8 theoretical amphiphile relative permittivities, $\boldsymbol{\varepsilon_a}$, ranging from 5-30. Previously, concentration had been measured on a weight basis, whereas in ***Figures 29a, 29b***, ***30***, and ***31*** concentration is modeled on a volume basis.

When the Walden product curve is a linear function of amphiphile concentration, conductivity of the system obeys the laws of classical electrochemistry, implying there are no ion-pairs present in the nonpolar solution. This linear relationship occurs when both a higher concentration of amphiphile is present within the solution, as well as at higher amphiphile relative permittivities. As both volume fraction of amphiphile , $\boldsymbol{\varphi}$, and relative permittivity of the amphiphile, $\boldsymbol{\varepsilon_a}$, increase, so does the relative permittivity of the overall solution, $\boldsymbol{\varepsilon}(\boldsymbol{\varphi})$, which decreases the *Bjerrum length* of the system, decreasing the likeliness that the solvated ions in solution will come close enough to one another to recombine into neutral ion-pairs.

All the curves in ***Figures 29***(***a*** and ***b***), ***30***, and ***31*** follow the same trend, a non-linearity (i.e. ion-pairs are present) between Walden product and amphiphile concentration is only observed at very low amphiphile concentration ranges and when the relative permittivity of the amphiphile is also extremely low (i.e. on the scale of the relative permittivity of a nonpolar liquid, $\boldsymbol{\varepsilon_n}$). For the amphiphile with the relative permittivity of 30, the graph appears linear across nearly the entire concentration spectra. ***Figure 29b*** expands the graph of ***Figure 29a*** to highlight the region in which concentration of added amphiphile is low, providing a more clear depiction of this behavior in which the dependence of conductivity multiplied by viscosity (Kη) on concentration deviates from linearity, indicating the presence of ion-pairs.

Theoretical values for ion size, $\boldsymbol{a}$, in ***Figure 29*** and ***Figure 30*** are both 1nm, while the concentration of ions in the pure amphiphile, $\boldsymbol{C_A}$, is decreased by an order of magnitude in ***Figure 30***, allowing for the effect ionic strength has on these systems to be examined. Based on the results illustrated in ***Figure 29*** and ***Figure 30*** it is clear that a decrease in the concentration of ions in the pure amphiphile, $\boldsymbol{C_A}$, increases the linearity between conductivity multiplied by viscosity and amphiphile concentration in all eight curves. This is consistent with the underlying principles of the *Ion-Pair Conductivity Model* which states, as the ionic strength of a nonpolar system decreases, less ions are present within the solution to form ion-pairs, thus, the eight curves in ***Figure 30*** appear more linear, across the entire amphiphile concentration spectra, due to a decrease in ion-pair formation in these nonpolar systems.

3.11.2.2 Ion Size

Next, theoretical values for the concentration of ions in the pure amphiphile, $\boldsymbol{C_A}$ (10^{-6}M), in ***Figure 29*** and ***Figure 31***, are held constant and ion size, $\boldsymbol{a}$, is varied from 1nm to 0.6 nm, respectively. As seen in ***Figure 31***, reducing ion size, $\boldsymbol{a}$, from 1nm to 0.6 nm, drastically expands the amphiphile concentration range in which ion-pairs are present in the solutions. Notably, ***Figure 31*** shows that almost all eight solutions have ion-pairs present across the entire amphiphile concentration spectra, some even at pure amphiphile. Additionally, unlike the data in ***Figure 29***, even the solution with an amphiphile relative permittivity, $\boldsymbol{\varepsilon_a}$, of 30 in ***Figure 31*** displays significant amphiphile concentration regions in which ion-pairs are present in the solution.

It is clear from ***Figures 31***, ***32*** and ***33*** that ion size plays an important role in the conductivity of a system. Specifically, there are two mechanisms by which ion size will impact the overall conductivity of the system; distance of closest ion approach, which favors large ions and ion mobility which favors small ions.

First, the hydrodynamic resistance that an ion experiences as it travels through a liquid will be directly impacted by the size of that ion. That hydrodynamic resistance is a function of the interfacial area between that ion and the surrounding liquid. An increase in ion size increases its surface area in contact with the material it is moving through, resulting in drag that limits the mobility of that ion, which in turn decreases its conductivity because conductivity is a function of ion mobility. The smaller the ion, the lower the hydrodynamic resistance experienced by that ion, thus increasing ion mobility, resulting in an increase in conductivity.

Second, ion size directly impacts the distance of closest ion approach, which will affect the ability of ion-pairs to form. Distance of closest ion approach, $\boldsymbol{a}$, is directly related to the intensity of the cation-anion attraction in a potential ion-pair. Smaller ions are able to approach each other at closer distances than larger ones can and, as a result, the attractive forces between these oppositely charged ions will be greater for the smaller ions. The stronger these attractive forces between anion and cation, the more likely it is that they will combine and form a neutral ion-pair, diminishing the conductivity of the system. As a result, as the size of the ions decreases, so does the number of free solvated ions in solution, due to the affinity of free ions to recombine into solvated ion-pairs as the distance between their attractive forces narrows. Therefore, as ion size decreases, so does the overall conductivity of the system.

Interestingly, these ion size driven conductivity mechanisms of nonpolar systems are at odds with one another: in terms of increasing conductivity, hydrodynamic size favors smaller ions while the distance of closest ion approach favors larger ions. Therefore, the conductivity of an amphiphile-nonpolar liquid solution, as a function of ion size, peaks at a *critical ion size,* $\boldsymbol{a_{cr}}$, whereby the balance between the two mechanisms is most favorable to the overall conductivity of the system. However, *critical ion size*, $\boldsymbol{a_{cr}}$, is only applicable in solutions in

which the environment for ion-pair formation exists, which is not always the case and a number of polar and nonpolar solutions exist in which ion-pairs are unable to be maintained in solution (e.g. very small *Bjerrum length*). Thus, the ability of the *Ion-Pair Conductivity Model* to allow us to predict the *critical ion size*, $\boldsymbol{a_{cr}}$, of a nonpolar system and examine the range of concentrations at which it is important is imperative when studying solutions in which ion-pair formation occurs.

Next, in order to validate the *Ion-Pair Conductivity Model* as a reliable model to investigate ion size in nonpolar media we examined a number of theoretical ion sizes, under various circumstances, while holding ionic strength and relative permittivity of the nonpolar solution constant. As anticipated, a critical ion size is identified where the Walden product reaches a maximum in both ***Figure 32*** and ***Figure 33***.

Theoretical values for the concentration of ions in the pure amphiphile, $\boldsymbol{C_A}$, (i.e. ionic strength), are varied from $1E^{-8}$ mol/L to $1E^{-7}$ mol/ L in ***Figure 32*** and ***Figure 33***, respectively, allowing for the effect ionic strength has on these systems to be examined. As seen in ***Figure 32*** when the ionic strength of the overall system is lowered, the role relative permittivity plays in such a system is also diminished, thus, significant overlap is observed in all six relative permittivity curves, implying the relative permittivity of the solution has a nearly negligible effect on both ion size and Walden product in the theoretical systems modeled in ***Figure 32***. Notably, a critical ion size of roughly 1.5nm diameter is identified for all six solutions.

However, when the ionic strength is increased from $1E^{-8}$ mol/L to $1E^{-7}$ mol/ L in ***Figure 33***, the role of relative permittivity in these theoretical solutions becomes much more prominent. As shown in ***Figure 33*** the six relative permittivity curves grow much more distinct covering a range of critical ion sizes (~0.5-1.5 nm), as ionic strength of the system

increases critical ion size is increasingly dependent upon the relative permittivity of the amphiphile.

The theoretical analysis of critical ion size put forth in ***Figures 32***and ***33*** indicates that ions with a size of 1.2 nm (±0.4 nm) most contribute to the overall conductivity of these nonpolar systems. These values were calculated from the average and standard deviation of the theoretical data. ***Figure 34*** represents a histogram of critical ion sizes in nonpolar media reported in the literature across 17 different publications[42,73,79,85,89-101], which are, for the most part, in good agreement with the theoretical predictions put forth by the *Ion-Pair Conductivity Model* in this section. While we make no claim that ***Figure 34*** covers the entirety of relevant research in this field, nor do we consider the methods by which these sizes were measured a factor, we do consider the data to be, at the very least, a strong benchmark for validating our findings.

3.11.2.3 Relative Permittivity Range Favorable for Ion-Pair Existence

Next, using the *Ion-Pair Conductivity Model* to examine when ion-pairs exist in solution, Walden product was plotted versus amphiphile relative permittivity, across the entire range of relative permittivities from $\boldsymbol{\varepsilon_a}$ = 5 to $\boldsymbol{\varepsilon_a}$ = 30 for three theoretical nonpolar systems with ion sizes of 0.6, 1, and 1.5 nm.

Theoretical values for the concentration of ions in the pure amphiphile, $\boldsymbol{C_A}$, (i.e. ionic strength), are varied from $1E^{-6}$ mol/L to $1E^{-2}$ mol/ L in ***Figure 35*** and ***Figure 36***, respectively, allowing for the effect of ionic strength on ion-pair formation as a function of ion size and relative permittivity in these systems to be examined. As seen in ***Figure 35*** , a lower ionic strength results in a significant transition in Walden plot (conductivity multiplied by viscosity) when the relative permittivity of the amphiphile is between ~2 and 10, implying that $\boldsymbol{\varepsilon_a}$ > 10 is

the threshold above which ion-pairs do not form, and thus the significance of critical ion size is no longer relevant.

As the ionic strength increases from $1E^{-6}$ mol/L to $1E^{-2}$ mol/ L in ***Figure 36***, the range of amphiphile relative permittivity, for all three theoretical solutions of various ion sizes, at which ion-pairs exists expands to approximately $\boldsymbol{\varepsilon_a} = 30$. While ion pairs are able to be present at much higher relative permittivities under these theoretical conditions, approaching a relative permittivity range of a low polar system, whereby classical electrochemistry, in which ion-pair formation does not exist, would begin to govern conductivity are still far lower than the relative permittivity of water, and other typical polar systems, where $\boldsymbol{\varepsilon_a} = 80$.

3.12 WATER CONTAMINATION IN NONPOLAR SYSTEMS AND THE SOURCE OF IONS C_A

In **Section 3.3** ionization as the result of water contamination was explored in various butanol-nonpolar liquid solutions. As illustrated in ***Figure 12***, the longer the dried pure butanol was exposed to ambient air the higher the solutions conductivity, highlighting the rather significant effect of water contamination on the ionization of these nonpolar systems. Additionally, as demonstrated in ***Figure 13***, titration of water into dried pure butanol also caused an increase in conductivity of the solution. Given butanol's hygroscopic nature (i.e. it readily absorbs moisture from ambient air) these results were exactly what was to be expected in these solutions under these experimental conditions. Therefore, the next step is to examine whether or not this phenomenon is exclusive to butanol or if other nonpolar systems are also susceptible to ionization via water contamination.

The role of water contamination in these nonpolar and semi-polar (i.e. amphiphilic) materials is not a trivial one, given the impact it has on the conductivity of these systems. Accordingly, we investigated the effect of water contamination on both Xiameter and SPAN nonionic surfactants (as well as Toluene) examined in **Section 3.4**.

Water content was continuously measured on a volume fraction basis, over a period of one to three minutes, using an 870 KF Titrino Plus manufactured by Metrohm, run in KFT Ipol setting.

Material	Water Content (% Vol.)
Toluene	0.02
OFX-5098	0.19
OFX-0400	0.85
SPAN 20	0.59
SPAN 80	0.41

Table 9*: Water Contamination Results from Karl-Fischer Titration Experiments.*

The data in ***Table 9*** shows that water content was lowest for nonpolar liquid toluene, 0.02 volume %, and highest for the nonionic surfactant OFX-0400, 0.85 volume %. Converting this data from volume fraction to concentration provides us with a water content range of 11 - 471 mol/m^3 for these five materials. Comparing this concentration of water data to the concentration of ions in the pure amphiphile, $\boldsymbol{C_A}$, data from the nonionic surfactant-toluene solutions discussed in **Section 3.4**, we see that the concentration of water measured herein is orders of magnitude larger than the concentration of ions in the pure amphiphile reported previously. While not all of the water present in these systems will automatically form ions that contribute to the overall conductivity of these nonpolar liquids, even if a very small percentage of them do, the impact this low number of newly formed ions would have on the conductivity of these system would still be significant, because the initial ionic concentration of these solutions is so low. The implication is that, even for non-polar liquids like toluene, there is adequate water present via contamination that ion concentration is not the limiting factor with regards to conductivity; rather, it is the concentration of the solvating agent, as well as the overall permittivity of the system, that impact the ability for ion-pairs to form.

Additionally, this data is also useful in providing a counter argument towards criticism of the *Ion-Pair Conductivity Model.* Specifically in the case of alcohols as amphiphiles, Gourdin-Bertin and Chassagne[102] criticized the mechanism of auto-dissociation and self-solvation of the alcohol molecules in toluene. These authors calculated the auto-dissociation rates for such mixtures and found that they were too high based on the findings of the *Ion-Pair Conductivity Model*. However, calculations carried out by Gourden-Berin et al. assumed that auto-dissociation was the sole source of ions in solution. The results discussed herein reaffirm the role of water contamination in ionization of these systems. The assumption that auto-dissociation is the sole source of ions in those mixtures is not necessarily valid.

3.12.1 THE IMPACT OF CONTAMINATION ON C_A

It has been demonstrated thus far that water can serve as a source of contamination, and therefore as a source of ions, in nonpolar systems with added amphiphile. While efforts were taken to minimize contamination via water (through use of anhydrous materials), Karl-Fischer titration experiments have proven that water is still present.

However, water is not the only possible contaminant in these systems. Nonionic surfactants, particularly those in the SPAN series, are known to have residual catalysts present, which are also a source of contamination. The concentration of ions in nonpolar systems is so low that trace impurities can have a non-negligible impact on the conductivity of mixtures of nonpolar media with added amphiphile.

As is described in the *Dissociation Model* (and accordingly, the *IPCM*) there exist two equilibrium dissociation reactions that occur in nonpolar systems (see ***Figure 1***). The first equilibrium dissociation reaction occurs as molecules dissociate into ions. The equilibrium in this case is between ions (which are then solvated) and neutral molecules. This is the dominant equilibrium dissociation reaction present in polar systems, and accordingly is the dominant reaction in classical aqueous electrochemistry.

However, in nonpolar systems there is a second equilibrium reaction present. This is the equilibrium reaction between free moving solvated ions and neutral ion-pairs that form due to long range electrostatic interactions. The details of this reaction were given in ***Section 1*** (see ***Eqs. 30*** and ***31***). The dissociation into free solvated ions is governed by Brownian motion, whereas the association into ion-pairs is governed by electrostatic interactions. Both of these mechanisms are well-defined, allowing for the *IPCM* to serve as a model, based on the *Dissociation Model*, for predicting conductivity in nonpolar media with added amphiphile across (nearly) the entire concentration range, from pure nonpolar media to pure amphiphile.

The first dissociation equilibrium reaction, between ions and neutral molecules, is much more difficult to define in the case of nonpolar systems for the reasons described above: the presence of contaminants, in combination with the very low concentration of total ions in these systems (making the impact of trace contaminants non-negligible), makes it very difficult to accurately describe this first dissociation equilibrium reaction. The exact species that are participating in this first dissociation equilibrium reaction are not well defined.

In classic electrochemistry only the first dissociation reaction is important, because ion-pairs are not present. However, due to concentration of ions being much higher, this reaction is typically well-defined.

In nonpolar electrochemisty both dissociation reactions are important. However, only the second dissociation reaction, between solvated ions and neutral ion-pairs, is well defined. It is this second equilibrium reaction that we seek to model using the *IPCM*, using this model to predict conductivity in nonpolar systems. The *IPCM* has two fitting parameters, ion size ($\boldsymbol{d_h}$) and concentration of ions in the amphiphile ($\boldsymbol{C_A}$) which serve as a theoretical treatment for the relevant parameters associated with the first equilibrium dissociation reaction.

3.12.1.1 CONDUCTIVITY, VISCOSITY, AND RELATIVE PERMITTIVITY PLOTTED VERSUS WEIGHT FRACTION

All of the measured data presented thus far has been plotted versus weight fraction of added amphiphile. More typically, such data would be plotted versus mole fraction of added amphiphile. However, in the case of mixtures of nonpolar media with added amphiphile, plotting data versus weight fraction of added amphiphile provides a more accurate representation.

As described above, the source of contaminant in nonpolar systems is ambiguous due to the very low concentration of ions in nonpolar systems, and the non-negligible effects that trace contamination can have on said systems. Since the exact source of ions is unknown, the

molecular weight of relevance is equally unknown. It is quite possible that ions present in a nonpolar system are the result of multiple species dissociating.

Because the relevant molecular weight is unknown, it is not possible to calculate the relevant mole fraction with respect to ions in solution. It is for this reason that we present the data on a weight fraction basis, which is well-defined for these systems. Weight fraction-basis also has the added benefit of being commonly used in industry.

3.13 THE ROLE OF VISCOSITY AND MOLECULAR CHAIN LENGTH IN NONPOLAR SYSTEMS: SHEAR RHEOLOGY

Thus far the *Ion-Pair Conductivity Model* has demonstrated the importance of viscosity, and its impact on ion mobility, on conductivity of nonpolar systems. Viscosity has been relegated to an input empirical parameter of a given amphiphile-nonpolar solution thus far, measured by a rheological instrument and used to help predict conductivity of these systems. While determination and use of viscosity in this manner is useful, a better understanding of the viscosity of such solutions, and Newtonian and non-Newtonian liquids in general, as well as the mixing rules that already exist for such systems, would allow the *Ion-Pair Conductivity Model* to rely less on empirically measured data, and provide a more robust tool for predicting the behavior of these systems.

Several viscosity mixing rules exist for polar and nonpolar media. In 1887, Arrhenius[103] proposed a dynamic viscosity mixing rule based on the mole fractions of the logarithms of the components of a liquid mixture. The ***Arrhenius mixing rule*** is defined as:

$$\boldsymbol{ln\,\eta_m = x_1\,ln\,\eta_1 + x_2 ln\,\eta_2} \qquad \textbf{\textit{Eq. 62}}$$

where $\boldsymbol{\eta}$ is dynamic viscosity, with subscript $\boldsymbol{m}$ corresponding to the overall mixture, and subscripts $\boldsymbol{1}$ and $\boldsymbol{2}$ corresponding to the components of the mixture, and $\boldsymbol{x}$ is mole fraction.

In 1949, Grunberg and Nissan expanded upon the *Arrhenius mixing rule* by adding parameter $\boldsymbol{d}$ to reflect molecular interactions within the solution, yielding the ***Grunberg-Nissan mixing rule***[104]:

$$\boldsymbol{\ln \eta_m = x_1 \ln \eta_1 + x_2 \ln \eta_2 + x_1 x_2 d} \qquad \textbf{\textit{Eq 63}}$$

This parameter $\boldsymbol{d}$ was a simply an empirical one, attempting to account for the additional attenuation observed beyond that predicted by the *Arrhenius mixing rule*.

Both the *Arrhenius mixing rule* (***Eq. 62***), and the expanded version proposed by Grunberg and Nissan (***Eq. 63***) ignore the molar volumes of the individual components. While ignoring molar volume may work in modeling systems where differences between the molar volumes of individual components is minimal, the same cannot be said when the differences in molar volumes are large. Thus, In 1964, Katti and Ghaudhri, taking into account molar volume, introduced the ***Katti-Ghaudhri mixing rule***[105]:

$$\ln \eta_m V_m = x_1 \ln \eta_1 V_1 + x_2 \ln \eta_2 V_2 \qquad \textit{Eq 64}$$

Where V is molar volume with subscript m corresponding to the overall mixture, and subscripts 1 and 2 corresponding to the components of the mixture.

Parameter d in ***Eq. 63*** was later replaced by the more generalized ΔG, the excess activation energy of the viscous flow (i.e. the sum of the intermolecular energies of the components E_{ij}) defined as:

$$\Delta G = \sum_i \sum_j x_i x_j E_{ij} \qquad \textit{Eq. 65}$$

Replacing parameter d in ***Eq. 63*** with ***Eq. 65***, ΔG, and generalizing for N components yields the ***Eyring mixing rule***[106]:

$$\ln \eta_m V_m = \sum_i^N x_i \ln \eta_i V_i + \frac{\Delta G}{RT} \qquad \textit{Eq. 66}$$

Where R is the universal gas constant and T is temperature.

For the purpose of examining binary mixtures, ***Eq. 65*** can be substituted into ***Eq. 66***, and limiting the number of elements to 2, yields the following mixing rule for dynamic viscosity of liquid mixtures, the ***Excess Activation Energy mixing rule (EAE)***[107]:

$$ln \eta_m V_m = x_1 ln \eta_1 V_1 + x_2 ln \eta_2 V_2 + x_1 x_2 \frac{E_{12}}{RT} \qquad \textit{Eq. 67}$$

Eq. 67 is similar to both the ***Grunberg-Nissan mixing rule*** and the ***Katti-Ghaudhri mixing rule***, but provides an explanation and mathematical representation for parameter d proposed by Grunberg and Nissan, where E_{12} accounts for the energy of molecular interactions between

the molecules of different components (i.e. the molecular interactions between components 1 and 2). This *Excess Activation Energy mixing rule* allows us to explore the extent to which intermolecular interactions affect the viscosity of these systems. By definition, parameter $\boldsymbol{E_{12}}$ must be constant regardless of the concentrations of the components, thus, $\boldsymbol{E_{12}}$ can be set as an adjustable parameter and solved for via viscosity versus concentration data. An approach first demonstrated by Monsalvo[108] et al. and expanded in this study.

The viscosity models described thus far are all classified as transition state theory, which states that viscosity (in particular, shear viscosity) is created by a molecule jumping from its initial position to an adjacent available location, overcoming an activation energy barrier to do so. As a result, the *Excess Activation Energy mixing rule*, argues that due to intermolecular forces between non-like molecules, an additional (i.e. excess) activation energy barrier must be overcome in order for a molecule to move to a new position.

Eq. 62, the *Arrhenius mixing rule*, is an absolute calculation (i.e. it does not contain any adjustable parameters). The *Excess Activation Energy mixing rule* has a single adjustable parameter, $\boldsymbol{E_{12}}$, which pertains to the energy of intermolecular forces. The ***Batchinski mixing rule***, used more recently in the field of polar and nonpolar systems, relies on two adjustable parameters[109,110]:

$$\boldsymbol{\eta_m = \frac{C}{V_m - b}} \qquad \textbf{Eq. 68}$$

Where $\boldsymbol{b}$ and $\boldsymbol{C}$ are substance-specific constants.

There are a wide variety of additional semi-empirical mixing rules to describe the viscosity of liquid mixtures: the hard-spheres model[111], the self-referencing approach[112], friction theory[113], and the free-volume model[114]. There are numerous of published papers which utilize these approaches[108,115-117]. The consensus among much of this work is that the simpler linear mixing rules described earlier (the Arrhenius mixing rule and the Grunberg-

Nissan mixing rule) are only applicable when the intermolecular interactions between unlike particles is weak. For stronger interactions more complicated theories are proposed. Friction theory is suggested by Monsalvo et al and Queimada et all[108,118], whereas the free-volume model is suggested in the work by Bloomfield and Dewan[116].

3.13.1 RESULTS

While earlier studies utilize computational simulations to solve for ***b*** and ***C***, we chose to use the semi-empirical *Excess Activation Energy mixing rule* along with the *Arrhenius mixing rule* and *Katti-Ghaudhri mixing rule*, to examine viscosity in two component non-Newtonian amphiphile (i.e. nonionic surfactant) and Newtonian nonpolar liquid solutions.

For these experiments' toluene was used as the Newtonian liquid. The non-Newtonian liquids were non-ionic surfactants, specifically SPAN 20, SPAN 80, OFX-5098, and OFX-0400. By looking at these four surfactants, we able to explore the role of chain length in influencing viscosity.

Material	Molecular Weight	Density	Viscosity		Sound Speed	Compressibility
			Dynamic	Longitudinal @ 100 MHz		
	[g/mol]	[g/cm^3]	[cP]	[cP]	[m/s]	10^{-10} [m^2/N]
Toluene	95.14	0.87	0.56	8.97	1305.20	6.77
SPAN 20	346.46	1.03	3505.88	227.50	1500.98	4.30
SPAN 80	428.61	0.99	1047.10	149.20	1466.98	4.69
OFX-5098	3225.90	1.08	219.16	65.26	1371.40	4.92
OFX-0400	3101.10	1.02	259.74	39.56	1180.04	7.04

***Table 10**: Intrinsic Properties of Non-Ionic Surfactants and Toluene: Molecular Weight, Density, Viscosity, Sound Speed, and Compressibility.*

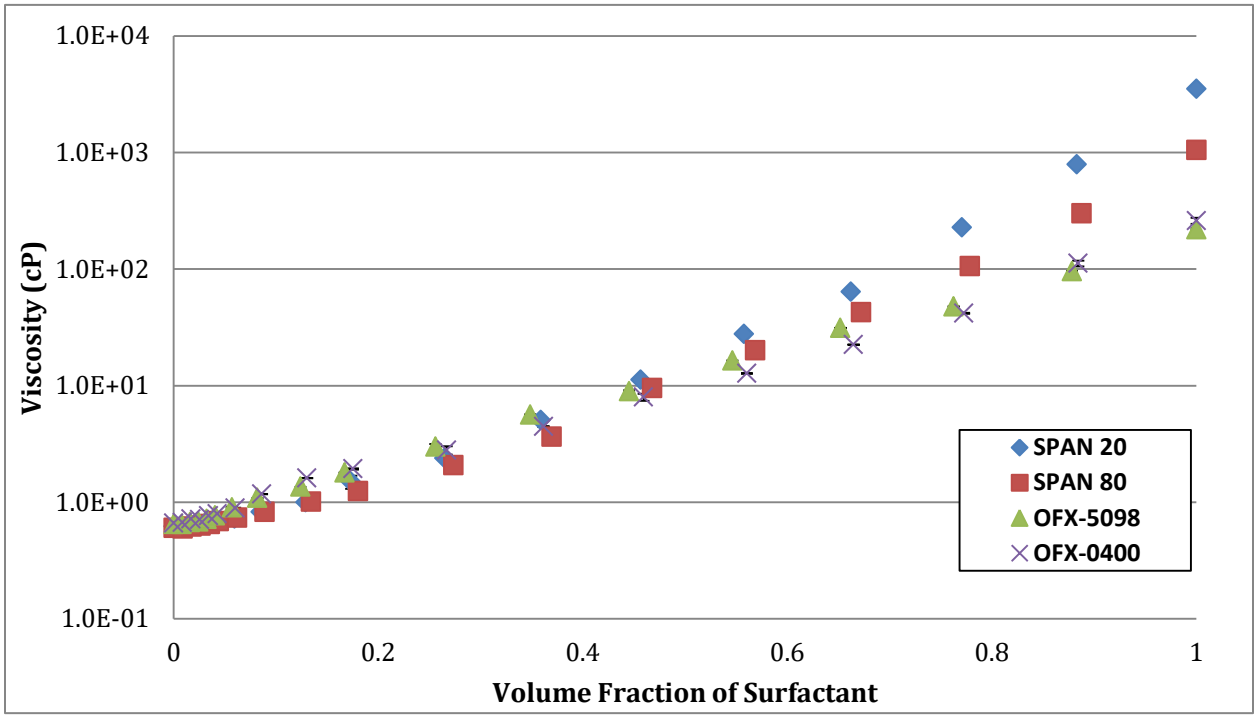

***Figure 37**: Experimental Viscosity versus Concentration of Amphiphile Data for mixtures of Non-Ionic Surfactant and Toluene. Logarithmic Scale*

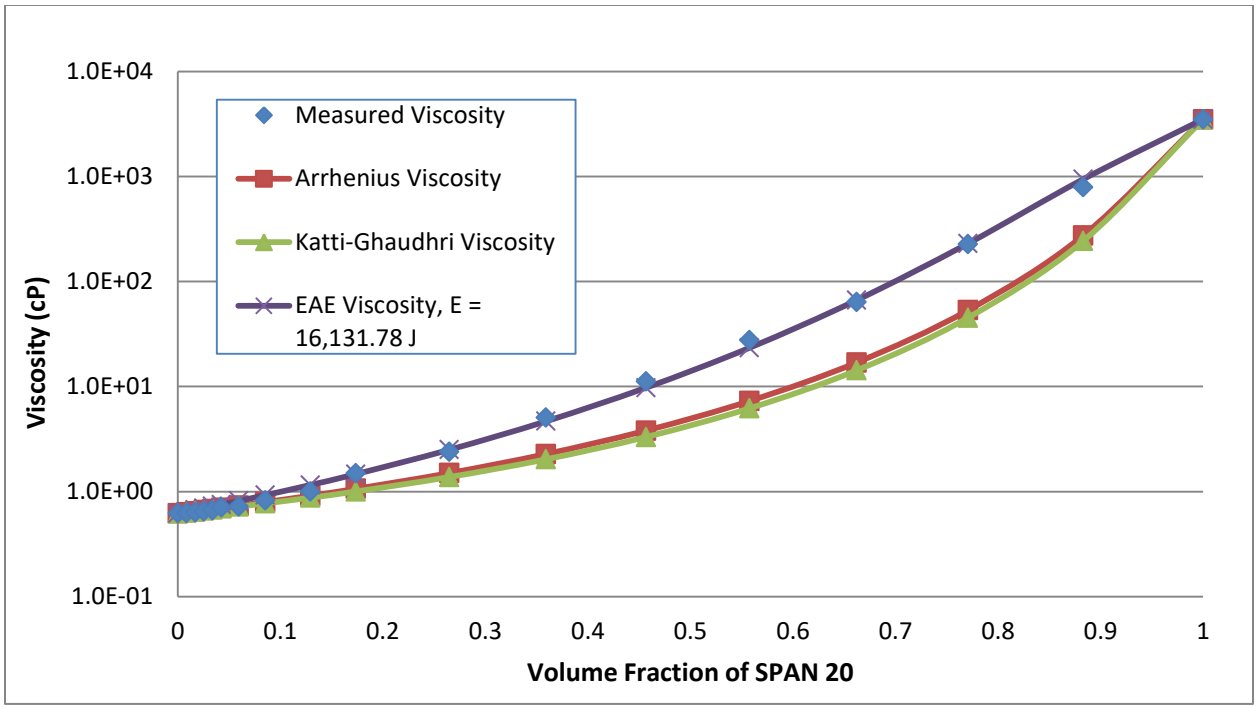

***Figure 38a**: Theoretical versus Measured Viscosity Data for Mixtures of SPAN 20 and Toluene. Logarithmic Scale*

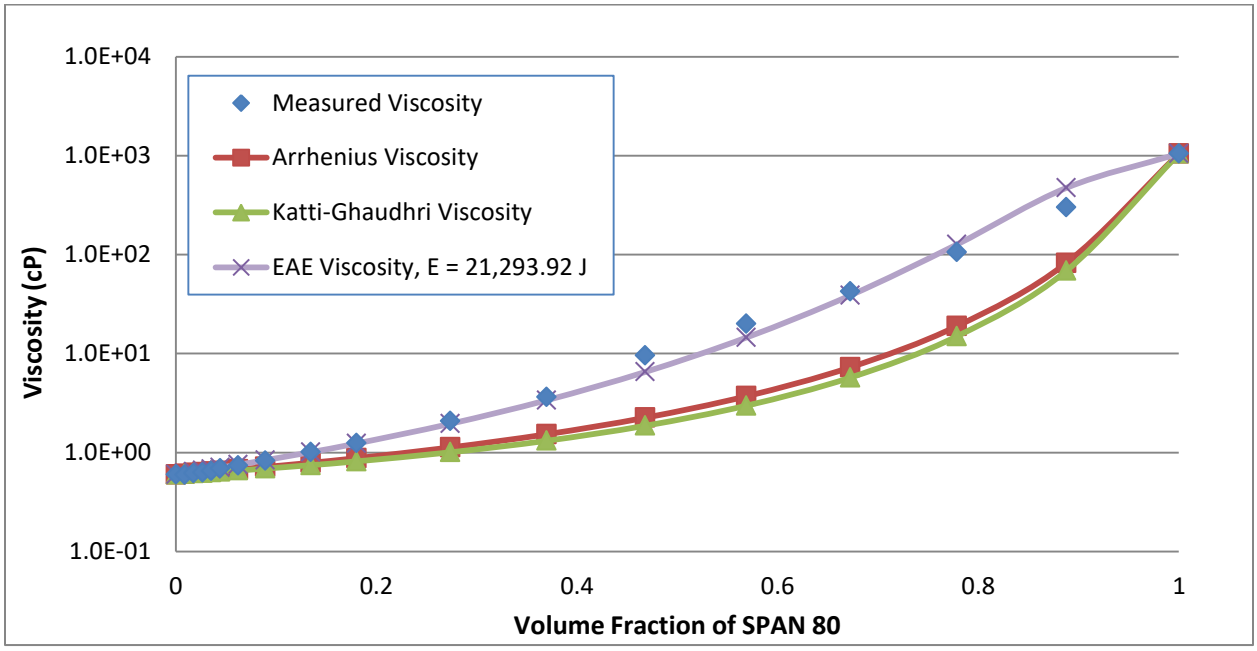

***Figure 38b**: Theoretical versus Measured Viscosity Data for Mixtures of SPAN 80 and Toluene. Logarithmic Scale*

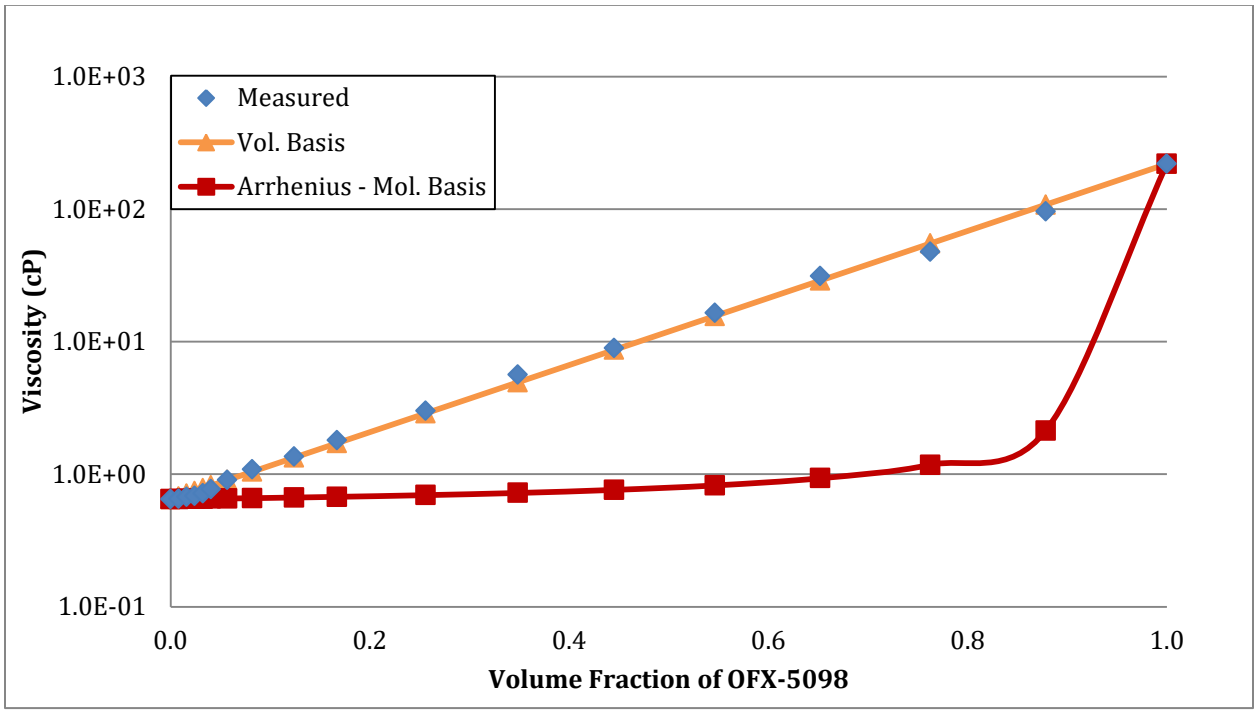

***Figure 39a**: Theoretical versus Measured Viscosity Data for Mixtures of OFX-5098 and Toluene. Logarithmic Scale*

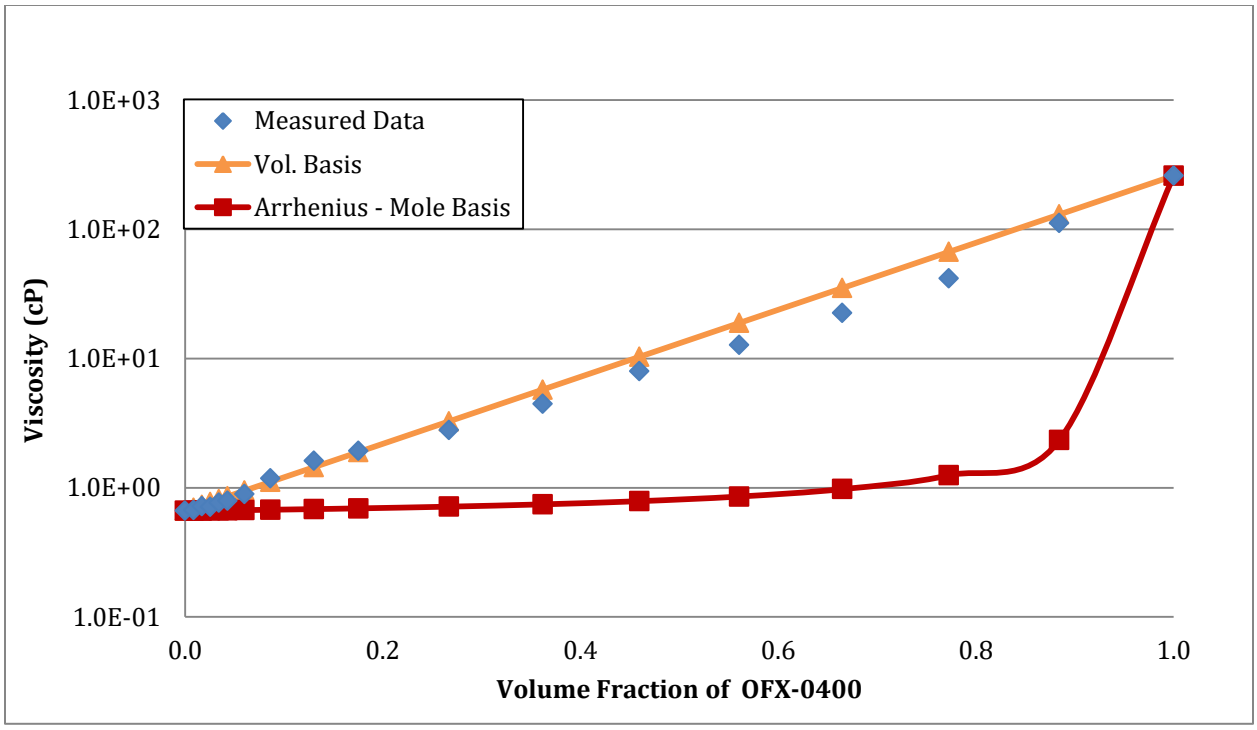

***Figure 39b**: Theoretical versus Measured Viscosity Data for Mixtures of OFX-0400 and Toluene.*

Logarithmic Scale

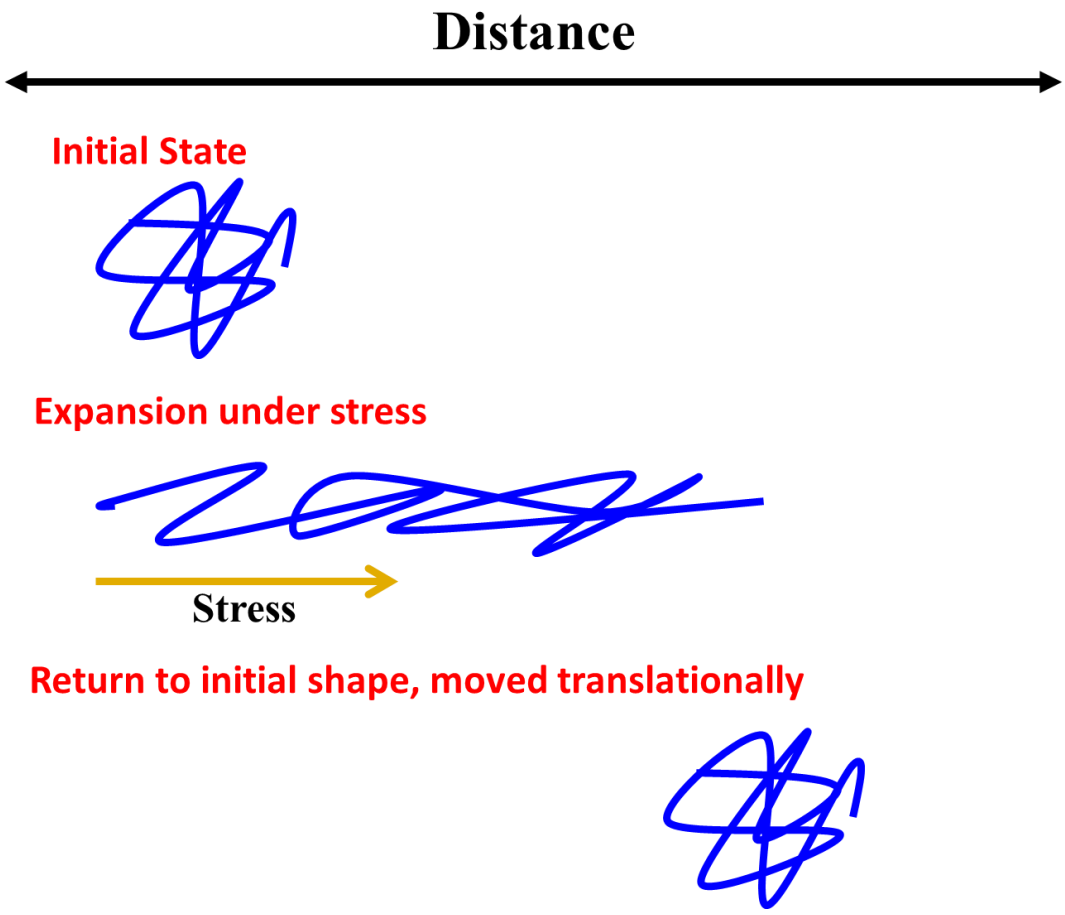

Figure 40*: Cartoon Depiction of Hypothesized Mechanism of Expanding and Collapsing of Long-Chain Surfactant Molecule.*

3.13.2 DISCUSSION

3.13.2.1 SPAN nonionic surfactant-toluene solutions

The molecular weight of the Xiameter surfactants is roughly ten times that of the SPAN surfactants. We can classify the Xiameter surfactants as "long-chain" surfactants, and the SPAN surfactants as "short-chain" surfactants. Sample preparation and the Cannon-Fenske viscometers, used for measuring viscosity in earlier **Section 3.4**, were the same for studying viscosity of these nonionic surfactant-toluene solutions.

Figure 37shows viscosity versus concentration of non-Newtonian amphiphile for all four nonionic surfactant-toluene solutions and ***Figure 38a*** and ***Figure 38b***, illustrate viscosity versus concentration of non-Newtonian amphiphile SPAN 20-toluene and SPAN 80-toluene solutions, respectively, as well as theoretical fits using the *Arrenhius mixing rule* and *the Katti-Ghaudhri mixing rule*. As seen in ***Figures 38a*** and ***38b***, both the *Arrenhius mixing rule* and *the Katti-Ghaudhri mixing rule* grossly underestimate and are unable to predict the experimental viscosity data, across most nonionic surfactant concentration ranges, from ***Figure 37***. However, using the *Excess Activation Energy mixing rule*, the fit improves significantly, becoming a near perfect predictor of the measured data for both SPAN short-chain surfactant-toluene solutions.

By solving for the optimal value of E_{12}, the intermolecular interaction energy between SPAN molecules and toluene can be explored. The calculated values for E_{12} for the SPAN-toluene solutions are as follows:

- SPAN 20 - 16131 J
- SPAN 80 – 21293 J

The above values for E_{12} are in agreement with the HLB data for these surfactants. Based on HLB number, SPAN 80, with an HLB number of 4.3, has a higher affinity for

toluene (which is hydrophobic) than SPAN 20, with an HLB number of 8.6, does. Similarly, the $\boldsymbol{E_{12}}$ value for SPAN 80 is higher than that of SPAN 20, implying that intermolecular interaction energy between SPAN 80 and toluene is higher than that for SPAN 20 and toluene, again indicating SPAN 80 has a higher affinity for toluene than SPAN 20.

Converting the $\boldsymbol{E_{12}}$ values, at 50 wt. % surfactant, to ΔG values:

- SPAN 20 - 4,033 J
- SPAN 80 – 5,323 J

Prior publications have also examined and reported ΔG values for similar nonpolar solutions (e.g. 1,1,1,2-tetrafluoroeethane (HFC-134a) with tetraethylene glycol dimethylether)[108]. While the reported $\boldsymbol{\Delta G}$ values for these nonpolar solutions were roughly half that of the values reported for the SPAN-toluene solutions presented hrein, they serve as a basis of comparison between $\boldsymbol{\Delta G}$ values for nonpolar liquid-liquid mixtures.

This analysis of for viscosity of nonpolar media with short-chain surfactants has not included the impact of surfactant self-assembly. It is known that above the critical micelle concentration (CMC) that surfactant molecules will self-assemble in structures such as micelles, bi-layers, and higher order structures depending on concentration. However, despite this omission the *Excess Activation Mixing Rules* is still able to accurately predict viscosity as a function of concentration, and provide insight into intermolecular interaction energies between SPAN surfactants and toluene, for both mixtures of nonpolar media and short-chain surfactants studied.

3.13.2.2 Xiameter nonionic surfactant-toluene solutions

As seen in ***Figure 39a*** and ***Figure 39b***, the long-chain Xiameter surfactants exhibited a linear volume-fraction dependence on viscosity, while the short-chain SPAN surfactants viscosity curves adhered to the more classically based mixing rules. Due to their increased length, the Xiameter surfactants are potentially more flexible, and therefore much more capable of deformation under the stress of a shear field. It is therefore possible that the mechanical energy dissipation is associated with this deformation.

If we assume that a long-chain surfactant molecule is anchored in location to a toluene molecule, then under an applied stress that long-chained surfactant molecule can begin to deform and stretch. When the stress is sufficient, eventually the surfactant molecule would release from the toluene molecule it was anchored, and then return to its original un-stretched shape, in a new location. From the perspective of the molecule, it undergoes cycles of expanding and collapsing (i.e. retraction) under the applied stress. Additionally, the molecule would be moving through space as a result of this cyclical motion. So, the motion of the molecule is the superposition of oscillation and translation. Therefore, there are two degrees of freedom associated with the motion of the molecule: oscillatory and translational. ***Figure 40*** is a cartoon which serves to demonstrate this behavior.

This second, oscillatory degree of freedom with regards to energy dissipation is similar to the Kelvin-Voigt model[118,119], and has been used for explaining excess ultrasound attenuation for dispersions in which the particles are linked by polymer strings[67]. According to this model, the first term, in the expansion of the equation for molecular displacement, is proportional to the length of displacement, while the second term is related to (and thus proportional to) the rate of displacement. It is this second term that is responsible for mechanical energy

dissipation, and therefore responsible for the viscosity of the system. The coefficient related to this term in the expansion is sometimes referred to as the "*second Hookean coefficient*."

According to this model, the viscosity of the system is dependent on the concentration of the non-Newtonian surfactant additive and the *second Hookean coefficient*, which corresponds to the relationship between stress and rate of strain. This concentration dependence on non-Newtonian surfactant additive is expressed mathematically as a volume-fraction dependence according to:

$$\boldsymbol{ln\,\eta_m = (1-\varphi)\,ln\,\eta_1 + \varphi ln\,\eta_2} \qquad \textbf{\textit{Eq. 69}}$$

Where $\boldsymbol{\phi}$ is the volume fraction of the non-Newtonian additive.

3.14 THE ROLE OF VISCOSITY AND MOLECULAR CHAIN LENGTH IN NONPOLAR SYSTEMS: LONGITUDINAL RHEOLOGY

While classic mixing rules are useful for predicting the conductivity of short-chain surfactant solutions, the assumptions they make and relationships they use to model viscosity in nonpolar systems fail entirely for long-chain surfactant solutions.

For systems in which the non-Newtonian liquids are long-chain surfactants, a superposition of translational and oscillational motion, as illustrated in ***Figure 40***, is used to describe these long-chain surfactant molecule's response to applied stress.

Ultrasound attenuation measurements apply a stress which results in predominantly oscillatory motion in liquid media[67]. As a result, the use of ultrasound attenuation measurements and, more specifically, measurements of high-frequency longitudinal rheology, allow for further exploration of the viscosity of these mixtures. While translational motion does exist under an applied acoustic stress (in the MHz range), it is comparatively negligible to the oscillatory motion. As is the case, ultrasound attenuation measurements allow us to single out the oscillatory degree of freedom, in order to explore the extent to which it contributes to the viscosity of the overall system, which is of specific interest for solutions with long-chain Xiameter surfactants due to their unique behavior under shear stress described in ***Section 3.13***.

3.14.1 RESULTS

Two parameters were measured in the case of these ultrasound experiments: sound speed and attenuation. ***Figures 41 a-d*** present attenuation versus frequency for all four nonionic surfactant-toluene solutions across the entire concentration range from pure nonionic surfactant to pure toluene.

Figure 42 presents sound speed versus nonionic surfactant concentration for all four surfactant-toluene mixtures.

Figure 43presents compressibility versus nonionic surfactant concentration data for all four of the surfactant-toluene mixtures.

Figures 44a-d present longitudinal viscosity versus frequency for all four nonionic surfactant-toluene solutions across the entire concentration range from pure nonionic surfactant to pure toluene.

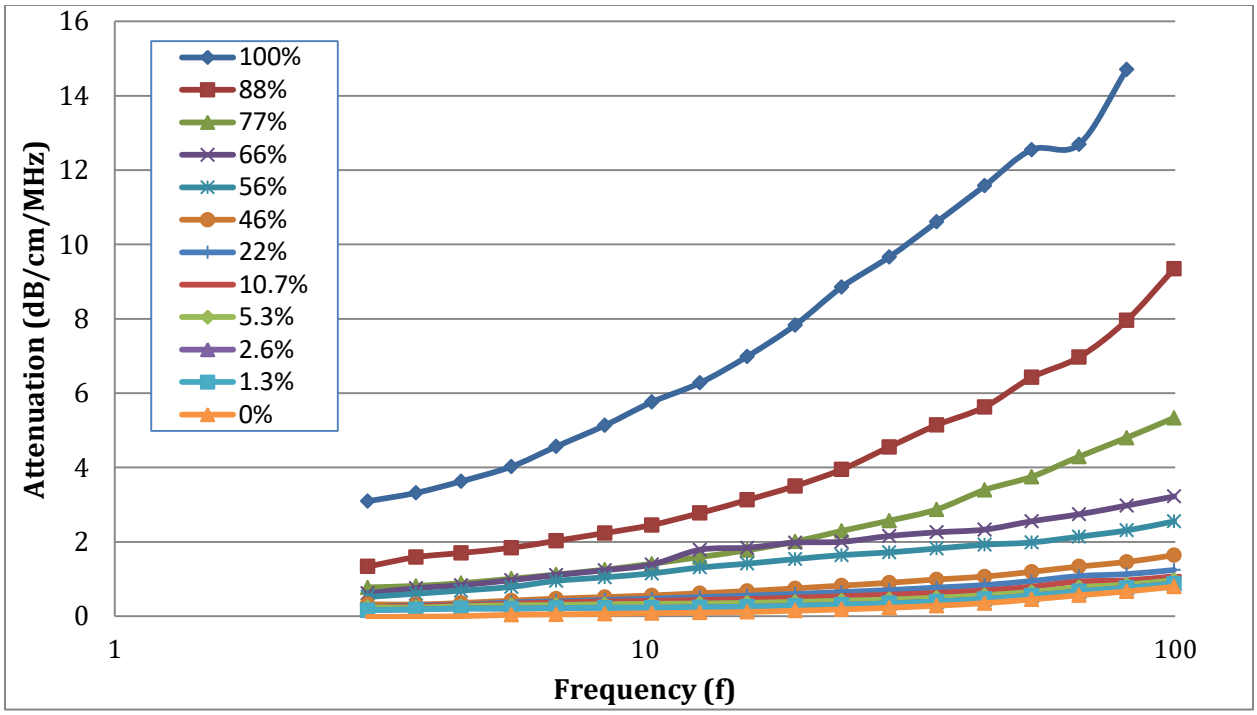

***Figure 41a**: Attenuation Versus Frequency for Nonionic Surfactant SPAN 20-Toluene Solutions. Values in legend correspond to concentration (volume %) of SPAN 20 in mixture. Linear Scale*

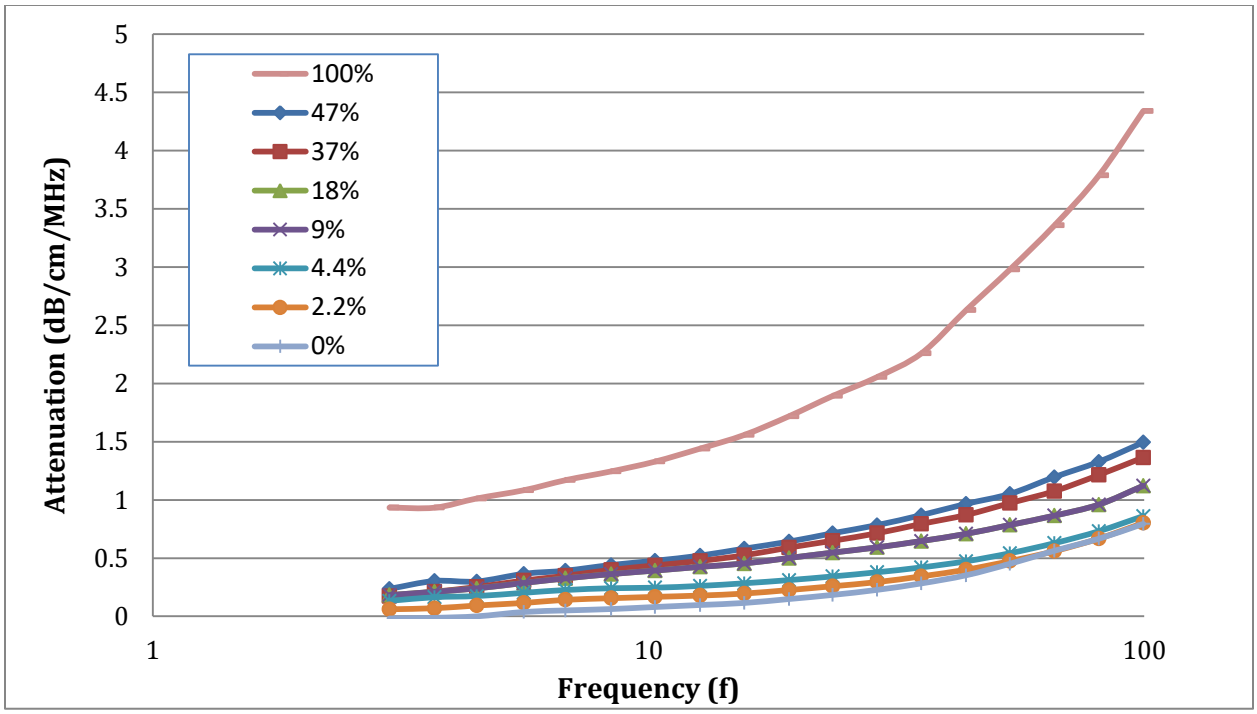

***Figure 41b**: Attenuation versus Frequency for Nonionic Surfactant SPAN 80-Toluene Solutions. Values in legend correspond to concentration (volume %) of SPAN 80 in mixture. Linear Scale*

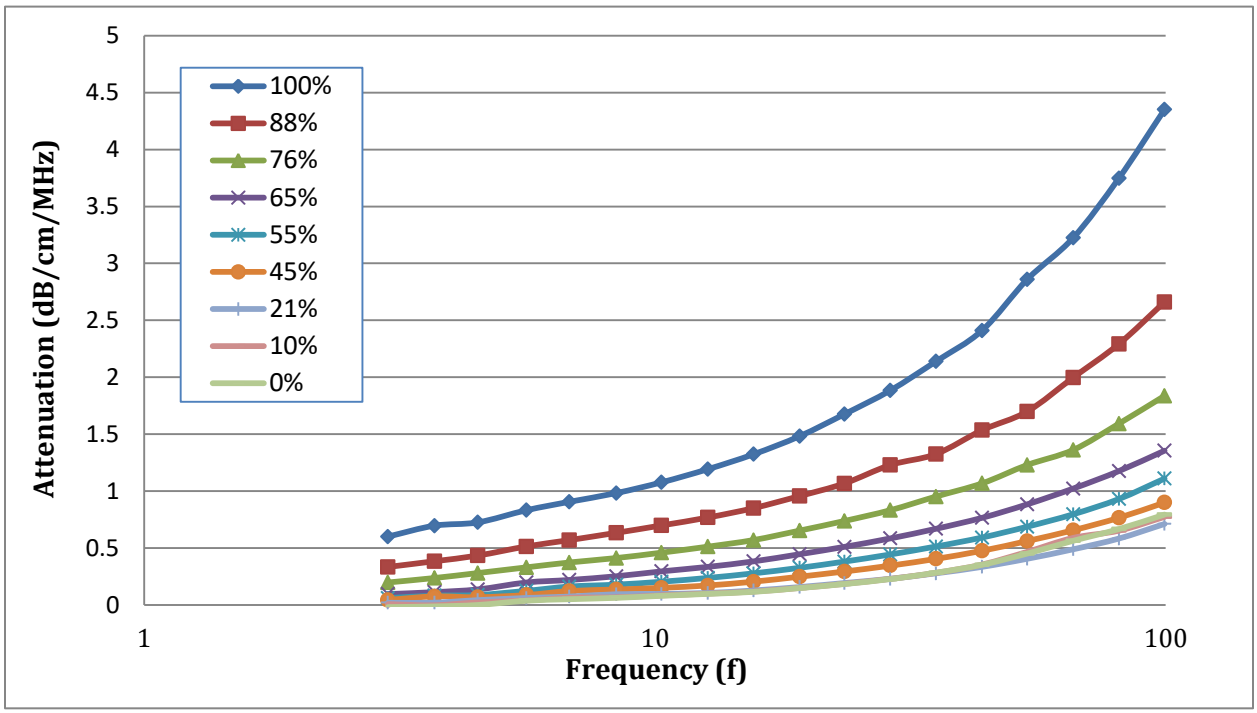

***Figure 41c**: Attenuation versus Frequency for Nonionic Surfactant OFX-5098-Toluene Solutions. Values in legend correspond to concentration (volume %) of OFX-5098 in mixture. Linear Scale*

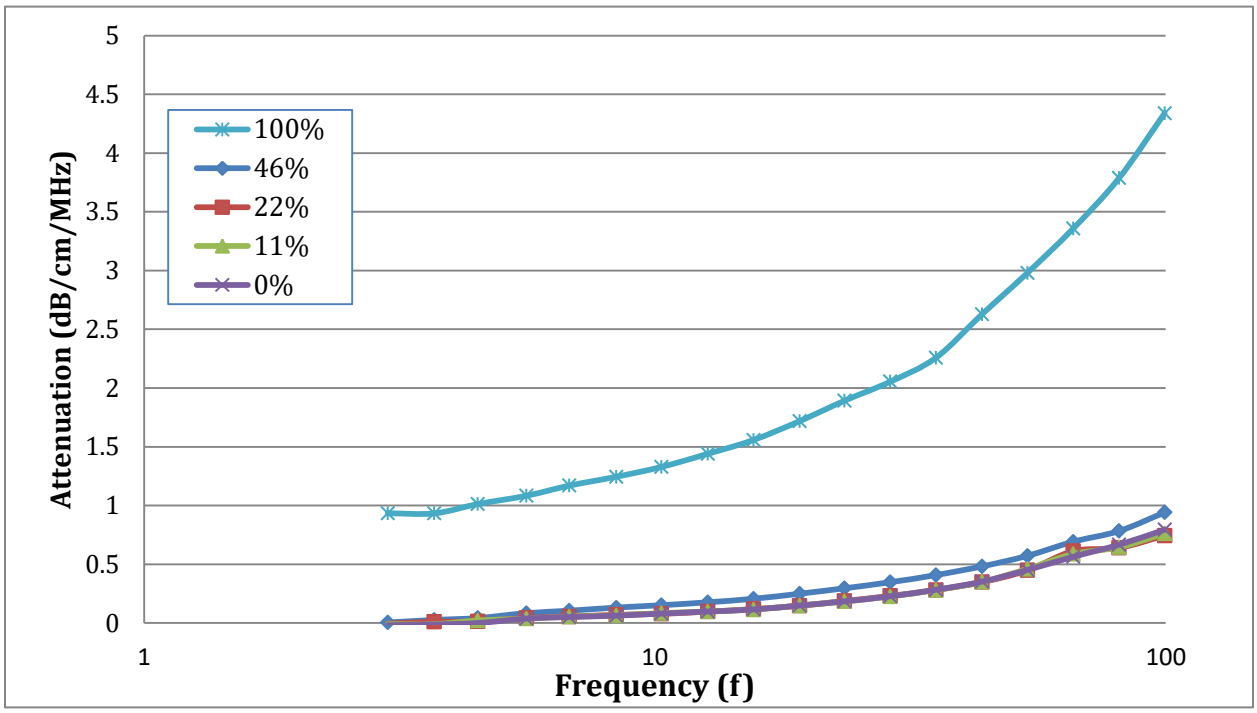

***Figure 41d**: Attenuation Versus Frequency of Non-Ionic Surfactant OFX-0400-Toluene Solutions. Values in legend correspond to concentration (volume %) of OFX-0400 in mixture. Linear Scale*

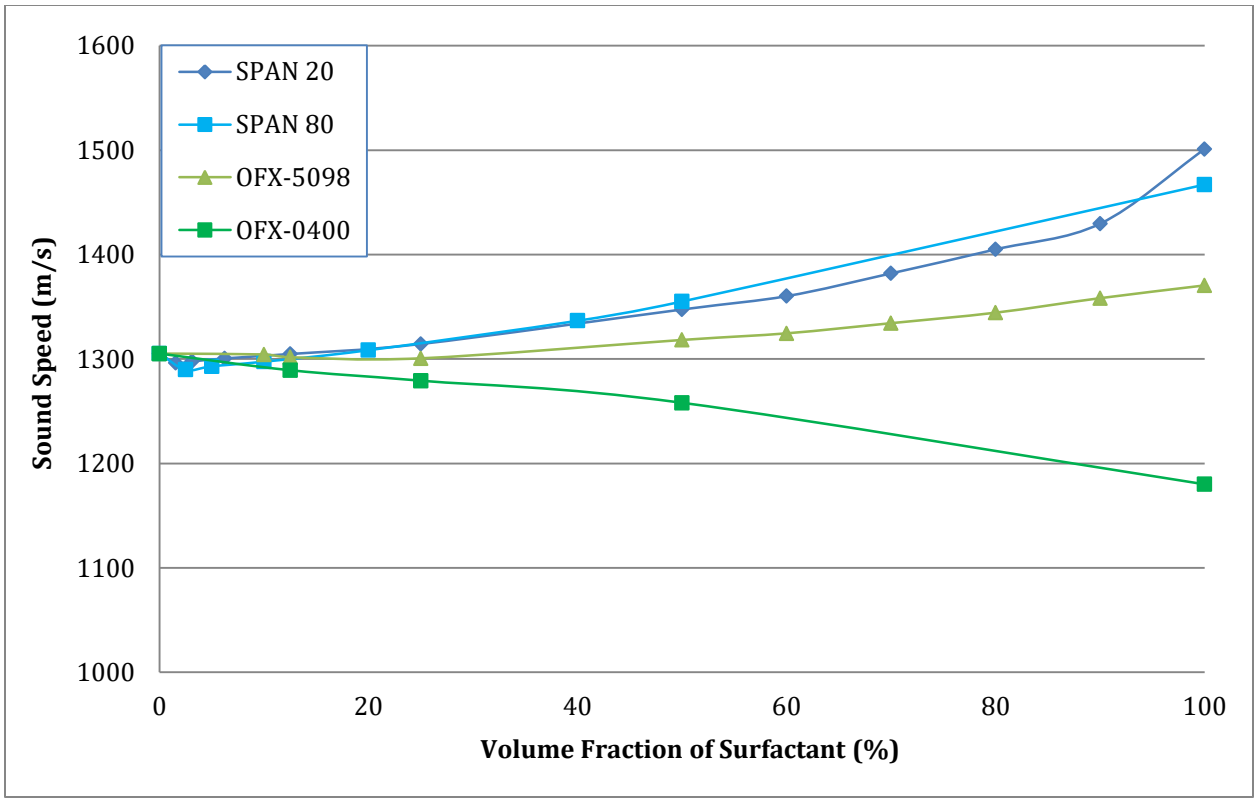

***Figure 42**: Sound Speed versus Nonionic Surfactant Concentration Nonionic Surfactant-Toluene Solutions. Legend Denotes Nonionic Surfactant in Mixture. Linear Scale*

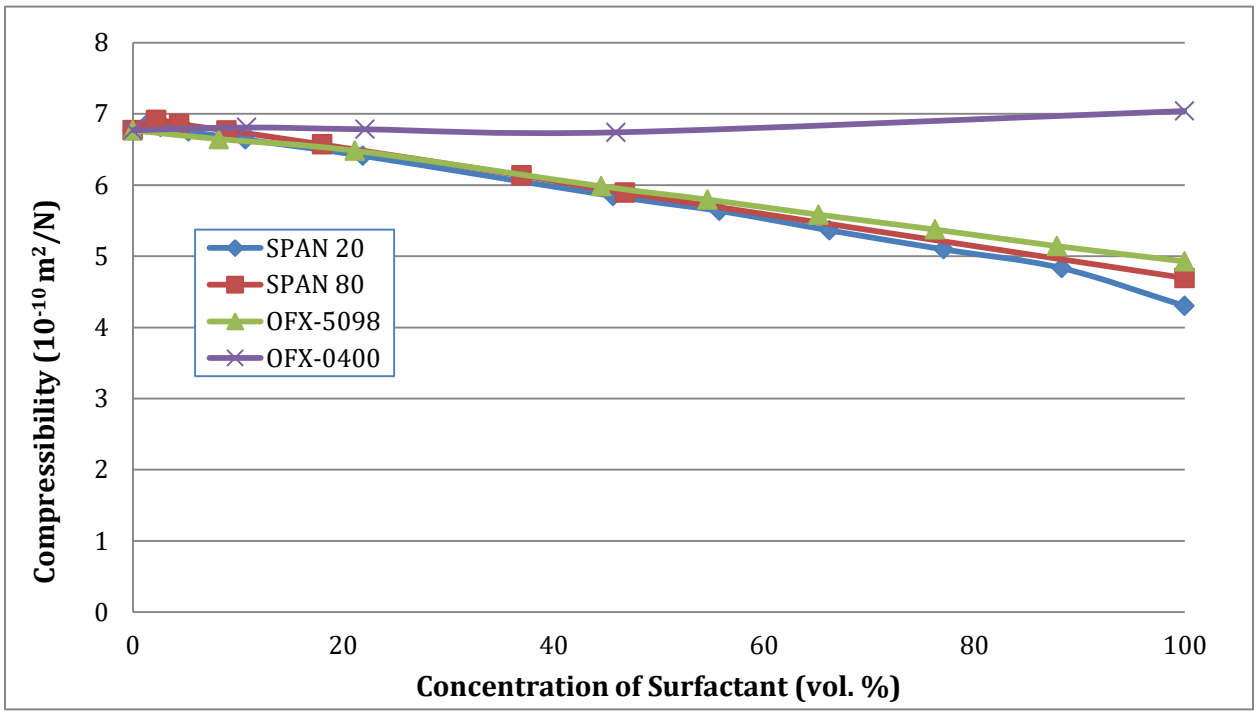

***Figure 43**: Compressibility versus Concentration of Amphiphile for Mixtures of Non-Ionic Surfactant and Toluene. Legend Denotes Nonionic Surfactant in Mixture. Linear Scale*

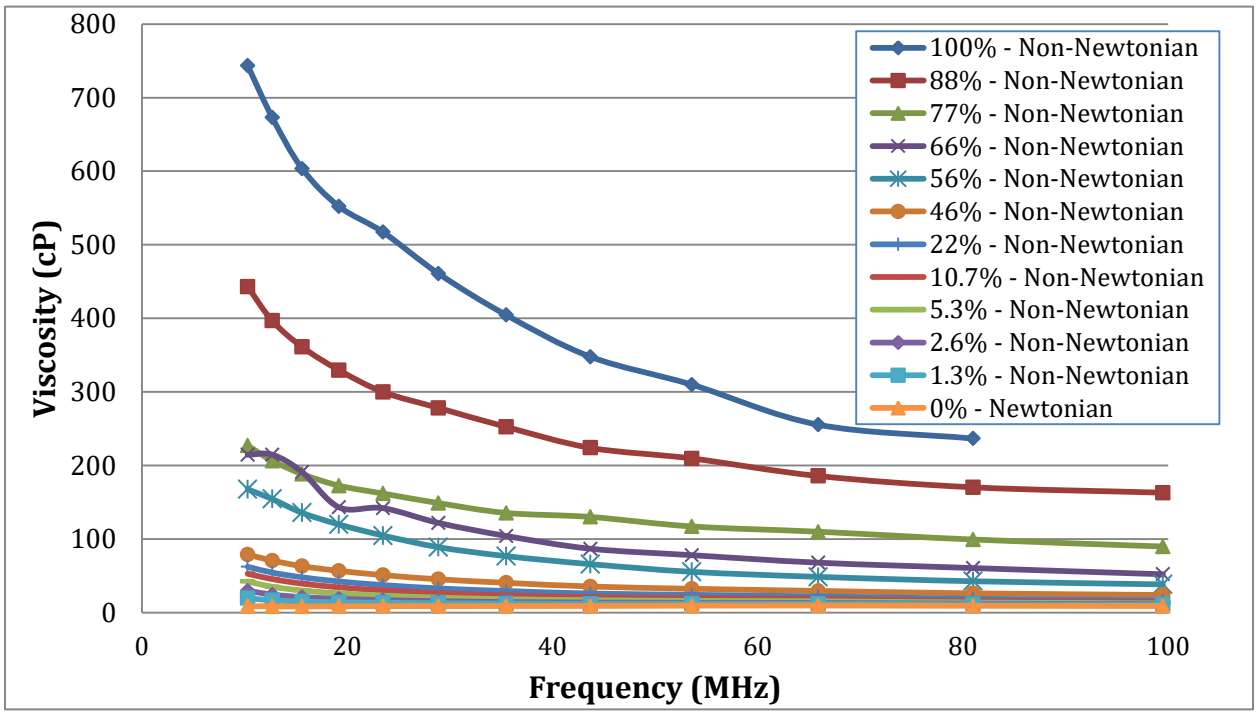

***Figure 44a**: Longitudinal Viscosity versus Frequency for Mixtures of Non-Ionic Surfactant and Toluene at Various Concentrations: SPAN 20. Information in legend corresponds to concentration of SPAN 20 (vol. %) in mixture with Toluene, and whether the DT-1202 reports that the mixture is Newtonian or Non-Newtonian under MHz stress. Linear Scale*

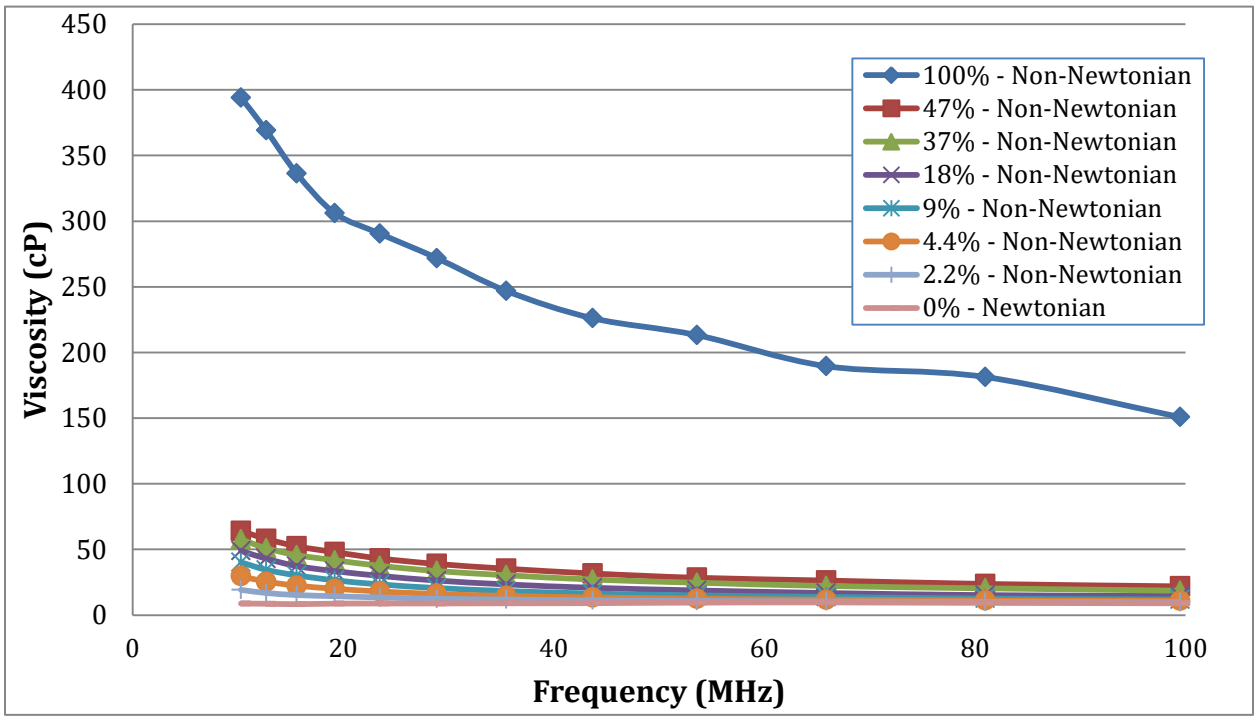

***Figure 44b**: Longitudinal Viscosity versus Frequency for Mixtures of Non-Ionic Surfactant and Toluene at Various Concentrations: SPAN 80. Information in legend corresponds to concentration of SPAN 80 (vol. %) in mixture with Toluene, and whether the DT-1202 reports that the mixture is Newtonian or Non-Newtonian under MHz stress. Linear Scale*

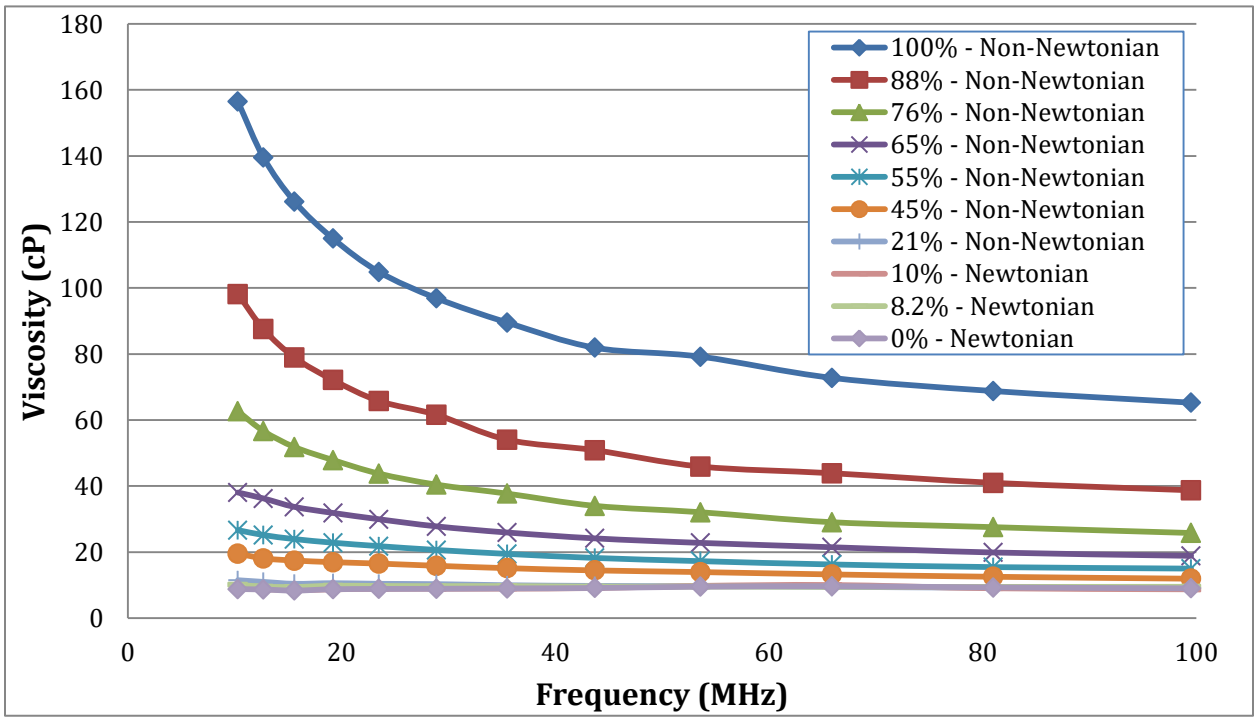

***Figure 44c**: Longitudinal Viscosity versus Frequency for Mixtures of Non-Ionic Surfactant and Toluene at Various Concentrations: OFX-5098. Information in legend corresponds to concentration of OFX-5098 (vol. %) in mixture with Toluene, and whether the DT-1202 reports that the mixture is Newtonian or Non-Newtonian under MHz stress. Linear Scale*

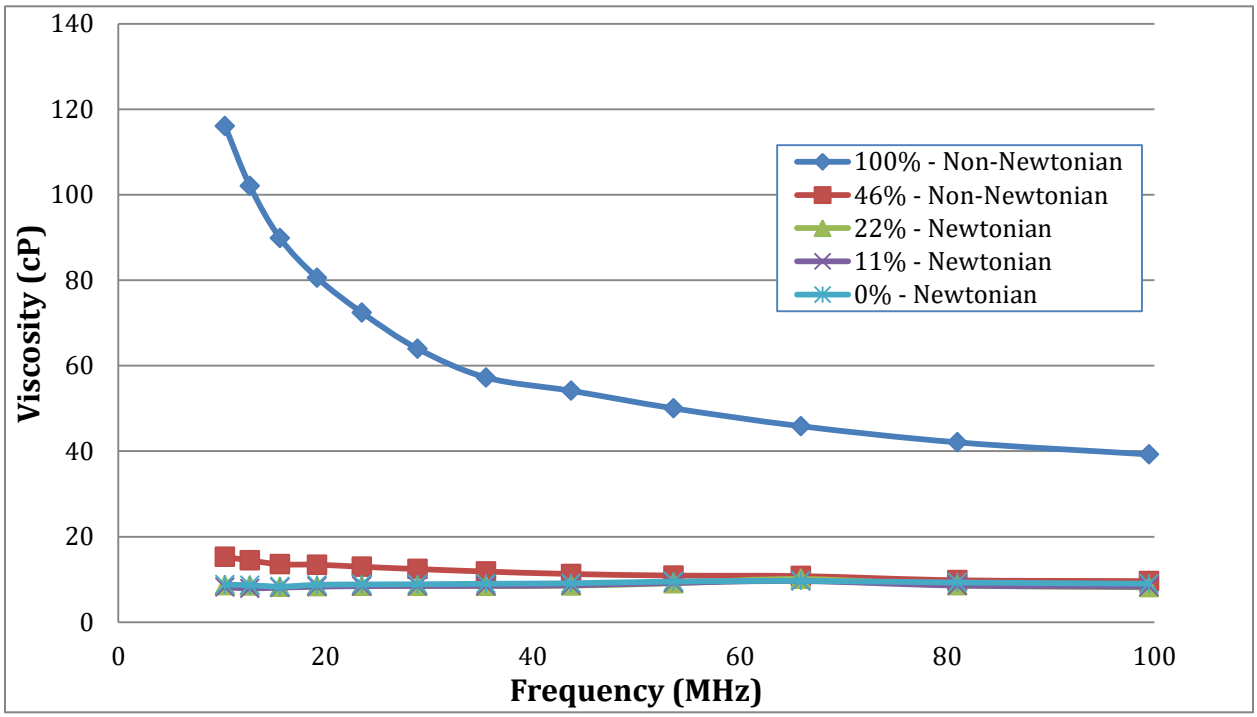

***Figure 44d**: Longitudinal Viscosity versus Frequency for Mixtures of Non-Ionic Surfactant and Toluene at Various Concentrations: OFX-0400. Information in legend corresponds to concentration of OFX-0400 (vol. %) in mixture with Toluene, and whether the DT-1202 reports that the mixture is Newtonian or Non-Newtonian under MHz stress. Linear Scale.*

3.14.2 DISCUSSION

The data in ***Figures 41 a-d*** and ***Figure 42*** are experimental longitudinal raw data for all four nonionic surfactant-toluene solutions for attenuation frequency spectra and sound speed, respectively. This raw data is then used for determining solution properties that are more commonly associated with rheology, specifically compressibility (from sound speed) and longitudinal viscosity (from attenuation spectra).

Compressibility, $\boldsymbol{\beta}$, is calculated from sound speed according to the following equation[66]:

$$\boldsymbol{\beta} = \frac{\mathbf{1}}{\boldsymbol{V^2\rho}} \qquad \textit{Eq. 70}$$

Where $\boldsymbol{V}$ is sound speed of the solution, and $\boldsymbol{\rho}$ is density. This compressibility $\boldsymbol{\beta}$ is the isothermal compressibility of the system and is a measure of the relative volume change of the material in response to a stress. In this case the applied stress is pressure via an ultrasonic sound pulse, and therefore the direction of the stress is normal to the interface. This sets longitudinal rheology, and accordingly longitudinal isothermal compressibility, apart from the more common shear rheology: the direction of applied stress is tangential to the surface (i.e. interface) for shear rheology, whereas it is normal to the surface in longitudinal rheology.

Figure 43 presents the compressibility for mixtures of nonionic surfactant and toluene as a function of concentration of nonionic surfactant, for all concentrations from pure toluene to pure nonionic surfactant. For solutions in which the nonionic surfactant is SPAN 20, SPAN 80, and OFX-5098, the compressibility decreases as a function of surfactant concentration, which is due to sound speed increasing as a function of concentration in ***Figure 42***. However, for the solution in which the nonionic surfactant was OFX-0400 the opposite was true: compressibility increased slightly as a function of surfactant concentration, due to sound speed diminishing as a function of surfactant concentration.

Figures 41 a-d present attenuation versus frequency graphs for all four nonionic surfactant-toluene solutions across the entire concentration range from pure nonionic surfactant to pure toluene. Longitudinal viscosity is then calculated from these attenuation spectra according to the following equation[67,120]:

$$\eta_{long} = \frac{2\alpha\rho V^3}{\omega^2} \qquad \textit{Eq. 71}$$

Where ω is ultrasound frequency, α is attenuation, ρ is density and V is sound speed of the overall mixture.

Figures 44 a-d present longitudinal viscosity versus frequency for all four nonionic surfactant-toluene solutions across the entire concentration spectra from pure nonionic surfactant to pure toluene. The instrument used in these experiments (Dispersion Technology DT-1202) is also capable of determining whether a liquid is Newtonian or non-Newtonian, while accounting for experimental error in measurement, on the megahertz scale. The viscosity of a Newtonian liquid is independent of frequency, while the viscosity of a non-Newtonian liquid is dependent upon frequency (noted in the ***Figure 44 a-d*** legends next to each curves concentration vol. %).

At high concentrations of nonionic surfactant all of the mixtures behaved as non-Newtonian liquids. The threshold at which the nonionic surfactant-toluene solutions transitioned from non-Newtonian to Newtonian are:

- SPAN 20 - below 1.2 vol. %
- SPAN 80 - below 1.2 vol. %
- Xiameter OFX-5098 - above 10 vol. %
- Xiameter OFX-0400 - above 22 vol. %

As was the case in the shear rheology studies in **Section 3.13**, the solutions longitudinal rheological behavior is governed by the surfactants chain length.

The short-chain SPAN surfactant-toluene solutions behave as non-Newtonian liquids across nearly the entire concentration spectra. In fact, the solutions only behave as a Newtonian liquid when the solution is pure toluene (i.e. 0 vol. % SPAN surfactant). The non-Newtonian behavior observed by these SPAN-toluene solutions across nearly the entire concentration spectra is likely the result of micelle formation or other self-assembly of surfactant molecules, whose response to longitudinal stress is frequency dependent.

The long-chain Xiameter nonionic surfactant-toluene solutions behaved as Newtonian liquids across a much broader nonionic surfactant concentration range (~0-22 vol .% for the OFX-0400-toluene solution and ~0-10 vol. % for the OFX-5098-toluene solution). The non-Newtonian behavior for these long-chain nonionic surfactant-toluene solutions at very high nonionic surfactant concentration ranges (e.g. over 50 vol. %) is likely driven by the macroscopic structure formed within the mixture. However, as the sample is diluted and the concentration of surfactant decreases, that macroscopic structure disappears, and the contribution from individual surfactant molecules is negligible. In fact, at the concentrations at which the mixtures become Newtonian and below, the attenuation curves for the mixtures are indistinguishable from that of pure toluene.

The measured attenuation spectra in ***Figures 41 a-d*** and corresponding longitudinal viscosity data in ***Figures 44 a-d*** imply that for the long-chain Xiameter-toluene solutions, oscillation of the Xiameter surfactant molecules in an ultrasound wave does not contribute to the viscosity of the system. Therefore, this oscillatory motion is effectively purely elastic: it is thermodynamically reversible and does not cause any mechanical energy dissipation. However, despite both Xiameter surfactants exhibiting this elastic oscillatory motion under the stress of an ultrasound wave, their compressibility curves, illustrated in ***Figure 43***, are quite different.

Exploring multiple types of rheology (i.e. shear rheology and high frequency longitudinal rheology), and examining material characteristics pertaining to those rheological properties (i.e. compressibility, the role of oscillational motion, ultrasound attenuation, sound speed, etc.), emphasizes the importance and value of complex rheological characterization for liquid mixtures, specifically solutions of non-polar media and nonionic surfactant. Utilization of multiple rheological measurement techniques allows for a more comprehensive understanding of liquid mixture behavior, which can serve to improve our understanding of viscosity and the impact it has on conductivity in nonpolar systems, the *Ion-Pair Conductivity Model*, and other models used for describing the laws that govern nonpolar systems.

IV. CONCLUSION

As we've become a more technologically advanced society, the relevance of nonpolar electrochemistry and its application in modern scientific innovation has garnered renewed attention, amplifying the importance of improving our understanding of the fundamental mechanisms by which ionization occurs (i.e. by which ions are maintained in nonpolar liquids). Modern technologies such as electrophoretic displays, a-polar paints, electrorheological fluids, electrostatic lithography, etc. all rely on ionization in nonpolar systems to function properly.

The purpose of the work carried out herein was to further explore the field of nonpolar electrochemistry to improve our overall understanding of the mechanisms by which ionization in nonpolar systems occurs and to introduce a robust theoretical approach capable of modeling conductivity in nonpolar systems that accounts for the effects neutral ion-pair formation has on such systems. Advanced knowledge and the ability to accurately model and predict the electrochemical nature of these liquids allows for the intrinsic properties that govern these systems to be controlled and optimally employed in real-world environments.

Early research carried out by Kohlrausch, Arrhenius, Bjerrum, Debye, Hückel, Onsager, Fuoss and others serve as the basis of our theoretical understanding of charge transport in the field of nonpolar electrochemistry. However, most, if not all, of the theories put forth to date have been almost entirely limited to dilute solutions. The restrictions applied to additive (i.e. amphiphile) concentration in these models inhibits our ability to investigate and interpret data across an array of nonpolar solutions and impedes our understanding of the underlying mechanisms which drive these systems.

Alcohol-nonpolar solutions serve as straightforward media for studying conductivity in nonpolar systems due to the inherent simplicity of these solutions. The ionized alcohol molecules exist in solution due to an "auto-dissociation" reaction, followed by a "self-solvation"

reaction via the surrounding neutral alcohol molecules present in the solution. Therefore, by way of the *Dissociation Model*, and the preliminary work done by Bjerrum, Onsager, Fuoss and others, development of a general, yet robust model for predicting conductivity as a function of ionization in nonpolar systems is made possible. The *Ion-Pair Conductivity Model*, as it's introduced herein, is named as such to emphasize the important role that ion-pairs play in the overall conductivity of these systems. Experimental verification and analyzation of the *Ion-Pair Conductivity Model* is then evaluated under a variety of conditions across a wide array of nonpolar systems to both investigate and demonstrate the applicability of this new model in nonpolar media.

The first group of nonpolar systems examined consisted of eight amphiphile-nonpolar liquid solutions. Toluene was chosen as the nonpolar liquid and eight straight chain alcohols, with a carbon chain of increasing length, were chosen as the amphiphiles, which allowed for the effects that increased carbon chain length had on the conductivity and relative permittivity of these mixtures to be studied exclusively. Conductivity as a function concentration of these two-component solutions were then measured and modeled. The focus of this work centered around the examination of the conductivity curves, specifically identifying and analyzing the concentration regions in which ion-pairs were and were not present, and the subsequent impact they had on both the linear and exponential relationships observed between concentration and conductivity. Results of which led to the conclusion that these important relationships, evident in all eight conductivity curves, are dependent upon the relationship between *Bjerrum length*, $\boldsymbol{\lambda}$ as a function of the relative permittivity, $\boldsymbol{\varepsilon}$ and amphiphile concentration of the system.

Good agreement between the *Ion-Pair Conductivity Model* and experimental data were found for all eight two-component systems examined, with slight deviation reported at very

low alcohol concentrations and at very high concentrations for long-chain alcohols (i.e. hexanol, heptanol and octanol), proving this new theoretical model is capable of accurately predicting the same conductivity trends found in the experimental data.

Next, to study the impact that nonpolar chemistry has on conductivity, the amphiphile in these binary solutions was kept constant and the nonpolar liquid was varied. Butanol was chosen as the amphiphile and toluene, hexane and heptane were chosen as the nonpolar liquids.

The experimental data for all three butanol-nonpolar liquid solutions illustrated nearly identical conductivity curves regardless of the nonpolar liquid used in the solution, indicating that the chemistry of the nonpolar liquid does not impact the conductivity of these systems. Rather, it is the relative permittivity of the nonpolar liquid that is important. These experimental results are in direct agreement with the conductivity curve predicted by the *Ion-Pair Conductivity Model*, reaffirming the model's assumption that it is the relative permittivity, not the chemistry of the nonpolar liquid (a parameter which the model omits all together), that drives ionization in nonpolar media.

While solutions consisting of alcohols as the added amphiphile in nonpolar media do have practical applications, they are rather limited in scope. Accordingly, the next step was to analyze nonionic surfactants as the amphiphile, since they are more commonly used for real-world purposes.

The first nonionic surfactants examined were OFX-5098 and OFX-0400 (polyalkylene oxide-modified polydimethylsiloxanes), both from the Xiameter line of surfactants manufactured by Dow Corning. OFX-5098 and OFX-0400 have nearly the same viscosities and the exact same endcap, but different hydrophile-lipophile balance (HLB) numbers, allowing for the roll that HLB number plays with regards to conductivity in nonpolar systems to be

explored. Toluene was chosen as the nonpolar liquid. Conductivity, relative permittivity and viscosity measurements were then taken for each Xiameter-toluene solution across the entire nonionic surfactant concentration spectra.

The *Ion-Pair Conductivity Model* was in good agreement with the experimental data across nearly the entire Xiameter concentration range with some deviation between the theoretical and experimental conductivity curves observed at very high concentrations of Xiameter nonionic surfactant.

Next, SPAN 20 and SPAN 80 from the SPAN series of nonionic surfactants, manufactured by Sigma Aldrich were chosen as the amphiphile to be examined. The SPAN surfactants are well-known nonionic surfactants based on the sorbitan molecule and are widely used in both research and commercial applications for such functions as an emulsifier, wetter, and stabilizer. Again, toluene was chosen as the nonpolar liquid and conductivity, relative permittivity and viscosity measurements were taken for each SPAN-toluene solution across the entire nonionic surfactant concentration spectra.

Once more, the *Ion-Pair Conductivity Model* was in good agreement with the experimental data across nearly the entire SPAN concentration range with some deviation between the theoretical and experimental conductivity curves observed at very high concentrations of SPAN nonionic surfactant.

In the nonionic surfactant-toluene solution studies, the conductivity curves for the theoretical model deviated from the experimental data at high concentrations of nonionic surfactant. This deviation is likely the result of the non-Newtonian nature of these amphiphiles and the large contrast between the two components viscosities. In the prior amphiphile-toluene experiments, in which the amphiphile was an alcohol, the difference in viscosities of the two components were minimal, therefore, only simple mixing rules were required to

estimate the viscosity of the system. However, in terms of these nonionic surfactant-toluene solutions, where the nonionic surfactant's viscosity is significantly higher than that of its nonpolar counterpart, toluene, a more precise means of measuring the viscosity data for these systems is required.

According to the *Ion-Pair Conductivity Model*, there are five critical parameters of a nonpolar system that impact the conductivity of any two-component amphiphile-nonpolar liquid solution: the relative permittivity of the amphiphile, $\boldsymbol{\varepsilon_a}$, the volume fraction of the amphiphile in the overall solution, , the concentration of ions in the pure amphiphile, $\boldsymbol{C_A}$, Ion size in solution, $\boldsymbol{a}$, and the viscosity of the system, $\boldsymbol{\eta}$.

The *Ion-Pair Conductivity Model* further states that only when the environment within a given nonpolar system, and subsequently the five driving properties of such a system allow for it, will ion-pair formation occur within the nonpolar solution. Ion-pairs will only be present within a nonpolar system, across a specific concentration range, when the properties of the solution create an ideal atmosphere for ion-pairs to form.

Based on the results presented herein it is clear that a decrease in the concentration of ions in the pure amphiphile, $\boldsymbol{C_A}$, increases the linearity between *Walden Plot* (conductivity multiplied by viscosity) and amphiphile concentration in all eight theoretical amphiphile relative permittivity, $\boldsymbol{\varepsilon_a}$, curves. This is consistent with the underlying principles of the *Ion-Pair Conductivity Model* which states that, as the concentration of ions in a nonpolar system decreases, less ions are present within the solution to form ion-pairs, thus, a linear relationship between *Walden Plot* and amphiphile concentration is observed due to a decrease in ion-pair formation in these nonpolar systems.

Next, theoretical values for ion size, $\boldsymbol{a}$, are varied. It is clear from the data reported herein that reducing ion size, $\boldsymbol{a}$, drastically expands the amphiphile concentration range in

which ion-pairs are present in the solutions, highlighting the important role that ion size plays in the conductivity of nonpolar systems. Specifically, there are two mechanisms by which ion size will impact the overall conductivity of the system; distance of closest ion approach, $\boldsymbol{q}$, which favors large ions and hydrodynamic size (i.e. ion mobility) which favors small ions. Notably, these ion size driven conductivity mechanisms of nonpolar systems are at odds with one another. Therefore, the conductivity of an amphiphile-nonpolar liquid solution, as a function of ion size, peaks at a *critical ion size,* $\boldsymbol{a_{cr}}$, whereby the balance between the two mechanisms is most favorable to the overall conductivity of the system.

Thus, the ability of the *Ion-Pair Conductivity Model* to allow us to predict the *critical ion size*, $\boldsymbol{a_{cr}}$, of a nonpolar system and examine the range of concentrations at which it is important is imperative when studying solutions in which ion-pair formation occurs. As anticipated, the *Ion-Pair Conductivity Model*, under various circumstances, across a range of theoretical ion sizes, is able to identify a critical ion size where the Walden product reaches a maximum.

The *Ion-Pair Conductivity Model* states that ion-pairs form when solvated ions combine into neutral entities. However, those ions can come from several sources. As stated previously, ionization in nonpolar systems where alcohol is the amphiphile can be attributed to the auto-dissociation of the alcohol molecules. Additionally, ionization can also be the result of dissociation of surfactant molecules, water contamination, or other types of contaminants.

Comparing this concentration of water data to the concentration of ions in the pure amphiphile, $\boldsymbol{C_A}$, the concentration of water measured herein is orders of magnitude larger than the concentration of ions in the pure amphiphile reported previously. While not all of the water present in these systems will automatically form ions that contribute to the overall conductivity of these nonpolar liquids, even if a very small percentage of them do, the impact this low number of newly formed ions would have on the conductivity of these system would

still be significant, because the initial ionic concentration of these solutions is so low. Implying that, even for non-polar liquids, there is adequate water present via contamination that ion concentration is not the limiting factor with regards to conductivity; rather, it is the concentration of the solvating agent, as well as the overall permittivity of the system, that impacts the ability for ion-pairs to form in these nonpolar systems.

Thus *Ion-Pair Conductivity Model* has demonstrated the importance that viscosity, and its impact on ion mobility, plays with regards to conductivity of nonpolar systems. A better understanding of the viscosity of such solutions, and the applicability of already established mixing rules for such liquid mixtures, would allow the *Ion-Pair Conductivity Model* to rely less on empirically measured data, and provide a more robust tool for predicting the behavior of these systems.

Molecular chain length of added non-Newtonian liquid (i.e. amphiphile) was explored with regards to its impact on viscosity. For short-chain surfactants the "excess activation energy mixing rule," based on classic mixing rules, successfully predicted the conductivity of mixtures studied across the entire concentration range. This allowed for the intermolecular interaction energies for these systems to be explored.

For systems in which the added non-Newtonian liquids were long-chain surfactants, a hypothesis was presented to explain deviation from classic mixing rules with regards to viscosity, describing a superposition of translational and oscillational motion of the long-chain surfactant, and justifying why these systems adhere to a simple volume fraction-based mixing rule.

High frequency ultrasound measurements were made to explore the longitudinal viscosity of these systems and the concentrations at which they behave as Newtonian or non-Newtonian mixtures. These experiments demonstrated the value that more complex

rheological measurements, employing multiple viscosity measurement techniques, have on comprehensively exploring viscoelastic properties in liquid-liquid mixtures.

The *Ion-Pair Conductivity Model* developed and experimentally justified herein serves as a comprehensive tool for exploring conductivity in non-polar systems, emphasizing the crucial role ion-pair formation plays. It expands upon the *Dissociation Model*, and its range of applicability, to encompass the entire concentration range for nonpolar media with added amphiphile. Its success in accurately predicting conductivity, and its vast range of applicability, make it a valuable tool in the field of nonpolar electrochemistry.

V. FUTURE WORK

Future work with regards to the *Ion-Pair Conductivity Model (IPCM)* should begin by focusing on improving the quality of fit between theoretical and experimental data. It should also focus on the range of applicability and limitations of the *IPCM* as it is described here.

The *IPCM* showed deviation from experimental results for mixtures in which the added amphiphile was nonionic surfactant, at high concentrations of surfactant in the mixture (above ~80 wt. % for all four mixtures studied). This deviation was hypothesized to be the result of differences between the macroscopic viscosity of the system measured via Cannon-Fenske Viscometers, and the "micro-viscosity" experienced by the ion as it travels through the media. An image of an ion moving within a cage was used to describe this phenomenon, in which the nanometer-scale movement of the ion was not impacted by the cage which is of a much larger scale. The viscosity measurements conducted in this work serve as a useful starting point for more complex rheological analysis, but there is still much room for improvement.

More detailed viscosity measurements which can account for the differences between micro and macro viscosity would serve to improve the quality of the *IPCM*. If the hypothesis proposed is correct, then the viscosity experienced by the ion would be much lower than the measured viscosity, which would account for the increased mobility, and therefore increased viscosity, that the experimental data shows when compared to the model. Acoustic spectroscopy using particles of known size is one method by which micro-viscosity can be explored[67].

Establishing a concentration-based model for viscosity that could then be included in the *IPCM* equation would improve the *IPCM*; the model would not rely on empirical viscosity data (as was the case for mixtures in which the added amphiphile was nonionic surfactant). However, while an exponential dependence of viscosity on concentration was found for the

systems with nonionic surfactants, the fact that a simple volume-fraction based mixing rule was adequate for the systems in which alcohols were the amphiphiles implies that the data contained here within is not sufficient for providing a generalized viscosity rule which can be implemented into the *IPCM*. The differences in behavior between short and long chain surfactants further justifies the need for additional research in order to establish such a concentration-based model for viscosity that can be included in the *IPCM.*

The complex behavior of long-chain surfactants with regards to viscosity discussed ***Section 3.14*** warrants further scrutiny. Additional experimentation needs to be carried out to confirm the theory of continuous expanding and collapsing of long-chain surfactant molecules. Additionally, the inflection point at which the systems viscosity, and subsequently the molecular chain length of the molecule, transitions from being governed by classical mixing rules to volume-fraction based mixing rules warrants further consideration.

Light scattering measurements could be used to explore the size of these long chain surfactant molecules, and the structures they form (i.e. micelles), when suspended in nonpolar media such as toluene. These measurements could help improve our understanding of long-chain surfactant behavior in nonpolar systems, and whether our hypothesized theory of continuous expanding and collapsing of long-chain surfactant molecules is valid.

Models for viscosity in mixtures of nonpolar media with short-chain surfactants can also be improved by consideration of self-assembly and the impact that self-assembly has on viscosity in nonpolar systems. Light scattering could serve as a useful tool in this endeavor as well, by exploring micelle size as a function of concentration of added nonionic surfactant.

Furthermore, at this point, viscosity has only been investigated in systems in which toluene was the Newtonian liquid. Thus, exploration of additional Newtonian liquids and the effects they have on viscosity of nonpolar systems would help further our understanding of the

underlying mechanisms which drive the mixing rules for other Newtonian and non-Newtonian liquids as well.

The *IPCM* relies on a series of assumptions (see ***Section 1.3***) in order to present a final equation which can be readily applied to real-world systems. The validity of these assumptions, and the scenarios in which they are not applicable should be examined in future work. For example, *Assumption #1* states that the nonpolar media does not impact solvation of the ion by the amphiphile. However, this is known to not always be true. The fact that some surfactants work better in certain nonpolar liquids than others implies that the nonpolar media (i.e. chemistry of the nonpolar liquid) does play a role in surfactant self-assembly, and therefore will impact electrochemistry in nonpolar systems in which surfactant is used as additive[121]. Whether such an impact would be reflected in the *IPCM*, need to be accounted for by adjustments to the *IPCM,* or demonstrate a limitation of the *IPCM* with regards applicability, should be explored further. Similar considerations should be made for the other assumptions made in ***Section 1.3***, with future work exploring the validity of those assumptions.

The presence of ion-pairs was explored within the context of the *Ion-Pair Conductivity Model* through measurements of conductivity, and corresponding dependences of conductivity on concentration of added amphiphile. However, there are other possible measurement techniques, specifically Contrast Enhanced Neutron Scattering and Infrared (IR) Spectroscopy, which could serve as tools for demonstrating the presence of ion-pairs. IR Spectroscopy could be used to explore the presence of dipoles in these mixtures, which could provide evidence of ion-pair formation. Neutron scattering (specifically small angle neutron scattering) is used for exploring microstructures such as micelles. Accordingly it could be potentially used for exploring the structure of solvated ions in nonpolar systems.

The work carried out and reported herein focused on two-component systems of non-polar liquid and amphiphile. While such systems do have real-world applications, the logical next step would be to explore new categories of additives useful in relevant industries and more complex systems, such as three-component solutions in which multiple amphiphiles are used.

Numerous industrial processes exist that involve the use of multiple amphiphiles as "co-surfactants," capitalizing on the benefits that using surfactants in tandem with one another have on such systems. Examples of such applications include: personal care products[122,123], enhanced oil recovery[124,125], emulsion stabilization[126], and food production[127]. A better understanding of co-surfactant interaction, the structures they form, and the way that important system parameters such as conductivity are impacted by such dynamics could have a substantial impact on their application.

Lastly, ionic liquids, a unique class of liquids in which the entire liquid is considered to be composed of ions have, to date, yielded conductivity values significantly lower than expected. In fact, theoretical calculations carried out so far in such systems have reported negative mobility values for the ions in solution, which, based on what we know so far, is simply not possible[128]. Therefore, the *Ion-Pair Conductivity Model*, and its emphasis on ion-pairs, should be explored as a potential model to help better understand and explain this unique phenomenon found in such liquids.

VI. REFERENCES

1. Rieger, Philip H. *Electrochemistry*. 2nd ed., Springer, 1994.
2. Novotny, V. "Applications of Nonaqueous Colloids." *Colloids and Surfaces*, vol. 24, no. 4, June 1987, pp. 361–375.
3. Wang, Jing, et al. "Dispersion of Phthalocyanine Green G in Nonaqueous Medium Using Hyperdispersants and Application in E-Ink." *Journal of Dispersion Science and Technology*, vol. 27, no. 7, 2006, pp. 975–981.
4. Gacek, Matthew M., and John C. Berg. "Effect of Synergists on Organic Pigment Particle Charging in Apolar Media." *Electrophoresis*, vol. 35, no. 12-13, 2014, pp. 1766–1772
5. M. M. Gacek and J. C. Berg, "The role of acid–base effects on particle charging in apolar media," *Advances in Colloid and Interface Science*, **220**, 108 (2015).
6. Morrison ID. "Electrical charges in non-aqueous media." *Colloids Surf A* 1993;71:1–37.
7. Kaufman S, Singleterry CR. "Micelle formation by sulfonates in a nonpolar solvent." *J Colloid Sci* 1955;10(2):139–50..
8. Cametti C, Codastefano PA, Tartaglia P, Chen SH, Rouch J. "Electrical conductivity and percolation phenomena in water-in-oil microemulsions." *Phys Rev A* 1992;45(8):5358–61.
9. Faraday M. *Experimental Researches in Electricity*. London: Richard and John Edward Taylor; 1839.
10. Ehl, Rosemary Gene, and Aaron J. Ihde. "Faradays Electrochemical Laws and the Determination of Equivalent Weights." *Journal of Chemical Education*, vol. 31, no. 5, 1954, p. 226
11. Kraus CA, Fuoss RM. "Properties of electrolytic solutions. 1. Conductance as influenced by the dielectric constant of the solvent medium*." J Am Chem Soc* 1933;55(1):21–36.
12. Kablukoff Iwan. "Uber die elektrische Leitfahigkeit von Chlorwasser-stoff in verschiedenen Losungsmitteln". In: Ostwald W, van't Hoff JH, editors*. Zeitschrift fur Physikalische Chemie*, 4; 1889. p. 429–34.
13. Arrhenius S. "Recherches sur la conductivité galvanique des électrolytes." Stockholm: Uppsala Univ.; 1884.
14. Walter, J.H.; DeWayne, H.J.; "Electrolytic Conductance and the Conductances of the Halogen Acids in Water." *United States Department of Commerce*, NSRDS-NBS 33, 1970.
15. Onsager L. "Report on revision of the conductivity theory." *Trans Faraday Soc* 1927;23:341–9.
16. Plotnikov W. "Die elecktrische Leitahigkeit der Gemische von Brom und Ather". In: Ostwald W, van't Hoff JH, editors. Zeitschrift fur Physikalische Chemie, 57; 1906. p. 502–6.
17. Plotnikov. *Z Phys Chem* 1925;116:111.
18. Plotnikov, Jakubson. *Z Phys Chem* 1928;138:235.
19. Plotnikov, Kudra. *Z Phys Chem* 1929;145:625.

20. Dukhin AS, Goetz PJ. “How non-ionic “electrically neutral” surfactants enhance electrical conductivity and ion stability in non-polar liquids.” *J Electroanal Chem* 2006;588:44–50.
21. Walden P. Bull Acad Imp Sci St Petersburg 1913;7:934, referenced according to Walden P.” Salts, Acids, and Basis; Electrolytes;” *Stereochemistry*. New York: McGraw-Hill; 1929.
22. Walden. *Z Phys Chem* 1930;147:1.
23. McGraw-Hill Dictionary of Scientific & Technical Terms, 6E, The McGraw-Hill Companies, Inc. 2003.
24. Onsager L. ”Report on revision of the conductivity theory.” *Trans Faraday Soc* 1927;23:341–9.
25. P. Debye and E. Huckel “Zur Theorie der Elektrolyte. I. Gefrierpunktserniedrigung und verwandte Erscheinungen [The theory of electrolytes. I. Lowering of freezing point and related phenomena]”.*Physikalische Zeitschrift* 24: 185 (1923).
26. Bockris J, Reddy AK. *Modern electrochemistry*, vol.1. A Plenum/Rosetta edition; 1977
27. Bjerrum N. “A new form for the electrolyte dissociation theory*.” Proceedings of the 7th International Congress of Applied Chemistry,* Section X; 1929. p. 55–60 [London].
28. D. C. Prieve, B. A. Yezer, A. S. Khair, P. J. Sides, and J. W. Schneider.” Formation of Charge Carriers in Liquids.” *Advances in Colloid and Interface Science* (2016).
29. A. S. Dukhin and S. Parlia, “Ions, ion-pairs and inverse micelles in non-polar media”, *Current Opinion in Colloid and Interface Science*, 18, 93 (2013).
30. K. Izutsu. *Electrochemistry in Nonaqueous Solutions*, Second, Revised and Enlarged Edition. Wiley-VCH Verlag GmbH & Co. KGaA, Weinheim, ISBN: 978-3-527-32390-6 (2009).
31. Onsager L. “Deviation from Ohm's law in weak electrolytes.” *J Chem Phys*. 1934;2:599.
32. J. C. Justice. “An interpretation of distance parameter of the Fuoss-Onsager conductance equation in the case of ionic association.” *Electrochimica Acta*, 16, 701 (1971).
33. Prieve DC, Haggard JD, Fu R, Sides PJ, Bethea R. “Two independent measurement of Debye length in dopped nonploar liquids.” *Langmuir* 2008;24:1120–32.
34. Prieve DC. “Measurement of colloidal forces with TIRM*.” Adv Colloid Interf Sci* 1999;82:93–125.
35. Fuoss RM, Kraus CA. “Properties of electrolytic solutions. IV. The conductance minimum and the formation of triple ions due to the action of columbic forces.” *J Am Chem Soc* 1933;55(6):2387–99.
36. L.M. Varela, J. Carrete, M. Garcia, J.R. Rodriguez, L.J. Gallego, M. Turmine and O. Cabeza (2011). *Pseudolattice Theory of Ionic Liquids: Theory, Properties, New Approaches,* Prof. Alexander Kokorin (Ed.)
37. Fuoss RM. “Ionic association. I. Derivation of constants from conductance data.” *J Am Chem Soc* 1957;79(13):3301–3.

38. Fuoss RM. “Ionic association. III. The equilibrium between ion pairs and free ions.” *J Am Chem Soc* 1958;80(19):5059–61.
39. W. R. Gilkerson. “Application of free volume theory to ion pair dissociation constant.” *J. Chem. Phys.*, 25(6), 1199 (1956).
40. J. T. Dennison and J. B. Ramsey, “The Free Energy, Enthalpy and Entropy of Dissociation of Some Perchlorates in Ethylene Chloride and Ethylidene Chloride.” *J. Amer. Chem. Soc.,* 77, 2615 (1955).
41. Fuoss, R.M., and Karus, C. A. “Ionic association. II.” *J Am. Chem. Soc*. 79, 3304 (1957)
42. Dukhin, A., Parlia, S. “Ion-pair conductivity theory fitting measured data for various alcohol-toluene mixtures across entire concentration range” *Journal of The Electrochemical Society*, 162 (4) H1-H8 (2015)
43. Kitahara A. “Zeta potential in non-aqueous media and its effect on dispersion stability.” *Prog Org Coat* 1973/4;2:81–98.
44. Kitahara A. *Nonaqueous systems. In: Kitahara A, Watanabe A, ditors. Electrical phenomena at interfaces.* Marcel Decker; 1984.
45. Nelson SM, Pink RC. “Solutions of metal soaps in organic solvents. Part IV. Direct current conductivity in solutions of some metal oleates in toluene.” *J Chem Soc* 1954:4412–7.
46. Mathews MB, Mattoon RW. “Micelles in Non-Aqueous Media.” *J Chem Phys* 1949;17:496–7.
47. B. A. Yezer, A. S. Khair, P. J. Sides, and D. C. Prieve, “Determination of charge carrier concentration in doped nonpolar liquids by impedance spectroscopy in presence of charge adsorption,” *JCIS*, 469, 325 (2016).
48. A. Bombard and A. S. Dukhin, “Ionization of a nonpolar liquid with and Alcohol,” *Langmuir*, 30(15), 4517 (2014).
49. Verwey EJW. “The charge distribution in the water molecule and the calculation of the intermolecular forces.” *Recl Trav Chim* Pays-Bas Belg 1941;60:887.
50. Verwey EJW. “The interaction of ion and solvent in aqueous solutions of electrolytes.” *Recl Trav Chim* Pays-Bas Belg 1942;61:127.
51. Eicke HF, Borkovec M, Das-Gupta B. “Conductivity of water-in-oil microemulsions: a quantitative charge fluctuation model.” *J Phys Chem* 1989; 93:314–7.
52. Cametti C, Codastefano PA, Tartaglia P, Chen SH, Rouch J. “Electrical conductivity and percolation phenomena in water-in-oil microemulsions.” *Phys Rev A* 1992;45(8):5358–61.
53. Collins, Kim. “Why continuum electrostatics theories cannot explain biological structure, polyelectrolytes or ionic strength effects in ion-protein interactions.” *Biophysical Chemistry.* 167, 43-59 (2012)
54. Falcone, R. Dario, et al. “What Are the Factors That Control Non-Aqueous/AOT/n-Heptane Reverse Micelle Sizes? A Dynamic Light Scattering Study.” *Physical Chemistry Chemical Physics*, 11, 47 (2009)

55. G. Begona, R. Alcalde, S. Aparicio, and J. M. Leal. "The N-methylpyrrolidone–(C1– C10) alkan-1-ols solvent systems." *J. Chem. Phys.* 4, 1170 (2002).
56. "Toluene Physical Properties" Sigma-Aldrich Solvent Center. Sigma-Aldrich. Web. July 10th, 2014.
57. Dow Corning Corp., "XIAMETER brand Silicone Polyether Products," 95-1112-01Product Data Sheet, 2012 [Revised May. 2016].
58. Dow Corning Corp, "XIAMETER™ OFX-5098 Fluid", Form No. 95-836-01 B. 2017
59. Dow Corning Corp, "DOWSIL™ OFX-0400 Fluid", Form No. 26-1990-01 A 2017
60. Millipore Sigma, "Safety Data Sheet for Span® 20," 840119 08/22/2013
61. Millipore Sigma, "Safety Data Sheet for Span® 80," 1338-43-8 03/19/2019
62. Angel Cart´on, Gerardo Gonz´alez, Angeles I˜niguez, and Jose Luis Cabezas. "Separation of Ethanol-water Mixtures Using 3A Molecular Sieve." *Journal of Chemical Technology and Biotechnology*, 39(2), 125 (1987).
63. Dispersion Technology Inc. DT-700 Non-Aqueous Conductivity Probe. Retrieved November 12, 2019, from http://www.dispersion.com
64. Brookhaven Instruments., BI-870 Dielectric Constant Meter. Retrieved July 20, 2019, from http://www.brookhaveninstruments.com
65. Fan T. 2001. Viscosity Measurement Using Cannon-Fenske Viscometers. 2 p. (Instructions) http://www.prrc.nmt.edu/groups/petrophysics/media/pdf/viscometer.pdf (July 20th, 2019)
66. Dispersion Technology Inc. DT-1202 Acoustic and Electroacoustic Spectrometer . Retrieved November 12, 2019, from http://www.dispersion.com
67. A. S. Dukhin and J. P. Goetz, "Characterization of Liquids, Nano- and Microparticulates, and Porous Bodies using Ultrasound", *Elsevier* (2010).
68. Metrohm AG. 870 KF Titrino Plus Manual. Jan 21, 2015. www.metrohm.com
69. G. Bego˜na, R. Alcalde, S. Aparicio, and J. M. Leal. "The N-methylpyrrolidone–(C_1–C_{10}) alkan-1-ols solvent systems." *Phys. Chem. Chem. Phys.* 4, 1170 (2002).
70. "Toluene Physical Properties" Sigma-Aldrich Solvent Center. Sigma-Aldrich. Web. July 10th, 2014. http://www.sigmaaldrich.com/chemistry/solvents/toluene-center.html.
71. A. Maryott and E. Smith. "Table of Dielectric Constants of Pure Liquids." *National Bureau of Standards Circular* 514, 1 (1951).
72. M. Prego, E. Rilo, E. Carballo, C. Franjo, E. Jimenez, and O. Cabeza "Electrical conductivity data of alcohols from 273 to 333 K", *J. of Molecular Liquids*, 102/1-3, 83 (2003).
73. Parlia, S., Dukhin, A., Somasundaran, P., "Ion-pair conductivity theory: mixtures of butanol with various non-polar liquids and water." *Journal of The Electrochemical Society,* 163 (7) H1-H6 (2016)
74. PubChem. US National Library of Medicine, "Hexane". Retreived November 11, 2019 from https://pubchem.ncbi.nlm.nih.gov/compound/hexane

75. PubChem. US National Library of Medicine, "Heptane". Retreived November 11, 2019 from https://pubchem.ncbi.nlm.nih.gov/compound/heptane
76. PubChem. US National Library of Medicine, "Toluene". Retreived November 11, 2019 from https://pubchem.ncbi.nlm.nih.gov/compound/Toluene
77. David R. Burfield and Rogher H. Smithers. "Desiccant Efficiency in Solvent and Reagent Drying. 7. Alcohols." *J. Org. Chem*., 48(14), 2420 (1983).
78. Peter D¨urre. "Biobutanol: An attractive biofuel". *Biotechnology journal* 2.12 01 Dec 2007: 1525. Wiley. 22 Feb 2016.
79. Parlia, S., Dukhin, A., Somasundaran, P., "Ion-pair conductivity theory: mixtures of non-polar media with non-ionic surfactant." *Journal of The Electrochemical Society*, 164 (12) E1-E5 (2017)
80. Q. Guo, V. Singh, and S. H. Behrens, "Electric charging in non-polar dispersions due to non-ionazable surfactants," *Langmuir*, 26(5), 3203 (2010).
81. C. E. Espinosa, Q. Guo, V. Singh, and S. H. Behrens, "Particle charging and charge screening in nonpolar dispersions with non-ionic surfactants," *Langmuir*, 26(22), 16941 (2010).
82. S. Poovarodom and J. C. Berg, "Effect of particle and surfactant acid-base properties on charging of colloids in apolar media*," J. Coll. and Interface Sci*., 346, 370–377 (2010).
83. PubChem. US National Library of Medicine, "Sorbitan". Retreived November 11, 2019 from https://pubchem.ncbi.nlm.nih.gov/compound/sorbitan
84. P. Walden, Bull. Acad. Imp. Sci., St. Petersburg, 7, 934 (1913), referenced according to P.Walden, "Salts, Acids, and Basis; Electrolytes; Stereochemistry,",McGraw-Hill, New York, (1929).
85. S. Parlia, A. S. Dukhin, and P. Somasundaran, "Ion-Pair Conductivity Theory IV: SPAN Surfactants in Toluene and the Role of Viscosity." *J. of the Electrochemical Society*, 165(5), H1 (2018).
86. R. N. Zia and J. F. Brady, "Microviscosity, microdiffusivity, and normal stresses in colloidal dispersions," *J. of Rheology*, 56, 1175 (2012).
87. T. G. Mason and D. A. Weitz, "Optical measurements of frequency-dependent linear viscoelastic moduli of complex fluids," *Phys. Rev. Lett*., 74(7), 1250 (1995).
88. S. Parlia, A. S. Dukhin, and P. Somasundaran, "Ion-Pair Conductivity Theory V: Critical Ion Size and Range of Ion-Pair Existence." *J. of the Electrochemical Society*, 165(14), E1-E9 (2018).
89. N. O. Mchedlov-Petrossyan, I. N. Palval, A. V. Lebed, and E. M. Nikiforova, "Association of the picrate ion with cation of various nature in solvents of medium and low relative permittivity. An UV/Vis spectroscopic and conductometric study", *Journal of Molecular Liquids*, 145, 158 (2009).
90. S. Kaufman and C. R. Singleterry, "Micelle formation by sulfonates in a nonpolar solvent", *Journal of Colloid Science*, 10(2), 139 (1955).

91. K. Miyoshi, “Comparison of the conductance equations of Fuoss-Onsager, Fuoss-Hsia and Pitts with the data of bis(2,9-dimethyl-1,10-phenanthroline)Cu(1) Perchlorate”, *Bulletin of the Chem. Soc. Japan*, 46, 426 (1973). 524
92. N. O. Mchedlov-Petrossyan, I. N. Palval, A. Lebed, and E. M. Nikiforova, “Association of the picrate ion with cations of various nature in solvents of medium and low relative permittivity. An UV/Vis spectroscopic and conductometric study”, *J. of Molecular Liquid*s, 145, 158 (2009).
93. H. Sadek and R. Fuoss, “Electrolyte solvent interaction. VI. Tetrabutylammonium bromide in nitrobenzene-carbon tetrachloride mixtures”, *J. Am. Chem. Soc.* 1954, 76, 23, 5905-5909
94. M. F. Hsu, E. R. Dufresne, and D. A. Weitz, “Charge stabilization in nonpolar solvents”, *Langmuir*, 21(11), 4881 (2005).
95. A. Denat, B. Gosse, and J. P. Gosse, “Electrical conduction of solutions of an ionic surfactant in hydrocarbons”, *J. of Electrostatics*, 12, 197 (1982).
96. S. K. Sainis, J. W.Merrill, and E. R. Dufresne, “Electrostatic interactions of colloidal particles at vanishing ionic strength”, *Langmuir*, 24, 13334 (2008).
97. P. M. Bowyer, A. Ledwith, and D. C. Sherrington, “Ion-pair dissociation equilibria for hexachloroantimonate salts of stable organic cations in dichloromethane”, *J. Chem. Soc., B*, 1511 (1971).
98. C. A. Kraus and G. S. Hooper, “The dielectric properties of solutions of electrolytes in non-polar solvent”, *Proc. of the National Academy of Sci*., 19(#11), 939 (1933).
99. A. P. Abbot and D. J. Schiffrin, “Conductivity of tetra-alkyammonium salts in polyaromatic solvents”, *J. Chem. Soc. Faraday Trans*., 86(9), 1453 (1990).
100. K. Mpoukouvalas, D. Turp, M. Wagner, K. Mullen, H-J. Butt, and G. Floudas, “Dissociation and charge transport in salts of dendronized ions in solvents of low polarity”, *J. of Physical Chemistry*, 115, 5801 (2011).
101. P. Debye and E. . H¨uckel, "Zur Theorie der Elektrolyte. I. Gefrierpunktserniedrigung und verwandte Erscheinungen [The theory of electrolytes. I. Lowering of freezing point and related phenomena]". *Physikalische Zeitschrift*, 24: 185. (1923).
102. Gourdin-Bertin, S., Chassagne, C. “Application of classical thermodynamics to the conductivity in non-polar media.” *J Chem Phys.* 2016 Jun 28;144(24):244501
103. S. Arrhenius, Über die Innere Reibung Verdünnter Wässeriger Lösungen, *Z. Phys. Chem*. 1 (1887) (1887) 2855–3298.
104. L. Grunberg, A.H. Nissan, “Mixture law for viscosity”, *Nature* 164 (1949) (1949) 799–800.
105. P.K. Katti, M.M. Chaudhri, “Viscosities of binary mixtures of benzyl acetate with dioxane, aniline, and m-cresol*,” J. Chem. Eng. Data* 9 (1964) (1964) 442–443.
106. S. Glasstone, K.J. Laidler, H. Eyring, “The Theory of Rate Processes, the Kinetics of Chemical Reactions, Viscosity, Diffusion, and Electrochemical Phenomena”, *McGraw Hill*, New York, 1941.

107. Dukhin, A., Parlia, S., Somasundaran, P., "Rheology of non-Newtonian liquid mixtures and the role of molecular chain length." *J. of Colloid and Interface Science.* (2019)
108. M.A. Monsalvo, A. Baylauc, P. Reghem, S.E. Quinones-Cisneros, C. Boned, "Viscosity measurements and correlations of binary mixtures: 1,1,1,2-tetrafluoroeethane (HFC-134a) + tetraethylene glycol dimethylether (TEGDME)", *J. Fluid Phase Equilibria* 233 (2005) 1–8.
109. A.J. Batchinski, "Untersuchungen über die innere Reibung der Flüssigkeiten" II*, Z. Phys. Chem*. 84 (1913) 643.
110. V. Pisarev, S. Mistry, "Volume-based mixing rules for viscosities of methane þ n-butane liquid mixtures," *Fluid Phase Equilibria* 484 (2019) 98–105.
111. M.J. Assael, J.H. Dymind, M. Papadaki, P.M. Ptterson, "Correlation and prediction of dense fluid transport coefficients: II. Simple molecular fluids." *J. Fluid Phase Equilibria* 75 (1992) 245–255.
112. M. Kanti, H. Zhou, S. Ye, C. Boned, B. Lagourette, P. Saint-Cuirons, P. Xans, F.J.J. Montel, "Viscosity of liquid hydrocarbons, mixtures and petroleum cuts, as a function of pressure and temperature." *Phys. Chem*. (1989) 3860–3864.
113. S.E. Quinones-Cisneros, C.K. Zeberg-Mikkelsen, E.H.J. Stenby , "The friction theory (f-theory) for viscosity modeling." *Fluid Phase Equilibria* 169 (2000) 249–276.
114. A. Allal, M. Moha-Quchane, C. Boned, "A New Free Volume Model for Dynamic Viscosity and Density of Dense Fluids Versus Pressure and Temperature." *J. Phys. Chem. Liq*. 39 (2001) 1–30.
115. A.J. Queimada, I.M. Marrucho, J.A.P. Coutinho, E.H. Stenby, "Viscosity and liquid density of asymmetric n-alkane mixtures: measurement and modeling," *Int. J. Thermophys.* 26 (1) (2005) 47–61.
116. V.A. Bloomfield, R.K. Dewan, "Viscosity of liquid mixtures," *J. Phys. Chem.* 75 (20) (1971) 3113–3119.
117. A. Laesecke, R.F. Hafer, D.J. Morris, "Saturated-liquid viscosity of ten binary and ternary alternative refrigerant mixtures. Part 1: measurements," *J. Chem. Eng. Data* 46 (2001) 433–445
118. R.I. Tanner, *Engineering Rheology*, Oxford University Press, 1988.
119. C.W. Macosco, *Rheology. Principles, measurements and applications,* Wiley- VCH, 1994.
120. A. Zelenev, "Application of acoustic spectroscopy to the characterization of surfactant solutions, emulsions, and microemulsions: d–limonene–water–C12EO7–isopropanol system," *J. Surf. Deterg.* (2019).
121. Shrestha, Lok Kumar, et al. "Shape, Size, and Structural Control of Reverse Micelles in Diglycerol Monomyristate Nonionic Surfactant System." The Journal of Physical Chemistry B, vol. 111, no. 7, (2007)
122. Bhadani, A., Shrestha, R., Koura, S., Endo, T., Sakai, K., Abe, M., Sakai, H., Self-aggregation properties of new ester-based gemini surfactants and their rheological

behavior in the presence of cosurfactant — monolaurin.“ Colloids and Surfaces A: Physicochem. Eng. Aspects 461 (2014) 258–266
123. Wertz, J., Goffinet, P., inventors; Near-neutral pH detergents containing anionic surfactant, cosurfactant and fatty acid, US Patent US4561998A, Dec. 31st 1985
124. Bera, A., Mandal, A., “Microemulsions: a novel approach to enhanced oil recovery: a review.” J Petrol Explor Prod Technol (2015) 5:255–268
125. Gogarty, W., Olson, R., inventors; Marathon Oil Co, Assignee; Use of microemulsions in miscible-type oil recovery procedure, US Patent US3254714A, June 7th, 1965
126. Farago, B. and Richter, D. and Huang, J. S. and Safran, S. A. and Milner, S. T., “Shape and size fluctuations of microemulsion droplets: The role of cosurfactant.” Phys. Rev. Lett. 65: 26, (1990) 3348-3351
127. Li, Y., McClements, D., “Influence of cosurfactant on the behavior of structured emulsions under simulated intestinal lipolysis conditions” Food Hydrocolloids, 40 (2014) 96-103
128. Gebbie, M., Valtiner, M., Banquy, X., Fox, E., Henderson, A., “Ionic liquids behave as dilute electrolyte solutions. PNAS 110: 24 (2013) 9674-9679

A. APPENDIX

A.1 DATA FOR ALCOHOL-NONPOLAR MIXTURES

A.1.1 CONDUCTIVITY

Methanol-Toluene Mixtures:

Concentration of Methanol (wt. %)	Conductivity (S/m)	Standard Deviation
100	2.95E-04	8.76E-07
90	2.53E-04	6.75E-07
80	2.21E-04	1.71E-06
70	2.04E-04	5.27E-07
60	1.74E-04	7.89E-07
50	1.44E-04	2.10E-06
40	1.14E-04	3.16E-07
36.84	9.13E-05	1.76E-07
33.33	7.82E-05	1.58E-07
29.41	6.20E-05	1.55E-07
25.00	4.24E-05	1.03E-07
20.00	1.77E-05	5.16E-08
14.29	2.79E-06	5.16E-09
10.45	2.93E-07	1.05E-09
7.69	5.46E-08	1.32E-10
4.76	2.80E-09	2.04E-10
2.44	2.61E-10	9.45E-12
0.83	7.47E-11	9.45E-12

Ethanol-Toluene Mixtures:

Concentration of Ethanol (wt. %)	Conductivity (S/m)	Standard Deviation
100	1.06E-04	3.16E-07
90	9.22E-05	1.23E-07
80	8.43E-05	1.62E-07
70	7.66E-05	1.52E-07
60	6.51E-05	1.29E-07
50	4.95E-05	8.76E-08
40	2.95E-05	1.17E-07
31.43	1.06E-05	8.77E-08
29.41	7.64E-06	1.37E-08
25.00	3.22E-06	7.89E-09
20.00	8.40E-07	1.49E-09
14.29	8.89E-08	1.90E-10
10.45	1.32E-08	1.26E-10
7.69	2.26E-09	1.96E-11
4.76	3.05E-10	1.02E-11
2.44	1.45E-10	3.30E-11
0.83	1.58E-10	7.79E-12
0.00	1.01E-10	6.87E-12

Propanol-Toluene Mixtures

Concentration of Propanol (wt. %)	Conductivity (S/m)	Standard Deviation
100.00	2.45E-05	2.24E-07
90.00	2.19E-05	6.75E-08
80.00	2.04E-05	4.71E-08
70.00	1.81E-05	4.71E-08
60.00	1.40E-05	1.79E-11
50.00	8.65E-06	1.18E-08
40.00	3.35E-06	7.07E-09
29.41	7.62E-07	1.12E-12
25.00	3.28E-07	7.38E-10
20.00	8.86E-08	5.54E-10
14.29	1.44E-08	1.66E-10
10.45	3.59E-09	6.33E-11
6.25	6.71E-10	2.17E-11
4.76	9.13E-11	6.14E-12
2.44	5.73E-11	3.92E-12
0.83	5.56E-11	2.95E-12
0.00	4.76E-11	2.58E-11

Butanol-Toluene Mixtures

Concentration of Butanol (wt. %)	Conductivity (S/m)	Standard Deviation
100.00	7.36E-06	1.91E-08
90.00	6.28E-06	5.16E-09
80.00	5.63E-06	6.75E-09
70.00	4.56E-06	1.64E-08
60.00	2.85E-06	1.05E-08
50.00	1.50E-06	1.03E-08
40.00	4.79E-07	3.60E-09
33.33	1.33E-07	4.83E-10
28.57	4.56E-08	5.68E-11
24.05	1.36E-08	2.27E-11
20.00	4.00E-09	1.85E-11
17.81	1.98E-09	1.75E-11
15.49	9.37E-10	1.42E-11
13.04	3.62E-10	3.96E-12
10.45	1.10E-10	1.17E-11
7.69	4.73E-11	5.20E-12
5.51	3.06E-11	2.15E-12
4.00	2.80E-11	4.02E-12
2.44	2.98E-11	2.51E-12
0.83	2.97E-11	3.29E-12
0.00	2.55E-11	2.53E-12

Pentanol-Toluene Mixtures:

Concentration of Pentanol (wt. %)	Conductivity (S/m)	Standard Deviation
100.00	6.47E-06	2.15E-08
90.00	4.99E-06	1.03E-08
80.00	3.69E-06	9.49E-09
70.00	2.30E-06	4.22E-09
60.00	1.09E-06	6.32E-10
50.00	4.12E-07	1.10E-09
40.00	1.12E-07	5.16E-10
29.41	7.48E-09	3.25E-11
25.00	2.64E-09	2.80E-11
20.00	7.09E-10	6.18E-12
16.67	2.26E-10	7.33E-12
14.29	1.03E-10	5.45E-12
10.45	3.54E-11	2.32E-12
3.23	1.56E-11	3.67E-12
0.00	1.50E-11	2.78E-12

Hexanol-Toluene Mixtures:

Concentration of Hexanol (wt. %)	Conductivity (S/m)	Standard Deviation
100.00	7.79E-06	1.64E-08
90.00	4.91E-06	1.14E-08
80.00	2.73E-06	4.46E-22
70.00	1.22E-06	3.16E-10
60.00	4.08E-07	5.16E-10
50.00	1.02E-07	5.16E-10
40.00	1.82E-08	5.68E-11
33.33	3.83E-09	1.48E-11
29.41	1.85E-09	9.66E-12
25.00	7.38E-10	1.08E-11
21.05	3.32E-10	7.47E-12
17.81	1.28E-10	6.81E-12
15.49	8.87E-11	3.95E-12
13.04	6.17E-11	5.35E-12
10.45	4.55E-11	4.79E-12
4.76	2.11E-11	2.86E-12
0.00	2.18E-11	5.81E-12

Heptanol-Toluene Mixtures:

Concentration of Heptanol (wt. %)	Conductivity (S/m)	Standard Deviation
100.00	2.44E-06	1.08E-09
90.00	1.65E-06	8.64E-08
80.00	8.68E-07	2.83E-09
70.00	3.74E-07	2.31E-09
60.00	1.07E-07	1.03E-09
50.00	2.35E-08	2.32E-10
40.00	5.08E-09	2.95E-11
36.84	2.91E-09	2.45E-11
33.33	1.47E-09	7.32E-11
29.41	7.81E-10	9.32E-12
25.00	3.01E-10	6.78E-12
22.08	1.64E-10	1.17E-11
20.00	9.17E-11	2.99E-12
17.81	5.99E-11	3.93E-12
15.49	4.33E-11	3.44E-12
13.04	2.60E-11	3.42E-12
9.09	1.74E-11	3.34E-12
3.23	1.40E-11	3.70E-12
0.00	1.19E-11	2.76E-12

Octanol-Toluene Mixtures:

Concentration of Octanol (wt. %)	Conductivity (S/m)	Standard Deviation
100.00	1.53E-06	4.30E-08
90.00	8.38E-07	1.37E-09
80.00	3.96E-07	1.17E-09
70.00	1.50E-07	5.16E-10
60.00	4.59E-08	5.99E-10
50.00	1.40E-08	2.50E-10
40.00	3.45E-09	7.92E-11
35.97	2.05E-09	1.26E-11
33.33	1.36E-09	1.16E-11
29.41	7.58E-10	8.66E-12
25.00	3.75E-10	1.32E-11
21.05	1.95E-10	7.78E-12
17.81	1.08E-10	5.06E-12
14.29	6.69E-11	3.95E-12
10.45	4.92E-11	3.85E-12
4.76	2.98E-11	5.17E-12
0.00	2.49E-11	2.57E-12

Butanol-Hexane Mixtures:

Concentration of Butanol (wt. %)	Conductivity (S/m)	Standard Deviation
0	7.23E-12	3.25E-12
1	1.01E-11	3.86E-12
2	1.20E-11	2.65E-12
3	1.24E-11	2.94E-12
4	1.24E-11	3.67E-12
5	1.13E-11	2.89E-12
7	1.14E-11	3.11E-12
10	1.73E-11	3.12E-12
15	5.13E-11	3.68E-12
20	4.59E-10	1.69E-11
30	1.59E-08	3.90E-10
40	2.73E-07	6.29E-09
50	1.22E-06	4.66E-08
60	2.79E-06	1.34E-07
70	4.47E-06	2.14E-07
80	5.94E-06	3.21E-07
90	6.91E-06	2.49E-07
100	7.04E-06	2.76E-08

Butanol-Heptane Mixtures:

Concentration of Butanol (wt. %)	Conductivity (S/m)	Standard Deviation
0	1.03E-11	3.54E-12
1	9.75E-12	2.83E-12
2	9.78E-12	2.47E-12
3	1.01E-11	3.23E-12
4	1.33E-11	2.99E-12
5	1.09E-11	2.64E-12
7	1.37E-11	3.04E-12
10	2.06E-11	3.16E-12
15	7.58E-11	6.00E-12
20	6.43E-10	3.32E-11
30	2.25E-08	1.30E-09
40	2.22E-07	4.58E-09
50	9.51E-07	1.41E-08
60	2.32E-06	2.89E-08
70	4.02E-06	3.09E-08
80	5.61E-06	6.93E-08
90	6.53E-06	1.29E-07
100	7.57E-06	8.43E-07

A.1.2 RELATIVE PERMITTIVITY

Methanol-Toluene Mixtures:

Concentration of Methanol (wt. %)	Relative Permittivity
100	33.2
90	30.7
80	27.4
70	24.7
60	21.3
50	17.6
40	13.2
30	9.7
20	6.58
10	3.82
7	3.29
5	2.88
3	2.68
0	2.37

Ethanol-Toluene Mixtures:

Concentration of Ethanol (wt. %)	Relative Permittivity
100	24.1
80	19.8
60	14.9
50	13.3
40	9.62
30	7.32
20	4.96
10	3.42
7	3
5	2.8
3	2.61
0	2.36

Propanol-Toluene Mixtures:

Concentration of Propanol (wt. %)	Relative Permittivity
100	20.1
80	16.04
60	12
50	9.82
40	7.7
30	5.47
20	3.95
10	2.93
7	2.71
5	2.61
3	2.51
0	2.37

Butanol-Toluene Mixtures:

Concentration of Butanol (wt. %)	Relative Permittivity
100	17.27
80	13.56
60	9.86
50	7.95
40	6.15
30	4.58
20	3.53
10	2.82
7	2.68
5	2.58
3	2.49
2	2.46
1	2.41
0	2.38

Pentanol-Toluene Mixtures:

Concentration of Pentanol (wt. %)	Relative Permittivity
100	14.65
90	13.21
80	11.46
70	9.7
60	7.95
50	6.36
40	4.96
30	3.94
20	3.21
10	2.71
7.73	2.63
3	2.48
0	2.39

Hexanol-Toluene Mixtures:

Concentration of Hexanol (wt. %)	Relative Permittivity
100	12.57
80	9.63
60	6.72
50	5.38
40	4.3
30	3.55
20	3.04
10	2.7
7	2.59
3	2.48
0	2.38

Heptanol-Toluene Mixtures:

Concentration of Heptanol (wt. %)	Relative Permittivity
100	11.3
90	9.82
80	8.47
60	5.82
50	4.74
40	3.81
30	3.26
20	2.88
10	2.62
7	2.53
3	2.44
1	2.29
0	2.37

Octanol-Toluene Mixtures:

Concentration (wt. %)	Relative Permittivity
100	9.43
80	7.12
60	4.87
50	4.07
40	3.51
30	3.07
20	2.77
10	2.57
7	2.49
5	2.46
3	2.42
1	2.39
0	2.36

A.2 DATA FOR NONIONIC SURFACTANT-NONPOLAR MIXTURES

A.2.1 CONDUCTIVITY

Xiameter OFX-5098 - Toluene Mixtures:

Concentration of OFX-5098 (wt. %)	Conductivity (S/m)	Standard Deviation
100	4.17E-07	5.42E-10
90	3.94E-07	2.15E-10
80	2.85E-07	6.97E-10
70	1.79E-07	1.19E-09
60	9.36E-08	2.00E-10
50	4.57E-08	6.28E-11
40	2.10E-08	5.23E-11
30	7.71E-09	2.18E-11
20	3.45E-09	1.07E-11
15	2.34E-09	1.13E-11
10	1.43E-09	1.59E-11
7	1.08E-09	1.35E-11
5	8.15E-10	8.83E-12
4	7.08E-10	9.18E-12
3	6.45E-10	1.77E-11
2	4.54E-10	1.13E-11
1	3.04E-10	1.41E-11
0	1.59E-11	3.53E-12

Xiameter OFX-0400 - Toluene Mixtures:

Concentration of OFX-0400 (wt. %)	Conductivity (S/m)	Standard Deviation
100	1.50667E-07	6.57167E-11
90	1.37948E-07	1.12932E-10
80	8.76721E-08	1.45913E-10
70	5.51104E-08	8.30323E-11
60	3.23721E-08	2.01191E-10
50	1.58109E-08	1.36202E-10
40	8.84455E-09	1.78679E-11
30	4.98203E-09	2.91436E-11
20	2.87453E-09	1.77918E-11
15	2.01933E-09	1.85615E-11
10	1.30313E-09	1.90482E-11
7	9.60123E-10	2.94492E-11
5	7.63901E-10	1.91587E-11
4	6.77844E-10	1.56894E-11
3	5.79176E-10	1.5734E-11
2	4.49414E-10	1.69961E-11
1	4.22032E-10	8.86548E-12
0	2.73328E-11	5.4543E-12

SPAN 20 - Toluene Mixtures:

Concentration of SPAN 20 (wt. %)	Conductivity (S/m)	Standard Deviation
0	2.11E-11	3.11E-12
1	5.96E-08	7.48E-11
2	1.77E-07	1.11E-10
3	3.08E-07	4.49E-09
4	3.92E-07	7.04E-10
5	4.85E-07	1.74E-09
7	6.58E-07	1.04E-08
10	9.04E-07	1.88E-09
15	1.33E-06	3.71E-09
20	1.82E-06	3.79E-09
30	2.54E-06	7.72E-10
40	3.45E-06	1.46E-08
50	4.54E-06	1.43E-08
60	4.40E-06	1.06E-08
70	3.77E-06	7.07E-09
80	3.17E-06	3.00E-09
90	2.66E-06	2.02E-08
100	2.25E-06	1.35E-08

SPAN 80 - Toluene Mixtures

Concentration of SPAN 80 (wt. %)	Conductivity (S/m)	Standard Deviation
0	3.67E-11	1.93E-11
1	1.15E-08	4.83E-10
2	2.60E-08	6.37E-10
3	3.67E-08	5.90E-10
4	4.47E-08	7.53E-10
5	5.52E-08	8.83E-10
7	7.39E-08	1.44E-09
10	1.01E-07	1.31E-09
15	1.50E-07	3.58E-09
20	2.05E-07	3.46E-09
30	3.22E-07	5.85E-09
40	4.46E-07	7.25E-09
50	5.69E-07	2.90E-09
60	6.14E-07	2.61E-09
70	5.98E-07	1.86E-09
80	5.32E-07	2.38E-09
90	3.74E-07	2.41E-10
100	2.12E-07	1.39E-10

A.2.2 RELATIVE PERMITTIVITY

Xiameter OFX-5098 - Toluene Mixtures:

Concentration of OFX-5098 (wt. %)	Relative Permittivity
100	6.1
90	5.7
80	5.2
70	4.7
60	4.2
50	3.8
40	3.4
30	3.1
20	2.9
15	2.7
10	2.6
7	2.5
5	2.5
4	2.5
3	2.4
2	2.4
1	2.4
0	2.4

Xiameter OFX-0400 - Toluene Mixtures:

Concentration of OFX-0400 (wt. %)	Relative Permittivity
100	4.7
90	4.4
80	4.2
70	3.9
60	3.6
50	3.3
40	3.1
30	2.9
20	2.7
15	2.6
10	2.5
7	2.5
5	2.4
4	2.4
3	2.4
2	2.4
1	2.3
0	2.3

SPAN 20 - Toluene Mixtures:

Concentration of SPAN 20 (wt. %)	Relative Permittivity
0	2.3
1	2.4
2	2.43
3	2.46
4	2.49
5	2.52
7	2.57
10	2.66
15	2.84
20	3.03
30	3.39
40	3.72
50	4.45
60	5.05
70	5.63
80	6.62
90	7.06
100	8.52

SPAN 80 - Toluene Mixtures:

Concentration of SPAN 80 (wt. %)	Relative Permittivity
0	2.36
1	2.39
2	2.41
3	2.43
4	2.44
5	2.46
7	2.49
10	2.55
15	2.65
20	2.75
30	2.96
40	3.2
50	3.55
60	3.78
70	4.1
80	4.39
90	4.75
100	5.11

A.2.3 VISCOSITY

OFX-5098 - Toluene Mixtures:

Concentration of OFX-5098 (wt. %)	Viscosity (cP)	Standard Deviation
0	0.648	0.003
1	0.650	0.014
2	0.673	0.013
3	0.685	0.009
4	0.717	0.008
5	0.771	0.014
7	0.903	0.008
10	1.087	0.001
15	1.356	0.003
20	1.798	0.004
30	3.000	0.159
40	5.640	0.053
50	8.945	0.173
60	16.443	0.045
70	31.242	0.143
80	47.592	0.472
90	95.857	0.538
100	219.163	4.282

OFX-0400 - Toluene Mixtures:

Concentration of OFX-0400 (wt. %)	Viscosity (cP)	Standard Deviation
0	0.662	0.034
1	0.671	0.011
2	0.720	0.006
3	0.711	0.003
4	0.763	0.012
5	0.793	0.004
7	0.892	0.008
10	1.178	0.004
15	1.616	0.006
20	1.933	0.023
30	2.797	0.228
40	4.463	0.051
50	7.974	0.568
60	12.751	0.061
70	22.466	0.109
80	41.785	0.522
90	111.788	6.286
100	259.738	15.245

SPAN 20 - Toluene Mixtures:

Concentration of SPAN 20 (wt. %)	Viscosity (cP)	Standard Deviation
0	0.620	0.000
1	0.625	0.002
2	0.632	0.013
3	0.646	0.004
4	0.663	0.019
5	0.702	0.024
7	0.721	0.001
10	0.824	0.058
15	1.001	0.018
20	1.498	0.191
30	2.386	0.053
40	5.071	0.008
50	11.205	0.056
60	27.716	0.585
70	63.798	0.357
80	227.390	3.387
90	788.055	2.546
100	3505.875	

SPAN 80 - Toluene Mixtures:

Concentration of SPAN 80 (wt. %)	Viscosity (cP)	Standard Deviation
0	0.600	
1	0.594	0.0003
2	0.616	0.001
3	0.628	0.0004
4	0.650	0.001
5	0.689	0.001
7	0.739	0.002
10	0.823	0.003
15	1.007	0.002
20	1.245	0.000
30	2.073	0.008
40	3.636	0.031
50	9.521	0.092
60	20.015	0.410
70	42.518	0.220
80	105.733	1.964
90	300.725	11.080
100	1047.095	

A.3 ATTENUATION DATA

A.3.1 ATTENUATION DATA

SPAN 20 - Toluene Mixtures

Volume Fraction of SPAN 20 (%):	100	88	77	66	56	46
Frequency (MHz)	**Attenuation (dB/cm/MHz)**					
3	3.091	1.336	0.775	0.618	0.518	0.320
3.7	3.317	1.587	0.815	0.752	0.605	0.315
4.5	3.627	1.701	0.888	0.835	0.688	0.357
5.6	4.025	1.841	1.008	0.969	0.789	0.419
6.8	4.563	2.027	1.120	1.107	0.950	0.472
8.4	5.131	2.236	1.252	1.237	1.047	0.513
10.3	5.759	2.453	1.412	1.390	1.153	0.558
12.7	6.276	2.775	1.591	1.788	1.309	0.617
15.6	6.990	3.126	1.775	1.843	1.413	0.676
19.2	7.833	3.503	2.008	1.980	1.536	0.749
23.5	8.855	3.947	2.295	2.002	1.644	0.823
28.9	9.664	4.553	2.570	2.158	1.717	0.899
35.5	10.606	5.142	2.873	2.256	1.821	0.989
43.7	11.578	5.627	3.395	2.330	1.924	1.066
53.6	12.548	6.423	3.751	2.554	1.985	1.194
65.9	12.696	6.970	4.293	2.742	2.140	1.337
81	14.704	7.959	4.801	2.977	2.308	1.460
99.5		9.344	5.337	3.221	2.552	1.641

Volume Fraction of SPAN 20 (%):	22	10.7	5.3	2.6	1.3	0
Frequency (MHz)	**Attenuation (dB/cm/MHz)**					
3	0.229	0.232	0.242	0.162	0.162	-0.019
3.7	0.294	0.278	0.235	0.183	0.183	-0.013
4.5	0.306	0.295	0.268	0.208	0.208	0.000
5.6	0.374	0.339	0.293	0.206	0.206	0.038
6.8	0.400	0.366	0.303	0.220	0.220	0.051
8.4	0.440	0.397	0.321	0.228	0.228	0.063
10.3	0.473	0.411	0.334	0.227	0.227	0.080
12.7	0.513	0.437	0.341	0.241	0.241	0.097
15.6	0.554	0.465	0.360	0.254	0.254	0.115
19.2	0.599	0.499	0.386	0.279	0.279	0.149
23.5	0.651	0.538	0.416	0.307	0.307	0.184
28.9	0.704	0.579	0.451	0.346	0.346	0.227
35.5	0.771	0.630	0.498	0.396	0.396	0.283
43.7	0.838	0.695	0.565	0.462	0.462	0.353
53.6	0.947	0.795	0.655	0.555	0.555	0.452
65.9	1.080	0.932	0.778	0.668	0.668	0.564
81	1.133	0.965	0.852	0.762	0.762	0.666
99.5	1.243	1.072	0.965	0.877	0.877	0.794

SPAN 80 - Toluene Mixtures:

Volume Fraction of SPAN 80 (%):	100	47	37	18
Frequency (MHz)	**Attenuation (dB/cm/MHz)**			
3	0.934	0.236	0.174	0.183
3.7	0.933	0.304	0.211	0.211
4.5	1.012	0.299	0.252	0.240
5.6	1.083	0.365	0.307	0.287
6.8	1.169	0.392	0.348	0.326
8.4	1.245	0.441	0.399	0.363
10.3	1.329	0.478	0.437	0.393
12.7	1.440	0.522	0.476	0.425
15.6	1.558	0.582	0.524	0.454
19.2	1.719	0.642	0.591	0.501
23.5	1.892	0.714	0.649	0.547
28.9	2.055	0.784	0.713	0.592
35.5	2.258	0.869	0.794	0.647
43.7	2.629	0.966	0.871	0.708
53.6	2.980	1.052	0.973	0.785
65.9	3.358	1.197	1.076	0.865
81	3.787	1.328	1.214	0.960
99.5	4.339	1.494	1.364	1.121

Volume Fraction of SPAN 80 (%):	9	4.4	2.2	0
Frequency (MHz)	**Attenuation (dB/cm/MHz)**			
3	0.183	0.133	0.061	-0.019
3.7	0.211	0.164	0.070	-0.013
4.5	0.240	0.174	0.093	0.000
5.6	0.287	0.202	0.115	0.038
6.8	0.326	0.226	0.142	0.051
8.4	0.363	0.241	0.155	0.063
10.3	0.393	0.246	0.167	0.080
12.7	0.425	0.261	0.179	0.097
15.6	0.454	0.284	0.196	0.115
19.2	0.501	0.311	0.226	0.149
23.5	0.547	0.343	0.259	0.184
28.9	0.592	0.379	0.294	0.227
35.5	0.647	0.420	0.344	0.283
43.7	0.708	0.473	0.400	0.353
53.6	0.785	0.542	0.474	0.452
65.9	0.865	0.629	0.560	0.564
81	0.960	0.731	0.668	0.666
99.5	1.121	0.861	0.802	0.794

OFX-5098 - Toluene Mixtures:

Volume Fraction of OFX-5098 (%):	100	88	76	65
Frequency (MHz)	**Attenuation (dB/cm/MHz)**			
3	0.601	0.334	0.197	0.096
3.7	0.696	0.384	0.237	0.113
4.5	0.725	0.434	0.280	0.137
5.6	0.832	0.514	0.330	0.197
6.8	0.906	0.570	0.373	0.220
8.4	0.983	0.634	0.412	0.252
10.3	1.077	0.699	0.459	0.295
12.7	1.193	0.768	0.512	0.335
15.6	1.324	0.851	0.570	0.383
19.2	1.482	0.957	0.653	0.446
23.5	1.676	1.067	0.738	0.511
28.9	1.884	1.229	0.832	0.585
35.5	2.139	1.325	0.952	0.669
43.7	2.411	1.535	1.068	0.765
53.6	2.860	1.700	1.230	0.884
65.9	3.224	1.997	1.362	1.022
81	3.748	2.293	1.592	1.176
99.5	4.351	2.661	1.837	1.355

Volume Fraction of OFX-5098 (%):	55	45	21	10	0
Frequency (MHz)	**Attenuation (dB/cm/MHz)**				
3	0.060	0.045	0.019	0.006	-0.019
3.7	0.082	0.075	0.020	-0.002	-0.013
4.5	0.087	0.068	0.043	0.023	0.000
5.6	0.124	0.087	0.061	0.040	0.038
6.8	0.162	0.122	0.074	0.064	0.051
8.4	0.179	0.136	0.094	0.067	0.063
10.3	0.204	0.151	0.097	0.084	0.080
12.7	0.238	0.171	0.106	0.100	0.097
15.6	0.278	0.205	0.127	0.118	0.115
19.2	0.326	0.248	0.157	0.149	0.149
23.5	0.381	0.294	0.193	0.185	0.184
28.9	0.444	0.346	0.230	0.229	0.227
35.5	0.513	0.405	0.278	0.282	0.283
43.7	0.592	0.476	0.335	0.355	0.353
53.6	0.688	0.562	0.406	0.467	0.452
65.9	0.796	0.656	0.489	0.589	0.564
81	0.931	0.766	0.583	0.653	0.666
99.5	1.110	0.899	0.712	0.774	0.794

OFX-0400 - Toluene Mixtures:

Volume Fraction of OFX-0400 (%):	100	46	22	11	0
Frequency (MHz)	**Attenuation (dB/cm/MHz)**				
3	0.934	0.004	-0.006	-0.010	-0.019
3.7	0.933	0.026	0.010	-0.010	-0.013
4.5	1.012	0.042	0.014	0.022	0.000
5.6	1.083	0.084	0.043	0.037	0.038
6.8	1.169	0.105	0.055	0.054	0.051
8.4	1.245	0.131	0.070	0.065	0.063
10.3	1.329	0.151	0.078	0.085	0.080
12.7	1.440	0.176	0.097	0.098	0.097
15.6	1.558	0.206	0.119	0.115	0.115
19.2	1.719	0.249	0.147	0.148	0.149
23.5	1.892	0.296	0.187	0.183	0.184
28.9	2.055	0.347	0.231	0.226	0.227
35.5	2.258	0.408	0.281	0.281	0.283
43.7	2.629	0.482	0.348	0.349	0.353
53.6	2.980	0.572	0.448	0.461	0.452
65.9	3.358	0.692	0.612	0.588	0.564
81	3.787	0.783	0.639	0.644	0.666
99.5	4.339	0.941	0.744	0.762	0.794

A.3.2 SOUND SPEED

SPAN 20 - Toluene Mixtures

Volume Fraction of SPAN 20 (%)	Sound Speed (m/s)	Standard Deviation
100.00	1500.98	8.00
88.32	1429.54	6.46
77.07	1404.97	1.44
66.22	1381.99	3.48
55.76	1360.17	1.94
45.66	1347.42	2.35
21.88	1314.38	1.08
10.72	1304.80	1.36
5.30	1300.56	1.15
2.64	1297.66	1.34
1.32	1296.20	1.09
0.00	1305.20	1.94

SPAN 80 - Toluene Mixtures:

Volume Fraction of SPAN 80(%)	Sound Speed (m/s)	Standard Deviation
100.00	1466.98	2.55
46.79	1355.08	2.06
36.96	1336.60	1.48
18.02	1308.44	1.02
8.90	1297.46	0.69
4.42	1293.02	1.49
2.20	1289.68	0.45
0.00	1305.20	1.94

OFX-5098 - Toluene Mixtures:

Volume Fraction of OFX-5098 (%)	Sound Speed (m/s)	Standard Deviation
100.00	1370.48	1.42
87.84	1358.26	2.04
76.25	1344.38	0.65
65.19	1334.32	1.03
54.63	1324.58	1.21
44.53	1318.24	0.79
21.11	1300.66	0.59
10.29	1301.72	0.78
8.19	1304.38	1.04
0.00	1305.20	1.94

OFX-0400 - Toluene Mixtures:

Volume Fraction of OFX-0400 (%)	Sound Speed (m/s)	Standard Deviation
100.00	1180.04	0.94
45.95	1258.10	0.95
22.08	1279.26	1.11
10.83	1289.30	0.79
0.00	1305.20	1.94

A.3.3 COMPRESSIBILITY

SPAN 20 - Toluene Mixtures

Volume Fraction of SPAN 20 (%)	Compressibility (10^{-10} m^2/N)
100.00	4.301
88.32	4.832
77.07	5.096
66.22	5.363
55.76	5.636
45.66	5.845
21.88	6.409
10.72	6.639
5.30	6.751
2.64	6.815
1.32	6.848
0.00	6.771

SPAN 80 - Toluene Mixtures:

Volume Fraction of SPAN 80 (%)	Compressibility (10^{-10} m^2/N)
100.00	4.694
46.79	5.891
36.96	6.135
18.02	6.570
8.90	6.766
4.42	6.856
2.20	6.913
0.00	6.771

OFX-5098 - Toluene Mixtures:

Volume Fraction of OFX-5098 (%)	Compressibility (10^{-10} m^2/N)
100.00	4.927
87.84	5.142
76.25	5.375
65.19	5.584
54.63	5.796
44.53	5.983
21.11	6.482
8.19	6.645
0.00	6.771

OFX-0400 - Toluene Mixtures:

Volume Fraction of OFX-0400 (%)	Compressibility (10^{-10} m^2/N)
100.00	7.041
45.95	6.741
22.08	6.784
10.83	6.809
0.00	6.771